Targeting Lipid Signalling in Cancer

Inauguraldissertation

zur
Erlangung der Würde eines Doktors der Philosophie
vorgelegt der
Philosophisch-Naturwissenschaftlichen Fakultät
der Universität Basel

von

Vladimir Cmiljanović
aus
Serbien

Basel 2010

UNI
BASEL

Genehmigt von der Philosophisch-Naturwissenschaftlichen Fakultät
auf Antrag von

Prof. Dr. Bernd Giese
Prof. Dr. Andreas Pfaltz

Basel, den 08.12.2009

Prof. Dr. Eberhard Parlow
Dekan

Für meine Prinzessinnen von Bottmingen, Nicole und Janina Mila

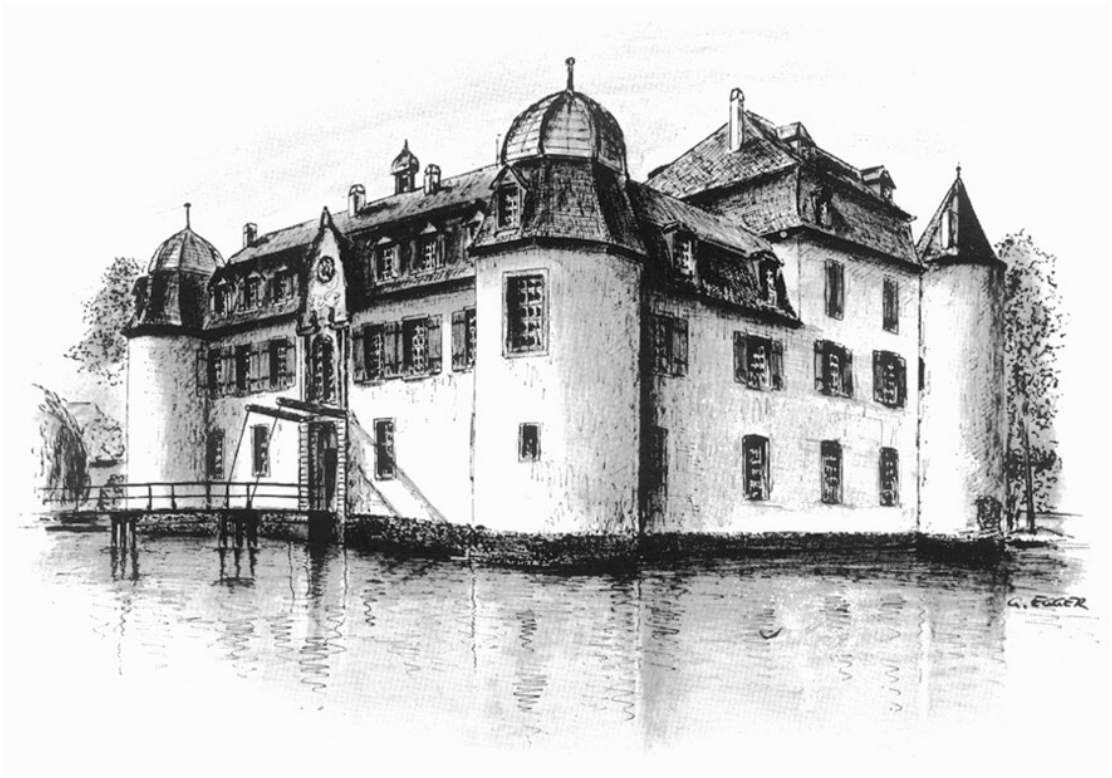

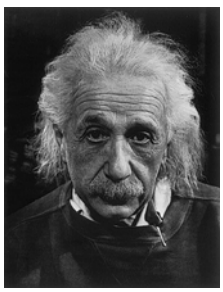

„Zwei Dinge sind zu unserer Arbeit nötig: Unermüdliche Ausdauer und die Bereitschaft, etwas, in das man viel Zeit und Arbeit gesteckt hat, wieder wegzuwerfen.“
Albert Einstein

Die vorliegende Arbeit wurde unter Anleitung von Prof. Dr. Bernd Giese und Prof. Dr. Matthias Wymann in der Zeit von März 2006 bis November 2009 im Departement Chemie und Departement für Biomedizin der Universität Basel angefertigt.

Auszüge dieser Arbeit wurden bereits veröffentlicht:

Cmiljanovic, V., Marone, R., Giese, B., Wymann, MP., ***Targeting phosphoinositide 3-kinase—Moving towards therapy***. Biochimica et Biophysica Acta, 2007. 1784(1): p. 159-185.

Marone, R., Erhart, D., Mertz, AC., Bohnacker, T., Schnell, C., Cmiljanovic, V., Stauffer, F., Garcia-Echeverria, C., Giese, B., Maira, S-M., Wymann, MP., ***Targeting melanoma with dual phosphoinositide 3-kinase/mammalian target of rapamycin inhibitors***. Molecular Cancer Research, 2009. 7(4): p. 601-613.

Cmiljanovic, V., Cmiljanovic, N., Giese, B., Wymann, MP., ***Triazine, pyrimidine and pyridine analogs and their use as therapeutic agents and diagnostic probes***. International WTO Patent ***.

Cmiljanovic, V., Cmiljanovic, N., Giese, B., Wymann, MP., ***Spirocyclic compounds and their use as therapeutic agents and diagnostic probes***. Patent ***.

Cmiljanovic, V., Cmiljanovic, N., Giese, B., Wymann, MP., ***Heterocyclic compounds and their use as therapeutic agents and diagnostic probes***. Patent ***.

Inhaltsverzeichnis

Dank (Acknowledgments)

Meinen geschätzten Doktorvätern, Prof. Dr. Bernd Giese und Prof. Dr. Matthias Wymann, danke ich ganz herzlich dafür, dass sie mir die Möglichkeit gaben ein hochaktuelles und sehr interessantes Thema zu bearbeiten. Besonders bedanken möchte ich mich dabei für das entgegengebrachte Vertrauen, die stete Unterstützung und Beratung, sowie die vielen Freiheiten, welche mir bei der Bearbeitung des gewählten Themas gewährt wurden.

Für die Korreferenz dieser Dissertation danke ich herzlich Prof. Dr. Andreas Pfaltz.

Ein grosser Dank geht an meine Schwester, Nataša Cmiljanović, die innerhalb ihrer Dissertationsarbeit im Arbeitskreis Giese-Wymann an demselben Forschungsprojekt mit anderen Schwerpunkten arbeitete und die mit ihrer fachlichen Hilfe, ihrem Engagement und ihrem Teamgeist einen wichtigen Beitrag zu dieser Arbeit leistete.

Besonders dankbar bin ich meinen fleissigen und ehrgeizigen Masterstudenten Jasmina Bogdanović, Alexander Sele, Manuela Jörg, Valentina Volić, Gabriel Schäfer, Heiko Gselinger und Samantha Brianza, die mit ihren hervorragenden Masterarbeiten und Wahlpraktika einen wichtigen Beitrag zum Erfolg dieses Dissertationsprojekts beigetragen haben.

Ganz herzlich danke ich Dr. Romina Marone (Arbeitskreis vom Prof. Dr. Matthias Wymann), die unermüdlich und mit hoher Präzision die biologische Aktivität vieler chemischen Verbindungen bestimmte und deren besondere Hilfe zu einer erfolgreichen und fruchtbaren Zusammenarbeit des Instituts für Organische Chemie und Instituts für Biomedizin führte. Ebenfalls danke ich Frau Ann Mertz (Arbeitskreis vom Prof. Dr. Matthias Wymann) für ihre Bemühungen an der Entwicklung von high-throughput screening assays.

Bei Dr. Marketa Zvelebil von The Institute of Cancer Research, Breakthrough Breast Cancer Research Centre, London, UK, möchte ich mich ganz herzlich bedanken für ihre Unterstützungen bei strukturellen Studien (computational studies and high-throughput molecular modelling studies). Bei Prof. Dr. Roger L. Williams und Frau Xuxiao Zhang von MRC Laboratory of Molecular Biology, University of Cambridge, UK, möchte ich mich ganz herzlich bedanken für die aufwendigen Röntgenstrukturaufklärungen von mehreren Enzym-Inhibitor-Komplexen.

Ein besonderer Dank geht an Prof. Dr. Nathanael S. Gray von Department of Biological Chemistry and Molecur Pharmacology, Dana-Farber Cancer Institute, Harvard Medical School, Harvard University, Boston, USA, für die zahlreichen und nützlichen Disskussionen in der Medizinal Chemie.

Dank gebührt ebenfalls Dr. Daniel Häussinger für die Strukturaufklärung komplexerer chemischen Moleküle. Sämtliche Elementaranalysen führte Werner Kirsch durch. Markus Neuburger danke ich für die Durchführung der Röntgenstrukturanalysen von kleinen chemischen Molekülen. Bei der Verfeinerung der Strukturen wurde er unterstützt von Dr. Silvia Schaffner.

Allen derzeitigen und ehemaligen Mitgliedern der Arbeitskreise Giese, Wymann, Pfaltz, Woggon, Mayor, Constable und Wennemers danke ich für die anregenden Diskussionen, produktive und freundschaftliche Arbeitsatmosphäre.

Herrn Maurus Maier, Herrn Andres Koller und Kollegen vom Werkstatt des Instituts für Organische Chemie danke ich herzlich für die zahlreichen Reparaturen der verschiedenen Maschinen, nötig für die Herstellung von biologisch aktiven Substanzen im multi-Gramm Massstab.

Der Wissens- und Technologietransfer Stelle der Universität Basel (insbesondere Herrn Mathias Weiss und Frau Hannah Greiner) danke ich herzlich für den Schutz des geistigen Eigentums sowie der aktiven Vermarktung neuer Technologien erforscht während diesem Dissertationsprojekt.

Meinen Eltern danke ich besonders für Ihre moralische Unterstützung.

Der allergrösste Dank geht an meine Frau Nicole, die während der ganzen Zeit meiner Dissertation trotz vieler Labornächte geduldig blieb und immer an mich glaubte, und an meine Tochter Janina Mila, die das Herz ihrer Eltern für immer erobert hat.

Für die finanzielle Unterstützung danke ich dem Schweizerischen Nationalfond und der Universität Basel.

1. Introduction

Phosphoinositide 3-kinases (PI3Ks) play an important role in a variety of cellular activities, including mitogenic signalling and cell survival, cytoskeletal remodelling, metabolic control, proliferation and vesicular trafficking. Consistent with their function *in cell* survival and growth, the gene for the class Iα PI3K catalytic subunit is a common site of cancer mutations. Ongoing structural studies of these enzymes and the complexes they make with their regulatory subunits have helped to clarify the mechanistic basis of this role in tumor development. The broad spectrum of biological activities associated with various isotypes of class I PI3Ks has led to an intense search for isotype-specific inhibitors as tools in mammalian cell biology and for therapeutic application. With the review "*Targeting phosphoinositide 3-kinase—Moving towards therapy"* (published at *Biochimica et Biophysica Acta*, 2007) we summarized the most important aspects of lipid kinase signalling in inflammation, cancer and metabolic disease, and discussed emerging strategies for therapeutic intervention. Last but not least, we reviewed as first the progress of >400 recent patents covering pharmaceutical targeting of PI3K. Due to its uniqueness, this review has been highly-cited within last 2 years (>100 citations in journals with good- to highest-impact factor).

Available online at www.sciencedirect.com
ScienceDirect
Biochimica et Biophysica Acta 1784 (2008) 159–185
www.elsevier.com/locate/bbapap

Review

Targeting phosphoinositide 3-kinase—Moving towards therapy

Romina Marone [a,1], Vladimir Cmiljanovic [b,1], Bernd Giese [b], Matthias P. Wymann [a,*]

[a] Institute of Biochemistry and Genetics, Department of Biomedicine, University of Basel, Mattenstrasse 28, CH-4058 Basel, Switzerland
[b] Department of Chemistry, University of Basel, CH-4056 Basel, Switzerland

Received 15 August 2007; received in revised form 28 September 2007; accepted 5 October 2007
Available online 12 October 2007

Abstract

Phosphoinositide 3-kinases (PI3K) orchestrate cell responses including mitogenic signaling, cell survival and growth, metabolic control, vesicular trafficking, degranulation, cytoskeletal rearrangement and migration. Deregulation of the PI3K pathway occurs by activating mutations in growth factor receptors or the PIK3CA locus coding for PI3Kα, by loss of function of the lipid phosphatase and tensin homolog deleted in chromosome ten (PTEN/MMAC/TEP1), by the up-regulation of protein kinase B (PKB/Akt), or the impairment of the tuberous sclerosis complex (TSC1/2). All these events are linked to growth and proliferation, and have thus prompted a significant interest in the pharmaceutical targeting of the PI3K pathway in cancer. Genetic targeting of PI3Kγ (p110γ) and PI3Kδ (p110δ) in mice has underlined a central role of these PI3K isoforms in inflammation and allergy, as they modulate chemotaxis of leukocytes and degranulation in mast cells. Proof-of-concept molecules selective for PI3Kγ have already successfully alleviated disease progress in murine models of rheumatoid arthritis and lupus erythematosus. As targeting PI3K moves forward to therapy of chronic, non-fatal disease, safety concerns for PI3K inhibitors increase. Many of the present inhibitor series interfere with target of rapamycin (TOR), DNA-dependent protein kinase (DNA-PK_{cs}) and activity of the ataxia telangiectasia mutated gene product (ATM). Here we review the current disease-relevant knowledge for isoform-specific PI3K function in the above mentioned diseases, and review the progress of >400 recent patents covering pharmaceutical targeting of PI3K. Currently, several drugs targeting the PI3K pathway have entered clinical trials (phase I) for solid tumors and suppression of tissue damage after myocardial infarction (phases I,II).

Keywords: PI3K; Cancer; Inflammation; Allergy; Pharmacology; Drug development

1. Introduction to phosphoinositide 3-kinases (PI3Ks)

Phosphoinositide 3-kinases (PI3Ks) were early on identified as lipid kinases associated with viral oncogens [1–3], and for the last 20 years, the connection between cancer and PI3K has been further substantiated [4–6]. PI3Ks have since been recognized to modulate a wide range of cellular activities, and to be central to the growth and metabolic control. Although not discussed in depth in the following, early work in model organisms, like *D. melanogaster* [7,8], *C. elegans* [9,10], *D. discoideum* (for references see [11]) and *S. cerevisiae* [12], has significantly contributed to the elucidation of the function of members of the PI3K family [13].

Genetically modified mice targeting the PI3K pathway, and the elucidation of human hereditary disease like Cowden's syndrome, tuberous sclerosis, ataxia telangiectasia, X-linked myotubular myopathy and Charcot-Marie-Tooth neuropathy, have provided further insight in the cellular and systemic role of phosphoinositide signaling. Deregulation of phosphoinositide levels, and in particular the product of class I PI3Ks, PtdIns $(3,4,5)P_3$, is involved in the pathogenesis of cancer, chronic inflammation, allergy, metabolic disease, diabetes and cardiovascular problems. Here we focus to review PI3K activation and signaling in the aforementioned human diseases, and give an overview of the progress that was made towards pharmacological targeting of PI3K.

* Corresponding author. Institute Biochemistry and Genetics, Centre of Biomedicine, Department of Clinical and Biological Sciences, DKBW, University of Basel, Mattenstrasse 28, CH-4058 Basel, Switzerland. Tel.: +41 61 695 3046; fax: +41 61 267 3566.
E-mail address: Matthias.Wymann@UniBas.ch (M.P. Wymann).
[1] Equal contribution.

1570-9639/$ - see front matter © 2007 Elsevier B.V. All rights reserved.
doi:10.1016/j.bbapap.2007.10.003

2. Phosphoinositide kinases and related proteins

2.1. The phosphoinositide 3-kinase (PI3K) family

PI3Ks are a family of enzymes, which phosphorylate the 3′-OH position of the inositol ring of phosphoinositides. They have been divided into three classes on the basis of structural features and in vitro lipid substrate specificity (Fig. 1, Table 1; and [14,15]).

Class I PI3Ks form heterodimers, which consist of one of the four closely related ~110 kDa catalytic subunits, and an associated regulatory subunit belonging to two distinct families. In vitro they are capable to convert PtdIns to PtdIns-3-*P*, PtdIns-4-*P* to PtdIns(3,4)P_2, and PtdIns(4,5)P_2 to PtdIns(3,4,5)P_3, but the in vivo substrate is PtdIns(4,5)P_2 [16,17]. Class I PI3Ks are activated by a large variety of cell-surface receptors, comprising growth factor receptors as well as G protein-coupled receptors (for a review see [18]).

Class II PI3Ks are capable to phosphorylate PtdIns and PtdIns-4-*P* in vitro, but their relevant in vivo substrates are still under investigation. This class of large (170–200 kDa) enzymes has three members, all characterized by a C-terminal C2 homology domain, which is Ca^{2+}-insensitive due to the lack of a conserved aspartate residue [19]. No adaptor molecules for class II PI3Ks have been identified so far. It was claimed, that members of this class have a different sensitivity to the classical PI3K inhibitors LY294002 and wortmannin. In fact, PI3KC2α is more resistant to both inhibitors when compared to members of the class I PI3Ks, while PI3KC2β is sensitive to wortmannin, but quite resistant to LY294002. These differences in inhibitor sensitivity are, however, insufficient to distinguish biological roles of such PI3Ks. Although class II PI3Ks have been localized to the trans-Golgi network and low-density microsomes, their mode of action is still poorly understood. Mainly the PI3KC2α isoform has been reported to associate with clathrin and has been attributed a role in clathrin assembly and clathrin-mediated vesicular trafficking [20,21]. A growing list of stimuli was described to activate class II PI3Ks, including chemokines (MCP-1), cytokines (leptin and TNFα), LPA, insulin, and other data show association of the class II enzymes with EGF-, PDGF- and SCF-receptors. Recently, it was demonstrated that PI3KC2β might be involved in LPA-induced cell migration of ovarian and cervical cancer cells [22].

Class III PI3Ks are solely able to phosphorylate PtdIns, and thus generate only PtdIns-3-*P*. The single member of this class is Vps34, of which the *S. cerevisiae* Vps34p (vacuolar protein sorting mutant 34 protein) is the prototype, and has been shown to play an essential role in trafficking of newly synthesized proteins from the Golgi to the yeast vacuole, an organelle equivalent to lysosomes in mammals [12]. In *S. cerevisiae*, Vps34p forms a complex with the N-terminal myristoylated Ser/Thr protein kinase Vps15p, which is required for activation and recruitment of Vps34p to Golgi membranes [23]. In mammals, Vps34p is associated with the orthologue of yeast Vps15p, p150 (also called hVps15), which targets hVps34p to Rab5-positive endosomes. Therefore, it appears that hVps34p is also central to endocytosis and vesicular trafficking [24,25]. As it has been demonstrated in yeast, Vps34p forms two distinct complexes with Vps15p, Atg6/Vps30p and either Atg14 or Vps38 [26]. Interestingly, deletion of Atg14 leads to defects in autophagy, while deletion of Vps38 causes a vacuolar-sorting defect. Mammalian orthologues of Atg14 and Vps38 have not been identified yet. The mammalian orthologue of Atg6/Vps30p is Beclin-1, which is capable to bind hVps34p directly. Down regulation of Beclin-1 in cells leads to minimal defects in autophagy and vesicular trafficking [27]. Mice heterozygous for Beclin-1 (Beclin-$1^{+/-}$) show decreased autophagy and enhanced tumor formation [28,29]. In the last years, a lot of attention was given to the requirement of Vps34p in the induction of autophagy in nutrient, amino acid, as well as glucose-deprived cells. Recent data suggest a role of Vps34p in the activation of mTOR downstream of amino acids, resulting in mTOR-dependent phosphorylation of $p70^{S6K1}$ and 4E-BP1 [30–32].

2.2. The phosphoinositide 4-kinases

Phosphoinositide 4-kinases (PI4Ks) phosphorylate the 4′-OH position of the inositol ring of PtdIns, and thereby generate PtdIns-4-*P* [33]. This lipid can then be further phosphorylated by PtdIns-4-*P* 5-kinases to generate PtdIns (4,5)P_2, which is the main source for phospholipase C and PI3K signaling at the plasma membrane. Four PI4Ks isoforms are known: PI4KIIα and β, and PI4KIIIα and β (for alternative names see Table 1). Type II PI4Ks have a palmitoylation sequence on a conserved stretch of cysteines, which localizes the enzymes to intracellular membranes, mainly to the trans-Golgi network and endosomes [34]. On the other hand, PI4KIIIα is mainly localized to the endoplasmic reticulum, to some extent in the nucleus and at the plasma membrane [35,36], and its highest expression is found in the nervous system [37,38]. At the plasma membrane, the lipid kinase has been found to be associated with $P2_{X7}$ ion channels, which are involved in cytoskeletal remodeling and membrane blebbing [39]. PI4KIIIβ is primary localized at the Golgi, and in small amounts in the nucleus [36,40]. It regulates trafficking of membranes from the Golgi to the plasma membrane and shuttling of intra-Golgi membrane to basolateral compartments. PI4Ks are also present on secretory and synaptic vesicles, but the predominant isoforms have not been defined yet. The PI4KIIIs are most closely related to PI3Ks and are sensitive to inhibition by wortmannin (for a review see [33]).

2.3. PI3K-related protein kinases

This class of PI3K-related proteins, referred to as class IV PI3Ks, consists of high molecular weight enzymes with a catalytic core similar to PI3Ks and PI4Ks (Fig. 1, Table 1), and include the target of rapamycin (mTOR, also known as FRAP), DNA-dependent protein kinase (DNA-PK_{cs}), the ataxia telangiectasia mutated gene product (ATM), ataxia telangiectasia-related (ATR), SMG-1 and transformation/transcription domain-

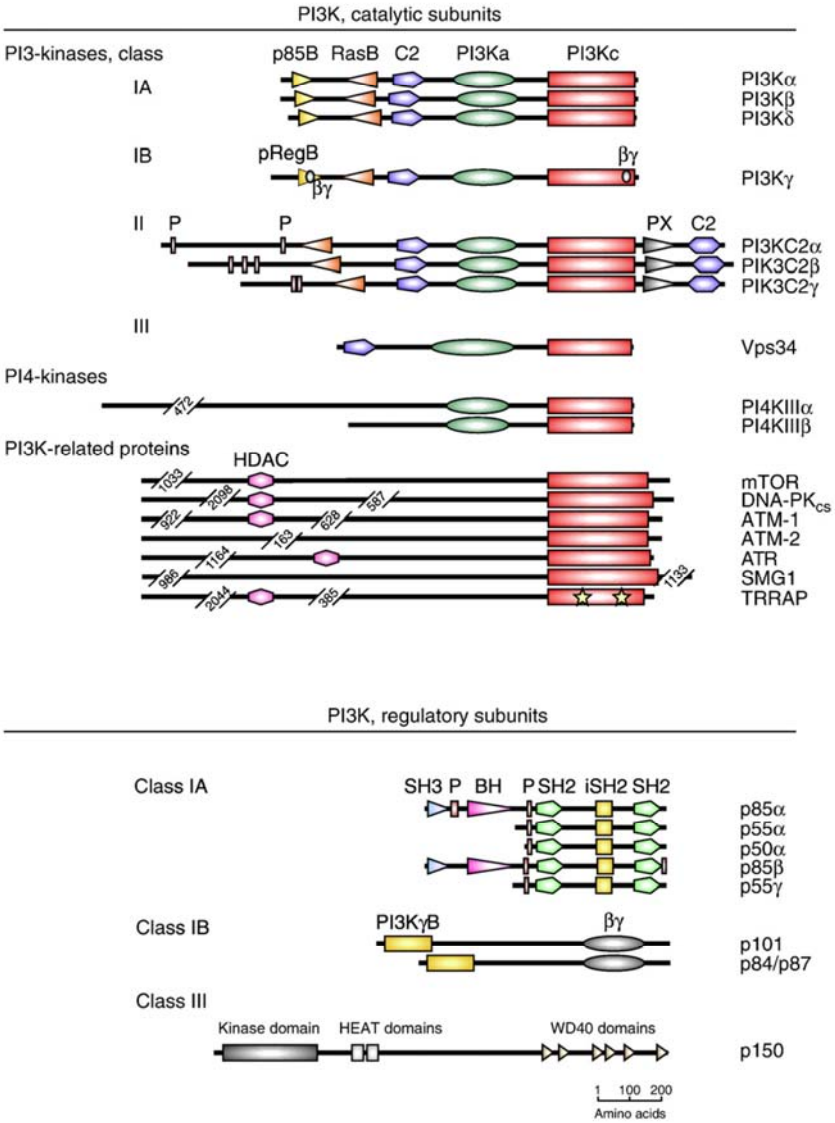

Fig. 1. Domain structure of phosphoinositide 3-kinases (PI3Ks), PI4Ks and PI3K-related proteins' catalytic and regulatory subunits. All catalytic subunits of the depicted kinases share a core catalytic domain (PI3Kc), which contains the ATP-binding site. In the case of TRRAP this domain has no kinase activity due to mutations in conserved residues (shown as stars). At their N-terminus, the catalytic domains of PI3K class I have a regulatory subunit binding domain (p85B binds p85/55/50 regulatory subunits; pRegB binds p101 and p84/87^{PIKAP} proteins), followed by a Ras-binding domain (RasB), a C2 domain (protein kinase C homology domain 2) and a PI3K accessory (helical) domain (PI3Ka). PI3Kγ contains interaction sites for βγ subunits of trimeric G proteins in the pRegB and the PI3Kc domains. PI3Ks of the class II do not have a known adaptor subunit-binding site in front of their RasB site, but display two to three proline-rich (P) stretches, as well as a PX (phox) and an additional C2 domain at the C-terminus. The catalytic subunit of the class III enzyme Vps34 is composed only of the C2, PI3Ka and PI3Kc domains. The PI3K-related proteins are large enzymes sharing only the PI3Kc domain with PI3Ks and PI4Ks. Some members of this class contain also an HDAC (histone deacetylase) domain. The regulatory subunits of class IA PI3Ks contain a proline-rich region, two SH2 (Src-homology 2) domains, as well as an iSH2 region (with a coiled-coil structure), which interacts with the catalytic subunit. p85α and p85β have at the N-terminus an additional SH3 (Src-homology 3) and BH (BCR homology) domain. The structure of p101 and p84/87^{PIKAP} is not well explored. The N-terminus is required for association with PI3Kγ, and Gβγ interaction is mediated by the C-terminal part of these adaptors. The adaptor of the class III PI3K Vps34 is the Ser/Thr protein kinase p150 (hVps15). Besides the kinase domain, this protein contains HEAT (Huntington, Elongation Factor 3, PR65/A, TOR) domains and a series of WD40 repeats. In the case of the PI4K and the PI3K-related proteins, only part of the protein is depicted here, and the number of excised amino acids is displayed. Abbreviations: ATM, ataxia telangiectasia mutated; ATR, ataxia telangiectasia-related; BH, BCR homology domain; C2, protein kinase C homology domain 2; DNA-PK$_{cs}$, catalytic subunit of DNA-dependent protein kinase; HDAC, histone deacetylase; HEAT, Huntington, Elongation Factor 3, PR65/A, TOR; iSH2, inter-SH2; mTOR, mammalian target of rapamycin; P, proline-rich region; PX, phox; TRRAP, transformation/transcription domain-associated protein.

Table 1
PI3Ks, PI4Ks and class IV PI3Ks family members

Locus	Common name	SwissProt/protein [UniProt]	Accession number Hs	Interacts with	Reference MIM	Gene map Hs/Mm
Class I PI3Ks						
Catalytic subunits						
PIK3CA	p110α, PI3Kα	PK3CA_human	NM_006218	PIK3r1, PIK3r2, PIK3r3, Ras	[233] MIM 171834	3q26.3/3 12.4cM
PIK3CB	p110β, PI3Kβ	PK3CB_human	NM_006219	PIK3r1, PIK3r2, PIK3r3, Ras	[234] MIM 602925	3q22.3/9 E4
PIK3CG	p110γ, PI3Kγ	PK3CG_human	NM_002649	Trimeric G protein βγ subunits, PIK3r5, PIK3r6, PDE3B, MEK, Ras	[235] MIM 601232	7q22.3/12 B
PIK3CD	p110δ, PI3Kδ	PK3CD_human	NM_005026	PIK3r1, PIK3r2, PIK3r3, Ras	[236,237] MIM 602839	1p36.2/4 E2
Regulatory subunits						
PIK3r1	p85α/p55α/p50α	P85A_human	NM_181523 NM_181504 NM_181524	PIK3ca, PIK3cb, PIK3cd, IRS, Rac, Src, CIP85/Ruk	[238] MIM 171833	5q13.1/13 50.0cM
PIK3r2	p85β/p55β	P85B_human	NM_005027	PIK3ca, PIK3cb, PIK3cd, IRS, Rac, Src, CIP85/Ruk	[239] MIM 171833	19q13.2–13.4/ 8 33.5cM
PIK3r3	p55γ	p55g_human	NM_003629	PIK3ca, PIK3cb, PIK3cd, IRS	[240] MIM 606076	1p34.1/4 D1
PIK3r5	p101	PI3R5_human	NM_014308	PIK3cg, βγ	[241]	17p13.1/11B3
PIK3r6	p84/p87^{PIKAP}	PI3R6_human	AY753192	PIK3cg, βγ	[242]	17p13.1/11 B3
Class II PI3Ks						
PIK3C2A	PI3K-C2α	P3C2A_human	NM_002645	Clathrin, dynactin	[243] MIM 603601	11p15.5–p14/7 53.0cM
PIK3C2B	PI3K-C2β	P3C2B_human	NM_002646	Clathrin, Grb2	[244] MIM 602838	1q32/1 E4
PIK3C2G	PI3K-C2γ	P3C2G_human	NM_004570		[245] MIM 609001	12p12/6 70.0cM
Class III PI3K						
Catalytic subunits						
PIK3C3	Vps34p	PK3C3_human	NM_002647	PIK3r4 (p150, Vps15p), Beclin1	[246] MIM 602609	18q12.3/18 B1
Regulatory subunits						
PIK3r4	p150, Vps15	PI3R4_human	NM_014602	PIK3C3 (Vps34p)	[247] MIM 602610	3q22.1/9 56.0cM
PI4Ks						
PI4K2A	PI4KIIα, PI4K2A, PI4K55	P4K2A_human	NM_018425		[264–266] MIM 609763	10q24 19 47.0cM
PI4K2B	PI4KIIβ, PI4K2B, PI4K55	P4K2B_human	NM_018323	TCR-CD3 zeta chain	[264–266]	4p15.2 5 C1
PIK4CA	PI4K230, PI4KIIIα	PI4KA_human	NM_058004 NM_002650		[248] MIM 600286	22q11.21/16 A3
PIK4CB	PI4K92, PI4KIIIβ	PI4KB_human	NM_002651	NCS-1/frequenin (?)	[249] MIM 302758	1q21/3 F2.1
PI3K-related protein kinases, class IV PI3Ks						
FRAP1	mTOR, FRAP, FRAP2, RAFT1, RAPT1, FLJ44809	FRAP_human	NM_004958	mTORC1: FKBP12, Raptor, Rheb, mLST8 mTORC2: Rictor, hSIN1, mLST8	[250] MIM 601231	1p36.2/4 71.0cM
PRKDC	DNA-PKcs, HYRC, p350, DNAPK, DNPK1, HYRC1, XRCC7	PRKDC_human	NM_006904	DNA, KU70 and KU80, XRCC4, DNA ligase IV, Artemis	[198,251] MIM 600899	8q11/16 9.2cM
ATM	ATM, AT1, ATA, ATC, ATD, ATE, ATDC, TEL1, TELO1	ATM_human	NM_000051 NM_138292	DNA, p53, Abl1, BRCA1, NBN/nibrin, TERF1, RAD17, EEF1E1, Artemis, MYST1, HTATIP	[252] MIM 607585	11q22–33/9 30.0cM
ATR	ATR, FRP1, MEC1, SCKL, SCKL1	ATR_human	NM_001184	DNA, ATRIP, RAD17, MSH2, HDAC2, Bcr/Abl, Claspin, EEF1E1	[253] MIM 601215	3q22–q24/9 E4
SMG1	SMG1, ATX, LIP, 61E3.4, KIAA0421	SMG1_human	NM_015092	PKC iota, NMD complex	[254,255] MIM 607032	16p12.3/
TRRAP	Tra1, TR-AP, PAF400, STAF40	TRRAP_human	NM_003496	c-Myc, E2F1, E2F4, p53, GCN5L2, PCAF complex, STAGA complex, BAF53 complex	[256,257] MIM 603015	7q21.2–q22.1/5 G2

associated protein (TRRAP). The first five members are active protein serine–threonine kinases that are involved in cell growth control and genome/transcriptome surveillance [41,42]. DNA-PK$_{cs}$, ATM, ATR and SMG-1 are involved in DNA-damage responses. The first two are primarily responsible for double strand break (DSB) repair, whereas ATR and SMG-1

respond to ultraviolet-induced stress as well as DSB [43,44]. SMG-1 is involved also in mRNA surveillance mechanisms [45]. The only active kinase not involved in DNA-damage is mTOR, which is regulated by growth factors and nutrient availability, and coordinates protein synthesis, cell growth and proliferation [46].

3. PI3K class I activation and signaling

The PI3K pathway is a key signaling transduction cascade controlling the regulation of cell growth, proliferation, survival as well as cell migration. PI3Ks are activated by a wide variety of different stimuli including growth factors, inflammatory mediators, hormones, neurotransmitters, and immunoglobulins and antigens [18,47]. The class IA PI3K isoforms PI3Kα, β and δ, are all bound to one of the p85/p55/p50 regulatory subunits, which all harbor two SH2 domains that bind with high affinity to phosphorylated Tyr-X-X-Met motifs. These motifs are present in activated growth factor receptors, their substrates and numerous adaptor proteins (Fig. 2).

PI3Kγ, the only class IB PI3K, associates with the adaptor proteins p101 or p84/p87^{PIKAP}, and is activated and translocated to the plasma membrane by βγ subunits of trimeric G proteins (Fig. 2). Activation of class I PI3Ks leads to the production of PtdIns(3,4,5)P_3, which recruits adaptor and effector proteins containing pleckstrin-homology (PH)-domains, e.g. protein kinase B (PKB/Akt). Once at the membrane, PKB/Akt is phosphorylated at Thr308 by phosphoinositide-dependent kinase 1 (PDK1). Full activation of PKB/Akt is achieved by phosphorylation of Ser473 within the hydrophobic motif by so-called PDK2 kinases, of which the mTOR complex 2 [48,49] and DNA-PK$_{cs}$ [50,51] seem to be the most relevant ones at present.

Once activated, PKB/Akt phosphorylates a plethora of proteins, regulating their activity either in a positive or negative manner [49]. These target molecules are involved in many different cellular outputs, which span from cell cycle progression to cell survival, degranulation, metabolism, ribosome biogenesis, translation, transcription, and cell motility (Fig. 3 and [52]).

The activation of the PI3K pathway is negatively regulated by the action of two phosphoinositide phosphatases. The SH2 domain-containing inositol phosphatase (SHIP) has a 5′-phosphoinositide phosphatase activity which converts PtdIns (3,4,5)P_3 to PtdIns(3,4)P_2 [53–55]. The other phosphatase is the phosphatase and tensin homolog deleted in chromosome ten (PTEN; also MMAC for mutated in multiple advanced cancers; or TEP1, TGF-β-regulated and epithelial cell enriched phosphatase 1), which hydrolyzes PtdIns(3,4,5)P_3 to PtdIns (4,5)P_2 [56]. PTEN is often mutated, deleted or down-regulated

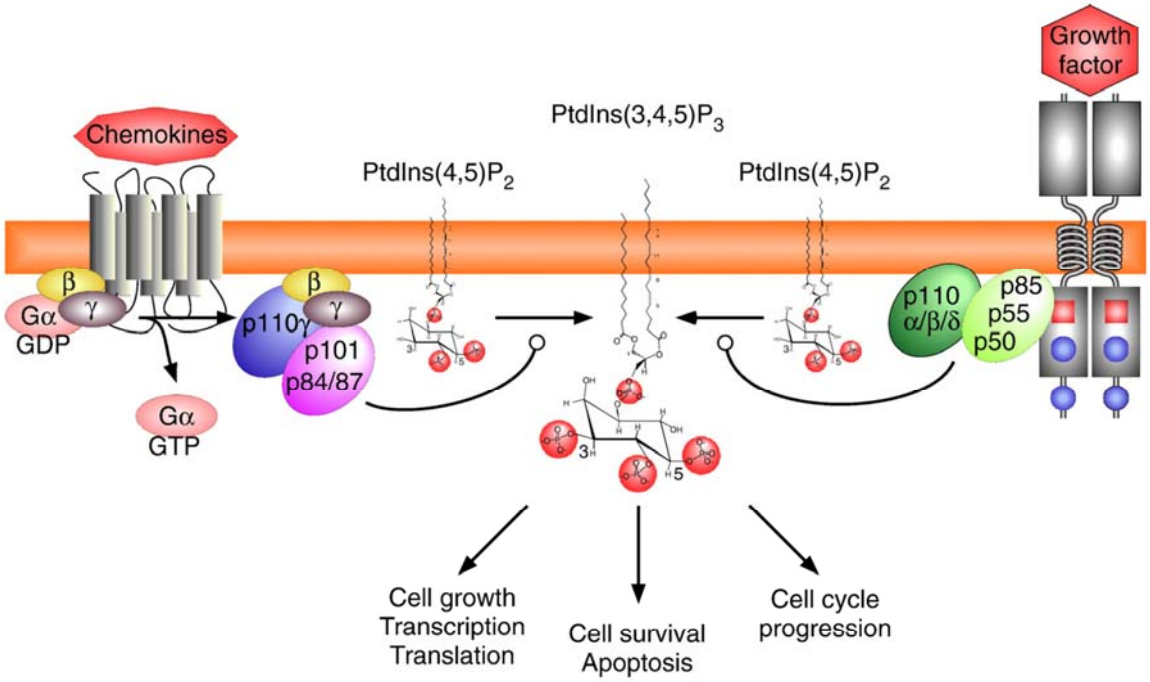

Fig. 2. Simplified activation scheme of class I PI3Ks. Heterodimeric PI3Kα, PI3Kβ, and PI3Kδ complexes are activated downstream of growth factors, cytokine receptors and their substrates, whereas PI3Kγ activation is triggered downstream of G protein-coupled receptors (GPCRs). Binding of growth factors to their cognate receptor leads to receptor dimerisation and auto-phosphorylation of multiple tyrosines (pY, blue circle), which can be located in pYxxM motifs (blue squares). These act as docking sites for the SH2 domains present in the PI3K regulatory subunits p85, p55, and p50. This translocates the catalytic PI3K subunit to the plasma membrane to initiate the conversion of PtdIns(4,5)P_2 to PtdIns(3,4,5)P_3. PtdIns(3,4,5)P_3 then recruits proteins with a pleckstrin homology (PH) domain and amplifies the growth factor signaling cascade. In the case of PI3Kγ, binding of chemokines to GPCRs induces the dissociation of heterotrimeric G_i-proteins. Free $G_{\beta\gamma}$ subunits interact with PI3Kγ and the adaptor proteins p101 and p84/87^{PIKAP}, usually triggering transient, high amplitude signals of PtdIns(3,4,5)P_3.

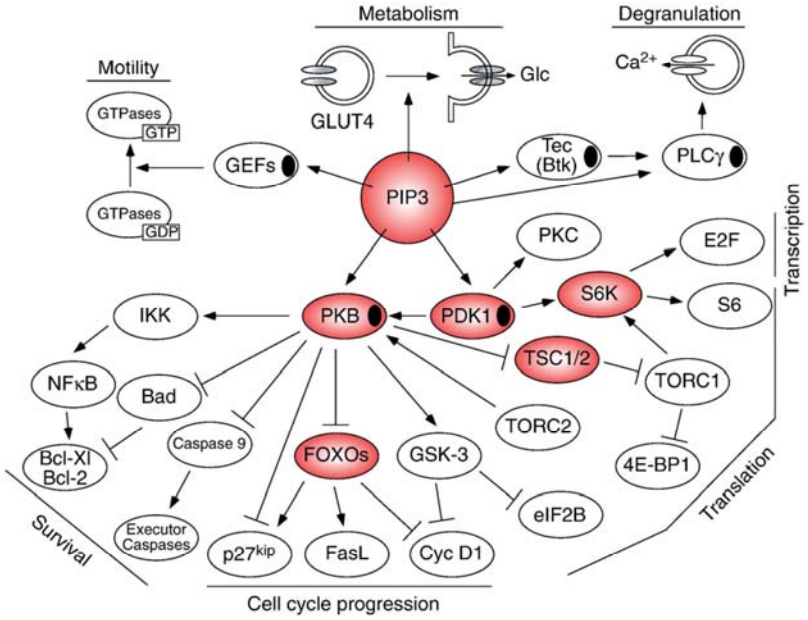

Fig. 3. Central role of the PI3K pathway in cell growth, proliferation, survival, and motility. PtdIns(3,4,5)-trisphosphate [PIP_3; PtdIns(3,4,5)P_3] is produced exclusively by class I PI3Ks, and recruits proteins with pleckstrin homology domains (PH domain, black oval). Translocation of PKB/Akt promotes its phosphorylation by phosphoinositide-dependent kinase 1 (PDK1→Thr308) and PDK2 (→Ser473) activities. Double phosphorylated and fully activated, PKB/Akt phosphorylates and inactivates members of the FOXO transcription factor family, and they are trapped in the cytosol in their phosphorylated form due to interaction with 14-3-3 proteins. At this stage, transcription of cyclin D1 is up-regulated, whereas $p27^{Kip1}$ is down-regulated, resulting in cell proliferation. Additionally, phosphorylated PKB/Akt has an anti-apoptotic action via the regulation of IKK, Bad and caspase 9. To proliferate, cells have to reach a critical size, which is controlled by the mTOR complex 1 (mTORC1), which triggers S6 kinase (S6K), linking to transcription and translation. PtdIns(3,4,5)P_3 also contributes to the translocation of GLUT4 glucose transporter containing vesicles to the plasma membrane. PtdIns(3,4,5)P_3 also activates GEFs, which in turn act on small GTPases such as Rac and Cdc42, and stimulate cell motility. Translocation of Tec family members and PLCγ leads to increase in intracellular Ca^{2+} concentration, and subsequent degranulation (e.g. in mast cells and granulocytes). PtdIns(3,4,5)P_3 controls a variety of signaling molecules – which, when mutated or deleted – promote disease such as cancer, inflammation and allergy, autoimmune disorders as well as cardiovascular disease (relevant molecules marked in red). Abbreviations: 4E-BP1, eukaryotic initiation factor 4F binding protein; Bad, Bcl2-antagonist of cell death; Bcl-Xl/Bcl-2, Bcl-Xl/Bcl-2-antagonist causing cell death; Cyc D1, cyclin D1; eIF2B, eukaryotic initiation factor 2B; FasL, Fas ligand; FOXO, forkhead box O; GEF, guanine exchange factor; GSK-3, glycogen synthase kinase 3; IKK, inhibitory κB kinase; mTOR, mammalian target of rapamycin; NFκB, nuclear factor κB; PDK1, phosphoinositide-dependent kinase 1; PKB, protein kinase B (also called Akt); PKC, protein kinase C; PLCγ, phospholipase Cγ; S6K, S6 kinase; TSC, tuberous sclerosis complex; TSC1, hamartin; TSC2, tuberin.

in various tumors, which leads to a constitutive activation of the PI3K pathway [4–6].

3.1. Cell cycle progression

Cell cycle progression is tightly controlled by the oscillating expression of cyclins, and their interaction with cyclin-dependent kinases (CDKs) or CDK inhibitors. Active PKB/Akt is able to phosphorylate the class O of transcription factors (FOXOs) on three different sites. The latter allow binding of 14-3-3 proteins, which causes the retention of the FOXO/14-3-3 complex in the cytosol [57]. The absence of FOXO from the nucleus increases transcription of cyclin D1 and reduces transcription of the CDK inhibitor $p27^{Kip1}$ [58,59]. Moreover, phosphorylated PKB/Akt blocks the activity of glycogen synthase kinase 3β (GSK3β), resulting in the accumulation of cyclin D1, since it is no longer targeted for degradation to the proteasome by GSK3β [60]. An increase in the levels of cyclin D1 and a reduction in $p27^{Kip}$ are the conditions required for the cells to pass the transition between G1 and S phase [60,61].

3.2. Cell survival and apoptosis

The activation of the PI3K/PKB pathway has an anti-apoptotic effect. Here, PKB/Akt phosphorylates and inhibits caspase 9, a protease crucial in the initiation of the apoptotic cascade [62]. PKB/Akt also phosphorylates the death promoter BAD at Ser136, and thus releases the anti-apoptotic proteins Bcl-2 and Bcl-X_L [63,64]. PKB/Akt can also activate and phosphorylate I-κB kinase. This kinase in turn phosphorylates and inactivates the inhibitor I-κB, which then releases the transcription factor NF-κB. As a consequence, the latter translocates to the nucleus and activates transcription of anti-apoptotic proteins such as Bcl-2 and Bcl-X_L [65,66]. Finally, inactivation and cytosolic retention of FOXO as mentioned above, leads to a block in transcription of FasL, and thus intercepts ligand-induced apoptosis.

3.3. Cell growth, transcription, and translation

In order to proliferate and divide, the cells have to reach a certain cell size. PKB/Akt and the nutrient sensor mTOR

collaborate to control cell size and growth. PKB/Akt phosphorylates and inhibits TSC2 (tuberin), which in a complex with TSC1 (hamartin) forms the tuberous sclerosis complex [67]. Once phosphorylated, the complex is no longer able to suppress Rheb, which can now be loaded with GTP and act positively on mTOR. Active mTOR phosphorylates and inhibits the eIF4E binding proteins (4E-BPs), promoting the translation of 5′-terminal cap 7′-methyl guanosine containing mRNAs [46]. Moreover, mTOR activates $p70^{S6K}$, which in turn phosphorylates the ribosomal protein S6, a protein essential for the regulation of cell size. As a consequence, protein and lipid biosynthesis are on, and cells can now increase in size and enter the cell cycle [68,69].

4. PI3Ks in disease

As described above, activation of the PI3K/PKB signaling cascade has a positive effect on cell growth, survival and proliferation. Constitutive up-regulation of PI3K signaling can have a deleterious effect on cells leading to uncontrolled proliferation, enhanced migration and adhesion-independent growth. These events favor not only the formation of malignant tumors, but also the development of inflammatory and autoimmune disease [5,6,13].

4.1. PI3Ks in chronic inflammation and allergy

All cell types express PI3Kα and PI3Kβ, whereas PI3Kδ and PI3Kγ are mainly expressed in leukocytes. PI3Kγ is also present at low concentration in smooth muscle cells, endothelia and cardiomyocytes [5,70–73]. Mice lacking PI3Kα or PI3Kβ die during embryonic development, which has prevented the evaluation of the role of these isoforms in the immune system [74,75]. In contrast, mice without functional PI3Kδ or expressing a catalytically inactive version of PI3Kδ ("knock-in") [76–78] or PI3Kγ [79–81] are viable and fertile, and show attenuated function of immune cells. PI3Kδ "knock-out" and "knock-in" mice have an impaired development of the marginal zone B-cells and peritoneal B1-cells. Moreover, signaling downstream of the B-cell receptor (BCR) is attenuated or completely abolished. In mice with non-functional PI3Kδ, peripheral T-cells have a more pronounced naïve phenotype, as when compared to PI3Kδ null animals. In addition, PI3Kδ "knock-in" mice have an elevated amount of Foxp3+ T-regulatory cells in the thymus, whereas in all other peripheral organs the proportion of Foxp3+ cells is reduced [82]. It has been speculated that some auto-reactive thymocytes do not undergo apoptosis and differentiate into T-regulatory cells. PI3Kδ "knock-in" T-cells have some mild defects in T-cell receptor (TCR) signaling, showing a reduced phosphorylation of the PI3K effector PKB/Akt upon stimulation. On the other hand, T-cells of PI3Kγ null mice display significant differentiation and signaling defects. These mice have an impaired thymocyte selection resulting in less double-positive cells and an altered $CD4^+$ to $CD8^+$ ratio [83]. Moreover, TCR activation in peripheral T-cells leads to a reduced proliferation and cytokine production. New data are suggesting a role for PI3Kγ in the reduction of $CD4^+$ memory T-cells survival [84]. B-cells of PI3Kγ null mice do not have differentiation and functional defects.

Recent data show that PI3Kγ null and PI3Kδ "knock-in", double mutant mice have severe defects in thymocyte differentiation (reduced numbers of thymocytes, in particular of $CD4^+/CD8^+$ double-positive cells), and display loss of thymus structure, and atrophy of thymus and spleen [85,86]. In addition, the number of B-cells was reduced to levels similar to that of the PI3Kδ single "knock-in" mice. Interestingly, these mice show signs of inflammation in multiple organs including stomach and salivary glands. Until recently, very little was known about natural killer (NK) cells development and differentiation in PI3K mutant mice [87,88]. PI3Kδ "knock-in", but not PI3Kγ null mice, have reduced numbers of NK and NKT cells. When compared to each single mutant, the double PI3Kγ/PI3Kδ mutant mice have an even more pronounced reduction in the number of NK but not NKT cells [89]. Double mutant mice also illustrated that PI3Kδ is important for cytokine secretion, and both isoforms cooperate during NK cells development and cytotoxicity.

Importantly, macrophages, dendritic cells and granulocytes derived from PI3Kγ null mice show impaired migration towards chemokines and sites of inflammation [90,91], and mast cells derived from PI3Kγ null and PI3Kδ "knock-in" mice do not show maximal reaction in allergic responses [92,93].

Allergy and inflammation involve the activation of tissue resident mast cells and macrophages, followed by the invasion of effector cells like monocytes, neutrophils and more mast cell precursors to the inflamed area. PI3Kγ is required for chemokine-dependent migration of neutrophils, macrophages [79] and mast cells [94] to the site of infection and consequent clearance of infection.

Mast cells express the high affinity receptor for IgE (FcεRI) on their surface, which makes them primary effectors in allergic responses, asthma and atopic dermatitis. Their activation is induced by antigen/IgE-mediated cross-linking of FcεRI receptors, followed by the phosphorylation of immuno-receptor tyrosine-based motifs (ITAMs) on the receptor's β and γ chains by protein tyrosine kinase Lyn and subsequently recruitment of Syk. This protein tyrosine cascade culminates in the phosphorylation of multiple tyrosines on membrane-anchored adapters LAT and NTAL/LAB [95], as well as Grb2-associated binder 2 (Gab2; [96]). Then translocation of PI3K class IA and production of PtdIns(3,4,5)P_3 initiates the activation of Bruton's tyrosine kinase (Btk) and phospholipase Cγ (PLCγ). A full-scale activation is achieved by the opening of calcium channels in the plasma membrane, and the release mediators such as histamine and heparin from mast cell granules [97].

Mast cells express G protein-coupled receptors (GPCRs), among them also adenosine receptors. Bone marrow-derived mast cells from PI3Kγ null mice display attenuated degranulation as compared to wild type cells when stimulated with antigen/IgE. It has been shown that the adenosine-mediated activation of PI3Kγ cooperates with the protein tyrosine kinase downstream of FCεRI receptors. As a consequence, PI3Kγ "knock-out" mice are completely protected against systemic anaphylaxis [92,98].

Mice expressing a kinase-inactive version of PI3Kδ also display a partial impaired antigen-IgE inflammatory response and bone marrow mast cells derived from these mice have migratory defect in response to stem cell factor [93]. However, in comparison to PI3Kγ null mice, PI3Kδ "knock-in" mice are only partially protected against anaphylactic allergic responses, attributing to PI3Kγ a central role in allergic response.

Rheumatoid arthritis (RA) is a chronic systemic inflammatory autoimmune disorder affecting ~1% of the population, and is characterized by the inflammation of the joints, causes cartilage and bone erosion terminating in joint destruction. Other tissues including skin, blood vessels, heart, lungs and muscles can also be affected.

T-cells, mainly $CD4^+$ memory cells invade the synovial membrane and start to secrete IL-2 and IFN-γ leading to the activation of monocytes, macrophages and fibroblasts. These cells then produce pro-inflammatory cytokines such has TNF-α, IL-1 and IL-6, which are critical in the onset of the chronic inflammation [99,100]. A variety of cells contribute to the progression of RA: T-cells, B-cells, and plasma cells, which produce auto-antibodies recognizing type II collagen and proteoglycans; macrophages, mast cells, dendritic cells, neutrophils and fibroblasts accumulate in high numbers in the synovial membrane. In addition, in the proliferating synovial membrane neovascularization takes place.

As described above, PI3Kγ and PI3Kδ are essential for T-cell and B-cell development and function, and they are required for neutrophil and mast cell migration as well as for mast cell degranulation in allergic responses. These results suggest that these PI3K isoforms may be valuable targets in inflammatory disorders such as RA. Mouse models to study RA and the effect of different drugs are the collagen-induced arthritis (CIA) and the passive αCII-IA models [101–104]. In CIA, type II collagen is injected intra-dermally to develop typical features of RA, including cell infiltration in the synovial space, hyperplasia, and disruption of pannus, joint cartilage and bone. For the initiation of CIA, T- and B-cells are required. In the passive αCII-IA model, where type II collagen-specific monoclonal antibodies are injected to initiate RA, disease progresses independently of T- and B-cells, reflecting more the effector phase of the disease. Experiments performed in PI3Kγ null mice showed that mutant mice are protected from RA progression independently of the model used: wild type mice injected with type II collagen, or with type II collagen-specific antibodies, showed attenuated joint inflammation and progression to RA, when the animals were treated with PI3Kγ inhibitors semi-therapeutically (treatment at disease onset) and therapeutically (treatment when disease was established; [105]). A hallmark of the pharmacological treatment was that the mice showed impaired neutrophil migration leading to a protection against RA development and reduced accumulation of neutrophils at the joints.

Systemic lupus erythematosus (SLE) is a chronic autoimmune inflammatory disease with a broad range of clinical presentations, affecting mostly women of African or Asian ancestry. Initially, it is characterized by the presence of autoreactive $CD4^+$ memory cells. These cells will induce polyclonal B-cell activation leading to B-cell expansion, hyper-gammaglobulinemia and production of anti-nuclear and anti-DNA antibodies. Approximately half of the patients will develop nephritis due to autoantibody complexes retained in the kidney, leading to the activation of the complement system, followed by infiltration of T-cells and macrophages. In the worst case, kidney inflammation progresses to glomerulonephritis, and eventually leads to renal failure.

Mice of the MRL strain – homozygous for the lymphoproliferation (*lpr*) mutation – develop spontaneously a lupus-like autoimmune disease including the generation of autoantibodies, abnormal amounts of auto-reactive $CD4^+$ cells and immune complexes in the kidney and in the salivary glands, and make them a suitable model for SLE studies [106,107]. These mice usually die 6 months after disease onset. Moreover, the $CD4^+$ cells of MRL-*lpr* mice have elevated levels of phosphorylated PKB/Akt as compared to wild type mice [108]. Importantly, also $CD4^+$ cells of SLE patients have high levels of pPKB/Akt. Furthermore, mice with constitutive activation of the PI3K pathway, e.g. caused by inactivation of PTEN or expression of $p65^{PI3K}$ (a truncated, activating form of the p85 regulatory subunit of PI3K) in T lymphocytes, develop a SLE-like phenotype [109,110]. On the other hand, expression of the $p65^{PI3K}$ transgene in T-cells of PI3Kγ null mice leads to milder SLE symptoms. In fact, these mice still have lymphoproliferation and T-cell infiltration disorders, but have reduced $CD4^+$ cell survival, less nephritis and a longer life span. These studies demonstrate that PI3Kγ plays a crucial role in SLE. Promising results have also been obtained using MRL-*lpr* mice treated with selective PI3Kγ inhibitors [108]. The treated mice had reduced numbers of $CD4^+$ cells and auto-antibodies, displayed reduced kidney malfunction, and lived longer than vehicle-treated controls. Current treatment for SLE is very heterogeneous due to the varying aggressiveness of the disease, and includes immunosuppressants, nonsteroidal anti-inflammatory drugs (NSAIDs), antimalarial drugs and corticosteroids, all with major side effects when used for long-term therapy. In mice, inhibition of PI3Kγ was well tolerated, and resulted in greater efficiency in comparison to the reference drug dexamethasone [111]. Altogether, murine models encourage the clinical development of PI3Kγ inhibitors for the treatment of SLE.

Atherosclerosis is a chronic inflammatory disease affecting arterial blood vessels, is characterized by deposits of oxidized low-density lipoproteins (LDLs), and is the primary cause of heart failure and stroke [112,113]. Macrophages and T lymphocytes are the first cells involved in the inflammatory process in atherosclerosis. Macrophages take up oxidized LDLs and convert to foam cells. It is known that oxidized LDLs activate the PI3K pathway in macrophages/foam cells [114,115]. In macrophages derived from PI3Kγ "knock-out" mice, PI3K downstream signaling was not activated upon exposure to oxidized LDLs. In addition, mice with a deletion of the apolipoprotein E gene ($apoE^{-/-}$) are prone to the development of an aggressive form of atherosclerosis [116,117], which was significantly reduced in the absence of PI3Kγ [118]. The amount of phosphorylated PKB/Akt, and other phosphorylated effector proteins (S6K, S6, GSK3β and FKHR), was

found to be reduced in atherosclerotic lesions of PI3Kγ$^{-/-}$/apoE$^{-/-}$ mice when compared to apoE$^{-/-}$, illustrating that the members of the PI3K class IA were not able to compensate for the deletion of PI3Kγ. These results clearly demonstrate that PI3Kγ has the potential to stabilize atherosclerosis at a pre-symptomatic stage, and might contribute to the alleviation of cardiovascular disorders.

Other inflammatory diseases: As described above, PI3Kγ and PI3Kδ are essential for the proper differentiation and functionality of T- and B-cells, mast cells, macrophages and neutrophils. In two different mouse models of acute pancreatitis (supramaximally stimulating doses of cerulein and choline-deficient ethionine-supplemented diet), PI3Kγ null mice fare better than wild type counterparts. The PI3Kγ null animals display increased apoptosis of acinar cells and a decreased infiltration of neutrophils in the pancreas [119]. Other diseases, where PI3K inhibition has a therapeutic potential are: i) psoriasis, in which T-cells, neutrophils, and macrophages are implicated [120,121], and ii) chronic obstructive pulmonary disease (COPD), which is mainly driven by macrophages, but also requires T-cells and neutrophils [122,123], and multiple sclerosis with T- and B- cells appear to be the major players [124,125].

4.2. Cardiovascular disease

More than 10 years ago, the first report of a role of the PI3K pathway in the control of cell and organ size was published: ectopic expression of the *Drosophila* class I PI3K Dp110 in wings, or in the eye marginal disks, resulted enlarged cells and tissues [8]. To investigate if PI3Ks were involved in the control of organ size in vertebrates, Shioi et al. overexpressed constitutively active PI3Kα in the heart of mice [126]. Mice overexpressing the active PI3Kα had an enlarged heart. Cardiac hypertrophy was mediated by increased cell size, not cell number. Interestingly, neither cardiac architecture nor cardiac function was changed in PI3Kα transgenic mice. Moreover, even a bigger increase in heart size was obtained, when a constitutive form of PKB/Akt was expressed [127]. This phenotype was completely reverted following treatment with the mTOR inhibitor rapamycin, demonstrating that PKB/Akt signaling is relayed via mTOR to control heart size. Another way to constitutively activate the PI3K pathway is the cardiomyocyte-specific inactivation of the lipid phosphatase PTEN, which also triggers heart hypertrophy and culminates in reduced cardiac contractility [128].

PI3Kγ, activated downstream of GPCRs, is expressed in the heart at low levels. PI3Kγ deficient mice display no changes in heart size and heart rate. Interestingly, targeting of PI3Kγ in PTEN deficient hearts leads a restoration of contractility. It seems that PI3Kα, and other members of the class IA PI3Ks mainly control heart size [129], whereas PI3Kγ influences contractility.

Hypertrophy can also be induced by cardiac pressure overload, e.g. by transverse aortic constriction (TAC). In the TAC model, PI3Kγ null mice suffered fibrosis and chamber dilatation leading to acute heart failure. Mice expressing catalytically inactive PI3Kγ (PI3Kγ$^{KD/KD}$), however, developed less hypertrophy as compared to wild type mice, and did not show signs of apoptosis and fibrosis. During theses studies it was found that the lipid kinase activity of PI3Kγ was not vital to the control of heart contractility, but that the PI3Kγ protein was required as a scaffold for phosphodiesterase 3B activity and cAMP breakdown [70]. Recent studies demonstrated that PI3Kγ and PI3Kδ regulated infarct size after ischemia/reperfusion injuries. In agreement, animals treated with the PI3Kγ/δ inhibitor TG100-115, developed diminished inflammatory responses and edema formation, while tissue repair processes like endothelial cell mitogenesis were left intact [130,131]. After promising results obtained in rodent and porcine models, phases I and II clinical trials with acute myocardial infarction patients are currently in progress.

4.3. Cancer

PI3K controls cell growth, proliferation, and cell survival, which constitute critical steps towards tumor formation and malignant cell dissemination. Aberrations of PI3K signaling are found in various tumors. The most frequent ones are loss or attenuation of PTEN function and mutations in PI3Kα, both leading to elevated PtdIns(3,4,5)P_3 levels [4–6,13]. Activating mutations, truncations and change in expression levels have been reported for the p85 regulatory subunit, the downstream effectors PDK1, PKB/Akt, S6K, TSC1/2, members of the forkhead family and in TCL1 [132,133]. Additionally, mutations have been identified in activators of PI3K, like the epidermal growth factor receptor (EGFR), the platelet-derived growth factor receptor (PDGFR) and Bcr-Abl [5,132,134].

The phosphatase PTEN dephosphorylates PtdIns(3,4,5)P_3 at the 3′ position and reverses the action of PI3K. A number of tumors have alterations in the level of expression of this protein, in the methylation of the PTEN locus, or loss of heterozygosity. Germline mutations [135,136] have been found in around 80% of patients with Cowden's syndrome [137], and less frequently in diseases like the Bannayan-Riley-Ruvalcaba syndrome (60%; [138]), the Proteus syndrome (up to 20%; [139]) and the Proteus-like syndrome (up to 50%; [140]). Cowden's disease is characterized by presence of multiple hamartomas, and the patients have a high risk of developing breast, thyroid and endometrial cancers [141]. In Cowden's disease, as well as in Bannayan-Riley-Ruvalcaba syndrome, PTEN mutations are mostly missense and non-sense localized in exons 5,7 and 8 that contain the phosphatase domain. In tumor cells a large number of frameshift mutations are found, which are usually absent in the genetic syndromes. Sporadic mutations are found in more than 50% of glioma, melanoma, prostate, endometrial and ovarian cancers and to a lesser extent in breast cancer [142–144]. Furthermore, some tumor cells down-regulate PTEN by promoter hyper-methylation. This is seen in more than 50% of breast and prostate tumors, as well as in melanoma, endometrial, colorectal cancer and leukemia [145–148]. Loss of function of PTEN is usually a late step in tumor progression occurring in advanced tumor stages or even after metastasis [5,6,42].

The PIK3CA gene encodes the PI3Kα catalytic subunit. This gene is amplified in different tumors, especially in ovarian, cervix and lung cancers [149–151]. Mutations are also found in more than 30% of solid tumors including colorectal, gastric, brain, breast, certain brain tumors, ovarian, lung, and hepatocellular carcinomas [133,152]. They are localized mainly in two hotspots: the helical and the catalytic domain [153]. In the helical domain, residues E542 and E545 are often mutated to lysine, whereas in the kinase domain residue H1047 is changed to arginine. A rationale for the molecular mechanism on how the above mutations activate PI3Kα, has been provided on the basis of structural resolution of a co-crystallized p85 inter-SH2 domain interacting with the N-terminus of the PI3Kα catalytic subunit [154]. The three PI3Kα mutant proteins above display elevated lipid kinase activity as compared to wild type PI3Kα, and have the potential to transform chicken-embryo fibroblasts and NIH 3T3 cells. Transfected with mutated PI3Kα, these cells show constitutive phosphorylation of PKB/Akt and of downstream proteins S6K, 4E-BP1 and forkhead transcription factors [155–157]. As a result, these cells are able to proliferate better in 2D and in 3D culture settings, and display reduced levels of apoptosis as compared to wild type cells, when grown in the absence of fetal calf serum [157]. Moreover, PIK3CA mutant cells have an increased migratory and invasive capacity in vitro and in vivo. Altogether, this suggests that expression of a constitutive active form of PI3Kα allows cells to survive and even migrate in suboptimal environmental conditions, and that PI3Kα contributes to tumor formation and metastasis.

LKB1, is a serine–threonine protein kinase activating AMP-dependent protein kinase (AMPK). AMPK signals to TSC2, which results in mTOR inhibition [159]. LKB1 is defective in Peutz-Jeghers syndrome, a familial colorectal polyp disorder, in which patients are also predisposed to early-onset cancers in other tissues [160].

TSC: mutation or loss of heterozygosity in TSC gives rise to the tuberous sclerosis syndrome, an autosomal dominant disorder characterized by the development of hamartomas in a variety of organs [158]. The TSC syndrome is seldom associated with malignancy, but patients have an increased risk to develop clear-cell renal carcinomas.

Target of rapamycin (mTOR) complexes 1 and 2 integrate growth factor signaling (via PI3K/PKB and the Ras/MAPK cascade), energy status (LKB1 and AMPK) and nutrient detection. TOR is positively regulated by PKB/Akt, which phosphorylates the negative regulator TSC2 in the tuberous sclerosis complex (TSC), resulting in activation of the GTPase Rheb and mTOR. mTOR controls the 5′ cap-dependent translation via phosphorylation of the translational repressor 4E-BP1. Hyper-phosphorylated 4E-BP1 releases bound eIF4E, which is required for translation initiation modulated by the eIF4F complex. In parallel, mTOR stimulates translation of ribosomal proteins and therefore ribosome biogenesis via the activation of $p70^{S6K}$ [46]. Elevated expression of eIF4E is present in a variety of cancers, and correlates often with aggressive disease and poor prognosis [161].

Rapamycin, and its derivatives RAD001 and CCI-779, bind to FKBP12, and the complex blocks mTOR complex 1 (mTORC1, see below) activity very selectively. Various clinical trials were initiated using Rapamycin and derivatives, mostly in patients with tumors displaying elevated PI3K signaling and hyperactive mTOR. Promising results were obtained in mantle cell lymphoma, endometrial cancer and renal cell carcinoma [162]. Rapamycin and its derivatives possess anti-angiogenic activity because they counteract VEGF action [163]. This opens avenues for combinatorial treatments with conventional chemotherapy [164].

4.4. Metabolic disease

The mTOR cascade controls many steps of cellular metabolism, including protein biosynthesis, glucose homeostasis, and it has recently been shown that mTOR also modulates fat metabolism [46,165]. mTOR is present in two distinct complexes, mTORC1 and mTORC2. mTORC1 controls the activation of S6K and 4E-BP1, while mTORC2 phosphorylates PKB/Akt on Ser473, the so-called PDK2 site. It is assumed that only mTORC1 integrates nutrient and energy levels.

Insulin, via the insulin receptor tyrosine kinase, triggers phosphorylation of insulin receptor substrates (mainly IRS1 and IRS2). Specific phosphotyrosine motifs on IRS serve as docking sites for signaling molecules, such as the p85 adaptor subunits of PI3Ks class I. It has been demonstrated, however, that insulin is not able to drive $p70^{S6K}$ activation in the absence of amino acids and glucose [68]. mTOR "knock-out" mice die shortly after implantation due to defects in trophoblast differentiation and embryonic stem cells proliferation [166,167]. In contrast, S6K1 deficient mice are viable, but show developmental retardation, smaller pancreatic β-cell size, are hypoinsulinemic and are mildly glucose intolerant [42,168]. Interestingly, S6K1 null mice are protected against diet-induced obesity, probably due to a rise in lipolysis in adipose tissue and an increased metabolic rate in muscle and fat [168]. The above demonstrates the importance of the mTOR pathway in obesity and other metabolic diseases.

Obesity and diabetes: overweight (body mass index (BMI)> 25) and obesity (BMI>30) are among the greatest public health problems in the Western world of the 21st century. Prevalence is increasing globally, and estimations suggest that in Europe every third (//www.euro.who.int/obesity) and in United States (http://www.cdc.gov/nchs/fastats/overwt.htm) every second adult is affected. Weight excess is associated with diabetes mellitus type 2, cardiovascular disease, hypertension, stroke, gallbladder dysfunction, increase in cancer susceptibility and psychosocial problems. Diabetes type 2 is a metabolic disease starting with insulin resistance, developing towards variable insulin deficiency and hyperglycemia. It was shown that weight loss reduces the incidence of type 2 diabetes by 60% [169].

Nutrients, such as glucose and amino acids are not only metabolic fuels, but also important signaling molecules in so-called nutrient signaling pathways, which comprise the hexosamine signaling pathway, the mTOR signaling pathway, and the adenosine monophosphate-activated protein kinase (AMPK) signaling pathway [170]. They regulate energy metabolism, cell growth, proliferation, and survival. These

pathways are interconnected at various levels and linked to the action of insulin, which signals to the PI3K/PKB pathway. Attenuation of the PI3K-mTOR signaling cascade contributes to a diabetic phenotype. In fact, mice carrying an inactive heterozygous PI3Kα are smaller, have increased adipose tissue, show impaired glucose and insulin tolerance, and insulin resistance with hyperinsulinemia following fasting [171]. Interestingly, mice homozygous for a catalytically inactive PI3Kβ are viable, smaller and develop insulin resistance and mild diabetes later in life (Ciraolo et al.; 3rd Focused Meeting on PI3K signaling and disease; Bath, UK, November 2006, Abstract S010). Deletion of PKBβ/Akt2, an isoform abundant in muscles and liver, results in a diabetic phenotype in mice [172]. In agreement, point mutations in PKBβ/Akt2 are found in patients with a familial form of severe insulin resistance [173]. Moreover, elevated levels of the regulatory subunit p85, associated with decreased PI3K activity, were found in muscles of type 2 diabetic patients [174].

Not only fat, but also amino acids in excess contribute to insulin resistance via the inhibition of glucose uptake [168]. It was recently shown that S6K1-mediated IRS1 phosphorylation suppresses glucose uptake, providing a negative feedback from TORC1 [175].

A better understanding of the effect of amino acids, glucose, and fat uptake on pathways linked to insulin resistance, as well as genetic predispositions, will promote new strategies in treatment of metabolic diseases.

5. Validation and targeting of class I PI3Ks with low-molecular weight chemical compounds

Genetic approaches as described above have partially validated some individual PI3K isoforms as drug targets in complex disease conditions. For some PI3K isoforms, this was hampered by embryonic lethality (e.g. for PI3Kα and PI3Kβ "knock-out" mice [74,75]), potential developmental compensation and overlapping functions of other PI3K isoforms. Initially, validation of PI3Ks as drug targets was attempted using wortmannin and LY294002, which both target a broad range PI3K-related enzymes [18,176]. To exploit the promising biological data, the development of potent, stable and preferably isoform-specific PI3K inhibitors is essential. The identification of wortmannin [176–179] and LY294002 [180] has made the PI3K field easily accessible and spurred numerous publications (Fig. 4). Efforts to generate drug-like PI3K inhibitors were rare for a long time, but many pharmaceutical companies revived their interest in PI3K after the first demonstration that PI3Kγ played a role in inflammation [79–81]—and that life without PI3Kγ was possible. The finding that loss of PTEN correlated with tumor progression, and that PTEN was a lipid phosphatase, brought activities also back to PI3K as a drug target in cancer. Together, this has generated a burst of patents dealing with modulation of PI3K activity (Fig. 4). An overview of these activities is displayed in Table 2, with additional information available (Supplementary Table 1).

5.1. Phosphoinositide 3-kinase inhibitors

Lipid and protein kinases share structural similarities in their catalytic core. Most protein kinase inhibitors developed so far target the ATP-binding site, and there are only very few examples of allosteric protein kinase inhibitors [181,182]. In spite of the resemblance of ATP-binding sites among protein kinases, the production of specific inhibitors has been successful [181,182].

The mechanism of PI3K inhibition by wortmannin was elucidated 10 years ago (Fig. 4B) and allowed the prediction of other PI3K-related targets [176]. The recent availability of the crystal structure of PI3Kγ, free and in a complex with ATP [183], as well as bound to wortmannin, LY294002 and generic kinase inhibitors [184] has further accelerated drug development. Similar to protein kinases, the ATP-binding site of PI3K is located between a cleft formed by the N- and the C-terminal lobe of the catalytic domain (Fig. 5; data extracted from indicated PDB coordinates). Protein backbone and amino acid residues at Met804, Trp812, Glu880, Val882 and Met953 of PI3Kγ define a unique surface lining the ATP binding site, which provides more free space than typical protein kinases,

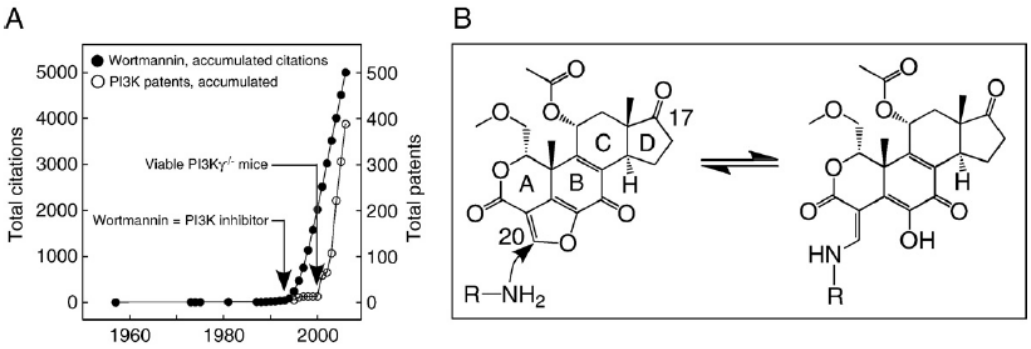

Fig. 4. (A) Accumulated numbers of published papers where wortmannin was used as a PI3K inhibitor (from PubMed, filled circles) are compared with the number of patents covering PI3K inhibitors (open circles, scale to the right). (B) Mechanism of PI3K inactivation by wortmannin. The nucleophile Lys802 in PI3Kα (Lys833 in PI3Kγ) within the ATP binding pocket attacks the furan ring of wortmannin at C20, resulting in a stable PI3K-wortmannin adduct.

Table 2
Specificity profile of PI 3-kinase inhibitors I [a]

Scaffold	Inhibitor	IC_{50} (μM) p110α / p110β / p110γ / p110δ	Name	Applicant	Comment	Literature patent
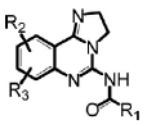	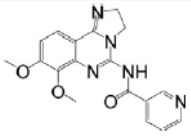	0.011 0.350 0.018 0.058	PIK-90/ BAY2-47	Bayer	Low mTOR activity Cell permeable	[221] WO2004029055
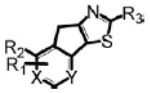	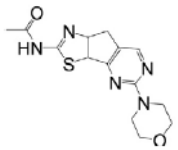	ND	Example 90	Boehringer	X=CH, N Y=CH, N PI3Kγ activity *	WO2006044729
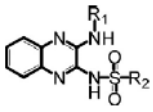	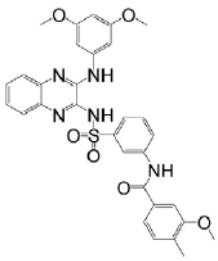	ND	XL765	Exelixis	PI3K and mTOR activity Clinical trial, phase I, solid tumors	WO2007044729
	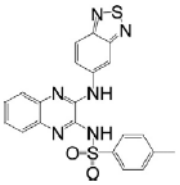	ND	XL147	Exelixis	Activity data not released Clinical trial, phase I, solid tumors	WO2007044729
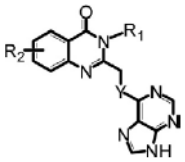	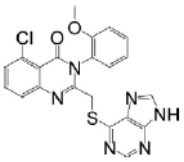	>200 11 17 0.18	PIK-39	ICOS	Selective p110δ inhibitor *	[221] WO0181346 WO03035075
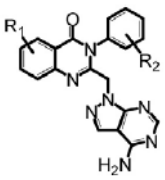	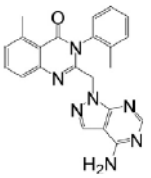	100 25 10 0.24	PIK-239	ICOS	Selective p110δ inhibitor	[221]
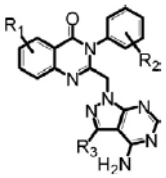	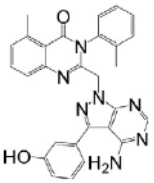	10 0.49 0.16 0.010	PIK-294	ICOS	Potent p110δ inhibitor Limited selectivity	[221]

Table 2 (*continued*)

Scaffold	Inhibitor	IC_{50} (μM) p110α / p110β / p110γ / p110δ	Name	Applicant	Comment	Literature patent
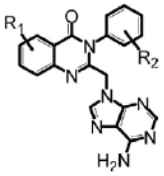	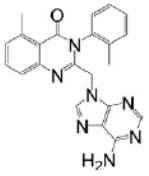	200 16 61 0.13	IC87114/D-030	ICOS	Selective p110δ inhibitor Cell permeable *	[227] [221] [218] [217] WO0181346
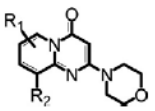	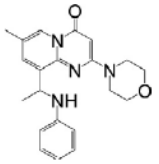	0.784 0.010 3.240 0.065	TGX-221	Kinacia	Selective PI3Kβ inhibitor Cell permeable *	[227] [222] WO2004016607 US2005085471
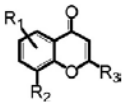	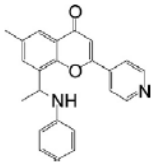	4.5 0.12 10 1	TGX-286	Kinacia	Blocks p110β in adipocytes	[221] WO2004016607 US2005085471
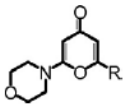	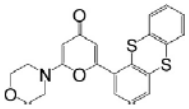	3.3 1.2 9.9 0.72	KU55399	Kudos	ATM inhibitor (5 nM) Represses HIV-1 infection *	[221] [258] WO03070726
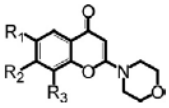	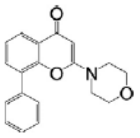	1–3 1–3 2 ND	LY294002	Lilly	Pan-PI3K inhibitor *	[180] WO0153266
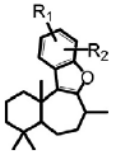	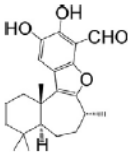	0.1 ND 1 ND	Liphagal	Marion et al.	Natural product, claimed to be a p110α inhibitor *	[209]
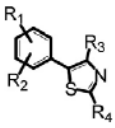	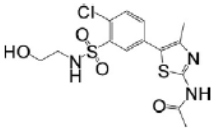	0.039 0.59 0.016 0.12	PIK-93	Novartis	Targets PI4KIIIβ (19 nM) *	[221] WO03072557
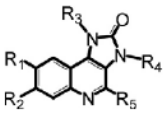	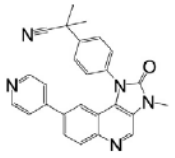	ND	ND	Novartis	Pan-PI3K inhibitor? *	WO2006122806

(*continued on next page*)

Table 2 (*continued*)

Scaffold	Inhibitor	IC_{50} (μM) p110α / p110β / p110γ / p110δ	Name	Applicant	Comment	Literature patent
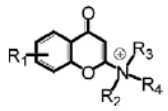	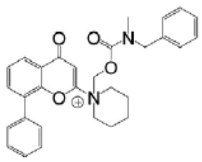	ND	AO44-62	Semafore	SF1126 inhibitor is the first broadspectrum PI3K inhibitor in clinical trial	WO2004089925
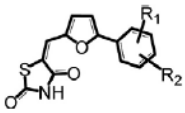	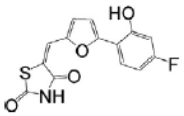	0.071 1.22 0.012 0.191	AS-252424	Serono	Cell permeable	[227] [229]
	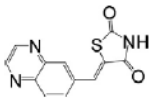	0.06 0.27 0.008 0.3	AS-605240	Serono	Used in vivo Cell permeable *	[105] WO2004007491
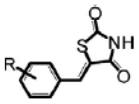	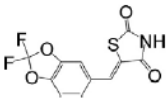	4.5 >20 0.25 >20	AS-604850	Serono	Lower (cellular) potency as compared to AS-605240	[105] WO2004007491
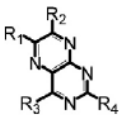	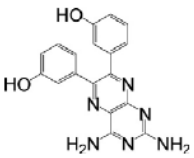	1.3 1.2 0.083 0.235	TG100-115	Targegen	PI3Kγ/PI3Kδ inhibitor Clinical trials, phase I, II; myocardial infarction	[130,131,231] WO2004030635 KR20050056227
	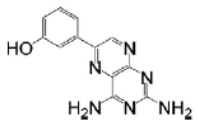	0.165 0.215 0.050 0.024	TG100-713	Targegen	PI3Kγ/PI3Kδ inhibitor	[130,131,231] WO2004030635 KR20050056227
	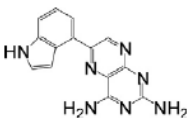	1.2 0.107 0.085 0.064	TG101-110	Targegen	PI3Kγ/PI3Kδ inhibitor	[130,131,231] WO2004030635 KR20050056227
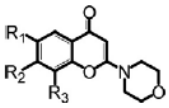	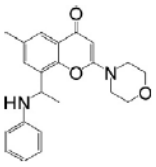	2.6 0.057 4.1 0.26	PIK-108	Thrombogenix	p110β/p110δ inhibitor DNA-PK inhibitor (12 nM) *	[221] WO0153266 WO2004016607
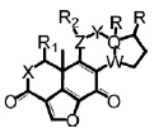	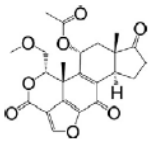	~0.004 ~0.004 ~0.004 ~0.004	Wortmannin	Wander AG, Lilly	X=O, CH_2 Y=CH_2, C• Z=C, C• Q=C, C• W=CH, C• High nM also active against DNA-PK, mTOR, ATR, ATM, PI4K, polo-like K *	[177,184,200,201, 249,259–261] EP0640339 JP7053370

Table 2 (*continued*)

Scaffold	Inhibitor	IC_{50} (μM) p110α p110β p110γ p110δ	Name	Applicant	Comment	Literature patent
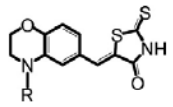	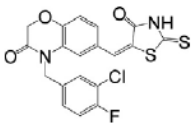	0.023 1.1 0.054 0.34	PIK-124	Warner Lambert	Pan-PI3K inhibitor *	[221] WO2004056820 WO2004052373
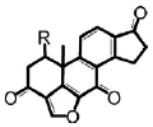	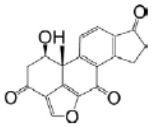	0.00013 ND ND ND	Demethoxy-viridin	Woscholski et al.	p85α/p110 dimer (3.4 nM) Cell permeable, very labile *	[195]
		π 0.006 1.3	PIK-75	Yamanouchi	DNA-PK inhibitor (2 nM)	π [221] ω [262]
	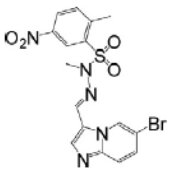	0.076 0.51			IC_{50} for A375 cell proliferation at 0.058 μM	[263] WO0183481 (DE60112272T) (EP1277754)
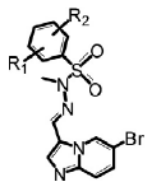		ω 0.0003 0.85 0.040 ND	Compound 8c	Yamanouchi	Effective in vivo	
	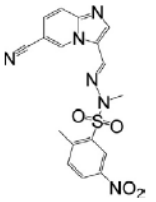	0.0003 ND ND ND	Compound 8h	Yamanouchi	IC_{50} of p110α at 260 pM IC_{50} of A375 cell proliferation at 0.033 μM	[265] WO0183481
		π 0.008 0.088 0.15 0.048	PI-103/10e	Yamanouchi	Targets PI3KC2β (26 nm), mTORC1 (20 nM), mTORC2 (83 nM), DNA-PK (2 nM), p235 (69 nM) *	π [221,225] ω [224] WO0183456 EP1277738 WO2004017950
	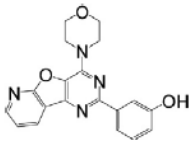	ω 0.002 0.003 0.015 0.003	PI-103/10e	Yamanouchi		
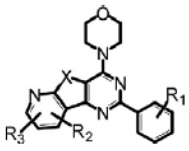	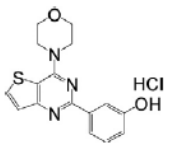	0.002 0.016 0.66 ND	15e	Yamanouchi	IC_{50} of A375 cell proliferation at 580 nM *	[226] WO2006046040 WO2006046031
	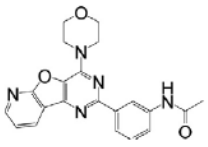	0.301 2.65 9.07 0.333	YM-024	Yamanouchi	Cell permeable	[227] WO0183456 (EP1277738) WO2006046031 WO06046040 WO2004017950

(*continued on next page*)

Table 2 (*continued*)

Scaffold	Inhibitor	IC_{50} (μM) p110α / p110β / p110γ / p110δ	Name	Applicant	Comment	Literature patent
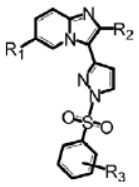	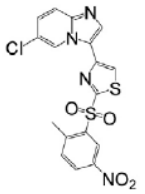	0.0028 0.17 0.23 ND	Compound 12	Yamanouchi	12 suppresses proliferative cellular activity (IC_{50}=0.21 μM) in vitro and in vivo mouse xenografts	[228,262] WO0183481 (DE60112272T) (EP1277754) US2002151549
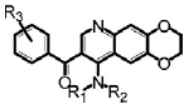	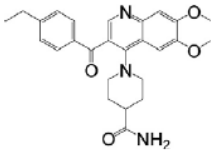	ND ND ND 30	Quinostatin	Yang et al.		[232]
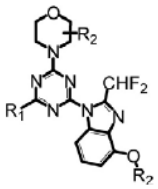	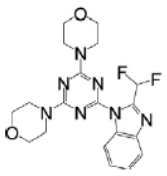	ND 0.017 0.053 0.006	ZSTK474	Zenyaku Kogyo	Pan-PI3K inhibitor Orally available Antitumor activity against human cancer xenografts *	[230] WO2005095389

*More scaffolds are presented in Supplementary Table.
ND, not defined.
Patents can be looked up in http://ep.espacenet.com/. Patents of Thrombogenix, Kinacia and Cerylid are listed under the respective applicant. Intellectual property transferred to Cerylid.
The same applies to Yamanouchi/Piramed and Onyx/Parke Davis/Warner Lambert/Pfizer and Serono/MerckSerono.
[a] Sorted in ascending order of patent applicant.

whose structures have been solved [184]. As predicted from biochemical studies [176,185], Lys833 interacts with the phosphate groups of ATP [184], and is critical for kinase activity.

5.2. PI3K-active natural products and their synthetic derivatives

Wortmannin and demethoxyviridin: wortmannin (Table 2) is a fungal product isolated from *Penicillium wortmanni* in 1957 [186], and its structure was fully elucidated 15 years later [187–190]. In studies performed at Wander AG, Bern (famous for the production of Ovomaltine), it was established early that wortmannin had an inhibitory effect on neutrophils [191]. The furan ring structure of wortmannin is crucial for its action, as derivatives with a modified furan ring are ineffective in biological assays [191]. After the characterization of wortmannin as a PI3K inhibitor [176–179], the covalent interaction of wortmannin with PI3K was established using 17-[^{3}H], 17-hydroxy wortmannin [192]. Wortmannin was subsequently shown to form an enamine at C20 after the attack of the conserved Lys802 of the PI3Kα catalytic subunit. This enamine is in equilibrium with a Schiff base (imine), is relatively stable at physiological pH, but is easily hydrolyzed under acidic conditions [176]. This covalent bond was confirmed biochemically for Lys833 in PI3Kγ [185] and also observed in the crystal structure of PI3Kγ in complex with wortmannin [184]. A detailed discussion of the reaction mechanism has been described in [193].

Demethoxyviridin (Table 2, isolated from *Nodulisporium hinnuleum*) is another inhibitor of PI3K, effective at nanomolar concentrations [194,195]. Demethoxyviridin has a similar reaction mechanism like the one of wortmannin, due to the identical furan ring system [196].

5.3. Structure–activity relationship (SAR) studies of wortmannin

In order to understand the structural requirements essential for PI3K inhibition, SAR studies of wortmannin were carried out by Norman et al. from Lilly [197]. The obtained results demonstrated that small substitutions on wortmannin have little effect on its in vitro activity, but again modifications of the electrophilicity of the furan ring dramatically changed the

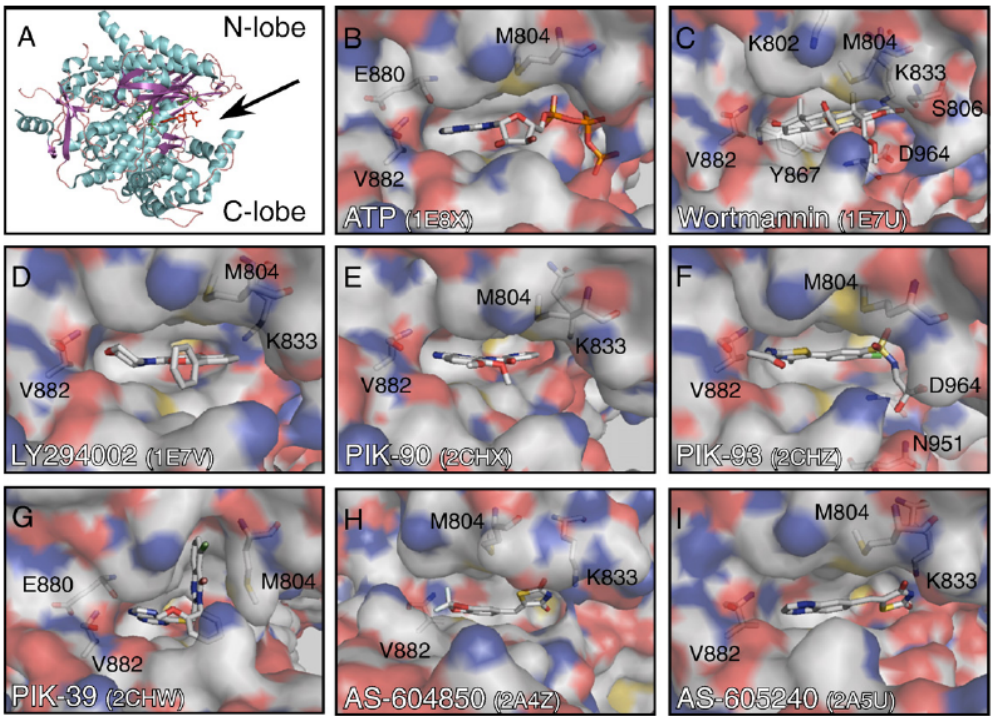

Fig. 5. Targeting phosphoinositide 3-kinase (PI3K) with small molecule ATP-competitive inhibitors. (A) Crystal structure of the ATP·PI3Kγ complex (from PDB coordinates as indicated, here 1E8X). A ribbon diagram is presented, where the secondary structure motifs are colored as follows: turquoise, α-helices; magenta, β-sheets; brown, loops, and in red the ATP located in the cleft between the N- and the C-terminal lobe of the catalytic subunit. (B) Surface diagram of ATP•PI3Kγ crystal structure zoomed into the ATP-binding site (1E8X). Numbers denote highlighted, prominent side chains mediating PI3K/ligand interactions. (C–I) Illustrations of inhibitor•PI3Kγ 3D structures demonstrating the interactions described in the text. Note in panel G) the altered Met804 position in the PIK-39·PI3Kγ structure [221]. For the PI3K isoform specificity of the depicted inhibitors consult text and data in Table 2.

inhibitory capacity of these derivatives. Moreover, this research established the importance of wortmannin's D ring, required for covalent PI3K binding (for a review see [193]).

As predicted by the covalent interaction of wortmannin and Lys802 in PI3Kα [176], the inhibitor cross-reacted with PI3K-related kinases mTOR, DNA-PKcs, ATM, ATR and PtdIns-4-kinase (type 3) at elevated concentrations [198–201]. As a consequence, wortmannin showed considerable toxicity at low doses in animal studies, with ~50% of animals dying at a daily dose of 1 mg/kg [18]. Metabolism of wortmannin to 17-OH-wortmannin by plasma carbonyl reductase could eventually potentiate toxic effects, as 17-OH-wortmannin is somewhat more potent than wortmannin itself [202]. Compounds with reduced liver toxicity as compared to wortmannin and improved inhibition of tumor cell proliferation were obtained from modifications of wortmannin's D ring. One of these compounds, PX-866 (Suppl. Table), successfully attenuated growth of tumor xenograft in mice at around 10 mg/kg [203].

5.4. Wortmannin and demethoxyviridin activity-based probes

Fluorescent derivatives of wortmannin and demethoxyviridin have been synthesized to generate covalent probes to identify cellular targets of wortmannin and demethoxyviridin [204]. Two chemical derivatives, 11-deacetylwortmannin and 17-hydroxywortmannin, were adopted for derivatisation with fluorophores. While substitution at C11 retained inhibitory potential, the C17 position was sensitive to derivatisation (Suppl. Table 1; [204]). Others produced bodipy and rhodamine C11-modified wortmannin derivatives, which were cell permeable and could be used to label intracellular targets [205–207]. Using rhodamine-C11-wortmannin, the binding site of the inhibitor to polo-like kinases (Plk1 and Plk3) was determined [208]. Plk1 activity is essential to cell viability and its potent inhibition by wortmannin may contribute to the compounds toxicity.

5.5. Low affinity natural compounds

Liphagal (Table 2) represents the first example of a meroterpenoid carbon skeleton of which the structure was elucidated. Liphagal was extracted from the sponge *Aka coralliphaga*, and was reported to inhibit PI3Kα at about 10-fold lower concentrations than against PI3Kγ (0.1 vs. 1 μM; [209]).

Caffeine and theophylline: studies on the effect of methylxanthines on the enzymatic activity of PI3Ks showed that caffeine (Suppl. Table) inhibits in vitro the PI3Ks of the class I (IC_{50}=75 μM for p110δ, 400 μM for p110α and p110β

and 1 mM for p110γ; [210]). Similar activities were described for theophylline (Suppl. Table), while other tested xanthines were even less active against PI3Ks.

Resveratrol: Resveratrol (3,5,4′-trihydroxystilbene; Suppl. Table) was initially characterized as phytoalexin, a toxic compound produced by higher plants [211]. Not much attention was given to resveratrol until 1992, when it was postulated, that its presence in red wine had cardio-protective effects [212]. Moreover, new data showed that resveratrol inhibits class IA PI3K by displacing ATP (in vitro and in cultured muscle cell lines; [213]). Resveratrol gained fame as a SIRT1 activator, protecting mice against diet-induced obesity, insulin resistance and ageing (see [214]).

5.6. Synthetic first generation PI3K inhibitors

The pan-PI3K inhibitor LY294002 (Table 2) was synthesized by Lilly in the early nineties. Although the reported IC_{50} value of LY294002 (1.4 μM; [180]) for class I PI3K is about 500-fold higher than that of wortmannin, LY294002 proved useful due to its superior chemical stability. LY294002 is the first synthetic PI3K inhibitor whose complex with PI3Kγ was structurally elucidated [184], showing that the morpholino oxygen makes a hydrogen bond with the backbone amide of Val882—a very conserved interaction that is shared by all current PI3K inhibitors and ATP (Fig. 5). The modification of the morpholino oxygen in LY294002 derivatives leads to a sharp drop in inhibitor activity. Other interactions occur with Lys833, Met804, Trp812 and Met953 [184]. Recent studies have shown that it is possible to reach a certain PI3K selectivity profile for derivatives from LY294002 [215]. As for wortmannin, LY294002 targets not only PI3K but also other kinases [216].

PI3Kδ inhibitor IC87114 and derivatives PIK-39, PIK-293 and PIK-294: ICOS Corporation has presented the first selective inhibitors of PI3Kδ, and one of them, the compound IC87114 (Table 2), has been used to explore the importance of PI3Kδ in neutrophil migration [217], and TNF1α-stimulated elastase exocytosis from neutrophils in a mouse model of inflammation [218]. In addition, it was shown that the selective inhibition of PI3Kδ could play a role in the pathophysiology of acute myeloid leukemia [219,220]. IC87114 inhibits p110δ at mid-nanomolar concentrations, and shows high in vitro selectivity (100–1000-fold) over other class I PI3Ks. Compound PIK-39 (Table 2) is structurally related to IC87114, but contains a mercaptopurine moiety. Molecular modeling of PIK-39 and IC87114/PI3K complexes showed a similar conformation of these compounds within the ATP binding site, and suggests that hydrogen bonds are formed with Val882 and Glu880 (Fig. 5; [221]. The unusual selectivity of PIK-39 is thought to be based in its structural geometry, which was suggested to induce a conformational transformation of Met804 opening a novel hydrophobic pocket between Met804 and Trp812. Compared to compounds PIK-90 and PI-103 (see below), PIK-39 does not use the advantage of the deep-affinity pocket of the ATP binding site. Therefore, the synthesis of PIK-39 derivative was accomplished, in order to exploit the depth of the affinity pocket of the ATP binding site [221]. A replacement of the mercaptopurine of PIK-39 by pyrazolopyrimidine substituted with an *m*-phenol, gave compound PIK-294 (Table 2), where the *m*-phenol moiety of PIK-294 was able to penetrate the "deep-affinity pocket" of the ATP-binding site, and thus increased in vitro inhibitor activity by ~20- to 60-fold [221].

PI3Kβ inhibitor TGX-221: Thrombogenix compound TGX-221 (Table 2, see under Kinacia) is a LY294002 analogue, able to inhibit selectively the PI3Kβ isoform in vitro. The chromone core of LY294002 was replaced with pyrido[1,2-*a*] pyrimidin-4-one and inserted into an aryl ring moiety, increasing the potency and selectivity against PI3Kβ [222]. TGX-221 is a low-nanomolar range inhibitor, shows about 1000-fold higher selectivity over PI3Kα, and is cell permeable. TGX-221 interfered with shear stress-induced PtdIns(3,4)P_2 production and integrin $\alpha_{IIb}\beta_3$-mediated adhesion in platelets, suggesting that inhibition of PI3Kβ might have an anti-thrombotic potential in vivo.

5.7. Synthetic second generation PI3K inhibitors

In the process of PI3K inhibitor development, several chemotypes belonging to arylthiazolidinones (PIK-124), pyridinylfuranopyrimidines (PI-103), phenylthiazoles (PIK-93) and imidazoquinazolines (PIK-90) were identified. These inhibitors are active against multiple PI3Ks and are useful to explore the overall importance of PI3K, as well as toxicity issues. PI-103 is a potent compound, which inhibits several critical enzymes in growth and proliferation (PI3Ks, mTOR complexes, DNA-PK_{cs}) at low-nanomolar concentration [221,223,224]. Much of the information concerning more recently developed PI3K inhibitors is confined to the patent literature. A side-by-side comparison and activity mapping performed by Knight et al. brought these inhibitors and their selectivity profiles to the attention of the academic community [221].

PI-103, 15e and YM-024: PI-103 (Table 2) belongs to the chemical class of pyridinylfuranopyrimidines and was developed from the precursor 4-morpholin-4-ylpyrido[3′,2′:4,5] thieno[3,2-*d*]pyrimidine (published name: compound 2a; see Suppl. Table; [225]). The PI-103 series originated from Yamanouchi, which transferred intellectual property to Piramed. It was shown recently that PI-103 reduced PKB/Akt phosphorylation through pan-PI3K inhibition (see Table 2), and induced G0/G1 cell-cycle arrest, due to its dual action on PI3K and mTOR. PI-103 at doses up to 100 mg/kg attenuated proliferation of glioma, breast, ovarian and cervical tumor cells in xenograft mouse models [223–225]. Although not orally applicable, PI-103 has the potential to be very useful as an experimental compound in cancer research in the future, last but not least due to the availability of pharmacological data [224].

A thieno[3,2-*d*]pyrimidine, compound 15e (Table 2), was recently reported as selective inhibitor for PI3Kα, which suppresses A375 tumor cell proliferation [226]. SAR studies showed the importance of the morpholino group, as seen before for LY294002 and PI-103, and the introduction of a *m*-phenol was essential for improved PI3Kα inhibitory activity. Unfortu-

nately, 15e seems to be of limited use in vivo due to poor pharmacokinetic properties and a short half-life (<10 min; [226]). Compound YM-024 from Yamanouchi was used together with IC87114, AS-252424 and TGX-221 to investigate the role of PI3K isoforms in the induction of the respiratory burst in TNF-α-primed, fMLP-stimulated neutrophils. A dominant role was found for PI3Kγ in the early and PI3Kδ in the late phase of the response [227].

PIK-93: the Novartis compound PIK-93 (Table 2) is the first reported PI4-kinase inhibitor, which is able to inhibit PI4KIIIβ at low-nanomolar range. In addition, this compound inhibits also potently PI3Kγ in vitro. PIK-93 also displays the typical hydrogen bonding to the backbone amide of Val882, and additional ones to the backbone carbonyl of Val882 and between its sulphonamide and Asp964 (Fig. 5).

PIK-90: besides Val882 H-binding, Bayer's imidazoquinazoline PIK-90 (Table 2) uses its pyridine ring to enter the hydrophobic affinity pocket of the ATP binding site, where it also interacts with Lys833. PIK-90 has a broad profile and inhibits PI3Kα, PI3Kγ, PI3Kδ, DNA-PK and PI3KC2s, and to a lesser degree PI3Kβ [221].

PIK-75 and compound 12: PIK-75 (Table 2) and compound 12 (Suppl. Table) belong to the class of imidazo[1,2-*a*]pyridines [221,228]. Compound 12 inhibits PI3Kα with an IC_{50} of 28 nM and inhibited cell proliferation of A375 and HeLa cells in vitro and reduced tumor growth in a mouse xenograft model. Besides

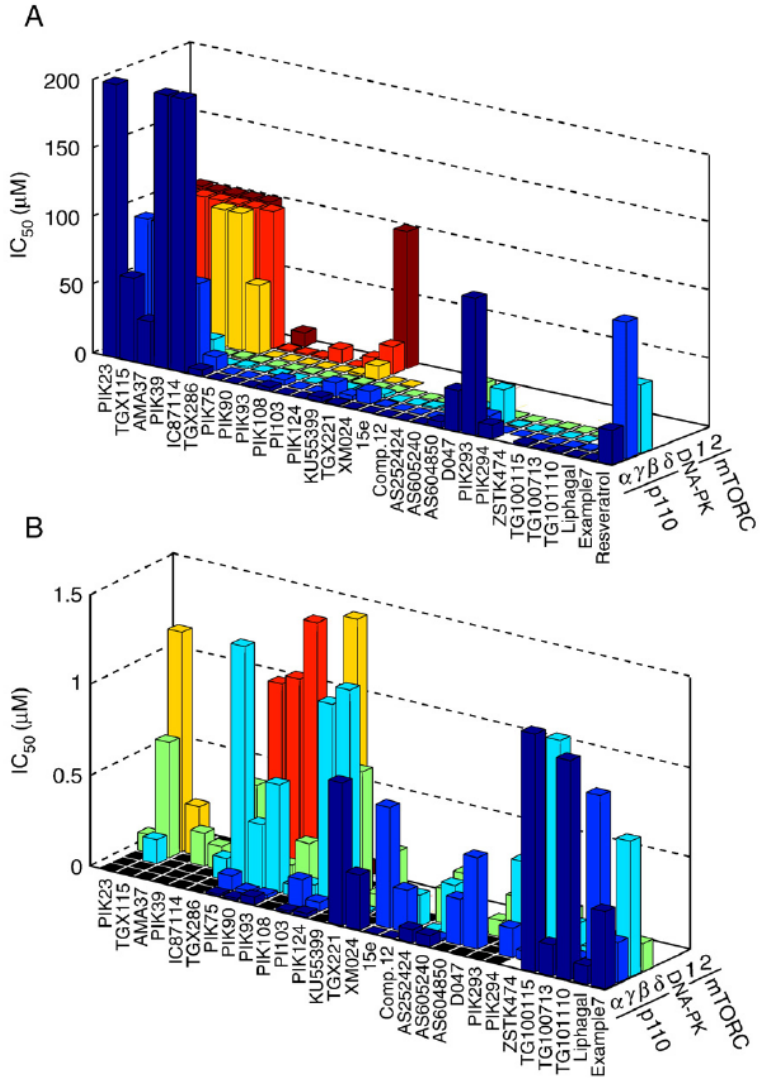

Fig. 6. Graphical overview of the in vitro specificity profile of PI3K inhibitors. IC_{50} values for the inhibition of class I PI3Ks, DNA-PKcs and mTOR complexes (mTORC1, 2) were extracted from literature and patents as indicated in Table 2 and Supplementary Table. Where no values were found, the base is left blank. (A) IC_{50} values depicted up to 200 μM allow the quick identification of "inhibition valleys". Isoform selective inhibitors are preferably plotted to the left. (B) IC_{50}s displayed up to 1.5 μM. Values exceeding the indicated scale were replaced by a square colored in black (only in bottom figure).

inhibition of PI3Kα, PIK-75 also inhibited DNA-PK, but not mTORC1 and mTORC2 [221].

Targeting PI3Kγ with AS-252424, AS-604850, AS-605240: these thiazolidinedione derivatives were the first examples of selective PI3Kγ inhibitors, and were used to block neutrophil chemotaxis in vitro and in vivo. In passive mouse models for rheumatoid arthritis these compounds minimized progression of joint destruction (see above and [105]). These compounds were co-crystallized with PI3Kγ, and key selectivity features of these compounds were identified (Fig. 5; [105]): i) the thiazolidinedione nitrogen makes a salt–bridge interaction with the side chain of Lys-833, and ii) the oxygen of the 1,3-benzodioxole ring of AS-604850 H-bonds with the backbone amide of Val882, while the nitrogen of the quinoxaline ring of AS-605240 forms the link to Val-882. Both inhibitors lacked notable activity against a wide panel of protein kinases at concentrations >1 μM [105]. AS-252424 belongs to a class of furan-2-ylmethylene thiazolidinediones and is an ATP-competitive PI3Kγ inhibitor. The SAR-optimization of the AS-252424 precursor, compound 5-(5-Phenyl-furan-2-ylmethylene)-thiazolidine-2,4-dione, demonstrated that the 2-hydroxy group on the phenyl ring plays a crucial role in inhibitor potency [229], and the introduction of a fluorine atom on the 4-position of the phenyl ring achieved reduction in activity against PI3Kα. With increased potency and efficacy, similar PI3Kγ inhibitors might develop into powerful anti-inflammatory agents.

ZSTK474 or 2-(2-difluoromethylbenzimidazol-1-yl)-4,6-dimorpholino-1,3,5-triazine (Table 2) was identified from a chemical library of about 1500 triazine derivatives at Zenyaku Kogyo, and selected for their ability to block tumor cell growth. Strong anti-proliferative activity was detected for ZSTK474, first without knowledge about its biological target, which was then identified as PI3K [230]. In preclinical studies ZSTK474 was orally administered to mice and displayed a strong anti-tumoral activity in xenograft models. Toxicity was reported to be moderate [230].

XL765 and XL147: According to patent literature, an inhibition of PI3K activity was found for quinoxaline derivatives, XL147 and XL765 (Table 2) by Exelixis. In preclinical studies it has been shown that XL765 selectively inhibits the activity of PI3K and mTOR. In comparison to XL765, compound XL147 was claimed to be more selective for PI3K. In several preclinical xenograft models, both compounds XL147 and XL765 seem to have shown efficacy as single agents and also in combination with chemotherapy. XL147 and XL765 have entered clinical studies (phase I) for treatment of solid tumors (information from www.exelixis.com).

TG100-115, TG100-713 and TG101-110: Targegen compounds TG100-115, TG100-713 and TG101-110 (Table 2) were identified by screening a family of pteridine derivatives against class I PI3Ks [130]. The compound TG100-115 was characterized as a selective PI3Kγ/δ inhibitor, which counteracted edema and inflammation. PI3Kγ/δ inhibition blocked VEGF signaling events central to late tissue damage after myocardial infarction. Molecular modeling studies revealed that TG100-115 interacts in the ATP binding pocket with the relevant Val882 and Glu880. Additionally, the 6′-substituted *m*-phenol of TG100-115 interacts outside ATP binding pocket with Asp841, forming an additional H-bridge. TG100-115 is currently in clinical studies (I, II) for acute myocardial infarction, as an acutely intravenously administered drug [231].

Quinostatin (Table 2), named after its quinoline core structure, was discovered in a high-throughput cell-based assay for modulators of mTOR signaling [232]. The interaction of quinostatin with PI3K (IC_{50}=~30 μM) was detected by the association of the PI3K p85/p110 complex with an affinity gel, produced by the attachment of a polyethylene glycol linker to the C3-position of quinostatin.

BEZ235 is a recent addition to molecules with anti-tumoral activity targeting the PI3K pathway. Produced by Novartis, it entered clinical trials recently (http://www.novartisoncology.com/page/bez235.jsp).

SF1126 was announced by Semafore to enter clinical trials as a pan-PI3K inhibitor, targeting cell growth, proliferation and angiogenesis (http://www.semaforepharma.com/pdf/PRESS_-_AACR_2005_SF1126_safe-efficacy_poster.pdf).

6. Conclusions and outlook

The pharmaceutical development of PI3K inhibitors has made a great leap forward during the last 5 years. Promising molecules have entered clinical trials for cancer therapy, inflammation and coronary heart disease. As summarized in Fig. 6, first inhibitors with some isoform specificity have been lanced. While inhibitor selectivity is often impressive when assessed in vitro, the in vivo selectivity, potency and efficacy often require further optimization, especially for the treatment of chronic non-fatal diseases, e.g. in inflammation and allergy. For some of the pan-PI3K developed for cancer therapy (e.g. BEZ235, PI-103, SF1126, XL765, XL147, ZSTK474), encouraging toxicity data has become available. Many experimental drugs are relatively well tolerated, even though the molecules cross-react with the whole PI3K family and PI3K-related kinases. As drugs targeting PI3K progress, gaps in knowledge of the specific function of the different PI3K isoforms should be closed. The race to occupy niches and markets in PI3K-dependent therapies is on.

Acknowledgements

We thank Poppy Fotiadou, Nathanael S. Gray, and David Woodmansee for the critical reading of the manuscript, and Natasa Cmiljanovic for data retrieval, and Federica Marone for help with graphical work. This work was supported by the Oncosuisse grant 01924-08-2006, the Swiss National Science Foundation, grants 3100A0-109718 and NCH1524 and the EU FP6 programme LSHG-CT-2003-502935.

Appendix A. Supplementary data

Supplementary data associated with this article can be found, in the online version, at doi:10.1016/j.bbapap.2007.10.003.

References

[1] M. Whitman, D.R. Kaplan, B. Schaffhausen, L. Cantley, T.M. Roberts, Association of phosphatidylinositol kinase activity with polyoma middle-T competent for transformation, Nature 315 (1985) 239–242.
[2] Y. Sugimoto, M. Whitman, L.C. Cantley, R.L. Erikson, Evidence that the Rous sarcoma virus transforming gene product phosphorylates phosphatidylinositol and diacylglycerol, Proc. Natl. Acad. Sci. U. S. A. 81 (1984) 2117–2121.
[3] I.G. Macara, G.V. Marinetti, P.C. Balduzzi, Transforming protein of avian sarcoma virus UR2 is associated with phosphatidylinositol kinase activity: possible role in tumorigenesis, Proc. Natl. Acad. Sci. U. S. A. 81 (1984) 2728–2732.
[4] M. Cully, H. You, A.J. Levine, T.W. Mak, Beyond PTEN mutations: the PI3K pathway as an integrator of multiple inputs during tumorigenesis, Nat. Rev., Cancer 6 (2006) 184–192.
[5] M.P. Wymann, R. Marone, Phosphoinositide 3-kinase in disease: timing, location, and scaffolding, Curr. Opin. Cell Biol. 17 (2005) 141–149.
[6] I. Vivanco, C.L. Sawyers, The phosphatidylinositol 3-kinase AKT pathway in human cancer, Nat. Rev., Cancer 2 (2002) 489–501.
[7] L.K. MacDougall, J. Domin, M.D. Waterfield, A family of phosphoinositide 3-kinases in *Drosophila* identifies a new mediator of signal transduction, Curr. Biol. 5 (1995) 1404–1415.
[8] S.J. Leevers, D. Weinkove, L.K. MacDougall, E. Hafen, M.D. Waterfield, The *Drosophila* phosphoinositide 3-kinase Dp110 promotes cell growth, EMBO J. 15 (1996) 6584–6594.
[9] J.Z. Morris, H.A. Tissenbaum, G. Ruvkun, A phosphatidylinositol-3-OH kinase family member regulating longevity and diapause in *Caenorhabditis elegans*, Nature 382 (1996) 536–539.
[10] L. Roggo, V. Bernard, A.L. Kovacs, A.M. Rose, F. Savoy, M. Zetka, M.P. Wymann, F. Muller, Membrane transport in *Caenorhabditis elegans*: an essential role for VPS34 at the nuclear membrane, EMBO J. 21 (2002) 1673–1683.
[11] L. Chen, M. Iijima, M. Tang, M.A. Landree, Y.E. Huang, Y. Xiong, P.A. Iglesias, P.N. Devreotes, PLA2 and PI3K/PTEN pathways act in parallel to mediate chemotaxis, Dev. Cell 12 (2007) 603–614.
[12] P.V. Schu, K. Takegawa, M.J. Fry, J.H. Stack, M.D. Waterfield, S.D. Emr, Phosphatidylinositol 3-kinase encoded by yeast VPS34 gene essential for protein sorting, Science 260 (1993) 88–91.
[13] J.A. Engelman, J. Luo, L.C. Cantley, The evolution of phosphatidylinositol 3-kinases as regulators of growth and metabolism, Nat. Rev., Genet. 7 (2006) 606–619.
[14] M.P. Wymann, L. Pirola, Structure and function of phosphoinositide 3-kinases, Biochim. Biophys. Acta 1436 (1998) 127–150.
[15] B. Vanhaesebroeck, S.J. Leevers, K. Ahmadi, J. Timms, R. Katso, P.C. Driscoll, R. Woscholski, P.J. Parker, M.D. Waterfield, Synthesis and function of 3-phosphorylated inositol lipids, Annu. Rev. Biochem. 70 (2001) 535–602.
[16] L.C. Cantley, The phosphoinositide 3-kinase pathway, Science 296 (2002) 1655–1657.
[17] L.R. Stephens, T.R. Jackson, P.T. Hawkins, Agonist-stimulated synthesis of phosphatidylinositol(3,4,5)-trisphosphate: a new intracellular signalling system? Biochim. Biophys. Acta 1179 (1993) 27–75.
[18] M.P. Wymann, M. Zvelebil, M. Laffargue, Phosphoinositide 3-kinase signaling—Which way to target? Trends Pharmacol. Sci. 24 (2003) 366–376.
[19] M. Falasca, T. Maffucci, Role of class II phosphoinositide 3-kinase in cell signaling, Biochem. Soc. Trans. 35 (2007) 211–214.
[20] J. Domin, I. Gaidarov, M.E. Smith, J.H. Keen, M.D. Waterfield, The class II phosphoinositide 3-kinase PI3K-C2alpha is concentrated in the trans-Golgi network and present in clathrin-coated vesicles, J. Biol. Chem. 275 (2000) 11943–11950.
[21] I. Gaidarov, M.E. Smith, J. Domin, J.H. Keen, The class II phosphoinositide 3-kinase C2alpha is activated by clathrin and regulates clathrin-mediated membrane trafficking, Mol. Cell 7 (2001) 443–449.
[22] T. Maffucci, F.T. Cooke, F.M. Foster, C.J. Traer, M.J. Fry, M. Falasca, Class II phosphoinositide 3-kinase defines a novel signaling pathway in cell migration, J. Cell Biol. 169 (2005) 789–799.
[23] P.K. Herman, J.H. Stack, S.D. Emr, An essential role for a protein and lipid kinase complex in secretory protein sorting, Trends Cell Biol. 2 (1992) 363–368.
[24] J.T. Murray, C. Panaretou, H. Stenmark, M. Miaczynska, J.M. Backer, Role of Rab5 in the recruitment of hVps34/p150 to the early endosome, Traffic 3 (2002) 416–427.
[25] S. Christoforidis, M. Miaczynska, K. Ashman, M. Wilm, L. Zhao, S.C. Yip, M.D. Waterfield, J.M. Backer, M. Zerial, Phosphatidylinositol-3-OH kinases are Rab5 effectors, Nat. Cell Biol. 1 (1999) 249–252.
[26] A. Kihara, T. Noda, N. Ishihara, Y. Ohsumi, Two distinct Vps34 phosphatidylinositol 3-kinase complexes function in autophagy and carboxypeptidase Y sorting in *Saccharomyces cerevisiae*, J. Cell Biol. 152 (2001) 519–530.
[27] A. Kihara, Y. Kabeya, Y. Ohsumi, T. Yoshimori, Beclin-phosphatidylinositol 3-kinase complex functions at the trans-Golgi network, EMBO Rep. 2 (2001) 330–335.
[28] X. Qu, J. Yu, G. Bhagat, N. Furuya, H. Hibshoosh, A. Troxel, J. Rosen, E.L. Eskelinen, N. Mizushima, Y. Ohsumi, G. Cattoretti, B. Levine, Promotion of tumorigenesis by heterozygous disruption of the beclin 1 autophagy gene, J. Clin. Invest. 112 (2003) 1809–1820.
[29] Z. Yue, S. Jin, C. Yang, A.J. Levine, N. Heintz, Beclin 1, an autophagy gene essential for early embryonic development, is a haploinsufficient tumor suppressor, Proc. Natl. Acad. Sci. U. S. A. 100 (2003) 15077–15082.
[30] S.G. Dann, G. Thomas, The amino acid sensitive TOR pathway from yeast to mammals, FEBS Lett. 580 (2006) 2821–2829.
[31] P. Gulati, G. Thomas, Nutrient sensing in the mTOR/S6K1 signalling pathway, Biochem. Soc. Trans. 35 (2007) 236–238.
[32] T. Nobukuni, S.C. Kozma, G. Thomas, hvps34, an ancient player, enters a growing game: mTOR Complex1/S6K1 signaling, Curr. Opin. Cell Biol. 19 (2007) 135–141.
[33] A. Balla, T. Balla, Phosphatidylinositol 4-kinases: old enzymes with emerging functions, Trends Cell Biol. 16 (2006) 351–361.
[34] A. Balla, G. Tuymetova, M. Barshishat, M. Geiszt, T. Balla, Characterization of type II phosphatidylinositol 4-kinase isoforms reveals association of the enzymes with endosomal vesicular compartments, J. Biol. Chem. 277 (2002) 20041–20050.
[35] L.M.J. Heilmeyer, G.J. Vereb, G. Vereb, A. Kakuk, I. Szivak, Mammalian phosphatidylinositol 4-kinases, IUBMB Life 55 (2003) 59–65.
[36] K. Wong, D. Meyers, L.C. Cantley, Subcellular locations of phosphatidylinositol 4-kinase isoforms, J. Biol. Chem. 272 (1997) 13236–13241.
[37] A. Balla, G. Vereb, H. Gulkan, T. Gehrmann, P. Gergely, L.M.J. Heilmeyer, M. Antal, Immunohistochemical localisation of two phosphatidylinositol 4-kinase isoforms, PI4K230 and PI4K92, in the central nervous system of rats, Exp. Brain Res. 134 (2000) 279–288.
[38] A. Zolyomi, X. Zhao, G.J. Downing, T. Balla, Localization of two distinct type III phosphatidylinositol 4-kinase enzyme mRNAs in the rat, Am. J. Physiol., Cell Physiol. 278 (2000) C914–C920.
[39] M. Kim, L.H. Jiang, H.L. Wilson, R.A. North, A. Surprenant, Proteomic and functional evidence for a P2X7 receptor signalling complex, EMBO J. 20 (2001) 6347–6358.
[40] P. de Graaf, E.E. Klapisz, T.K. Schulz, A.F. Cremers, A.J. Verkleij, P.M. van Bergen en Henegouwen, Nuclear localization of phosphatidylinositol 4-kinase beta, J. Cell Sci. 115 (2002) 1769–1775.
[41] Y. Shiloh, ATM and related protein kinases: safeguarding genome integrity, Nat. Rev., Cancer 3 (2003) 155–168.
[42] R.T. Abraham, PI 3-kinase related kinases: 'big' players in stress-induced signaling pathways, DNA Repair (Amst.) 3 (2004) 883–887.
[43] D. Durocher, S.P. Jackson, DNA-PK, ATM and ATR as sensors of DNA damage: variations on a theme? Curr. Opin. Cell Biol. 13 (2001) 225–231.
[44] K. Hiom, DNA repair: how to PIKK a partner, Curr. Biol. 15 (2005) R473–R475.
[45] A. Yamashita, I. Kashima, S. Ohno, The role of SMG-1 in nonsense-mediated mRNA decay, Biochim. Biophys. Acta 1754 (2005) 305–315.
[46] S. Wullschleger, R. Loewith, M.N. Hall, TOR signaling in growth and metabolism, Cell 124 (2006) 471–484.
[47] P.T. Hawkins, K.E. Anderson, K. Davidson, L.R. Stephens, Signalling through Class I PI3Ks in mammalian cells, Biochem. Soc. Trans. 34 (2006) 647–662.

[48] P. Polak, M.N. Hall, mTORC2 caught in a SINful Akt, Dev. Cell 11 (2006) 433–434.
[49] B.D. Manning, L.C. Cantley, AKT/PKB signaling: navigating downstream, Cell 129 (2007) 1261–1274.
[50] J. Feng, J. Park, P. Cron, D. Hess, B.A. Hemmings, Identification of a PKB/Akt hydrophobic motif Ser-473 kinase as DNA-dependent protein kinase, J. Biol. Chem. 279 (2004) 41189–41196.
[51] M. Hanada, J. Feng, B.A. Hemmings, Structure, regulation and function of PKB/AKT—A major therapeutic target, Biochim. Biophys. Acta 1697 (2004) 3–16.
[52] D.P. Brazil, J. Park, B.A. Hemmings, PKB binding proteins. Getting in on the Akt, Cell 111 (2002) 293–303.
[53] M.V. Kisseleva, M.P. Wilson, P.W. Majerus, The isolation and characterization of a cDNA encoding phospholipid-specific inositol polyphosphate 5-phosphatase, J. Biol. Chem. 275 (2000) 20110–20116.
[54] L.R. Rohrschneider, J.F. Fuller, I. Wolf, Y. Liu, D.M. Lucas, Structure, function, and biology of SHIP proteins, Genes Dev. 14 (2000) 505–520.
[55] J. Kalesnikoff, L.M. Sly, M.R. Hughes, T. Buchse, M.J. Rauh, L.P. Cao, V. Lam, A. Mui, M. Huber, G. Krystal, The role of SHIP in cytokine-induced signaling, Rev. Physiol., Biochem. Pharmacol. 149 (2003) 87–103.
[56] V. Stambolic, A. Suzuki, J.L. de la Pompa, G.M. Brothers, C. Mirtsos, T. Sasaki, J. Ruland, J.M. Penninger, D.P. Siderovski, T.W. Mak, Negative regulation of PKB/Akt-dependent cell survival by the tumor suppressor PTEN, Cell 95 (1998) 29–39.
[57] B.M. Burgering, G.J. Kops, Cell cycle and death control: long live forkheads, Trends Biochem. Sci. 27 (2002) 352–360.
[58] B. Alvarez, C. Martinez-A, B.M. Burgering, A.C. Carrera, Forkhead transcription factors contribute to execution of the mitotic programme in mammals, Nature 413 (2001) 744–747.
[59] B.M. Burgering, R.H. Medema, Decisions on life and death: FOXO forkhead transcription factors are in command when PKB/Akt is off duty, J. Leukoc. Biol. 73 (2003) 689–701.
[60] J. Liang, J.M. Slingerland, Multiple roles of the PI3K/PKB (Akt) pathway in cell cycle progression, Cell Cycle 2 (2003) 339–345.
[61] F. Foijer, H. te Riele, Check, double check: the G2 barrier to cancer, Cell Cycle 5 (2006) 831–836.
[62] M.H. Cardone, N. Roy, H.R. Stennicke, G.S. Salvesen, T.F. Franke, E. Stanbridge, S. Frisch, J.C. Reed, Regulation of cell death protease caspase-9 by phosphorylation, Science 282 (1998) 1318–1321.
[63] L. del Peso, M. Gonzalez-Garcia, C. Page, R. Herrera, G. Nunez, Interleukin-3-induced phosphorylation of BAD through the protein kinase Akt, Science 278 (1997) 687–689.
[64] S.R. Datta, H. Dudek, X. Tao, S. Masters, H. Fu, Y. Gotoh, M.E. Greenberg, Akt phosphorylation of BAD couples survival signals to the cell-intrinsic death machinery, Cell 91 (1997) 231–241.
[65] Q. Li, I.M. Verma, NF-kappaB regulation in the immune system, Nat. Rev., Immunol. 2 (2002) 725–734.
[66] O.N. Ozes, L.D. Mayo, J.A. Gustin, S.R. Pfeffer, L.M. Pfeffer, D.B. Donner, NF-kappaB activation by tumour necrosis factor requires the Akt serine-threonine kinase, Nature 401 (1999) 82–85.
[67] D. Pan, J. Dong, Y. Zhang, X. Gao, Tuberous sclerosis complex: from *Drosophila* to human disease, Trends Cell Biol. 14 (2004) 78–85.
[68] N. Hay, N. Sonenberg, Upstream and downstream of mTOR, Genes Dev. 18 (2004) 1926–1945.
[69] D.E. Martin, M.N. Hall, The expanding TOR signaling network, Curr. Opin. Cell Biol. 17 (2005) 158–166.
[70] E. Patrucco, A. Notte, L. Barberis, G. Selvetella, A. Maffei, M. Brancaccio, S. Marengo, G. Russo, O. Azzolino, S.D. Rybalkin, L. Silengo, F. Altruda, R. Wetzker, M.P. Wymann, G. Lembo, E. Hirsch, PI3Kgamma modulates the cardiac response to chronic pressure overload by distinct kinase-dependent and -independent effects, Cell 118 (2004) 375–387.
[71] C. Vecchione, E. Patrucco, G. Marino, L. Barberis, R. Poulet, A. Aretini, A. Maffei, M.T. Gentile, M. Storto, O. Azzolino, M. Brancaccio, G.L. Colussi, U. Bettarini, F. Altruda, L. Silengo, G. Tarone, M.P. Wymann, E. Hirsch, G. Lembo, Protection from angiotensin II-mediated vasculotoxic and hypertensive response in mice lacking PI3Kgamma, J. Exp. Med. 201 (2005) 1217–1228.
[72] G. Alloatti, A. Marcantoni, R. Levi, M.P. Gallo, L. Del Sorbo, E. Patrucco, L. Barberis, D. Malan, O. Azzolino, M. Wymann, E. Hirsch, G. Montrucchio, Phosphoinositide 3-kinase gamma controls autonomic regulation of the mouse heart through Gi-independent downregulation of cAMP level, FEBS Lett. 579 (2005) 133–140.
[73] K. Okkenhaug, B. Vanhaesebroeck, PI3K in lymphocyte development, differentiation and activation, Nat. Rev., Immunol. 3 (2003) 317–330.
[74] L. Bi, I. Okabe, D.J. Bernard, A. Wynshaw-Boris, R.L. Nussbaum, Proliferative defect and embryonic lethality in mice homozygous for a deletion in the p110alpha subunit of phosphoinositide 3-kinase, J. Biol. Chem. 274 (1999) 10963–10968.
[75] L. Bi, I. Okabe, D.J. Bernard, R.L. Nussbaum, Early embryonic lethality in mice deficient in the p110beta catalytic subunit of PI 3-kinase, Mamm. Genome 13 (2002) 169–172.
[76] K. Okkenhaug, A. Bilancio, G. Farjot, H. Priddle, S. Sancho, E. Peskett, W. Pearce, S.E. Meek, A. Salpekar, M.D. Waterfield, A.J. Smith, B. Vanhaesebroeck, Impaired B and T cell antigen receptor signaling in p110delta PI 3-kinase mutant mice, Science 297 (2002) 1031–1034.
[77] E. Clayton, G. Bardi, S.E. Bell, D. Chantry, C.P. Downes, A. Gray, L.A. Humphries, D. Rawlings, H. Reynolds, E. Vigorito, M. Turner, A crucial role for the p110delta subunit of phosphatidylinositol 3-kinase in B cell development and activation, J. Exp. Med. 196 (2002) 753–763.
[78] S.T. Jou, N. Carpino, Y. Takahashi, R. Piekorz, J.R. Chao, N. Carpino, D. Wang, J.N. Ihle, Essential, nonredundant role for the phosphoinositide 3-kinase p110delta in signaling by the B-cell receptor complex, Mol. Cell. Biol. 22 (2002) 8580–8591.
[79] E. Hirsch, V.L. Katanaev, C. Garlanda, O. Azzolino, L. Pirola, L. Silengo, S. Sozzani, A. Mantovani, F. Altruda, M.P. Wymann, Central role for G protein-coupled phosphoinositide 3-kinase gamma in inflammation, Science 287 (2000) 1049–1053.
[80] Z. Li, H. Jiang, W. Xie, Z. Zhang, A.V. Smrcka, D. Wu, Roles of PLC-beta2 and -beta3 and PI3Kgamma in chemoattractant-mediated signal transduction, Science 287 (2000) 1046–1049.
[81] T. Sasaki, J. Irie-Sasaki, R.G. Jones, A.J. Oliveira-dos-Santos, W.L. Stanford, B. Bolon, A. Wakeham, A. Itie, D. Bouchard, I. Kozieradzki, N. Joza, T.W. Mak, P.S. Ohashi, A. Suzuki, J.M. Penninger, Function of PI3Kgamma in thymocyte development, T cell activation, and neutrophil migration, Science 287 (2000) 1040–1046.
[82] D.T. Patton, O.A. Garden, W.P. Pearce, L.E. Clough, C.R. Monk, E. Leung, W.C. Rowan, S. Sancho, L.S. Walker, B. Vanhaesebroeck, K. Okkenhaug, Cutting edge: the phosphoinositide 3-kinase p110 delta is critical for the function of $CD4^+$ $CD25^+$ Foxp3+ regulatory T cells, J. Immunol. 177 (2006) 6598–6602.
[83] L. Rodriguez-Borlado, D.F. Barber, C. Hernandez, M.A. Rodriguez-Marcos, A. Sanchez, E. Hirsch, M. Wymann, C. Martinez-A, A.C. Carrera, Phosphatidylinositol 3-kinase regulates the CD4/CD8 T cell differentiation ratio, J. Immunol. 170 (2003) 4475–4482.
[84] D.F. Barber, A. Bartolome, C. Hernandez, J.M. Flores, C. Fernandez-Arias, L. Rodriguez-Borlado, E. Hirsch, M. Wymann, D. Balomenos, A.C. Carrera, Class IB-phosphatidylinositol 3-kinase (PI3K) deficiency ameliorates IA-PI3K-induced systemic lupus but not T cell invasion, J. Immunol. 176 (2006) 589–593.
[85] L.M. Webb, E. Vigorito, M.P. Wymann, E. Hirsch, M. Turner, Cutting edge: T cell development requires the combined activities of the p110gamma and p110delta catalytic isoforms of phosphatidylinositol 3-kinase, J. Immunol. 175 (2005) 2783–2787.
[86] H. Ji, F. Rintelen, C. Waltzinger, D. Bertschy Meier, A. Bilancio, W. Pearce, E. Hirsch, M.P. Wymann, T. Ruckle, M. Camps, B. Vanhaesebroeck, K. Okkenhaug, C. Rommel, Inactivation of PI3K{gamma} and PI3K{delta} distorts T cell development and causes multiple organ inflammation, Blood (2007).
[87] H. Suzuki, Y. Terauchi, M. Fujiwara, S. Aizawa, Y. Yazaki, T. Kadowaki, S. Koyasu, Xid-like immunodeficiency in mice with disruption of the p85alpha subunit of phosphoinositide 3-kinase, Science 283 (1999) 390–392.

[88] A. Saudemont, K. Okkenhaug, F. Colucci, p110delta is required for innate immunity to transplantable lymphomas, Biochem. Soc. Trans. 35 (2007) 183–185.
[89] N. Kim, A. Saudemont, L. Webb, M. Camps, T. Ruckle, E. Hirsch, M. Turner, F. Colucci, The p110delta catalytic isoform of PI3K is a key player in NK cell development and cytokine secretion, Blood (2007).
[90] G.E. Jones, E. Prigmore, R. Calvez, C. Hogan, G.A. Dunn, E. Hirsch, M.P. Wymann, A.J. Ridley, Requirement for PI 3-kinase gamma in macrophage migration to MCP-1 and CSF-1, Exp. Cell Res. 290 (2003) 120–131.
[91] A. Del Prete, W. Vermi, E. Dander, K. Otero, L. Barberis, W. Luini, S. Bernasconi, M. Sironi, A. Santoro, C. Garlanda, F. Facchetti, M.P. Wymann, A. Vecchi, E. Hirsch, A. Mantovani, S. Sozzani, Defective dendritic cell migration and activation of adaptive immunity in PI3Kgamma-deficient mice, EMBO J. 23 (2004) 3505–3515.
[92] M. Laffargue, R. Calvez, P. Finan, A. Trifilieff, M. Barbier, F. Altruda, E. Hirsch, M.P. Wymann, Phosphoinositide 3-kinase gamma is an essential amplifier of mast cell function, Immunity 16 (2002) 441–451.
[93] K. Ali, A. Bilancio, M. Thomas, W. Pearce, A.M. Gilfillan, C. Tkaczyk, N. Kuehn, A. Gray, J. Giddings, E. Peskett, R. Fox, I. Bruce, C. Walker, C. Sawyer, K. Okkenhaug, P. Finan, B. Vanhaesebroeck, Essential role for the p110delta phosphoinositide 3-kinase in the allergic response, Nature 431 (2004) 1007–1011.
[94] J. Kitaura, T. Kinoshita, M. Matsumoto, S. Chung, Y. Kawakami, M. Leitges, D. Wu, C.A. Lowell, T. Kawakami, IgE and IgE+Ag-mediated mast cell migration in an autocrine/paracrine fashion, Blood 105 (2005) 3222–3229.
[95] J. Rivera, NTAL/LAB and LAT: a balancing act in mast-cell activation and function, Trends Immunol. 26 (2005) 119–122.
[96] H. Gu, K. Saito, L.D. Klaman, J. Shen, T. Fleming, Y. Wang, J.C. Pratt, G. Lin, B. Lim, J.P. Kinet, B.G. Neel, Essential role for Gab2 in the allergic response, Nature 412 (2001) 186–190.
[97] S. Kraft, J.P. Kinet, New developments in FcepsilonRI regulation, function and inhibition, Nat. Rev., Immunol. 7 (2007) 365–378.
[98] M.P. Wymann, K. Bjorklof, R. Calvez, P. Finan, M. Thomast, A. Trifilieff, M. Barbier, F. Altruda, E. Hirsch, M. Laffargue, Phosphoinositide 3-kinase gamma: a key modulator in inflammation and allergy, Biochem. Soc. Trans. 31 (2003) 275–280.
[99] G.S. Firestein, Evolving concepts of rheumatoid arthritis, Nature 423 (2003) 356–361.
[100] G. Steiner, Auto-antibodies and autoreactive T-cells in rheumatoid arthritis: pathogenetic players and diagnostic tools, Clin. Rev. Allergy Immunol. 32 (2007) 23–36.
[101] K. Terato, K.A. Hasty, R.A. Reife, M.A. Cremer, A.H. Kang, J.M. Stuart, Induction of arthritis with monoclonal antibodies to collagen, J. Immunol. 148 (1992) 2103–2108.
[102] J.M. Stuart, A.S. Townes, A.H. Kang, Collagen autoimmune arthritis, Annu. Rev. Immunol. 2 (1984) 199–218.
[103] D.E. Trentham, Collagen arthritis as a relevant model for rheumatoid arthritis, Arthritis Rheum. 25 (1982) 911–916.
[104] S.S. Kerwar, M.E. Englert, R.A. McReynolds, M.J. Landes, J.M. Lloyd, A.L. Oronsky, F.J. Wilson, Type II collagen-induced arthritis. Studies with purified anticollagen immunoglobulin, Arthritis Rheum. 26 (1983) 1120–1131.
[105] M. Camps, T. Ruckle, H. Ji, V. Ardissone, F. Rintelen, J. Shaw, C. Ferrandi, C. Chabert, C. Gillieron, B. Francon, T. Martin, D. Gretener, D. Perrin, D. Leroy, P.A. Vitte, E. Hirsch, M.P. Wymann, R. Cirillo, M.K. Schwarz, C. Rommel, Blockade of PI3Kgamma suppresses joint inflammation and damage in mouse models of rheumatoid arthritis, Nat. Med. 11 (2005) 936–943.
[106] G.G. Singer, A.C. Carrera, A. Marshak-Rothstein, C. Martinez, A.K. Abbas, Apoptosis, Fas and systemic autoimmunity: the MRL-lpr/lpr model, Curr. Opin. Immunol. 6 (1994) 913–920.
[107] P.L. Cohen, R.A. Eisenberg, Lpr and gld: single gene models of systemic autoimmunity and lymphoproliferative disease, Annu. Rev. Immunol. 9 (1991) 243–269.
[108] D.F. Barber, A. Bartolome, C. Hernandez, J.M. Flores, C. Redondo, C. Fernandez-Arias, M. Camps, T. Ruckle, M.K. Schwarz, S. Rodriguez, C. Martinez-A, D. Balomenos, C. Rommel, A.C. Carrera, PI3Kgamma inhibition blocks glomerulonephritis and extends lifespan in a mouse model of systemic lupus, Nat. Med. 11 (2005) 933–935.
[109] A. Di Cristofano, P. Kotsi, Y.F. Peng, C. Cordon-Cardo, K.B. Elkon, P.P. Pandolfi, Impaired Fas response and autoimmunity in Pten+/− mice, Science 285 (1999) 2122–2125.
[110] L.R. Borlado, C. Redondo, B. Alvarez, C. Jimenez, L.M. Criado, J. Flores, M.A. Marcos, C. Martinez-A, D. Balomenos, A.C. Carrera, Increased phosphoinositide 3-kinase activity induces a lymphoproliferative disorder and contributes to tumor generation in vivo, FASEB J. 14 (2000) 895–903.
[111] W.W. Chatham, R.P. Kimberly, Treatment of lupus with corticosteroids, Lupus 10 (2001) 140–147.
[112] A.J. Lusis, Atherosclerosis, Nature 407 (2000) 233–241.
[113] C.K. Glass, J.L. Witztum, Atherosclerosis. The road ahead, Cell 104 (2001) 503–516.
[114] T. Biwa, M. Sakai, T. Matsumura, S. Kobori, K. Kaneko, A. Miyazaki, H. Hakamata, S. Horiuchi, M. Shichiri, Sites of action of protein kinase C and phosphatidylinositol 3-kinase are distinct in oxidized low density lipoprotein-induced macrophage proliferation, J. Biol. Chem. 275 (2000) 5810–5816.
[115] T. Biwa, M. Sakai, M. Shichiri, S. Horiuchi, Granulocyte/macrophage colony-stimulating factor plays an essential role in oxidized low density lipoprotein-induced macrophage proliferation, J. Atheroscler. Thromb. 7 (2000) 14–20.
[116] A.S. Plump, J.D. Smith, T. Hayek, K. Aalto-Setala, A. Walsh, J.G. Verstuyft, E.M. Rubin, J.L. Breslow, Severe hypercholesterolemia and atherosclerosis in apolipoprotein E-deficient mice created by homologous recombination in ES cells, Cell 71 (1992) 343–353.
[117] Y. Nakashima, A.S. Plump, E.W. Raines, J.L. Breslow, R. Ross, ApoE-deficient mice develop lesions of all phases of atherosclerosis throughout the arterial tree, Arterioscler. Thromb. 14 (1994) 133–140.
[118] J.D. Chang, G.K. Sukhova, P. Libby, E. Schvartz, A.H. Lichtenstein, S.J. Field, C. Kennedy, S. Madhavarapu, J. Luo, D. Wu, L.C. Cantley, Deletion of the phosphoinositide 3-kinase p110gamma gene attenuates murine atherosclerosis, Proc. Natl. Acad. Sci. U. S. A. 104 (2007) 8077–8082.
[119] E. Lupia, A. Goffi, P. De Giuli, O. Azzolino, O. Bosco, E. Patrucco, M.C. Vivaldo, M. Ricca, M.P. Wymann, E. Hirsch, G. Montrucchio, G. Emanuelli, Ablation of phosphoinositide 3-kinase-gamma reduces the severity of acute pancreatitis, Am. J. Pathol. 165 (2004) 2003–2011.
[120] M.A. Lowes, A.M. Bowcock, J.G. Krueger, Pathogenesis and therapy of psoriasis, Nature 445 (2007) 866–873.
[121] M.P. Schon, W.H. Boehncke, Psoriasis, N. Engl. J. Med. 352 (2005) 1899–1912.
[122] S.D. Shapiro, COPD unwound, N. Engl. J. Med. 352 (2005) 2016–2019.
[123] K. Ito, G. Caramori, I.M. Adcock, Therapeutic potential of phosphatidylinositol 3-kinase inhibitors in inflammatory respiratory disease, J. Pharmacol. Exp. Ther. 321 (2007) 1–8.
[124] S.L. Hauser, J.R. Oksenberg, The neurobiology of multiple sclerosis: genes, inflammation, and neurodegeneration, Neuron 52 (2006) 61–76.
[125] B. Hemmer, J.J. Archelos, H.P. Hartung, New concepts in the immunopathogenesis of multiple sclerosis, Nat. Rev., Neurosci. 3 (2002) 291–301.
[126] T. Shioi, P.M. Kang, P.S. Douglas, J. Hampe, C.M. Yballe, J. Lawitts, L.C. Cantley, S. Izumo, The conserved phosphoinositide 3-kinase pathway determines heart size in mice, EMBO J. 19 (2000) 2537–2548.
[127] T. Shioi, J.R. McMullen, P.M. Kang, P.S. Douglas, T. Obata, T.F. Franke, L.C. Cantley, S. Izumo, Akt/protein kinase B promotes organ growth in transgenic mice, Mol. Cell. Biol. 22 (2002) 2799–2809.
[128] M.A. Crackower, G.Y. Oudit, I. Kozieradzki, R. Sarao, H. Sun, T. Sasaki, E. Hirsch, A. Suzuki, T. Shioi, J. Irie-Sasaki, R. Sah, H.Y. Cheng, V.O. Rybin, G. Lembo, L. Fratta, A.J. Oliveira-dos-Santos, J.L. Benovic, C.R. Kahn, S. Izumo, S.F. Steinberg, M.P. Wymann, P.H. Backx, J.M. Penninger, Regulation of myocardial contractility and cell size by distinct PI3K-PTEN signaling pathways, Cell 110 (2002) 737–749.
[129] J. Luo, J.R. McMullen, C.L. Sobkiw, L. Zhang, A.L. Dorfman, M.C. Sherwood, M.N. Logsdon, J.W. Horner, R.A. DePinho, S. Izumo, L.C. Cantley, Class IA phosphoinositide 3-kinase regulates heart size and physiological cardiac hypertrophy, Mol. Cell. Biol. 25 (2005) 9491–9502.

[130] J. Doukas, W. Wrasidlo, G. Noronha, E. Dneprovskaia, R. Fine, S. Weis, J. Hood, A. Demaria, R. Soll, D. Cheresh, Phosphoinositide 3-kinase gamma/delta inhibition limits infarct size after myocardial ischemia/reperfusion injury, Proc. Natl. Acad. Sci. U. S. A. 103 (2006) 19866–19871.
[131] J. Doukas, W. Wrasidlo, G. Noronha, E. Dneprovskaia, J. Hood, R. Soll, Isoform-selective PI3K inhibitors as novel therapeutics for the treatment of acute myocardial infarction, Biochem. Soc. Trans. 35 (2007) 204–206.
[132] B.T. Hennessy, D.L. Smith, P.T. Ram, Y. Lu, G.B. Mills, Exploiting the PI3K/AKT pathway for cancer drug discovery, Nat. Rev. Drug Discov. 4 (2005) 988–1004.
[133] A.G. Bader, S. Kang, L. Zhao, P.K. Vogt, Oncogenic PI3K deregulates transcription and translation, Nat. Rev., Cancer 5 (2005) 921–929.
[134] R.J. Shaw, L.C. Cantley, Ras, PI(3)K and mTOR signalling controls tumour cell growth, Nature 441 (2006) 424–430.
[135] K.A. Waite, C. Eng, Protean PTEN: form and function, Am. J. Hum. Genet. 70 (2002) 829–844.
[136] C. Eng, PTEN: one gene, many syndromes, Human Mutat. 22 (2003) 183–198.
[137] D. Liaw, D.J. Marsh, J. Li, P.L. Dahia, S.I. Wang, Z. Zheng, S. Bose, K.M. Call, H.C. Tsou, M. Peacocke, C. Eng, R. Parsons, Germline mutations of the PTEN gene in Cowden disease, an inherited breast and thyroid cancer syndrome, Nat. Genet. 16 (1997) 64–67.
[138] D.J. Marsh, P.L. Dahia, Z. Zheng, D. Liaw, R. Parsons, R.J. Gorlin, C. Eng, Germline mutations in PTEN are present in Bannayan-Zonana syndrome, Nat. Genet. 16 (1997) 333–334.
[139] J.M. Smith, E.P. Kirk, G. Theodosopoulos, G.M. Marshall, J. Walker, M. Rogers, M. Field, J.J. Brereton, D.J. Marsh, Germline mutation of the tumour suppressor PTEN in Proteus syndrome, J. Med. Genet. 39 (2002) 937–940.
[140] X.P. Zhou, D.J. Marsh, H. Hampel, J.B. Mulliken, O. Gimm, C. Eng, Germline and germline mosaic PTEN mutations associated with a Proteus-like syndrome of hemihypertrophy, lower limb asymmetry, arteriovenous malformations and lipomatosis, Hum. Mol. Genet. 9 (2000) 765–768.
[141] C. Eng, Will the real Cowden syndrome please stand up: revised diagnostic criteria, J. Med. Genet. 37 (2000) 828–830.
[142] J. Li, C. Yen, D. Liaw, K. Podsypanina, S. Bose, S.I. Wang, J. Puc, C. Miliaresis, L. Rodgers, R. McCombie, S.H. Bigner, B.C. Giovanella, M. Ittmann, B. Tycko, H. Hibshoosh, M.H. Wigler, R. Parsons, PTEN, a putative protein tyrosine phosphatase gene mutated in human brain, breast, and prostate cancer, Science 275 (1997) 1943–1947.
[143] P. Cairns, K. Okami, S. Halachmi, N. Halachmi, M. Esteller, J.G. Herman, J. Jen, W.B. Isaacs, G.S. Bova, D. Sidransky, Frequent inactivation of PTEN/MMAC1 in primary prostate cancer, Cancer Res. 57 (1997) 4997–5000.
[144] H. Wu, V. Goel, F.G. Haluska, PTEN signaling pathways in melanoma, Oncogene 22 (2003) 3113–3122.
[145] S. Khan, T. Kumagai, J. Vora, N. Bose, I. Sehgal, P.H. Koeffler, S. Bose, PTEN promoter is methylated in a proportion of invasive breast cancers, Int. J. Cancer 112 (2004) 407–410.
[146] A. Goel, C.N. Arnold, D. Niedzwiecki, J.M. Carethers, J.M. Dowell, L. Wasserman, C. Compton, R.J. Mayer, M.M. Bertagnolli, C.R. Boland, Frequent inactivation of PTEN by promoter hypermethylation in microsatellite instability-high sporadic colorectal cancers, Cancer Res. 64 (2004) 3014–3021.
[147] J.M. Stahl, A. Sharma, M. Cheung, M. Zimmerman, J.Q. Cheng, M.W. Bosenberg, M. Kester, L. Sandirasegarane, G.P. Robertson, Deregulated Akt3 activity promotes development of malignant melanoma, Cancer Res. 64 (2004) 7002–7010.
[148] A. Mirmohammadsadegh, A. Marini, S. Nambiar, M. Hassan, A. Tannapfel, T. Ruzicka, U.R. Hengge, Epigenetic silencing of the PTEN gene in melanoma, Cancer Res. 66 (2006) 6546–6552.
[149] L. Shayesteh, Y. Lu, W.L. Kuo, R. Baldocchi, T. Godfrey, C. Collins, D. Pinkel, B. Powell, G.B. Mills, J.W. Gray, PIK3CA is implicated as an oncogene in ovarian cancer, Nat. Genet. 21 (1999) 99–102.
[150] A. Zhang, S. Maner, R. Betz, T. Angstrom, U. Stendahl, F. Bergman, A. Zetterberg, K.L. Wallin, Genetic alterations in cervical carcinomas: frequent low-level amplifications of oncogenes are associated with human papillomavirus infection, Int. J. Cancer 101 (2002) 427–433.
[151] A. Racz, N. Brass, D. Heckel, S. Pahl, K. Remberger, E. Meese, Expression analysis of genes at 3q26-q27 involved in frequent amplification in squamous cell lung carcinoma, Eur. J. Cancer 35 (1999) 641–646.
[152] Y. Samuels, K. Ericson, Oncogenic PI3K and its role in cancer, Curr. Opin. Oncol. 18 (2006) 77–82.
[153] Y. Samuels, Z. Wang, A. Bardelli, N. Silliman, J. Ptak, S. Szabo, H. Yan, A. Gazdar, S.M. Powell, G.J. Riggins, J.K. Willson, S. Markowitz, K.W. Kinzler, B. Vogelstein, V.E. Velculescu, High frequency of mutations of the PIK3CA gene in human cancers, Science 304 (2004) 554.
[154] N. Miled, Y. Yan, W.C. Hon, O. Perisic, M. Zvelebil, Y. Inbar, D. Schneidman-Duhovny, H.J. Wolfson, J.M. Backer, R.L. Williams, Mechanism of two classes of cancer mutations in the phosphoinositide 3-kinase catalytic subunit, Science 317 (2007) 239–242.
[155] T. Ikenoue, F. Kanai, Y. Hikiba, T. Obata, Y. Tanaka, J. Imamura, M. Ohta, A. Jazag, B. Guleng, K. Tateishi, Y. Asaoka, M. Matsumura, T. Kawabe, M. Omata, Functional analysis of PIK3CA gene mutations in human colorectal cancer, Cancer Res. 65 (2005) 4562–4567.
[156] S. Kang, A.G. Bader, P.K. Vogt, Phosphatidylinositol 3-kinase mutations identified in human cancer are oncogenic, Proc. Natl. Acad. Sci. U. S. A. 102 (2005) 802–807.
[157] Y. Samuels, L.A.J. Diaz, O. Schmidt-Kittler, J.M. Cummins, L. Delong, I. Cheong, C. Rago, D.L. Huso, C. Lengauer, K.W. Kinzler, B. Vogelstein, V.E. Velculescu, Mutant PIK3CA promotes cell growth and invasion of human cancer cells, Cancer Cell 7 (2005) 561–573.
[158] J.P. Cheadle, M.P. Reeve, J.R. Sampson, D.J. Kwiatkowski, Molecular genetic advances in tuberous sclerosis, Hum. Genet. 107 (2000) 97–114.
[159] A. Woods, S.R. Johnstone, K. Dickerson, F.C. Leiper, L.G. Fryer, D. Neumann, U. Schlattner, T. Wallimann, M. Carlson, D. Carling, LKB1 is the upstream kinase in the AMP-activated protein kinase cascade, Curr. Biol. 13 (2003) 2004–2008.
[160] J. Boudeau, G. Sapkota, D.R. Alessi, LKB1, a protein kinase regulating cell proliferation and polarity, FEBS Lett. 546 (2003) 159–165.
[161] M.A. Bjornsti, P.J. Houghton, The TOR pathway: a target for cancer therapy, Nat. Rev., Cancer 4 (2004) 335–348.
[162] D.A. Guertin, D.M. Sabatini, Defining the role of mTOR in cancer, Cancer Cell 12 (2007) 9–22.
[163] M. Guba, P. von Breitenbuch, M. Steinbauer, G. Koehl, S. Flegel, M. Hornung, C.J. Bruns, C. Zuelke, S. Farkas, M. Anthuber, K.W. Jauch, E.K. Geissler, Rapamycin inhibits primary and metastatic tumor growth by antiangiogenesis: involvement of vascular endothelial growth factor, Nat. Med. 8 (2002) 128–135.
[164] I. Beuvink, A. Boulay, S. Fumagalli, F. Zilbermann, S. Ruetz, T. O'Reilly, F. Natt, J. Hall, H.A. Lane, G. Thomas, The mTOR inhibitor RAD001 sensitizes tumor cells to DNA-damaged induced apoptosis through inhibition of p21 translation, Cell 120 (2005) 747–759.
[165] S.G. Dann, A. Selvaraj, G. Thomas, mTOR Complex1-S6K1 signaling: at the crossroads of obesity, diabetes and cancer, Trends Mol. Med. 13 (2007) 252–259.
[166] Y.G. Gangloff, M. Mueller, S.G. Dann, P. Svoboda, M. Sticker, J.F. Spetz, S.H. Um, E.J. Brown, S. Cereghini, G. Thomas, S.C. Kozma, Disruption of the mouse mTOR gene leads to early postimplantation lethality and prohibits embryonic stem cell development, Mol. Cell. Biol. 24 (2004) 9508–9516.
[167] D.D. Sarbassov, S.M. Ali, S. Sengupta, J.H. Sheen, P.P. Hsu, A.F. Bagley, A.L. Markhard, D.M. Sabatini, Prolonged rapamycin treatment inhibits mTORC2 assembly and Akt/PKB, Mol. Cell 22 (2006) 159–168.
[168] S.H. Um, F. Frigerio, M. Watanabe, F. Picard, M. Joaquin, M. Sticker, S. Fumagalli, P.R. Allegrini, S.C. Kozma, J. Auwerx, G. Thomas, Absence of S6K1 protects against age- and diet-induced obesity while enhancing insulin sensitivity, Nature 431 (2004) 200–205.
[169] W.C. Knowler, E. Barrett-Connor, S.E. Fowler, R.F. Hamman, J.M. Lachin, E.A. Walker, D.M. Nathan, Reduction in the incidence of type 2 diabetes with lifestyle intervention or metformin, N. Engl. J. Med. 346 (2002) 393–403.

[170] S. Marshall, Role of insulin, adipocyte hormones, and nutrient-sensing pathways in regulating fuel metabolism and energy homeostasis: a nutritional perspective of diabetes, obesity, and cancer, Sci. STKE 2006 (2006) re7.
[171] L.C. Foukas, M. Claret, W. Pearce, K. Okkenhaug, S. Meek, E. Peskett, S. Sancho, A.J. Smith, D.J. Withers, B. Vanhaesebroeck, Critical role for the p110alpha phosphoinositide-3-OH kinase in growth and metabolic regulation, Nature 441 (2006) 366–370.
[172] H. Cho, J. Mu, J.K. Kim, J.L. Thorvaldsen, Q. Chu, E.B.r. Crenshaw, K.H. Kaestner, M.S. Bartolomei, G.I. Shulman, M.J. Birnbaum, Insulin resistance and a diabetes mellitus-like syndrome in mice lacking the protein kinase Akt2 (PKB beta), Science 292 (2001) 1728–1731.
[173] S. George, J.J. Rochford, C. Wolfrum, S.L. Gray, S. Schinner, J.C. Wilson, M.A. Soos, P.R. Murgatroyd, R.M. Williams, C.L. Acerini, D.B. Dunger, D. Barford, A.M. Umpleby, N.J. Wareham, H.A. Davies, A.J. Schafer, M. Stoffel, S. O'Rahilly, I. Barroso, A family with severe insulin resistance and diabetes due to a mutation in AKT2, Science 304 (2004) 1325–1328.
[174] G.K. Bandyopadhyay, J.G. Yu, J. Ofrecio, J.M. Olefsky, Increased p85/55/50 expression and decreased phosphotidylinositol 3-kinase activity in insulin-resistant human skeletal muscle, Diabetes 54 (2005) 2351–2359.
[175] F. Tremblay, M. Krebs, L. Dombrowski, A. Brehm, E. Bernroider, E. Roth, P. Nowotny, W. Waldhausl, A. Marette, M. Roden, Overactivation of S6 kinase 1 as a cause of human insulin resistance during increased amino acid availability, Diabetes 54 (2005) 2674–2684.
[176] M.P. Wymann, G. Bulgarelli-Leva, M.J. Zvelebil, L. Pirola, B. Vanhaesebroeck, M.D. Waterfield, G. Panayotou, Wortmannin inactivates phosphoinositide 3-kinase by covalent modification of Lys-802, a residue involved in the phosphate transfer reaction, Mol. Cell. Biol. 16 (1996) 1722–1733.
[177] A. Arcaro, M.P. Wymann, Wortmannin is a potent phosphatidylinositol 3-kinase inhibitor: the role of phosphatidylinositol 3,4,5-trisphosphate in neutrophil responses, Biochem. J. 296 (1993) 297–301.
[178] H. Yano, S. Nakanishi, K. Kimura, N. Hanai, Y. Saitoh, Y. Fukui, Y. Nonomura, Y. Matsuda, Inhibition of histamine secretion by wortmannin through the blockade of phosphatidylinositol 3-kinase in RBL-2H3 cells, J. Biol. Chem. 268 (1993) 25846–25856.
[179] M. Wymann, A. Arcaro, Platelet-derived growth factor-induced phosphatidylinositol 3-kinase activation mediates actin rearrangements in fibroblasts, Biochem. J. 3 (1994) 517–520 (298 Pt.).
[180] C.J. Vlahos, W.F. Matter, K.Y. Hui, R.F. Brown, A specific inhibitor of phosphatidylinositol 3-kinase, 2-(4-morpholinyl)-8-phenyl-4H-1-benzopyran-4-one (LY294002), J. Biol. Chem. 269 (1994) 5241–5248.
[181] B. Li, Y. Liu, T. Uno, N. Gray, Creating chemical diversity to target protein kinases, Comb. Chem. High Throughput Screen. 7 (2004) 453–472.
[182] K. Parang, G. Sun, Design strategies for protein kinase inhibitors, Curr. Opin. Drug Discov. Dev. 7 (2004) 617–629.
[183] E.H. Walker, O. Perisic, C. Ried, L. Stephens, R.L. Williams, Structural insights into phosphoinositide 3-kinase catalysis and signalling, Nature 402 (1999) 313–320.
[184] E.H. Walker, M.E. Pacold, O. Perisic, L. Stephens, P.T. Hawkins, M.P. Wymann, R.L. Williams, Structural determinants of phosphoinositide 3-kinase inhibition by wortmannin, LY294002, quercetin, myricetin, and staurosporine, Mol. Cell 6 (2000) 909–919.
[185] S. Stoyanova, G. Bulgarelli-Leva, C. Kirsch, T. Hanck, R. Klinger, R. Wetzker, M.P. Wymann, Lipid kinase and protein kinase activities of G-protein-coupled phosphoinositide 3-kinase gamma: structure–activity analysis and interactions with wortmannin, Biochem. J. 324 (1997) 489–495.
[186] P.W. Brian, P.J. Curtis, H.G. Hemming, G.L.F. Norris, Wortmannin, an antibiotic produced by *Penicillium wortmanni*, Trans. Br. Mycol. Soc. 40 (1957) 365–368.
[187] J. MacMillan, A.E. Vanstone, S.K. Yeboah, The structure of wortmannin, a steroidal fungal metabolite, J. Chem. Soc., Chem. Commun. 388 (1968) 613–614.
[188] J. MacMillan, A.E. Vanstone, S.K. Yeboah, Fungal products: Part III. Structure of wortmannin and some hydrolysis products, J. Chem. Soc. 1 (1972) 2898–2903.
[189] T.J. Simpson, M.W. Lunnon, J. MacMillan, Fungal products: Part 21. Biosynthesis of the fungal metabolite, wortmannin, from (1,2-13C2)-acetate, J. Chem. Soc., Perkin Trans. 1 (1979) 931–934.
[190] T.J. Petcher, H. Weber, Z. Kis, Crystal structure and absolute configuration of wortmannin and of wortmannin *p*-bromobenzoate, J. Chem. Soc., Chem. Commun. (1972) 1061–1062.
[191] M. Baggiolini, B. Dewald, J. Schnyder, W. Ruch, P.H. Cooper, T.G. Payne, Inhibition of the phagocytosis-induced respiratory burst by the fungal metabolite wortmannin and some analogues, Exp. Cell Res. 169 (1987) 408–418.
[192] M. Thelen, M.P. Wymann, H. Langen, Wortmannin binds specifically to 1-phosphatidylinositol 3-kinase while inhibiting guanine nucleotide-binding protein-coupled receptor signaling in neutrophil leukocytes, Proc. Natl. Acad. Sci. U. S. A. 91 (1994) 4960–4964.
[193] P. Wipf, R.J. Halter, Chemistry and biology of wortmannin, Org. Biomol. Chem. 3 (2005) 2053–2061.
[194] R.W. Bonser, N.T. Thompson, R.W. Randall, J.E. Tateson, G.D. Spacey, H.F. Hodson, L.G. Garland, Demethoxyviridin and wortmannin block phospholipase C and D activation in the human neutrophil, Br. J. Pharmacol. 103 (1991) 1237–1241.
[195] R. Woscholski, T. Kodaki, M. McKinnon, M.D. Waterfield, P.J. Parker, A comparison of demethoxyviridin and wortmannin as inhibitors of phosphatidylinositol 3-kinase, FEBS Lett. 342 (1994) 109–114.
[196] D.C. Aldridge, W.B. Turner, A.J. Geddes, B. Sheldrick, Demethoxyviridin and demethoxyviridiol: new fungal metabolites, J. Chem. Soc., Perkin Trans. 1 (1975) 943–945.
[197] B.H. Norman, C. Shih, J.E. Toth, J.E. Ray, J.A. Dodge, D.W. Johnson, P.G. Rutherford, R.M. Schultz, J.F. Worzalla, C.J. Vlahos, Studies on the mechanism of phosphatidylinositol 3-kinase inhibition by wortmannin and related analogs, J. Med. Chem. 39 (1996) 1106–1111.
[198] K.O. Hartley, D. Gell, G.C. Smith, H. Zhang, N. Divecha, M.A. Connelly, A. Admon, S.P. Lees-Miller, C.W. Anderson, S.P. Jackson, DNA-dependent protein kinase catalytic subunit: a relative of phosphatidylinositol 3-kinase and the ataxia telangiectasia gene product, Cell 82 (1995) 849–856.
[199] G.J. Brunn, J. Williams, C. Sabers, G. Wiederrecht, J.C.J. Lawrence, R.T. Abraham, Direct inhibition of the signaling functions of the mammalian target of rapamycin by the phosphoinositide 3-kinase inhibitors, wortmannin and LY294002, EMBO J. 15 (1996) 5256–5267.
[200] J.N. Sarkaria, R.S. Tibbetts, E.C. Busby, A.P. Kennedy, D.E. Hill, R.T. Abraham, Inhibition of phosphoinositide 3-kinase related kinases by the radiosensitizing agent wortmannin, Cancer Res. 58 (1998) 4375–4382.
[201] S. Banin, L. Moyal, S. Shieh, Y. Taya, C.W. Anderson, L. Chessa, N.I. Smorodinsky, C. Prives, Y. Reiss, Y. Shiloh, Y. Ziv, Enhanced phosphorylation of p53 by ATM in response to DNA damage, Science 281 (1998) 1674–1677.
[202] J.L. Holleran, J. Fourcade, M.J. Egorin, J.L. Eiseman, R.A. Parise, S.M. Musser, K.D. White, J.M. Covey, G.L. Forrest, S.S. Pan, In vitro metabolism of the phosphatidylinositol 3-kinase inhibitor, wortmannin, by carbonyl reductase, Drug Metab. Dispos. 32 (2004) 490–496.
[203] N.T. Ihle, R. Williams, S. Chow, W. Chew, M.I. Berggren, G. Paine-Murrieta, D.J. Minion, R.J. Halter, P. Wipf, R. Abraham, L. Kirkpatrick, G. Powis, Molecular pharmacology and antitumor activity of PX-866, a novel inhibitor of phosphoinositide-3-kinase signaling, Mol. Cancer Ther. 3 (2004) 763–772.
[204] J.L. Giner, K.A. Kehbein, J.A. Cook, M.C. Smith, C.J. Vlahos, J.A. Badwey, Synthesis of fluorescent derivatives of wortmannin and demethoxyviridin as probes for phosphatidylinositol 3-kinase, Bioorg. Med. Chem. Lett. 16 (2006) 2518–2521.
[205] H. Yuan, J. Luo, S. Field, R. Weissleder, L. Cantley, L. Josephson, Synthesis and activity of C11-modified wortmannin probes for PI3 kinase, Bioconjug. Chem. 16 (2005) 669–675.
[206] M.C. Yee, S.C. Fas, M.M. Stohlmeyer, T.J. Wandless, K.A. Cimprich, A cell-permeable, activity-based probe for protein and lipid kinases, J. Biol. Chem. 280 (2005) 29053–29059.
[207] Y. Liu, K.R. Shreder, W. Gai, S. Corral, D.K. Ferris, J.S. Rosenblum,

Wortmannin, a widely used phosphoinositide 3-kinase inhibitor, also potently inhibits mammalian polo-like kinase, Chem. Biol. 12 (2005) 99–107.
[208] Y. Liu, N. Jiang, J. Wu, W. Dai, J.S. Rosenblum, Polo-like kinases inhibited by wortmannin. Labeling site and downstream effects, J. Biol. Chem. 282 (2007) 2505–2511.
[209] F. Marion, D.E. Williams, B.O. Patrick, I. Hollander, R. Mallon, S.C. Kim, D.M. Roll, L. Feldberg, R. Van Soest, R.J. Andersen, Liphagal, a selective inhibitor of PI3 kinase alpha isolated from the sponge akacoralliphaga: structure elucidation and biomimetic synthesis, Org. Lett. 8 (2006) 321–324.
[210] L.C. Foukas, N. Daniele, C. Ktori, K.E. Anderson, J. Jensen, P.R. Shepherd, Direct effects of caffeine and theophylline on p110 delta and other phosphoinositide 3-kinases. Differential effects on lipid kinase and protein kinase activities, J. Biol. Chem. 277 (2002) 37124–37130.
[211] J.A. Baur, D.A. Sinclair, Therapeutic potential of resveratrol: the in vivo evidence, Nat. Rev., Drug Discov. 5 (2006) 493–506.
[212] E.H. Siemann, L.L. Creasy, Concentration of the phytoalexin resveratrol in wine, Am. J. Enol. Vitic. 43 (1992) 49–52.
[213] S. Frojdo, D. Cozzone, H. Vidal, L. Pirola, Resveratrol is a class IA phosphoinositide 3-kinase inhibitor, Biochem. J. 406 (2007) 511–518.
[214] M. Lagouge, C. Argmann, Z. Gerhart-Hines, H. Meziane, C. Lerin, F. Daussin, N. Messadeq, J. Milne, P. Lambert, P. Elliott, B. Geny, M. Laakso, P. Puigserver, J. Auwerx, Resveratrol improves mitochondrial function and protects against metabolic disease by activating SIRT1 and PGC-1alpha, Cell 127 (2006) 1109–1122.
[215] Z.A. Knight, G.G. Chiang, P.J. Alaimo, D.M. Kenski, C.B. Ho, K. Coan, R.T. Abraham, K.M. Shokat, Isoform-specific phosphoinositide 3-kinase inhibitors from an arylmorpholine scaffold, Bioorg. Med. Chem. 12 (2004) 4749–4759.
[216] S.I. Gharbi, M.J. Zvelebil, S.J. Shuttleworth, T. Hancox, N. Saghir, J.F. Timms, M.D. Waterfield, Exploring the specificity of the PI3K family inhibitor LY294002, Biochem. J. 404 (2007) 15–21.
[217] C. Sadhu, B. Masinovsky, K. Dick, C.G. Sowell, D.E. Staunton, Essential role of phosphoinositide 3-kinase delta in neutrophil directional movement, J. Immunol. 170 (2003) 2647–2654.
[218] C. Sadhu, K. Dick, W.T. Tino, D.E. Staunton, Selective role of PI3K delta in neutrophil inflammatory responses, Biochem. Biophys. Res. Commun. 308 (2003) 764–769.
[219] P. Sujobert, V. Bardet, P. Cornillet-Lefebvre, J.S. Hayflick, N. Prie, F. Verdier, B. Vanhaesebroeck, O. Muller, F. Pesce, N. Ifrah, M. Hunault-Berger, C. Berthou, B. Villemagne, E. Jourdan, B. Audhuy, E. Solary, B. Witz, J.L. Harousseau, C. Himberlin, T. Lamy, B. Lioure, J.Y. Cahn, F. Dreyfus, P. Mayeux, C. Lacombe, D. Bouscary, Essential role for the p110delta isoform in phosphoinositide 3-kinase activation and cell proliferation in acute myeloid leukemia, Blood 106 (2005) 1063–1066.
[220] C. Billottet, V.L. Grandage, R.E. Gale, A. Quattropani, C. Rommel, B. Vanhaesebroeck, A. Khwaja, A selective inhibitor of the p110delta isoform of PI 3-kinase inhibits AML cell proliferation and survival and increases the cytotoxic effects of VP16, Oncogene 25 (2006) 6648–6659.
[221] Z.A. Knight, B. Gonzalez, M.E. Feldman, E.R. Zunder, D.D. Goldenberg, O. Williams, R. Loewith, D. Stokoe, A. Balla, B. Toth, T. Balla, W.A. Weiss, R.L. Williams, K.M. Shokat, A pharmacological map of the PI3-K family defines a role for p110alpha in insulin signaling, Cell 125 (2006) 733–747.
[222] S.P. Jackson, S.M. Schoenwaelder, I. Goncalves, W.S. Nesbitt, C.L. Yap, C.E. Wright, V. Kenche, K.E. Anderson, S.M. Dopheide, Y. Yuan, S.A. Sturgeon, H. Prabaharan, P.E. Thompson, G.D. Smith, P.R. Shepherd, N. Daniele, S. Kulkarni, B. Abbott, D. Saylik, C. Jones, L. Lu, S. Giuliano, S.C. Hughan, J.A. Angus, A.D. Robertson, H.H. Salem, PI 3-kinase p110beta: a new target for antithrombotic therapy, Nat. Med. 11 (2005) 507–514.
[223] Q.W. Fan, Z.A. Knight, D.D. Goldenberg, W. Yu, K.E. Mostov, D. Stokoe, K.M. Shokat, W.A. Weiss, A dual PI3 kinase/mTOR inhibitor reveals emergent efficacy in glioma, Cancer Cell Int. 9 (2006) 341–349.
[224] F.I. Raynaud, S. Eccles, P.A. Clarke, A. Hayes, B. Nutley, S. Alix, A. Henley, F. Di-Stefano, Z. Ahmad, S. Guillard, L.M. Bjerke, L. Kelland, M. Valenti, L. Patterson, S. Gowan, A. de Haven Brandon, M. Hayakawa, H. Kaizawa, T. Koizumi, T. Ohishi, S. Patel, N. Saghir, P. Parker, M. Waterfield, P. Workman, Pharmacologic characterization of a potent inhibitor of class I phosphatidylinositide 3-kinases, Cancer Res. 67 (2007) 5840–5850.
[225] M. Hayakawa, H. Kaizawa, H. Moritomo, T. Koizumi, T. Ohishi, M. Yamano, M. Okada, M. Ohta, S. Tsukamoto, F.I. Raynaud, P. Workman, M.D. Waterfield, P. Parker, Synthesis and biological evaluation of pyrido[3′,2′:4,5]furo[3,2-*d*]pyrimidine derivatives as novel PI3 kinase p110alpha inhibitors, Bioorg. Med. Chem. Lett. 17 (2007) 2438–2442.
[226] M. Hayakawa, H. Kaizawa, H. Moritomo, T. Koizumi, T. Ohishi, M. Okada, M. Ohta, S. Tsukamoto, P. Parker, P. Workman, M. Waterfield, Synthesis and biological evaluation of 4-morpholino-2-phenylquinazolines and related derivatives as novel PI3 kinase p110alpha inhibitors, Bioorg. Med. Chem. 14 (2006) 6847–6858.
[227] A.M. Condliffe, K. Davidson, K.E. Anderson, C.D. Ellson, T. Crabbe, K. Okkenhaug, B. Vanhaesebroeck, M. Turner, L. Webb, M.P. Wymann, E. Hirsch, T. Ruckle, M. Camps, C. Rommel, S.P. Jackson, E.R. Chilvers, L.R. Stephens, P.T. Hawkins, Sequential activation of class IB and class IA PI3K is important for the primed respiratory burst of human but not murine neutrophils, Blood 106 (2005) 1432–1440.
[228] M. Hayakawa, H. Kaizawa, K. Kawaguchi, N. Ishikawa, T. Koizumi, T. Ohishi, M. Yamano, M. Okada, M. Ohta, S. Tsukamoto, F.I. Raynaud, M.D. Waterfield, P. Parker, P. Workman, Synthesis and biological evaluation of imidazo[1,2-*a*]pyridine derivatives as novel PI3 kinase p110alpha inhibitors, Bioorg. Med. Chem. 15 (2007) 403–412.
[229] V. Pomel, J. Klicic, D. Covini, D.D. Church, J.P. Shaw, K. Roulin, F. Burgat-Charvillon, D. Valognes, M. Camps, C. Chabert, C. Gillieron, B. Francon, D. Perrin, D. Leroy, D. Gretener, A. Nichols, P.A. Vitte, S. Carboni, C. Rommel, M.K. Schwarz, T. Ruckle, Furan-2-ylmethylene thiazolidinediones as novel, potent, and selective inhibitors of phosphoinositide 3-kinase gamma, J. Med. Chem. 49 (2006) 3857–3871.
[230] S. Yaguchi, Y. Fukui, I. Koshimizu, H. Yoshimi, T. Matsuno, H. Gouda, S. Hirono, K. Yamazaki, T. Yamori, Antitumor activity of ZSTK474, a new phosphatidylinositol 3-kinase inhibitor, J. Natl. Cancer Inst. 98 (2006) 545–556.
[231] M.S. Palanki, E. Dneprovskaia, J. Doukas, R.M. Fine, J. Hood, X. Kang, D. Lohse, M. Martin, G. Noronha, R.M. Soll, W. Wrasidlo, S. Yee, H. Zhu, Discovery of 3,3′-(2,4-diaminopteridine-6,7-diyl)diphenol as an isozyme-selective inhibitor of PI3K for the treatment of ischemia reperfusion injury associated with myocardial infarction, J. Med. Chem. 50 (2007) 4279–4294.
[232] J. Yang, A. Shamji, S. Matchacheep, S.L. Schreiber, Identification of a small-molecule inhibitor of class Ia PI3Ks with cell-based screening, Chem. Biol. 14 (2007) 371–377.
[233] S. Volinia, I. Hiles, E. Ormondroyd, D. Nizetic, R. Antonacci, M. Rocchi, M.D. Waterfield, Molecular cloning, cDNA sequence, and chromosomal localization of the human phosphatidylinositol 3-kinase p110 alpha (PIK3CA) gene, Genomics 24 (1994) 472–477.
[234] P. Hu, A. Mondino, E.Y. Skolnik, J. Schlessinger, Cloning of a novel, ubiquitously expressed human phosphatidylinositol 3-kinase and identification of its binding site on p85, Mol. Cell. Biol. 13 (1993) 7677–7688.
[235] B. Stoyanov, S. Volinia, T. Hanck, I. Rubio, M. Loubtchenkov, D. Malek, S. Stoyanova, B. Vanhaesebroeck, R. Dhand, B. Nurnberg, et al., Cloning and characterization of a G protein-activated human phosphoinositide-3 kinase, Science 269 (1995) 690–693.
[236] N. Seki, Y. Nimura, M. Ohira, T. Saito, S. Ichimiya, N. Nomura, A. Nakagawara, Identification and chromosome assignment of a human gene encoding a novel phosphatidylinositol-3 kinase, DNA Res. 4 (1997) 355–358.
[237] B. Vanhaesebroeck, M.J. Welham, K. Kotani, R. Stein, P.H. Warne, M.J. Zvelebil, K. Higashi, S. Volinia, J. Downward, M.D. Waterfield, P110delta, a novel phosphoinositide 3-kinase in leukocytes, Proc. Natl. Acad. Sci. U. S. A. 94 (1997) 4330–4335.
[238] S. Volinia, P. Patracchini, M. Otsu, I. Hiles, I. Gout, E. Calzolari, F. Bernardi, L. Rooke, M.D. Waterfield, Chromosomal localization of human p85 alpha, a subunit of phosphatidylinositol 3-kinase, and its homologue p85 beta, Oncogene 7 (1992) 789–793.
[239] J.W. Janssen, L. Schleithoff, C.R. Bartram, A.S. Schulz, An oncogenic fusion product of the phosphatidylinositol 3-kinase p85beta subunit and

HUMORF8, a putative deubiquitinating enzyme, Oncogene 16 (1998) 1767–1772.
[240] B.R. Dey, R.W. Furlanetto, S.P. Nissley, Cloning of human p55 gamma, a regulatory subunit of phosphatidylinositol 3-kinase, by a yeast two-hybrid library screen with the insulin-like growth factor-I receptor, Gene 209 (1998) 175–183.
[241] L.R. Stephens, A. Eguinoa, H. Erdjument-Bromage, M. Lui, F. Cooke, J. Coadwell, A.S. Smrcka, M. Thelen, K. Cadwallader, P. Tempst, P.T. Hawkins, The G beta gamma sensitivity of a PI3K is dependent upon a tightly associated adaptor, p101, Cell 89 (1997) 105–114.
[242] S. Suire, J. Coadwell, G.J. Ferguson, K. Davidson, P. Hawkins, L. Stephens, p84, a new Gbetagamma-activated regulatory subunit of the type IB phosphoinositide 3-kinase p110gamma, Curr. Biol. 15 (2005) 566–570.
[243] J. Domin, F. Pages, S. Volinia, S.E. Rittenhouse, M.J. Zvelebil, R.C. Stein, M.D. Waterfield, Cloning of a human phosphoinositide 3-kinase with a C2 domain that displays reduced sensitivity to the inhibitor wortmannin, Biochem. J. 326 (1997) 139–147.
[244] R.A. Brown, L.K. Ho, S.J. Weber-Hall, J.M. Shipley, M.J. Fry, Identification and cDNA cloning of a novel mammalian C2 domain-containing phosphoinositide 3-kinase, HsC2-PI3K, Biochem. Biophys. Res. Commun. 233 (1997) 537–544.
[245] M. Rozycka, Y.J. Lu, R.A. Brown, M.R. Lau, J.M. Shipley, M.J. Fry, cDNA cloning of a third human C2-domain-containing class II phosphoinositide 3-kinase, PI3K-C2gamma, and chromosomal assignment of this gene (PIK3C2G) to 12p12, Genomics 54 (1998) 569–574.
[246] S. Volinia, R. Dhand, B. Vanhaesebroeck, L.K. MacDougall, R. Stein, M.J. Zvelebil, J. Domin, C. Panaretou, M.D. Waterfield, A human phosphatidylinositol 3-kinase complex related to the yeast Vps34p-Vps15p protein sorting system, EMBO J. 14 (1995) 3339–3348.
[247] C. Panaretou, J. Domin, S. Cockcroft, M.D. Waterfield, Characterization of p150, an adaptor protein for the human phosphatidylinositol (PtdIns) 3-kinase. Substrate presentation by phosphatidylinositol transfer protein to the p150.Ptdins 3-kinase complex, J. Biol. Chem. 272 (1997) 2477–2485.
[248] K. Wong, L.C. Cantley, Cloning and characterization of a human phosphatidylinositol 4-kinase, J. Biol. Chem. 269 (1994) 28878–28884.
[249] R. Meyers, L.C. Cantley, Cloning and characterization of a wortmannin-sensitive human phosphatidylinositol 4-kinase, J. Biol. Chem. 272 (1997) 4384–4390.
[250] E.J. Brown, M.W. Albers, T.B. Shin, K. Ichikawa, C.T. Keith, W.S. Lane, S.L. Schreiber, A mammalian protein targeted by G1-arresting rapamycin-receptor complex, Nature 369 (1994) 756–758.
[251] J.D. Sipley, J.C. Menninger, K.O. Hartley, D.C. Ward, S.P. Jackson, C.W. Anderson, Gene for the catalytic subunit of the human DNA-activated protein kinase maps to the site of the XRCC7 gene on chromosome 8, Proc. Natl. Acad. Sci. U. S. A. 92 (1995) 7515–7519.
[252] K. Savitsky, A. Bar-Shira, S. Gilad, G. Rotman, Y. Ziv, L. Vanagaite, D.A. Tagle, S. Smith, T. Uziel, S. Sfez, M. Ashkenazi, I. Pecker, M. Frydman, R. Harnik, S.R. Patanjali, A. Simmons, G.A. Clines, A. Sartiel, R.A. Gatti, L. Chessa, O. Sanal, M.F. Lavin, N.G. Jaspers, A.M. Taylor, C.F. Arlett, T. Miki, S.M. Weissman, M. Lovett, F.S. Collins, Y. Shiloh, A single ataxia telangiectasia gene with a product similar to PI-3 kinase, Science 268 (1995) 1749–1753.
[253] K.A. Cimprich, T.B. Shin, C.T. Keith, S.L. Schreiber, cDNA cloning and gene mapping of a candidate human cell cycle checkpoint protein, Proc. Natl. Acad. Sci. U. S. A. 93 (1996) 2850–2855.
[254] M.T. Diaz-Meco, M.M. Municio, P. Sanchez, J. Lozano, J. Moscat, Lambda-interacting protein, a novel protein that specifically interacts with the zinc finger domain of the atypical protein kinase C isotype lambda/iota and stimulates its kinase activity in vitro and in vivo, Mol. Cell. Biol. 16 (1996) 105–114.
[255] A. Yamashita, T. Ohnishi, I. Kashima, Y. Taya, S. Ohno, Human SMG-1, a novel phosphatidylinositol 3-kinase-related protein kinase, associates with components of the mRNA surveillance complex and is involved in the regulation of nonsense-mediated mRNA decay, Genes Dev. 15 (2001) 2215–2228.
[256] S.B. McMahon, H.A. Van Buskirk, K.A. Dugan, T.D. Copeland, M.D. Cole, The novel ATM-related protein TRRAP is an essential cofactor for the c-Myc and E2F oncoproteins, Cell 94 (1998) 363–374.
[257] A. Vassilev, J. Yamauchi, T. Kotani, C. Prives, M.L. Avantaggiati, J. Qin, Y. Nakatani, The 400 kDa subunit of the PCAF histone acetylase complex belongs to the ATM superfamily, Mol. Cell 2 (1998) 869–875.
[258] A. Lau, K.M. Swinbank, P.S. Ahmed, D.L. Taylor, S.P. Jackson, G.C. Smith, M.J. O'Connor, Suppression of HIV-1 infection by a small molecule inhibitor of the ATM kinase, Nat. Cell Biol. 7 (2005) 493–500.
[259] G. Powis, R. Bonjouklian, M.M. Berggren, A. Gallegos, R. Abraham, C. Ashendel, L. Zalkow, W.F. Matter, J. Dodge, G. Grindey, et al., Wortmannin, a potent and selective inhibitor of phosphatidylinositol-3-kinase, Cancer Res. 54 (1994) 2419–2423.
[260] D.A. Fruman, R.E. Meyers, L.C. Cantley, Phosphoinositide kinases, Annu. Rev. Biochem. Allied Res. India 67 (1998) 481–507.
[261] G.C. Smith, S.P. Jackson, The DNA-dependent protein kinase, Genes Dev. 13 (1999) 916–934.
[262] M. Hayakawa, K. Kawaguchi, H. Kaizawa, T. Koizumi, T. Ohishi, M. Yamano, M. Okada, M. Ohta, S. Tsukamoto, F.I. Raynaud, P. Parker, P. Workman, M.D. Waterfield, Synthesis and biological evaluation of sulfonylhydrazone-substituted imidazo[1,2-*a*]pyridines as novel PI3 kinase p110alpha inhibitors, Bioorg. Med. Chem. 15 (2007) 5837–5844.
[263] J.D. Kendall, G.W. Rewcastle, R. Frederick, C. Mawson, W.A. Denny, E. S. Marshall, B.C. Baguley, C. Chaussade, S.P. Jackson, P.R. Shepherd, Synthesis, biological evaluation and molecular modelling of sulfonohydrazides as selective PI3K p110alpha inhibitors, Bioorg. Med. Chem. 15 (2007) 7677–7687.
[264] S. Minogue, J.S. Anderson, M.G. Waugh, M. dos Santos, S. Corless, R. Cramer, J.J. Hsuan, Cloning of a human type II phosphatidylinositol 4-kinase reveals a novel lipid kinase family, J. Biol. Chem. 276 (2001) 16635–16640.
[265] S. Minogue, J.S. Anderson, M.G. Waugh, M. dos Santos, S. Corless, R. Cramer, J.J. Hsuan, Cloning of a human type II phosphatidylinositol 4-kinase reveals a novel lipid kinase family, J. Biol. Chem. 276 (2001) 16635–16640.
[266] A. Balla, G. Tuymetova, M. Barshishat, M. Geiszt, T. Balla, Characterization of type II phosphatidylinositol 4-kinase isoforms reveals association of the enzymes with endosomal vesicular compartments, J. Biol. Chem. 277 (2002) 20041–20050.

2. Research Project

The pharmaceutical development of PI3K inhibitors has made a great leap forward during the last 7 years as described in previous introduction chapter. Promising molecules have entered clinical trials for cancer therapy, inflammation and coronary heart disease. The PI3K pathway clearly presents both a great therapeutic opportunity and a tremendous challenge for cancer therapy. While inhibitor selectivity is often impressive when assessed *in vitro*, the *in vivo* selectivity, potency and efficacy often require further optimization. There are several small molecular weight chemical compounds in clinical development that target the PI3K/Akt signalling pathway for the treatment of cancer. These include dual PI3K-mTOR inhibitors, PI3K inhibitors, Akt inhibitors and mTOR complex catalytic site inhibitors.

The goal of this work was to design and develop novel small molecular weight compounds able to selectively inhibit individual PI3K isoforms or PI3K-related proteins, with the aim to systematically validate these lipid kinases as drug targets in cancer and to proof the anti-cancer potential of novel compounds. Many of the PI3K inhibitors that are currently in clinical development inhibit all of the catalytic subunit isoforms of class IA PI3Ks (p110α, p110β, p110δ) whereas others inhibit only individual isoforms. It was not clear at the beginning of the project whether or not targeting: i) single PI3K isoform, ii) all class I PI3K isoforms, iii) PI3K/mTOR or iv) mTOR will be successful in cancer therapy. To contribute to the answer of this molecular oncology question, we identified the compounds under development by pharmaceutical industry through the intensive patent search and synthesized dual pan-PI3K/mTOR inhibitor PI-103 (Intelectual Property (IP) of *Roche*/*Piramed*, Switzerland/UK) and selective pan-PI3K[a] inhibitor ZSTK474 (IP of *Zenyaku*, Japan) in a multi-gram scale and successfully proved their anti-tumour activity *in vitro* and *in vivo* as well as their selectivity effect on melanoma[b] cancer. Additionally we did an in-depth analysis of >400 patents (~100-300 pages per patent!) with the aim to get an overview of chemical compounds able to inhibit PI3Ks. Representatives from different chemical classes of PI3K inhibitors were selected and compounds from each class were synthesized and activity against the class I PI3Ks measured *in vitro*. Based on this initial screen, a subset representing the most potent and selective agents was selected for further characterization. For most chemotypes, a negative control compound, inactive against all PI3Ks tested, was also synthesized. Through the further synthetic efforts, biological and X-ray characterization we could successfully

[a] pan-PI3K inhibitor means that such compound is able to inhibit class I PI3K family (PI3Kα, PI3Kβ, PI3Kγ, PI3Kδ) but not mTOR, which is a PI3K-related protein with similar catalytic function and structural homology.
[b] Melanoma is a malignant tumor of melanocytes, which are found predominantly in skin but also in the bowel and the eye. It is one of the less common types of skin cancer but causes the majority (75%) of skin cancer related deaths (http://www.aafp.org/afp/20000715/357.html).

obtain the binding mode of many compounds protected by pharmaceutical industry. The gained informations from such unique structure-activity-relationship studies we could successfully apply by developing novel drug discovery strategy, which we called matrix-template strategy, where modern medicinal chemistry techniques were combined with the aim to get novel highly active compounds which should close the gaps in knowledge of the specific function of the different PI3K isoforms.

3. Discussion and Results

3.1. Development of Pyridinylfuropyrimidine Derivatives for Cancer Therapy

Before the first promising results of pyridinylfuropyrimidine lipid kinase inhibitor PI-103 as an anti-cancer agent were published in 2006 [1], [2] we started to encode from Japanese the synthesis of pyridinylfuropyrimidine derivatives from the patent WO0183456A1 of the Japanese pharmaceutical company "Yamanouchi", with the aim to test few selected compounds against melanoma cancer, where the PI3K pathway is constitutively elevated. One of the selected compounds from the Yamanouchi patent was 3-(4-morpholinopyrido[3',2':4,5]furo[3,2-*d*]pyrimidin-2-yl)phenol (today known as PI-103), which we selected according to the previous published results from 2005 by Condliffe and colleagues, where the bioisoster[c] of PI-103, compound YM-024 or *N*-(3-(4-morpholinopyrido[3',2':4,5]furo[3,2-*d*]pyrimidin-2-yl)phenyl)acetamide (Figure 1) was identified as a class I PI3K inhibitor by studing which PI3K isoforms are responsible for modulating neutrophil responsiveness to infection and inflammation [3].

[c] In medicinal chemistry, bioisosteres are substituents or groups with similar physical or chemical properties that impart similar biological properties to a chemical compound. In drug design, the purpose of exchanging one bioisostere for another is to enhance the desired biological or physical properties of a compound without making significant changes in chemical structure. The main use of this term and it techniques are related to pharmaceutical sciences.

(12)特許協力条約に基づいて公開された国際出願

(19) 世界知的所有権機関
国際事務局

(43) 国際公開日
2001 年11 月8 日 (08.11.2001)

PCT

(10) 国際公開番号
WO 01/83456 A1

(51) 国際特許分類7: C07D 215/42, 239/94, 471/04, 491/147, 471/14, 495/14, 413/04, 401/04, 401/12, 409/04, 409/12, 405/04, 405/12, 403/04, 417/12, 487/04, 495/04, 491/048, A61K 31/5377, 31/519, 31/517, 31/541, 31/4355, 31/437, 31/4365, 31/4545, 31/496, A61P 35/00, 43/00

(21) 国際出願番号: PCT/JP01/03650

(22) 国際出願日: 2001 年4 月26 日 (26.04.2001)

(25) 国際出願の言語: 日本語

(26) 国際公開の言語: 日本語

(30) 優先権データ:
特願2000-128472 2000 年4 月27 日 (27.04.2000) JP

(71) 出願人 (米国を除く全ての指定国について): 山之内製薬株式会社 (YAMANOUCHI PHARMACEUTICAL CO., LTD.) [JP/JP]; 〒103-8411 東京都中央区日本橋本町二丁目3番11号 Tokyo (JP). ルードヴィッヒ インスティテュート フォア キャンサー リサーチ (LUDWIG INSTITUTE FOR CANCER RESEARCH) [US/US]; 10158 ニューヨーク州 ニューヨーク サードアベニュー605 New York (US). インペリアル キャンサー リサーチ テクノロジー リミテッド (IMPERIAL CANCER RESEARCH TECHNOLOGY LTD.) [GB/GB]; WC2A 3NL ロンドン サーディニア ストリート サーディニア ハウス London (GB).

(72) 発明者; および
(75) 発明者/出願人 (米国についてのみ): 早川昌彦 (HAYAKAWA, Masahiko) [JP/JP]. 貝沢弘行 (KAIZAWA, Hiroyuki) [JP/JP]. 森友博幸 (MORITOMO, Hiroyuki) [JP/JP]. 川口賀一 (KAWAGUCHI, Ken-ichi) [JP/JP]. 小泉智信 (KOIZUMI, Tomonobu) [JP/JP]. 山野真由美 (YAMANO, Mayumi) [JP/JP]. 松田光陽 (MATSUDA, Koyo) [JP/JP]. 岡田 稔 (OKADA, Minoru) [JP/JP]. 太田光昭 (OHTA, Mitsuaki) [JP/JP]; 〒305-8585 茨城県つくば市御幸が丘21 山之内製薬株式会社内 Ibaraki (JP).

(74) 代理人: 長井省三, 外 (NAGAI, Shozo et al.); 〒174-8612 東京都板橋区蓮根三丁目17番1号 山之内製薬株式会社 特許部内 Tokyo (JP).

(81) 指定国 (国内): AE, AG, AL, AM, AT, AU, AZ, BA, BB, BG, BR, BY, BZ, CA, CH, CN, CO, CR, CU, CZ, DE, DK, DM, DZ, EE, ES, FI, GB, GD, GE, GH, GM, HR, HU, ID, IL, IN, IS, JP, KE, KG, KR, KZ, LC, LK, LR, LS, LT, LU, LV, MA, MD, MG, MK, MN, MW, MX, MZ, NO, NZ, PL, PT, RO, RU, SD, SE, SG, SI, SK, SL, TJ, TM, TR, TT, TZ, UA, UG, US, UZ, VN, YU, ZA, ZW.

(84) 指定国 (広域): ARIPO 特許 (GH, GM, KE, LS, MW, MZ, SD, SL, SZ, TZ, UG, ZW). ユーラシア特許 (AM, AZ, BY, KG, KZ, MD, RU, TJ, TM). ヨーロッパ特許 (AT, BE, CH, CY, DE, DK, ES, FI, FR, GB, GR, IE, IT, LU, MC, NL, PT, SE, TR). OAPI 特許 (BF, BJ, CF, CG, CI, CM, GA, GN, GW, ML, MR, NE, SN, TD, TG).

添付公開書類:
— 国際調査報告書

2文字コード及び他の略語については、定期発行される各PCTガゼットの巻頭に掲載されている「コードと略語のガイダンスノート」を参照。

(54) Title: CONDENSED HETEROARYL DERIVATIVES

(54) 発明の名称: 縮合ヘテロアリール誘導体

(57) Abstract: Medicinal compositions which are useful as phosphatidylinositol 3-kinase (PI3K) inhibitors and anticancer agents; and novel bicyclic or tricyclic condensed heteroaryl derivatives or salts thereof having favorable effects of inhibiting PI3K and suppressing the proliferation of cancer cells.

(57) 要約:

フォスファチジルイノシトール３キナーゼ（PI3K）阻害剤並びに抗癌剤として有用な医薬組成物、並びに、良好なPI3K阻害作用並びに癌細胞増殖抑制作用を有する新規な二環式もしくは三環式縮合ヘテロアリール誘導体又はその塩を提供する。

WO 01/83456 A1

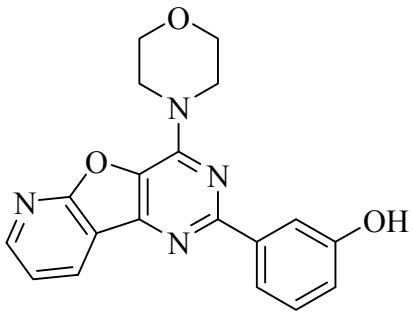

PI-103

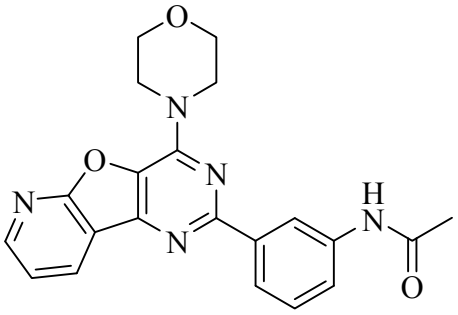

YM-024

Figure 1. Yamanouchi patent WO0183456A1 (left) and selected pyridinylfuropyrimidine derivatives, compounds PI-103 and YM-024 (right), which were synthesized with the aim to explore their anti-cancer activity and their selectivity against class I PI3K isoforms.

3.1.1. Synthesis of Pyridinylfuropyrimidine Derivative PI-103

The commercial available starting material 2-chloropyridine-3-carbonitrile **(1)** was treated with ethyl glycolate under basic conditions in the presence of 3-methylbutanol, where the aminofuropyridine **2** (AS3)[d] was obtained. Amide formation of **2** with 3-methoxybenzoyl chloride yielded the furopyridine **3** (AS7). Further ester hydrolysis of **3** and directly amide formation with methanolic ammonia yielded the amide **4**, which was cyclizated under basic conditions in ethanol after Mhaske and Argade [4] to the pyrimidinone **5** (AS18). Cleavage of the methyl group under acidic conditions, and further protection of the phenol group with acetic anhydride yielded the pyrimidinone **7** (AS21). Further treatment with phosphorus oxychloride ($POCl_3$) gave the chlorinated pyrimidine **8** (AS24), which was substituted on the chlorine position with morpholine to yield the desired compound **9** (PI-103). The same synthetic route could be successfully applied to produce PI-103 in a multi-gram scale (Figure 2) with the aim to explore its activity on *in vivo* cancer models, such as melanoma mice models.

[d] Original codes of the relevant compounds are presented in brackets.

Scheme 1.

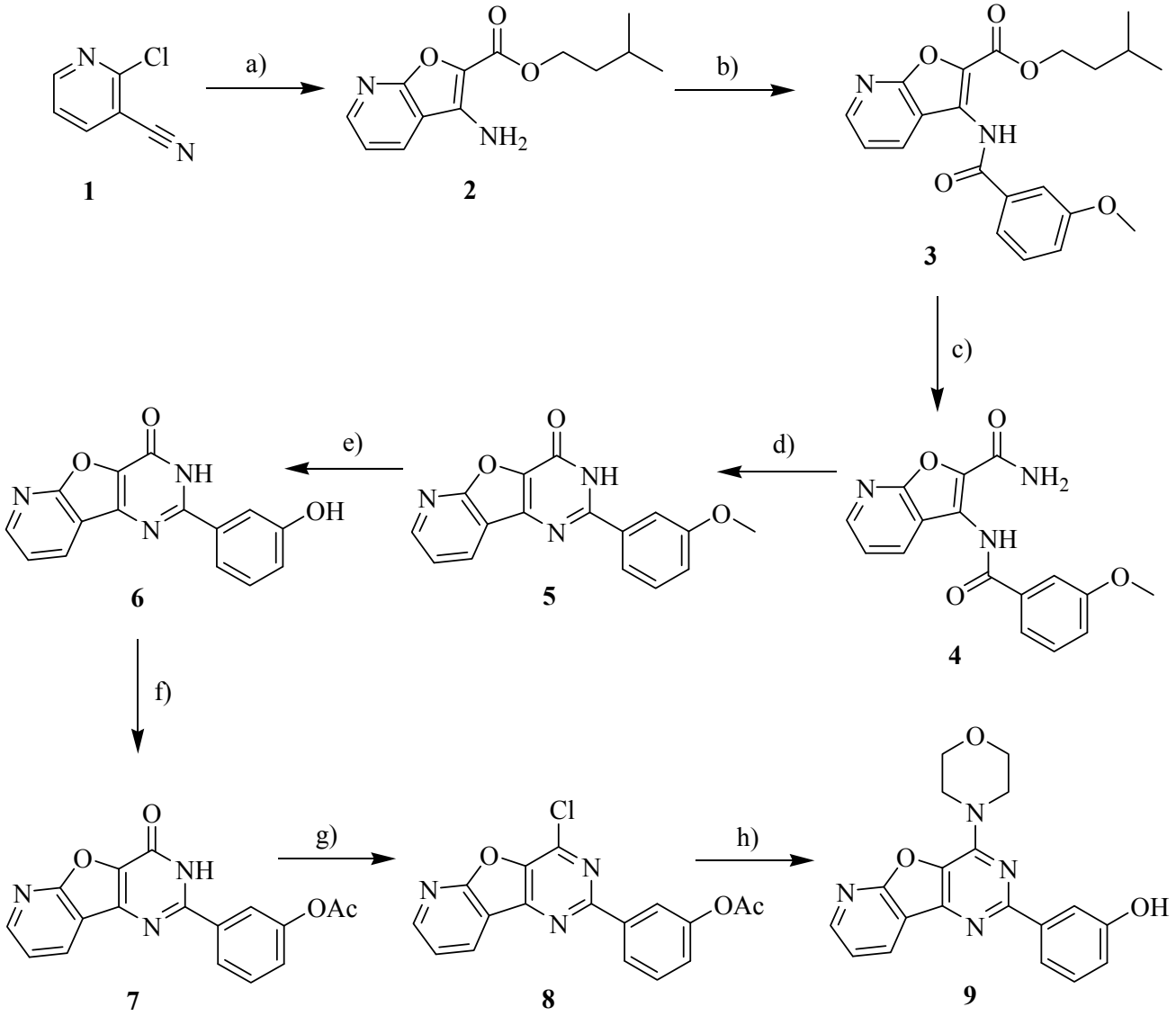

[a]Reagents and conditions: (a) ethyl glycolate (1.1 eq.), Na_2CO_3 (2.0 eq.), 3-methylbutanol, reflux, 72 h, 31%; (b) 3-methoxybenzoyl chloride (1.1 eq.), Et_3N (1.1 eq.), CH_2Cl_2, room temp., 28 h, 86%; (c) $NH_{3(sat.)}$, MeOH, room temp., 4 h, 100%; (d) 5% $NaOH_{(aq.)}$ (10 eq.), EtOH, reflux, 1 h, 90%; (e) $AcOH_{(conc.)}$, $HBr_{(conc.)}$, reflux, 8 h, 100%; (f) Ac_2O (~100 eq.), Et_3N (1.6 eq.), reflux, 1 h, 42%; (g) $POCl_3$ (100 eq.), reflux, 3 h,100%; (h) morpholine ($2.2^{-3.5}$ eq.), n-butanol, 105 °C, 4 h, 40%.

Figure 2. Pressure autoclave with glass tube magnetic drive was used for the multigram-scale synthesis of the inhibitor PI-103.

3.1.2. Biological Activity of PI-103 and its Mechanism of Action

A key challenge in targeting the PI3K family with small molecular weight compounds is to understand how individual PI3K isoforms control normal physiology, as this defines the therapeutic window for targeting a specific isoform. Cell-permeable small molecule inhibitors make it possible to directly assess the phenotypic consequences of inhibiting a kinase with a drug in a physiologically relevant model system.

After successful synthesis of PI-103 its biological activity *in vitro* for each class I PI3K isoform and in different cancer cell lines was proofed. A negative control compound **16**, inactive in tested cells, was also synthesized that differs from the active inhibitor by a single atom substitution (morpholino oxygen was exchanged with the piperidino carbon) (Table 1).

Table 1.

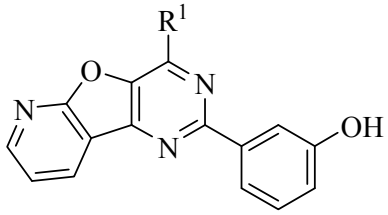

Compds	**R**	***In vitro* PI3Kalpha inhibition at 200nM**	In cell **inhibition**	
			pPKB/PKB 1 µM	**pPKB/PKB 10 µM**
			pS6 1 µM	**pS6 10 µM**
9 (PI-103)	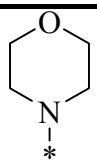	20	++++	++++
			+++	+++
16	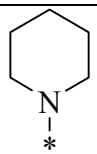	ND	-	-
			-	-

[a]Inhibitor efficacy and their cell permeability were measured by *in cell* Western inhibition assay on melanoma cell line A2058; "-" no activity, "+"/"++" poor activity; "+++" good activity; "++++" very good activity; *in vitro* PI3Kalpha inhibition was measured by *Kinase Glo* assay; given numbers represent %remaining activity, the smaller the value is the stronger is the inhibition.

At the same time the researcher from the University of San Francisko from the competitive lab of Prof. Kevan Shokat published a respectfull paper, where they described a similar synthesis of PI-103 (milligram-scale synthesis) and their observation that PI-103 is the first potent, synthetic

mTOR[e] inhibitor [1]. Additionally the authors found that PI-103 is able to target not only class I PI3K isoforms and mTOR but also DNA-PK[f] with low nanomolar activity, because all three target enzymes share similar sequence identity. To define targets critical for cancers driven by activation of PI3K, Shokat and colleagues screened a panel of potent and structurally divers drug-like molecules that target this enzyme family and found that only compound PI-103 effected proliferative arrest in glioma[g] cells, despite the ability of many other compounds to block PI3K signalling through its downstream effector, Akt (serine/threonine kinase). The unique cellular activity of PI-103 was traced directly to its dual inhibition of PI3K and mTOR.

To proof the anti-tumor effect of PI-103 and its dual nature inhibition we constructed an aggressive B16 mouse melanoma tumor model and administered PI-103 with no obvious toxicity. The anti-tumor effect of PI-103 was compared with the orraly available and also dual PI3K/mTOR inhibitors from pharmaceutical company "Novartis" (Basel, Switzerland), compounds NVP-BAG956, NVP-BBD130, and NVP-BEZ235 (Figure 3). The anti-tumor effect of dual inhibitors was compared with the anti-tumor effect of compound ZSTK474 (IP of pharmaceutical company "Zenyaku", Japan) (Figure 3), which selectively inhibits class I PI3Ks but not mTOR. In conclusion, compounds targeting PI3K and mTOR simultaneously were advantageous to attenuate melanoma growth and they develop their potential by targeting tumor growth directly and indirectly via their interference with angiogenesis [5]. Based on these results, we successfully presented that NVP-BEZ235, which has entered phase I/II clinical trials in patients with advanced solid tumors, has a potential in metastatic melanoma therapy [6]. Although PI-103 did not enter clinical trials due to its poor water solubility and therefore not oral application and its rapid *in vivo* metabolism [7], we showed that this compound has the potential to be very useful as an experimental compound in cancer research in the future, last but not least due to availability of pharmacological data. Moreover, PI-103 represents a lead for further optimization of this novel class of targeted molecular cancer therapeutic.

[e] mTOR or mammalian target of rapamycine is a serine/threonine protein kinase that regulates many cellular processes. It is a PI3K-related protein with similar catalytic activity and structural homology; mTOR is important drug target for cancer therapy.
[f] DNA-PK is DNA dependent protein kinase important for DNA repair.
[g] A glioma is a type of tumor that starts in the brain or spine. It is called a glioma because it arises from glial cells. The most common site of gliomas is the brain.

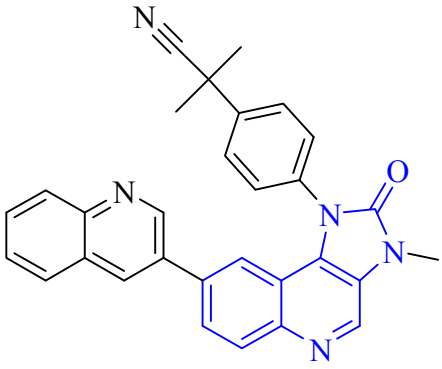

NVP-BEZ235
(Novartis)
Imidazo[4,5-c]quinolin core

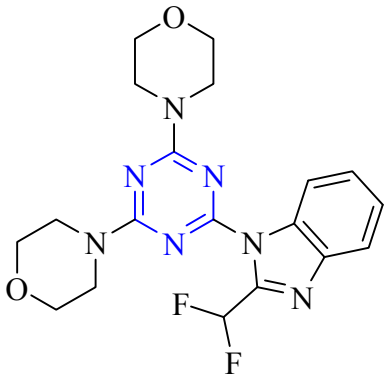

ZSTK474
(Zenyaku)
1,3,5-triazine core

Figure 3. Orally available PI3K/mTOR inhibitor NVP-BEZ235 (in clinical phase I/II) and selective class I PI3K inhibitor ZSTK474. Both molecules were used to study their anti-melanoma potential, which was compared with the anti-cancer potential of PI-103.

Targeting Melanoma with Dual Phosphoinositide 3-Kinase/ Mammalian Target of Rapamycin Inhibitors

Romina Marone,[1] Dominik Erhart,[1] Ann C. Mertz,[1] Thomas Bohnacker,[1] Christian Schnell,[3] Vladimir Cmiljanovic,[2] Frédéric Stauffer,[3] Carlos Garcia-Echeverria,[3] Bernd Giese,[2] Sauveur-Michel Maira,[3] and Matthias P. Wymann[1]

[1]Institute of Biochemistry and Genetics, Department of Biomedicine and [2]Department of Chemistry, University of Basel, and [3]Oncology Disease Area, Novartis Institutes for Biomedical Research, Basel, Switzerland

Abstract

Phosphoinositide 3-kinase (PI3K)/protein kinase B/Akt and Ras/mitogen-activated protein kinase pathways are often constitutively activated in melanoma and have thus been considered as promising drug targets. Exposure of melanoma cells to NVP-BAG956, NVP-BBD130, and NVP-BEZ235, a series of novel, potent, and stable dual PI3K/ mammalian target of rapamycin (mTOR) inhibitors, resulted in complete G1 growth arrest, reduction of cyclin D1, and increased levels of $p27^{KIP1}$, but negligible apoptosis. In contrast, treatment of melanoma with the pan-class I PI3K inhibitor ZSTK474 or the mTORC1 inhibitor rapamycin resulted only in minor reduction of cell proliferation. In a syngeneic B16 mouse melanoma tumor model, orally administered NVP-BBD130 and NVP-BEZ235 efficiently attenuated tumor growth at primary and lymph node metastatic sites with no obvious toxicity. Metastatic melanoma in inhibitor-treated mice displayed reduced numbers of proliferating and significantly smaller tumor cells. In addition, neovascularization was blocked and tumoral necrosis increased when compared with vehicle-treated mice. In conclusion, compounds targeting PI3K and mTOR simultaneously were advantageous to attenuate melanoma growth and they develop their potential by targeting tumor growth directly, and indirectly via their interference with angiogenesis. Based on the above results, NVP-BEZ235, which has entered phase I/II clinical trials in patients with advanced solid tumors, has a potential in metastatic melanoma therapy.
(Mol Cancer Res 2009;7(4):601–13)

Introduction

Cancer cells evolve from a benign, noninvasive state to metastatic tumors, which grow and proliferate aggressively and display diminished cell death out of their normal tissue context. This process is driven by the accumulation of genetic and epigenetic alterations (1), which leads to sustained inputs into multiple signal transduction pathways. Activation of phosphoinositide 3-kinase (PI3K) is a prominent relay to tumor growth as it promotes increase in cell mass and cell cycle entry, counteracts apoptosis, modulates cytoskeletal rearrangements, and enhances cell migration (2-4).

Excess growth factor expression, constitutively activated protein tyrosine kinase receptors (e.g., epidermal growth factor receptor, c-kit, platelet-derived growth factor receptor, Met), oncogenic Ras, loss of phosphatase and tensin homologue deleted in chromosome 10 (PTEN), and mutated PI3K can lead to an increase in the levels of the PI3K product PtdIns(3,4,5)P_3. The latter serves as a docking site for pleckstrin homology domain-containing proteins such as protein kinase B (PKB/ Akt) and guanine nucleotide exchange factors feeding into growth and metastasis (3, 5). A major output of PKB/Akt activation is the phosphorylation of tuberin in the tuberous sclerosis complex (TSC1/2), which releases the TSC1/ 2→Rheb→mammalian target of rapamycin (mTOR) pathway and leads to increased translation and transcription (6).

Metastatic melanoma is a tumor with an exceptionally bad prognosis. Melanoma display already at early stages often mutated B-Raf (V600E; 66%) or constitutively activated N-Ras (mutation Q61K/L/R, 20%). An increase in tumor aggressiveness is observed in metastatic melanoma, which often correlates with the loss of PTEN (up to 60%) or up-regulation of PKBγ/ Akt3 (43-67%). Mutations of PI3K itself, as observed in other tumors for PI3Kα (PIK3CA; ref. 7), are rare in cutaneous melanoma (8, 9); however, the PI3Kα protein was found to be up-regulated (10). Occasional mutations found in STK11/LKB1 (11) could also contribute to the activation of mTOR independent from PI3K in melanoma. Therefore, the Ras/mitogen-activated protein kinase (MAPK) and PI3K/mTOR signaling pathways were proposed as promising drug targets for the treatment of advanced melanoma (12).

Clinical trials targeting the MAPK pathway (single therapy with the B-Raf inhibitor sorafenib/Nexavar/BAY 43-9006; ref. 13) did not yield significant success in melanoma despite beneficial effects of sorafenib in the treatment of renal cell carcinoma (14). Now sorafenib is in clinical trials in combination with bevacizumab (Avastin), and other Raf inhibitors also entered clinical trials (PLX4032, Plexxikon; Raf265, Novartis). Trials with rapamycin derivatives targeting mTOR (CCI-779/temsirolimus, Wyeth) in melanoma had to be concluded too due to inefficacy (15). New clinical

Received 8/4/08; revised 11/7/08; accepted 12/14/08; published online 4/16/09.
Grant support: Swiss Cancer League (01924-08-2006), Swiss National Science Foundation (3100A0-109718), and EU FP6 programme EU LSHG-CT-2003-502935/BBW 03.0441-3 (M.P. Wymann).
The costs of publication of this article were defrayed in part by the payment of page charges. This article must therefore be hereby marked *advertisement* in accordance with 18 U.S.C. Section 1734 solely to indicate this fact.
Note: Supplementary data for this article are available at Molecular Cancer Research Online (http://mcr.aacrjournals.org/).
Matthias P. Wymann, Institute of Biochemistry and Genetics, Department of Biomedicine, University of Basel, Mattenstrasse 28, CH-4058 Basel, Switzerland. Phone: 41-61-695-3046; Fax: 41-61-267-3566. E-mail: Matthias.Wymann@UniBas.CH

doi:10.1158/1541-7786.MCR-08-0366

trials targeting Raf and mTOR simultaneously have been initiated recently.[4]

In preclinical models, the PI3K pathway was initially targeted with LY294002, a PI3K inhibitor with low potency, low specificity, and high toxicity (16). LY294002 and wortmannin inhibit the whole PI3K family and related proteins, including mTOR, PI4K, DNA-PK (17), and Polo-like kinases (18). Improvements in PI3K inhibitor potency and selectivity were made with the pyridofuropyrimidine PI103 (19-21), and, recently, the first orally administered pan-PI3K inhibitor ZSTK474 was presented (22, 23).

Here, we report for the first time in melanoma the action of PI3K/mTOR inhibitors with drug-like properties, including NVP-BEZ235, which has entered phase I/II clinical studies for patients with advanced solid malignancies. Our results reported herein provide a basis for the evaluation and rational of action of PI3K pathway targeting in solid tumors and document a significant efficiency and insignificant adverse effects of the compounds used.

Results

Dual PI3K/mTOR Inhibitors Block Proliferation of Melanoma Cells

Melanoma cells often show constitutive activation of the PI3K pathway due to mutations and attenuation of the phosphatase PTEN or changes in PKBγ expression. Here, a collection of human melanoma cell lines generated from different tumor stages and three mouse melanoma lines of the B16 family were used to investigate the susceptibility of melanoma to PI3K pathway inhibition. Currently, the effect of PI3K inhibition on cell proliferation is controversial (12, 22, 24-27); therefore, we first reevaluated the effect of the classic PI3K inhibitors wortmannin and LY294002. When cells were exposed to a single dose of inhibitor for 3 days, wortmannin was ineffective due to its limited stability (Fig. 1A and B). A set of newly identified, ATP-competitive PI3K/mTOR inhibitors, NVP-BAG956, NVP-BBD130, and NVP-BEZ235 (see Table 1; Supplementary Fig. S1; refs. 28, 29), showed a long-term effect on melanoma cell proliferation, superior to even much elevated concentrations of LY294002 (Fig. 1A and B). NVP compounds prevented growth (<20% of normal growth) in >85% of the tested melanoma lines, independent of the status of PTEN and BRaf (Supplementary Table S1) or the tumor stage the cells were derived from. The arrest in proliferation correlated with a reduction in cellular and nuclear size (data not shown). Interestingly, inhibitor-treated cells were able to reenter proliferation at a reduced rate and to gain normal cell volume when NVP-BAG956 and NVP-BEZ235 were removed, whereas cells exposed to NVP-BBD130 were arrested for up to 10 days and remained small (7 days in the absence of inhibitor; see Supplementary Fig. S2). Although in prolonged stasis, no significant cell death was observed.

To understand the mode of action of these novel compounds, we performed time course– and concentration-dependent experiments using malignant, aggressively growing cell lines, such as A2058, which have constitutively activated PI3K/PKB/Akt (Fig. 1C) and MAPK pathways (see Supplementary Fig. S3). All used PI3K inhibitors decreased phosphorylation of PKB/Akt, whereas the phosphorylation status of MAPK was not affected. The effect of wortmannin was short lived; levels of phosphorylated PKB/Akt were back to normal 2 to 4 hours after treatment. In the case of LY294002, the PKB/Akt phosphorylation was restored after 1 day. In contrast, a single addition of NVP compounds caused very prominent and prolonged dephosphorylation of PKB/Akt, even in melanoma showing PI3K inhibitor-resistant proliferation (e.g., C32; see Fig. 1A and C). The potency of the three novel inhibitors to block phosphorylation of PKB/Akt in A2058 cells was in the nmol/L range (IC_{50} value for NVP-BBD130 was 11 ± 4.6 nmol/L, for NVP-BEZ235 18 ± 6.4 nmol/L, and for NVP-BAG956 67 ± 25 nmol/L; Fig. 1D). In addition, inhibition of PKB/Akt phosphorylation correlated with loss of A2058 cell proliferation for NVP-BBD130 and NVP-BEZ235 (IC_{50} for NVP-BBD130 was 34 ± 2.6 nmol/L and for NVP-BEZ235 was 26 ± 2.5 nmol/L), whereas more of NVP-BAG956 was required to hinder proliferation (IC_{50} was 290 ± 20 nmol/L; see Fig. 1E). Altogether, when compared with the established compounds, the novel inhibitors exert prolonged action with superior stability in complex medium.

G1 Cell Cycle Arrest of Melanoma Cells Upon Treatment with PI3K/mTOR Inhibitors

The effect of PI3K inhibitors on the cell cycle is shown here in detail for A2058 melanoma cells (Fig. 2; more melanoma lines in Supplementary Table S2): Melanoma treated with wortmannin and LY294002 showed no significant shifts in cell cycle profiles compared with nontreated cells, whereas PC3M cells, which are very sensitive to PI3K inhibitors (Supplementary Fig. S4A; refs. 30-32), displayed a prominent cell cycle arrest in G1 with LY294002. NVP-BAG956, NVP-BBD130, and NVP-BEZ235 resulted in a complete arrest of most tumor cells in G1, which correlated with a lack of proliferation and DNA replication (as measured by [^{3}H]thymidine incorporation; Fig. 2B). PI3K inhibitor–resistant proliferation was observed in C32 melanomas, which consequently also showed no G1 arrest (Fig. 1A; Supplementary Table S2). Moreover, PI3K inhibition did not induce evident signs of apoptosis as monitored by the absence of sub-G1 peaks (Fig. 2A and data not shown) and Annexin V–positive cells (Supplementary Fig. S4B; Supplementary Table S2). PI3K/mTOR inhibitors thus have cytostatic, but no cytotoxic, effects on melanoma cells.

Cell cycle progression is regulated by the oscillating expression of cyclins and the inhibition of specific cyclin/cyclin-dependent kinase (Cdk) complexes by Cdk inhibitors. Expression of cyclin D1 is down-regulated in A2058 cells treated with NVP compounds and is somewhat reduced by treatment with LY294002 (Fig. 2C). A minor decrease in cyclin D1 was observed in control and wortmannin-treated cells, as they reached confluence at later stages. In inhibitor-resistant C32 cells, PI3K/mTOR inhibition caused compound-dependent elevations in cyclin D1 levels (Fig. 2C). Similarly, $p27^{Kip1}$ expression was clearly induced by NVP-BAG956, NVP-BBD130, and NVP-BEZ235 in A2058 cells but not in C32 cells.

To investigate stringency and rapidity of the cell cycle arrest in G1 induced by PI3K pathway inhibition, A2058 cells were synchronized with the microtubule disruptor nocodazole in G2-M and released subsequently in the presence of vehicle

[4] http://www.clinicaltrials.gov

or PI3K inhibitors: (*a*) the initial treatment with nocodazole arrested cells in G2-M (from 30% to 60% of cells in G2-M; Fig. 2D); (*b*) after nocodazole removal, control and wortmannin-treated cells showed a profile typical of proliferating cells after 24 h, whereas cells exposed to LY294002 required 48 h to restart proliferation. In the presence of NVP-BAG956, NVP-BBD130, or NVP-BEZ235, A2058 cells were only able to exit G2-M and then remained in G1 (Fig. 2D).

Primary and Metastatic Tumors Require the PI3K Pathway for Growth In vivo

To evaluate the efficacy of different PI3K/mTOR inhibitors *in vivo*, we used a syngeneic B16BL6 mouse melanoma model, in which cells, injected intradermally in both ears, rapidly progress to primary tumors and cervical lymph node metastasis. Treatment with vehicle control, PI3K/mTOR inhibitors, and a vascular endothelial growth factor receptor (VEGFR) protein tyrosine kinase inhibitor (PTK787) were started 7 days following tumor inoculation. A ~60% reduction in the primary tumor size was achieved with different doses and regimens of NVP-BBD130, NVP-BEZ235 and PI103 (Fig. 3A), and PTK787 (data not shown). Moreover, mice treated with NVP-BBD130, NVP-BEZ235, or PTK787 showed a significant reduction in the size of the cervical lymph node metastasis (Fig. 3B; PTK787: data not shown). For NVP-BBD130, tumor and metastasis size reduction correlated with a stringent reduction in the amount of phosphorylated PKB/Akt and $p70^{S6K}$ 2 hours after the last treatment (Fig. 4A). A partial recovery to basal level was seen after 16 hours. In addition, reduced expression of cyclin D1 and increased levels of $p27^{Kip1}$ were detected in metastatic tissue 2 hours after dosing (Fig. 4B). Intriguingly, treatment with PI103 at the concentration used here did not significantly reduce the mass of lymph node metastasis (Fig. 3B), which was in agreement with overshooting signals for phosphorylated PKB/Akt and $p70^{S6K}$ in primary and metastatic tumor tissue (Fig. 4A). As PI103 is cleared rapidly from the tumor (half life <2 hours; see ref. 20), these elevated and dose-dependent signals could represent a release of feedback loops in the PI3K/mTOR signaling system.

A closer analysis of metastatic sections revealed that cell size was decreased in tumor tissue from inhibitor-treated animals (Fig. 5A), but not in hepatocytes of the same mice. This is encouraging, as liver cell size dynamically responds to starvation and the current PI3K/mTOR treatment regimen seems not to fully mimic nutrient deprivation. Plasma levels of liver marker enzymes and proteins were also not significantly affected by the treatment with PI3K/mTOR inhibitors (except alanine aminotransferase; see Supplementary Table S3). Interestingly, PI3K inhibitor–mediated reduction in cell size went along with a decreased mitotic index (Fig. 5B). The few remaining mitotic cells were usually located around preexisting, large blood vessels. In addition to reduced cell proliferation, metastatic tissue from mice treated with NVP-BEZ235 displayed significantly increased necrosis levels compared with tumors from vehicle control–treated mice (Fig. 5C).

To survive and grow, tumors with a diameter larger than 1 mm require blood vessels to be fully supplied with nutrients and oxygen. Staining of metastatic sections for the endothelial cell marker CD31 revealed that NVP-BBD130 and NVP-BEZ235 completely abrogated neoangiogenesis in metastatic tissue, whereas vehicle control–, PI103-, or PTK787-treated tumors displayed a well-developed microvasculature (Fig. 6A; quantification in Fig. 6B). Large and preexisting blood vessels at the tumor border remained unaffected by all treatments (data not shown). Altogether, the above results show that the novel NVP compounds have a direct effect on tumor cell growth and proliferation, and exert, in addition, antiangiogenic effects supporting tumor necrosis.

PI3K/mTOR Inhibitors Are Well Tolerated

Tumor-bearing mice showed a disease-related drop in body weight by 5% to 10% and had >2-fold enlarged spleens when compared with healthy controls (Table 2). PI3K inhibitor–treated animals showed a less dramatic increase in spleen size and an overall tendency to regain body weight, reaching significance for PTK787 and NVP-BEZ235 (data not shown). The collected data illustrate that the tumor per se causes dramatic systemic changes, which were partially reversed by PI3K/mTOR inhibition. Interference with insulin-mediated glucose uptake also seemed negligible, as blood glucose levels did not significantly increase over concentrations determined in healthy and vehicle control–treated animals (Table 2).

PI3K and mTOR have been reported to play important roles in the immune system. Spleen and bone marrow of NVP-BBD130– and PI103-treated mice were therefore analyzed for adverse effects on immune cells. Tumor-bearing, vehicle control–treated mice displayed a reduction in the number of $CD3^+$ T cells, B cells, and natural killer cells, compared with healthy animals (Supplementary Table S4), and NVP-BBD130 treatment decreased lymphocyte counts in a statistically insignificant manner. Interestingly, treatment with PI103 resulted in an increase in the number of T cells, B cells, and natural killer cells back to levels similar to healthy control animals. Granulocytes, macrophages, and erythroid cell numbers were normal in the bone marrow of all tumor-bearing mice, and there was no indication that the applied PI3K/mTOR inhibitors interfered with hematopoiesis.

Cooperation of PI3K and mTOR in Melanoma Cell Proliferation

To discriminate between the importance of PI3K and mTOR, we ectopically expressed a constitutively active PKB/Akt (myristoylated PKB, Myr-PKB; ref. 33) to partially bypass the inhibitor-mediated block in PI3K signaling. To monitor PKB/Akt action, we used the mTOR-independent nuclear to cytoplasmic translocation of forkhead transcription factors (FOXO), which feed negatively into cell cycle progression and antiapoptotic events (34, 35). Nonphosphorylated FOXOs are localized to the nucleus but are retained in the cytoplasm when phosphorylated by PKB/Akt. In A2058 cells, PKB/Akt is maintained activated in a PI3K-dependent manner even in serum-free conditions, mainly due to the lack of the lipid phosphatase PTEN. As a consequence, ectopically expressed FOXO1 is quantitatively localized in the cytoplasm. Treatment of A2058 cells with NVP compounds caused a rapid inactivation of PKB/Akt and a subsequent translocation of FOXO1 to the nucleus (Fig. 7A). Stable expression of Myr-PKB in A2058

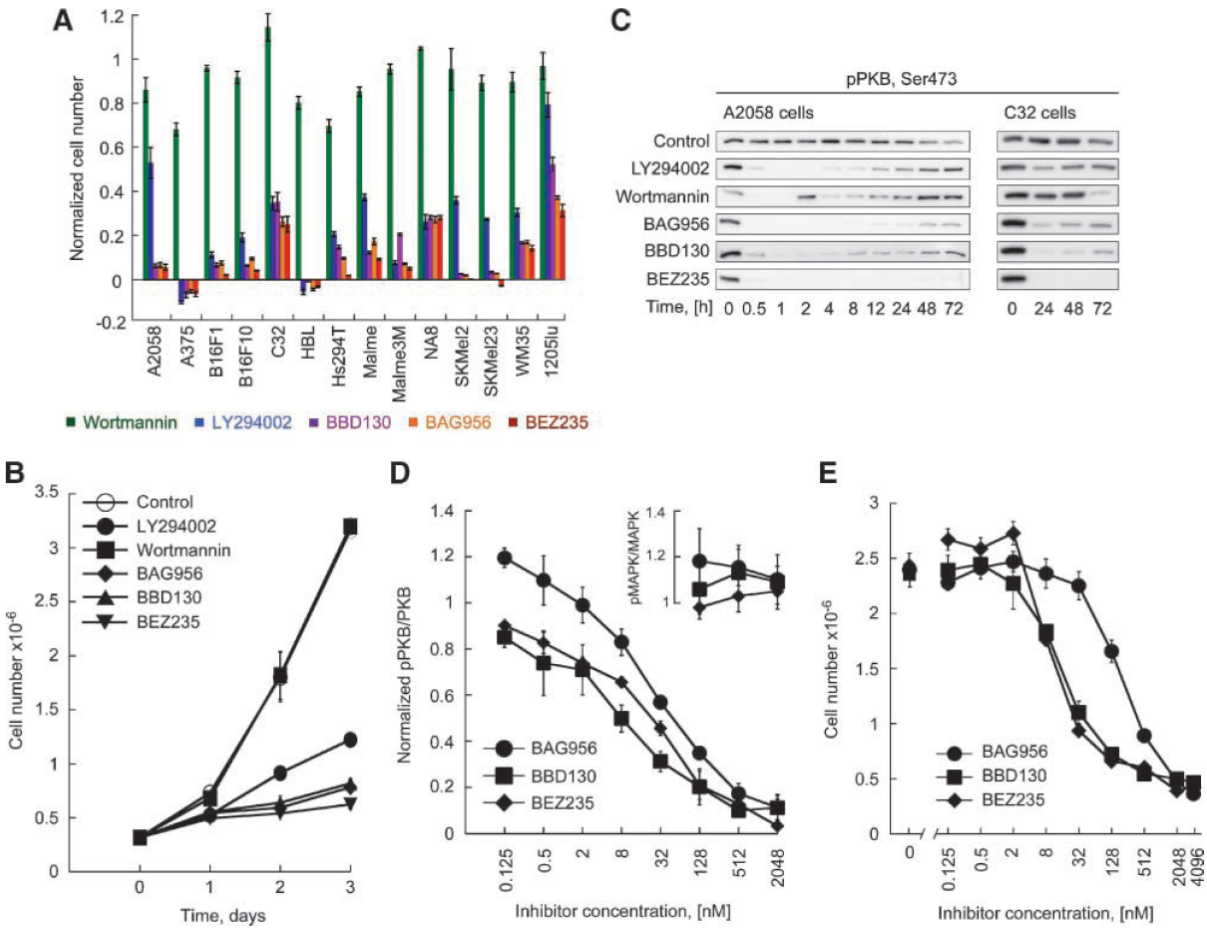

FIGURE 1. PI3K inhibitors affect proliferation and downstream signaling in melanoma cells. **A.** Antiproliferative effect of PI3K inhibitors. Melanoma cells were exposed to the indicated inhibitors (LY294002 at 25 μmol/L; wortmannin at 500 nmol/L; NVP-BAG956, NVP-BBD130, and NVP-BEZ235 at 1 μmol/L) for 3 d before cell numbers were determined. Cell numbers are depicted after the subtraction of initially seeded cells in relation to nontreated controls (ratio of treated over nontreated cultures). Columns, mean of triplicates; bars, SE. **B.** Time-dependent A2058 proliferation in the presence of PI3K inhibitors. A2058 cells were exposed to PI3K inhibitors at day 0 before cells were counted at the indicated time intervals. Points, mean of triplicates; bars, SE. **C.** Prolonged changes in phosphorylation of PKB/Akt upon PI3K inhibition. Phosphorylated PKB as detected in total cell lysates of A2058 and C32 cells treated with PI3K inhibitors for the indicated intervals are shown. An extended version of the figure is presented in Supplementary Fig. S3. **D.** Concentration-dependent inhibition of PKB phosphorylation. A2058 cells were exposed for 3 h to increasing concentrations of NVP-BAG956, NVP-BBD130, and NVP-BEZ235. Total cell lysates were subjected to immunoblotting for total and phosphorylated PKB or MAPK. Emerging signals were quantified using fluorescent secondary antibodies, and ratios of phosphosphorylated over nonphosphorylated kinases are displayed. Points, mean ($n > 3$); bars, SE. **E.** Inhibitory activity of PI3K inhibitors against melanoma cell proliferation. A2058 cells were treated at day 0 with increasing concentrations of NVP-BAG956, NVP-BBD130, and NVP-BEZ235. Cell proliferation was evaluated 3 d later. Points, mean of triplicates; bars, SE.

was sufficient to prevent nuclear translocation of exogenous FOXO1 in the presence of PI3K inhibitors, but did not rescue proliferation in the presence of, e.g., NVP-BEZ235 (Fig. 7B).

In serum-deprived HEK293 cells, Myr-PKB reconstituted phosphorylation of FOXO and GSK3β and also fed into mTOR signaling with phosphorylated $p70^{S6K}$, S6, and 4E-BP1 as readouts (Supplementary Fig. S5). Whereas FOXO and GSK-3β phosphorylation was to a large extent PI3K inhibitor resistant, signals downstream of mTOR were completely abrogated by NVP-BAG956, NVP-BBD130, NVP-BEZ235, and PI103, as well as by the mTORC1 inhibitor rapamycin. This corroborates mTOR inhibition by NVP compounds observed in TSC1 knockout mouse embryonic fibroblasts (Table 1; see ref. 28).

Recently, a selective pan-PI3K inhibitor without activity against mTOR (ZSTK474) was shown to block tumor cell growth with an overall 50% sensitivity rate (22, 23). To evaluate the requirement of a dual PI3K and mTOR inhibition to target melanoma, cells were comparatively exposed to NVP-BEZ235, ZSTK474, and/or rapamycin. The obtained results clearly illustrate that targeting either PI3K or mTOR in isolation can attenuate growth and proliferation of particularly sensitive cells (e.g., A375), whereas more resistant melanoma are only affected by the simultaneous targeting of PI3K and mTOR (Fig. 8A). Treatment of melanoma cells with a combination of ZSTK474 and rapamycin results in a more pronounced proliferation arrest compared with single compounds. The

differential modulation of the phosphorylation status of PKB and $p70^{S6K}$ by the various inhibitors in sensitive and more resistant cell lines shows that the degree of the coupling of PI3K to mTOR varies, and a retained activation of mTOR in the presence of PI3K inhibitor (as, e.g., in 1205lu cells; Fig. 8B) requires an efficient PI3K/mTOR dual-mode inhibitor to attenuate growth.

Discussion

The recognition that the PI3K pathway has gained as a putative target in cancer therapy (2-4) is reflected by a recent increase in patent literature covering novel PI3K inhibitors (36, 37) and documents the need for compounds with improved stability, efficacy, and potency. The newly developed series of ATP-competitive PI3K/mTOR inhibitors (28, 29), NVP-BAG956, NVP-BBD130, and NVP-BEZ235, fit these criteria, and NVP-BEZ235 has recently entered clinical trials. NVP-BEZ235 (28) and NVP-BBD130 (Supplementary Fig. S6) have advantageous pharmacologic profiles and show a high and sustained exposure in tumor tissue *in vivo*. Neither their effects in aggressive, metastatic tumors in syngeneic models nor the requirement of a dual inhibition of PI3K and mTOR was studied thus far.

Table 1. *In vitro* Inhibitory Activities of NVP Compounds and ZSTK474

A

Kinase type	Enzyme	NVP-BAG956 IC_{50} (μmol/L)	NVP-BBD130 IC_{50} (μmol/L)	NVP-BEZ235* IC_{50} (μmol/L)
Receptor TK	VEGFR1	2.56 ± 0.56	>10	>10
	Flt3	>10	>10	>10
	EGFR (HER1)	>10	>10	>10
	IGF1-R	>10	>10	>10
	EphB4	>10	>10	>10
	Ret	>10	>10	>10
	Tie-2 (Tek)	>10	>10	>10
	c-Met	>10	>10	>10
	FGFR-K650E	>10	>10	>10
Cytosolic TK	Fak	>10	>10	>10
	Jak2	>10	>10	>10
	c-Abl	>10	>10	>10
	c-Src	>10	>10	>10
Cytosolic S/TK	PKA	>10	>10	>10
	Akt (PKB)	>10	>10	>10
	PDK1†	0.24/0.26	>10	>10
	B-Raf–V600E	>10	>10	>10

B

	NVP-BAG956 IC_{50} (nmol/L)	NVP-BBD130 IC_{50} (nmol/L)	NVP-BEZ235* IC_{50} (nmol/L)	ZSTK474‡ IC_{50} (nmol/L)	PI103§ IC_{50} (nmol/L)
PI3Kα	56/56	72/71	4 ± 2	16	2/8
PI3Kβ	444/446	2,340/2,336	75 ± 45	44	3/88
PI3Kδ	34/35	201/201	7 ± 6	4.6	3/48
PI3Kγ	117/112	382/350	5 ± 4	49	15/150
mTOR	n.d.	n.d. [7.7]‖	20.7 [6.5]‖	>100,000	20-83

NOTE: *In vitro* activities of BAG956, BBD130, BEZ235, and ZSTK474. *In vitro* kinase assays were done with the indicated recombinant purified kinases in the presence of increasing concentration of the inhibitors (53).
Abbreviation: n.d., not determined.
*See Maira et al. (28).
†See Stauffer et al. (29).
‡See Kong and Yamori (23).
§See Fan et al. (19), Knight et al. (54), and Raynaud et al. (20).
‖Values in square brackets correspond to IC_{50} values obtained in TSC1 null mouse embryonic fibroblasts using phospho-S6 as output.

Incubation of asynchronously growing melanoma cells with NVP compounds resulted in a complete loss of PKB/Akt phosphorylation and induced growth arrest, but not apoptosis, which is in agreement with earlier reports for PI3K pathway inhibitors (12, 22, 26). The observed growth arrest was dose dependent and correlated with the loss of phosphorylation of PKB/Akt. Cells accumulated in the G1 cell cycle phase showing upregulation of the cell cycle inhibitor $p27^{Kip1}$, reduction in cyclin D1 levels, and a complete block of DNA synthesis. In all cell lines tested here, the effect of NVP compounds on cell proliferation was superior and prolonged when compared with the action of LY294002 and wortmannin. A small fraction of the cells tested responded only partially to PI3K/mTOR inhibition and consequently did not show a G1 arrest or changes in $p27^{Kip1}$. Increased cellular cyclin D1 has been previously associated with poor prognosis in many cancers and has also been reported to correlate with B-Raf inhibitor resistance in melanoma (38). Further studies will be required to determine if the inhibitor-induced increase in cyclin D1 levels depicted in C32 cells confers resistance to PI3K/mTOR inhibition in a general sense. Similarly, the low expression or mutation of the lipid phosphatase PTEN, a constitutive activation of the PI3K pathway, the presence of mutated Ras or Raf, or the p53 status cannot be currently translated into a reliable pattern to predict sensitivity of melanoma to PI3K/mTOR inhibition.

To assess the *in vivo* activity of NVP-BBD130 and NVP-BEZ235, a B16 melanoma model was used: This syngeneic mouse model allows the evaluation of pharmacologic effects on the progress of an aggressive primary tumor and the precise quantification of a secondary metastatic lymph node tumor. Moreover, other than in xenograft models, mice have here an intact immune system and the effects of drugs on immune cell counts can be monitored. This is important as melanoma patients mount spontaneous T cell–dependent responses against their tumor, which correlate with patient survival (39). One might thus anticipate that optimal treatment should not interfere with antitumoral immune responses.

NVP-BBD130 and NVP-BEZ235 could be administered orally and have excellent pharmacologic properties, whereas PI103 required i.p. application. Treatment of mice with different doses and regimens of inhibitors resulted in a ~60% reduction of the primary tumors independently of the inhibitor used. Size of lymph node metastasis was also greatly reduced in mice treated with NVP-BBD130 and NVP-BEZ235, whereas treatment with PI103 (10 mg/kg/d) had insignificant effects on the mass of metastasis. In a first report, Fan et al. (19) obtained an antitumoral activity of PI103 in glioma xenografts with doses as low as 5 mg/kg/d. In contrast, Raynaud et al. (20) used the same glioma tumor model and achieved comparable results only at 100 mg/kg/d and recently Chen et al. (21) showed that PI103 at 10 mg/kg/d was not efficacious as a single agent in a different glioblastoma model. In the melanoma model used

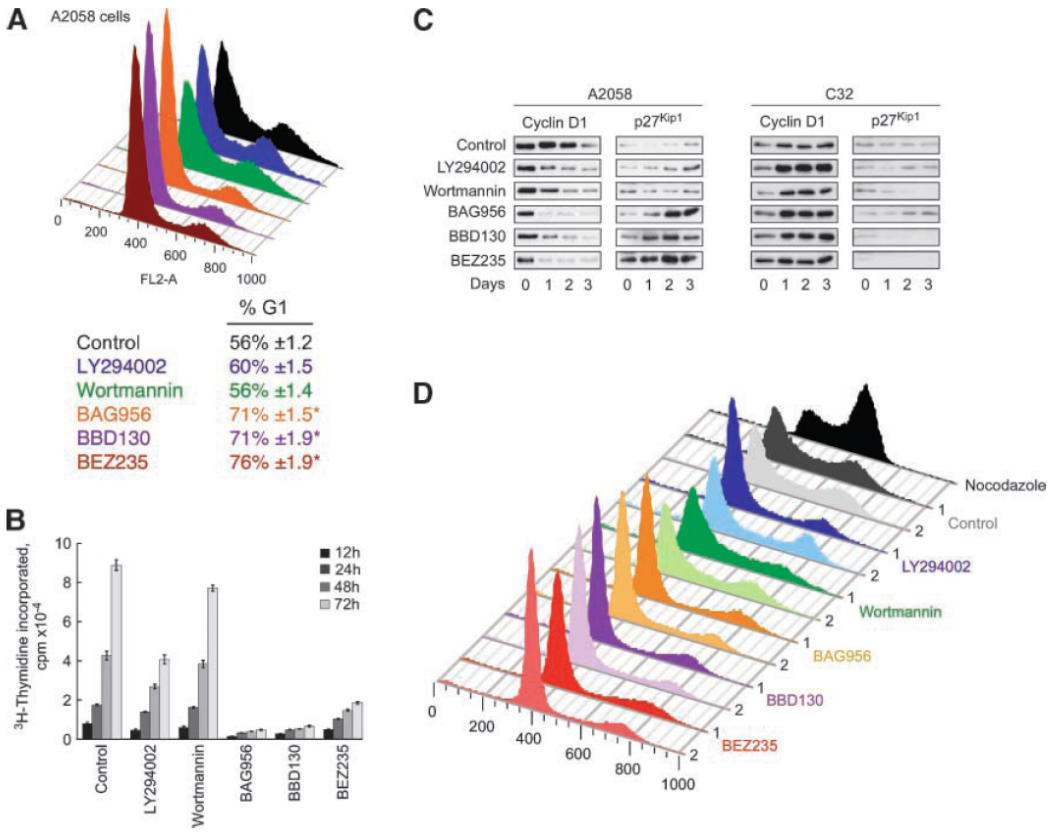

FIGURE 2. PI3K pathway inhibition causes growth arrest in G1 in melanoma. **A.** Determination of cell cycle profile changes by PI3K inhibitor treatment. A2058 melanoma cells were exposed to PI3K inhibitors for 3 d. Subsequently, the cell cycle profile was evaluated by fluorescence-activated cell sorting using propidium iodide staining. For more cell lines, see Supplementary Table S2. *, $P < 0.002$. **B.** PI3K and DNA replication. [^{3}H]thymidine incorporation into DNA was assessed in A2058 treated as above. Columns, mean ($n = 6$); bars, SE. **C.** Attenuation of PI3K activity affected cyclin D1 and cell cycle inhibitor p27^{Kip1} levels. A2058 and C32 cells, cultured with or without PI3K inhibitors, were lysed at the indicated times and assessed for cyclin D1 and p27^{Kip1} expression levels by immunoblotting. **D.** Evaluation of the role of PI3K in cell cycle transitions in melanoma cells. A2058 cells were synchronized in the G2-M phase by nocodazole treatment (*black curve*). Subsequently, cells were released from the nocodazole block and simultaneously exposed to the indicated PI3K inhibitors (*colored curves*). The cell cycle profile was then analyzed 1 and 2 d later as in **A**.

here, a dose of 10 mg/kg/d of PI103 was sufficient to attenuate primary tumor growth as observed for NVP-BEZ235, whereas a significant reduction in lymph node metastasis could not be detected. It is tempting to explain the lack of action on the lymph node metastasis by a restricted access of PI103 to metastatic tumor tissue. This is, however, challenged by the observation that increasing doses of PI103 caused a dose-dependent, paradoxical increase in phosphorylated PKB/Akt and p70^{S6K} in both the primary tumor and the metastasis in cervical lymph nodes. As Ser473 on PKB/Akt is mainly phosphorylated by TORC2 (40) in the absence of DNA damage (41, 42), and Thr389 phosphorylation on p70^{S6K} is mediated by TORC1, these phosphorylation patterns suggest that both mTOR complexes are in an overactivated state 2 hours after the last PI103 administration in a prolonged treatment scheme. As PI103 was used here at low doses and has a short half life (<2 hours; ref. 20), these results indicate that PI3K/mTOR signaling overshoots after a transient inhibition. BBD130, maintaining exposure to the tumor for a prolonged time (16 h/nmol/g), shows a clear reduction of Ser473 phosphorylation on PKB/Akt and Thr389 on p70^{S6K} until 16 hours after administration. The above result suggests that inhibitor half-life, exposure, and dosage frequency might affect the success of PI3K/mTOR modulation, and that phospho-PKB/Akt and phospho-p70^{S6K} need validation as biomarkers in conjunction with given compounds.

A close examination of melanoma tissue from mice treated with NVP-BBD130 and NVP-BEZ235 revealed that the mitotic index of metastatic cells in the cervical lymph nodes were reduced to more than half of untreated controls. This went along with a reduction in tumor cell mass, whereas cell size in other organs like the liver remained unaffected. The liver adapts to starvation by a reduction in cell size (43). As current PI3K/mTOR inhibitor treatments did not affect normal liver morphology, one may assume that nutrient uptake was functional. NVP-BBD130 at high single dose (40 mg/kg) showed a significant increase of the liver alanine aminotransferase in the plasma, which correlates with the increased liver retention of BBD130 compared with BEZ235 (Supplementary Fig. S6; ref. 28). Splitting the daily dose of NVP-BBD130 (2 × 20 mg/kg) reduced the

release of alanine aminotransferase. Moreover, we could not detect significant differences in blood glucose levels between inhibitor-treated and vehicle control mice, showing that the inhibition of the PI3Ks is not impairing the glucose homeostasis.

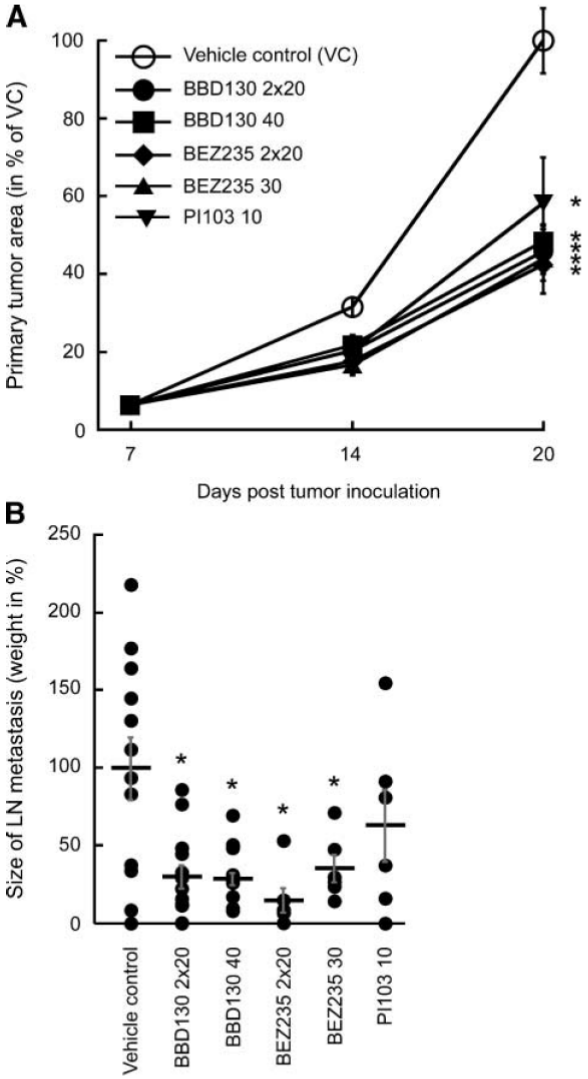

FIGURE 3. Antitumoral and antiangiogenic effect of PI3K inhibitors in the B16 mouse melanoma model. B16BL6 mouse melanoma cells were injected intradermally into ears of C57BL6 mice. One week later, tumors were established and treatment with vehicle and PI3K inhibitors (NVP-BBD130 at 40 mg/kg daily and 20 mg/kg twice daily, orally; NVP-BEZ235 at 40 mg/kg daily and 20 mg/kg twice daily, orally; PI103 at 10 mg/kg daily, i.p.) was started. Size of primary tumors was determined when indicated, whereas the mass of cervical lymph node metastasis was determined as the mice were sacrificed (*, $P < 0.05$ versus vehicle control group). **A.** Primary tumor size is depicted in percentage of the tumor size obtained in vehicle-treated (*VC*) animals 20 d after melanoma inoculation (for calculations, see Materials and Methods). Points, mean ($n > 6$); bars, SE. **B.** Formation of cervical lymph node metastasis. Mice were sacrificed 20 d after tumor inoculation and 2 wk of treatment with the indicated compounds. Cervical lymph node metastatic tissue was excised and weighted. Changes in metastatic mass are plotted in percentage of the mean end point of vehicle-treated animals. Points, mean ($n > 6$); bars, SE.

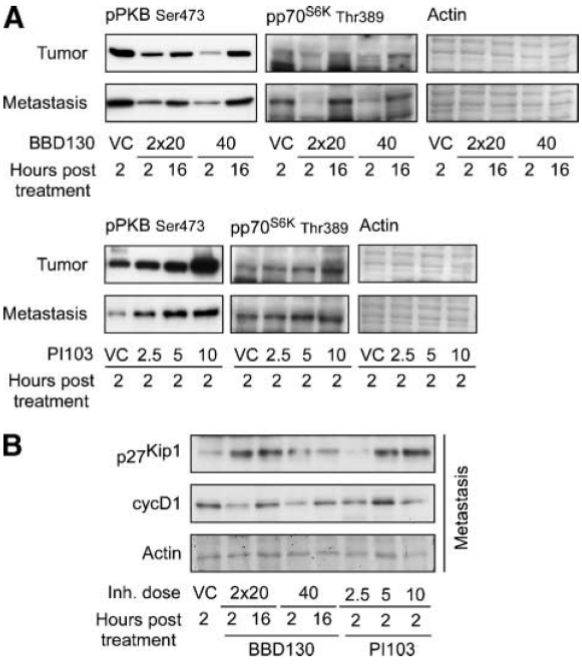

FIGURE 4. **A** and **B.** PI3K downstream signaling and cell cycle markers in tumor tissue. Tumor samples were collected at the indicated times after the last treatment with compound (posttreatment). Subsequently, total lysates of primary and metastatic tumors were resolved on SDS-PAGE and probed for phosphorylated PKB and $p70^{S6K}$, or $p27^{Kip1}$ and cyclin D1. Actin stained with Coomassie blue is shown as a loading control.

Angiogenesis is required for nutrient supply and growth of tumors beyond 1 mm (44) and has been shown to be sensitive to mTOR inhibition by rapamycin and its derivatives (45, 46). Supporting this notion, tumors excised from NVP-BBD130– and NVP-BEZ235–treated mice displayed a significant reduction in neovascularization, whereas large, preexisting blood vessels were not affected by targeting PI3K and mTOR. Intriguingly, mice treated with PI103 or the VEGFR inhibitor PTK787 showed no significant reduction in the amount of new blood vessels compared with vehicle control mice. Whereas NVP-BEZ235 and NVP-BBD130 are very potent PI3K and mTOR inhibitors, their effect on the VEGF receptor tyrosine kinase activity is negligible (IC_{50} for VEGFR1 >10 μmol/L). Despite this fact, they blocked the formation of new blood vessels more efficiently than PTK787. The PI3K/mTOR signaling pathway has been reported to control the expression of HIF-1 via activation of $p70^{S6K}$ and HDM2/MDM2. HIF-1 is the major regulator of VEGF transcriptional activity (47). Feedback loops from mTOR to PKB/Akt and PI3K activation have been reported (48), and also hypoxia-induced angiogenesis might require mTORC1 and mTORC2 (49). Therefore, NVP-BBD130 and NVP-BEZ235 interfere with VEGFR ligand production and VEGFR downstream signaling to block blood vessel formation and exert at the same time cytostatic effects on tumor cells. This dual action could explain the higher efficiency of NVP-BBD130 and NVP-BEZ235 compared with PTK787, an inhibitor more selectively targeting endothelial cells through VEGFR inhibition. The effect of

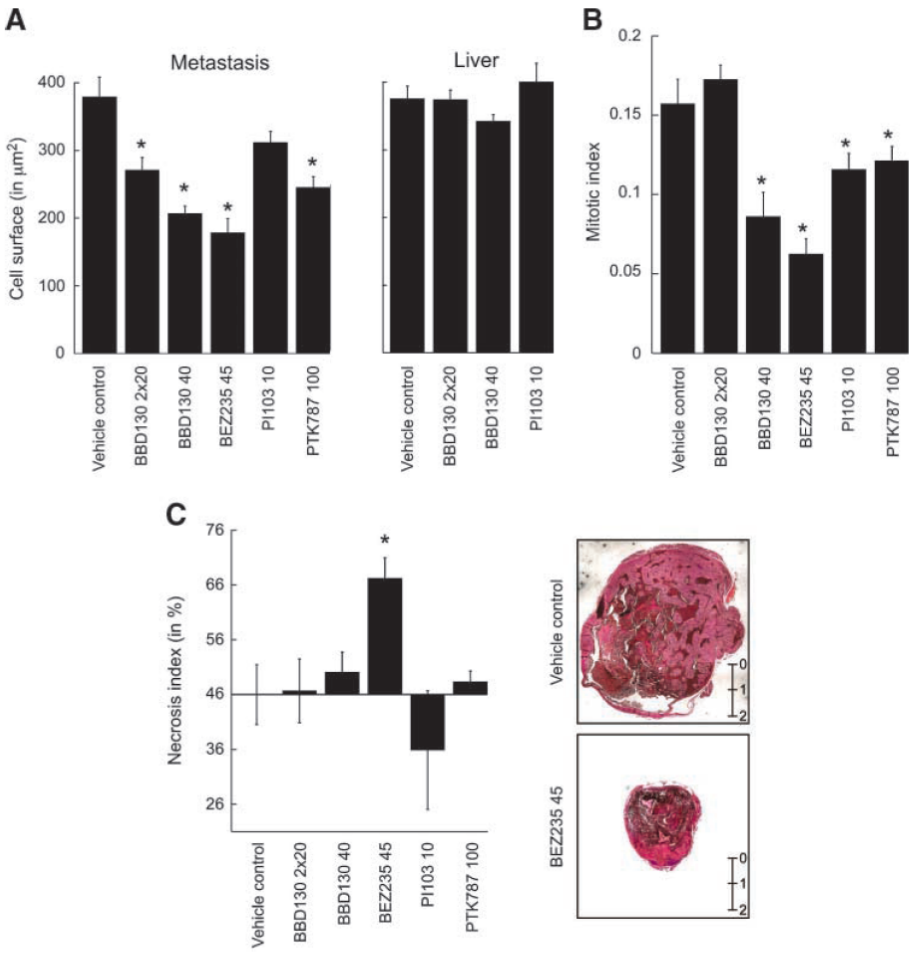

FIGURE 5. **A.** Tumor and hepatocyte cell size. Paraffin sections of metastatic melanoma and of liver tissue were stained with H&E, and cell size was measured as cross-section areas with ImageJ software. Columns, mean ($n > 300$); bars, SE. **B.** Mitotic index in metastatic tissue. Mitotic nuclei in lymph node metastasis were quantified in H&E-stained paraffin sections. Columns, mean ($n > 200$ cells); bars, SE. **C.** Necrosis in cervical lymph node metastasis. H&E-stained paraffin sections were analyzed for the presence of necrotic tissue and the percentage of necrotic cells was evaluated with the help of ImageJ. Columns, mean ($n > 4$); bars, SE. Scale in mm.

NVP-BBD130 and NVP-BEZ235 on neovascularization seemed to be crucial, as we noticed that tumor cells located in the vicinity of preexisting, large blood vessels still had some capacity to enter mitosis and displayed a nearly normal cell size (data not shown). It is therefore likely that the increased amount of necrotic tumor tissue observed in NVP-BEZ235–treated animals is caused by the very stringent targeting of neovascularization.

Our results indicate that the novel series of PI3K/TOR inhibitors attacks tumor progression by several molecular and physiologic mechanisms. To explore if the inhibition of mTOR in addition to PI3K is essential for blockage of tumor cell growth, we reintroduced constitutive PKB/Akt signaling in inhibitor-treated cells. When activated, PKB/Akt modulates directly and indirectly a range of transcription factors, among them the FOXOs. Here, NVP compounds abolished phosphorylation of FOXO1 by PKB/Akt, thus abrogating its binding to 14.3.3 proteins, which resulted in a translocation to the nucleus. Ectopic expression of constitutively active PKB/Akt (myr-PKB) yielded a PI3K inhibitor–resistant, cytosolic retention of FOXO1, but was unable to bypass the cell cycle arrest imposed by NVP compounds. This could be due to the fact that signals downstream of mTOR ($p70^{S6K}$, S6, and 4E-BP1 phosphorylation) remained inhibitor sensitive in the presence of constitutively active PKB/Akt.

Melanoma cells displayed a <50% drop in the rate of proliferation after high doses of rapamycin (mTOR inhibitor, 100 nmol/L) or <25% after ZSTK474 (pan-PI3K inhibitor, 1 µmol/L) treatment. NVP-BEZ235 is a pan-PI3K inhibitor but also blocks mTOR, targeting the ATP-binding site of TORC1 and TORC2 (28). Only the treatment of melanoma cells with dual inhibitors resulted in an efficient cytostatic, and in some rare cases cytotoxic, effect. The combination of rapamycin and ZSTK474 was more effective than either compound alone (<60%), but less effective than BEZ235. Whereas ZSTK474 inhibits class I PI3Ks, but not mTOR, rapamycin targets exclusively TORC1. Therefore, mTORC1 and simultaneously mTORC2 inhibition seems to be an important feature of NVP-BBD130 and NVP-BEZ235 action, which in combination with PI3K inhibition efficiently interferes with tumor growth *in vivo*.

In conclusion, inhibition of the PI3K/mTOR pathway via the nmol/L dual PI3K/mTOR inhibitors NVP-BBD130 and NVP-BEZ235 efficiently attenuates growth and proliferation of melanoma primary tumors and metastasis. Moreover, these

compounds efficiently target neovascularization, and NVP-BEZ235 augmented tumor necrosis. In all, the above results encourage clinical development of this compound series and the inclusion of patients with melanoma in ongoing phase I/II studies involving NVP-BEZ235.

Materials and Methods

Cell Culture

Melanoma cells were grown at 37°C in a 5% CO_2 atmosphere in DMEM (A2058, B16F1, B16F10, C32, HBL, Malme, Malme3M, NA8, SKMel2, and SKMel23 cells) or RPMI (A375, Hs294T, WM35, and 1205lu cells) supplemented with 10% heat-inactivated FCS, 1% L-glutamine, and 1% penicillin-streptomycin (all from Sigma). B16BL6 melanoma (from Dr. J. Fidler, Cancer Biology, The University of Texas M. D. Anderson Cancer Center, Houston, TX) were cultivated in MEM EBS (AMIMED) supplemented with 5% heat-inactivated FCS, 1% of each L-glutamine, penicillin-streptomycin, sodium pyruvate, nonessential amino acids, and 2% vitamins (stock solutions from AMIMED).

Proliferation and Cell Volume

One day after plating (7×10^3 cells/cm^2), melanoma cells were exposed to LY294002 (25 μmol/L); wortmannin (500 nmol/L); NVP-BAG956, NVP-BBD130, NVP-BEZ235, and ZSTK474 (1 μmol/L); and rapamycin (100 nmol/L). Compound concentrations were set 2 log units above the IC_{50} *in vitro* to ensure full PI3K inhibition, except for the μmol/L inhibitor LY294002. Cells were trypsinized and counted, and the volume was quantified using a Casy Counter and Analyser (Innovatis AG). To determine the nuclear volume, cells were resuspended in CASYton containing 0.5% Triton X-100, followed by repetitive pipetting (8×), before volume measurements.

Immunoblotting

Total cell lysates were prepared in NP40-based lysis buffer (pH 8.0, 20 mmol/L Tris-HCl, 138 mmol/L NaCl, 2.7 mmol/L KCl, 5% glycerol, 1 mmol/L $CaCl_2$, 1 mmol/L $MgCl_2$, 1% NP40, 20 μmol/L leupeptin, 18 μmol/L pepstatin, 1 mmol/L Na-O-vanadate, 20 mmol/L NaF, and 100 μmol/L phenylmethylsulfonyl fluoride). Proteins were separated on SDS-PAGE and transferred to Immobilon FL membranes (Millipore). Primary antibodies to PTEN, pSer^{473}-PKB/Akt, pThr308-PKB/Akt, pThr389-p70^{S6K}, pSer235/236-S6, pThr32-FOXO1, pSer9-GSK3β, 4E-BP1, and pThr37/46-4E-BP1 were from Cell Signaling Technology; primary antibodies to pMAPK and MAPK were from Sigma; the primary antibody to PKB was a kind gift of E. Hirsch (Turin, Italy); and primary antibodies to cyclin D1 and p27^{Kip1} were from Santa Cruz Biotechnology. Secondary antibodies (e.g., horseradish peroxidase–conjugated rabbit anti-mouse IgG and goat anti-rabbit IgG; Sigma) were visualized using enhanced chemiluminescence (Millipore), and fluorescent secondary antibodies (Alexa Fluor 680 or IRDye 800) were detected using the Odyssey IR reader (LICOR).

Cell Cycle and Apoptosis

Melanoma cells were plated (7×10^3/cm^2), and PI3K inhibitors (LY294002 at 25 μmol/L; wortmannin at 500 nmol/L; NVP-BAG956, NVP-BBD130, and NVP-BEZ235 at 1 μmol/L) were added 24 h later. After 3 d of exposure to inhibitors, cells were trypsinized and prepared for cell cycle and apoptosis analysis (50). For cell cycle evaluation, cells were fixed and permeabilized in PBS supplemented with 4% paraformaldehyde/1% bovine serum albumin/0.1% saponin for 30 min at 4°C, and subsequently washed with 1% bovine serum albumin/0.1% saponin in PBS. The pellet was resuspended in 0.1% Triton X-100/0.1% sodium citrate solution (pH 7.4) containing 50 μg/mL propidium iodide and 10 μg/mL DNase-free RNase and incubated for 8 h at 4°C

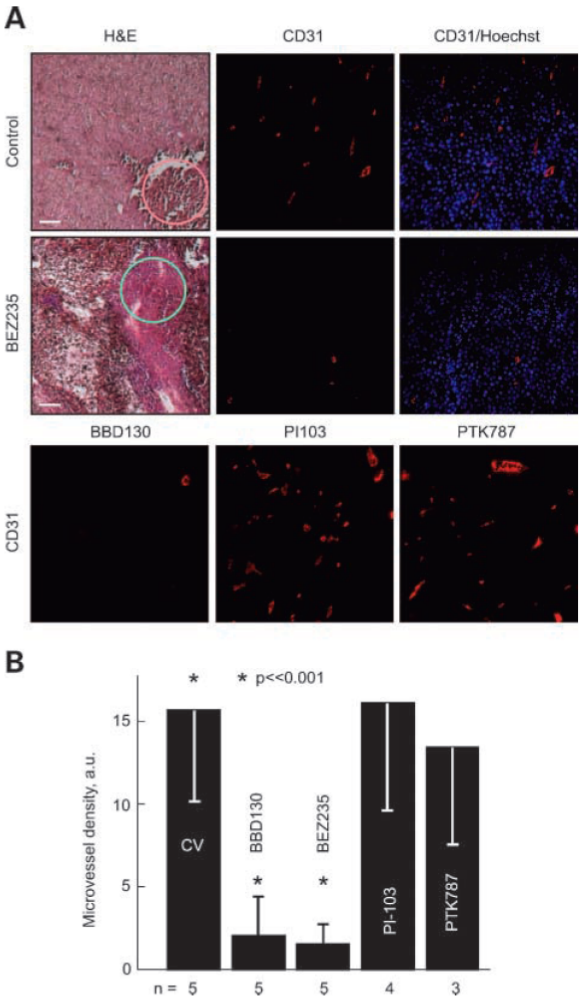

FIGURE 6. **A.** Effect of inhibitor treatment on neovascularization. Paraffin sections of metastatic tissue were stained with H&E (*left*), anti-CD31 anti-body to visualize the tumor vasculature (*red*), or Hoechst 33342 to stain nuclear DNA (*blue*). Nuclei are depicted in a picture merged with CD31 staining. **B.** Microvascular density was quantified in anti-CD31–stained slides as shown in **A**, using Hoechst staining to select regions with viable tissue (*green circle* in **A**). Necrotic tumor tissue was excluded from the evaluation (*red circle* in **A**). The number of metastases evaluated is indicated at the bottom of the graph (*n*; fields evaluated per tumor ≥4; *scale bar*, 0.1 mm).

Table 2. Effects of PI3K Inhibitors on Body, Spleen, and Liver Weights, and Glucose Levels in the B16 Mouse Melanoma Model

	Body weight (% change)	Spleen weight (mg)	Liver weight (mg)	Glucose* (mmol/L)
Healthy control	(19.3 ± 0.1 g)	73 ± 3	896 ± 34	10-15
Vehicle control	−4.5 ± 3.0	181 ± 29	869 ± 32	13.3 ± 0.7
BBD130 40 mg/kg/d	−6.6 ± 3.1	155 ± 23	821 ± 30	17.8 ± 2.4
BBD130 2 × 20 mg/kg/d	−3.7 ± 2.8	126 ± 10†	854 ± 34	12.6 ± 0.6
PI103 10 mg/kg/d	5.0 ± 2.8	219 ± 33	1,101 ± 25†	14.5 ± 1.3

NOTE: Effects of PI3K pathway inhibitors on body, spleen, and liver weights, and on glucose levels in the B16 melanoma mouse model. Mice were weighted weekly and sacrificed 13 days after initiation of treatment with the respective inhibitors for autopsy. Whole blood glucose was measured in samples drawn from the vena cava. During the experiment, the mice received water and food *ad libitum*. Data are presented as mean ± SE, $n > 6$.
*Healthy mice display normal blood glucose of 10 to 15 mmol/L, depending on their feeding status.
†$P < 0.05$ versus vehicle control group.

before fluorescence-activated cell sorting data acquisition (FACSCalibur, Becton Dickinson). Annexin V staining was done following the manufacturer's protocol (Becton Dickinson). In brief, cells were resuspended in 200 μL Annexin buffer [10 mmol/L HEPES (pH 7.4), 0.14 mol/L NaCl, 2.5 mmol/L $CaCl_2$] containing 2 μL of Cy5-labeled Annexin V (Becton Dickinson) and subsequently incubated 15 min at room temperature in the dark. Before cytometry, 2.5 μg of propidium iodide were added to the cells. Data were analyzed with FlowJo (Tree Star, Oregon Corporation).

DNA Synthesis and Thymidine Incorporation

A2058 cells were seeded in 96-well microtiter plates (2,000 per well) and 24 h later PI3K inhibitors (LY294002 at 25 μmol/L; wortmannin at 500 nmol/L; NVP-BAG956, NVP-BBD130, and NVP-BEZ235 at 1 μmol/L) were added for the indicated times. During the last 24 h of exposure to the inhibitors, 1 μCi of [^{3}H]thymidine was added per well. Subsequently, cells were harvested onto glass fiber filters using a cell harvester (FilterMate Harvester, Perkin-Elmer) and incorporated radioactivity was measured using a Perkin-Elmer MicroBeta TriLux.

Cell Cycle Synchronization

Melanoma cells were synchronized by incubation for 14 h with 1 μg/mL nocodazole in the medium described above. Subsequently, the cells were trypsinized, washed with PBS, and plated in the presence or absence of PI3K inhibitors (LY294002 at 25 μmol/L; wortmannin at 500 nmol/L; NVP-BAG956, NVP-BBD130, and NVP-BEZ235 at 1 μmol/L). The cell cycle profile was analyzed as described above.

In vivo *Mouse Melanoma Model*

B16BL6 mouse melanoma cells were grown until confluent, trypsinized, pelleted, and resuspended (50×10^6/mL) in Hanks buffer supplemented with 10% heat-inactivated FCS. Female C57BL/6 mice (Charles River) were anesthetized

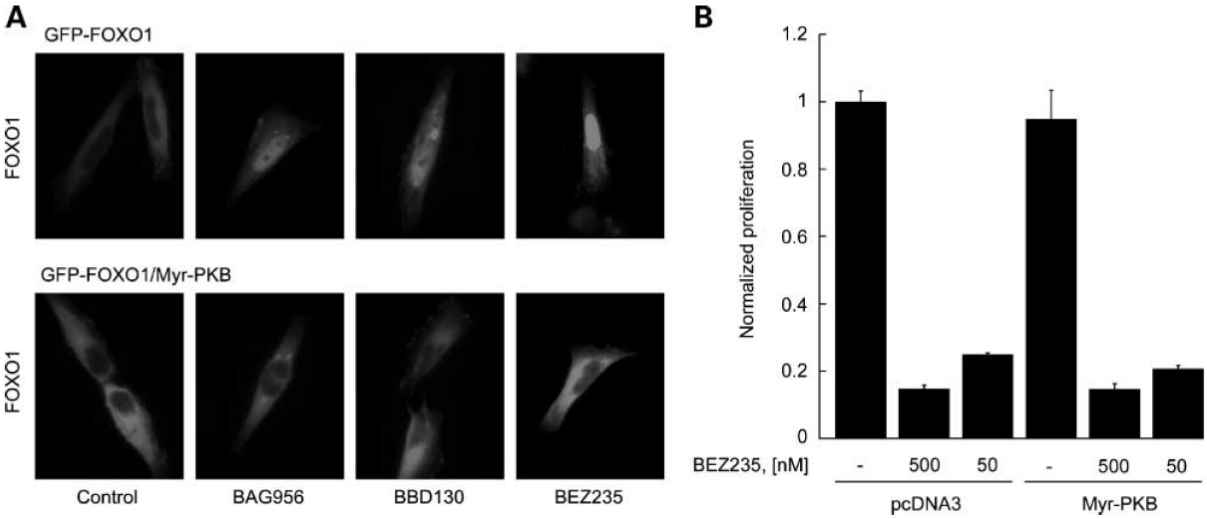

FIGURE 7. Requirement of PI3K and mTOR downstream signaling in melanoma proliferation. **A.** PI3K/PKB–dependent FOXO1 translocation to the nucleus. The localization of a GFP-FOXO1 (*red*) fusion protein was monitored in A2058 cells or A2058 cells stably expressing a myristoylated form of PKB after vehicle or the indicated PI3K inhibitors were added for 3 h. **B.** Constitutively active PKB does not rescue growth in the presence of PI3K/mTOR inhibitors. A2058 cells and A2058 cells stably expressing myristoylated PKB were ex-posed to NVP-BEZ235 for 3 d before cell numbers were determined (shown as percent of nontreated cells harboring a control plasmid). Columns, mean of triplicates; bars, SE.

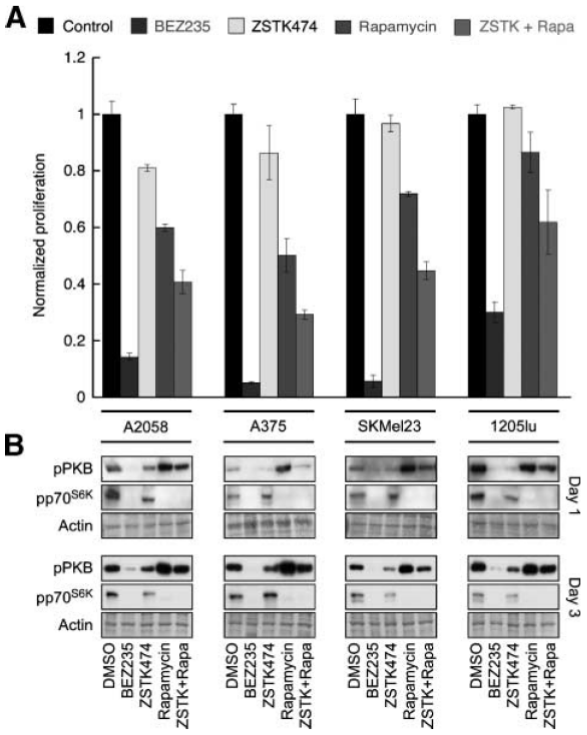

FIGURE 8. **A.** Antiproliferative effect of pan-PI3K, PI3K/mTOR, and mTOR inhibitors on melanoma cells. Melanoma cells were exposed to NVP-BEZ235 (1 μmol/L), ZSTK474 (1 μmol/L), and/or rapamycin (100 nmol/L). Proliferation was measured as above and is shown normalized to proliferation of vehicle-treated control cells. Columns, mean of triplicates; bars, SE. **B.** Changes in the phosphorylation of PKB and $p70^{S6K}$ upon PI3K and/or mTOR inhibition. Melanoma cells were exposed to inhibitors as indicated in **A** and total cell lysates were prepared 1 and 3 d later for detection of phosphorylated (Ser473) PKB and $p70^{S6K}$. Actin stained with Coomassie blue is shown as loading control.

with 3% isofluorane in O_2 (v/v) and placed on an operation table maintained at 37°C. Mouse ears were fixed with a double-sided tape over a steel cone and 1 μL of the cell suspension was injected intradermally using a microliter syringe with a 30-G needle. Primary tumor size was recorded every 7 d in mice anesthetized with isofluorane. One week after cell injection, oral treatment with vehicle control [10% NMP/PEG 300 (1-methyl-2-pyrrolidone/polyethylene glycol 300); 10:90, v/v], NVP-BBD130 (40 mg/kg daily and twice daily 20 mg/kg), NVP-BEZ235 (30 mg/kg daily and twice daily 20 mg/kg), PTK787 (100 mg/kg/d) and i.p. treatment with PI103 (2.5, 5, and 10 mg/kg/d) was started. NVP-BBD130, NVP-BEZ235, and PTK787 were dissolved by sonication in NMP and then the corresponding volume of PEG 300 was added. PI103 was instead dissolved in KZI (Cremophor EL/ethanol absolute 65:35, v/v) and the remaining volume (1:3, v/v) of 5% glucose (Braun Medical AG) was added. The inhibitors were given for the indicated period, before animals were sacrificed, and primary tumor, cervical lymph node metastases, spleen, liver, femurs, and blood (from the vena cava) were collected for further analysis.

The size of primary tumors at a given time point (=$area_t$) was determined by digital imaging as described in refs. (51, 52), and tumor progression was related to the tumor area at day 7 (=$area_{7days}$), and then expressed as percentage of the overall mean tumor size in untreated [vehicle control (VC)] animals (=mean_area_VC_{20days}). The depicted values were therefore calculated as follows:

$$\text{Primary tumor area } (\%) = [100 \times \text{area}_t/\text{area}_{7d}]/\text{mean\_area\_VC}_{20d}$$

A fraction of the primary tumors, metastases and liver samples were snap frozen in liquid nitrogen, the rest was fixed in 4% paraformaldehyde for paraffin embedding. Experiments were terminated (here at day 20) for ethical reasons.

Immunohistochemistry

Primary tumors, metastases, and liver tissues were embedded in paraffin using a Spin Tissue Processor (Microm International). Paraffin blocks were cut to 6-μm sections using the Microtome cool-cut HM355S (Microm International). For CD31 (antibody from Bachem AG) staining, tissue slides were deparaffinized using roticlean, and the antigen was unmasked by proteinase K treatment. The staining with the primary antibody was done overnight (antibody dilution 1:50). Subsequently, slides were incubated with a fluorescently labeled secondary antibody and Hoechst 33342 and mounted with crystal solution (Medite). For H&E staining, deparaffinized slides were incubated with hematoxylin solution followed by eosin and mounted with Cytoseal XYL (Medite).

Immune Cell Detection

Cell suspensions of spleen and bone marrow were generated and stained with different cell surface marker antibodies: monoclonal antibodies against CD3 (clone KT3), CD4 (RM4-5), CD8 (53-6.7), B220 (RA3-6B2), CD11b (M1/70), CD11c (HL3), GR1, and TERT were obtained from BD Biosciences PharMingen or eBioscience. The F4/80 antibody was from Serotec. Fluorescence was quantified on a FACS-Calibur.

Myr-PKB Transfection and GFP-FOXO Translocation

Cells were plated at $14 \times 10^3/cm^2$, and 24 h later were transfected with 0.1 $\mu g/cm^2$ pcDNA3-GFP-FOXO1 and/or pcDNA3-Myr-PKB expression plasmids using JetPEI (Brunschwig Chemie) following the manufacturer's protocol. The following day, cells were exposed to PI3K inhibitors (LY294002 at 25 μmol/L; wortmannin at 500 nmol/L; NVP-BAG956, NVP-BBD130, NVP-BEZ235, and PI103 at 1 μmol/L) or rapamycin (100 nmol/L) for 3 h. HEK293 cells were starved overnight in serum-free DMEM before treatment with the inhibitors.

For immunofluorescence, cells plated on glass coverslips ($21 \times 10^3/cm^2$) were fixed in PBS with 4% paraformaldehyde before nuclei were stained with Hoechst 33342. Coverslips were mounted on microscopy slides in Mowiol (Clariant GMbH). Images were acquired with OpenLab software (Improvision) on an Axiovert 200 M microscope (Zeiss) with a Plan-Achromat 63×/1.4 and an Orca ER II camera (Hamamatsu).

Disclosure of Potential Conflicts of Interest

No potential conflicts of interest were disclosed.

Acknowledgments

We thank Poppy Fotiadou for the critical reading of the manuscript; Mathias M. Hauri-Hohl for help with fluorescence-activated cell sorting analysis; Priska Reinhard for excellent technical assistance; Reinhard Dummer for inspiring discussions; Reinhard Dummer, Isaiah Fidler, Silvio Hemmi, Meenhard Herlyn, Adrian Ochsenbein, and Giulio Spagnoli for the supply of cell lines; Samuel Arnal for help with the *in vivo* experiment; Natasha Cmiljanovic for the synthesis of ZSTK474; and Karen C. Arden for the GFP-FOXO1 plasmid.

References

1. Vogelstein B, Kinzler KW. Cancer genes and the pathways they control. Nat Med 2004;10:789–99.

2. Vivanco I, Sawyers CL. The phosphatidylinositol 3-Kinase AKT pathway in human cancer. Nat Rev Cancer 2002;2:489–501.

3. Wymann MP, Marone R. Phosphoinositide 3-kinase in disease: timing, location, and scaffolding. Curr Opin Cell Biol 2005;17:141–9.

4. Engelman JA, Luo J, Cantley LC. The evolution of phosphatidylinositol 3-kinases as regulators of growth and metabolism. Nat Rev Genet 2006;7: 606–19.

5. Raftopoulou M, Hall A. Cell migration: Rho GTPases lead the way. Dev Biol 2004;265:23–32.

6. Bhaskar PT, Hay N. The two TORCs and Akt. Dev Cell 2007;12:487–502.

7. Samuels Y, Ericson K. Oncogenic PI3K and its role in cancer. Curr Opin Oncol 2006;18:77–82.

8. Omholt K, Krockel D, Ringborg U, Hansson J. Mutations of PIK3CA are rare in cutaneous melanoma. Melanoma Res 2006;16:197–200.

9. Curtin JA, Stark MS, Pinkel D, Hayward NK, Bastian BC. PI3-kinase subunits are infrequent somatic targets in melanoma. J Invest Dermatol 2006;126: 1660–3.

10. Stark M, Hayward N. Genome-wide loss of heterozygosity and copy number analysis in melanoma using high-density single-nucleotide polymorphism arrays. Cancer Res 2007;67:2632–42.

11. Guldberg P, thor Straten P, Ahrenkiel V, Seremet T, Kirkin AF, Zeuthen J. Somatic mutation of the Peutz-Jeghers syndrome gene, LKB1/STK11, in malignant melanoma. Oncogene 1999;18:1777–80.

12. Meier F, Busch S, Lasithiotakis K, et al. Combined targeting of MAPK and AKT signalling pathways is a promising strategy for melanoma treatment. Br J Dermatol 2007;.

13. Eisen T, Ahmad T, Flaherty KT, et al. Sorafenib in advanced melanoma: a Phase II randomised discontinuation trial analysis. Br J Cancer 2006;95: 581–6.

14. Ratain MJ, Eisen T, Stadler WM, et al. Phase II placebo-controlled randomized discontinuation trial of sorafenib in patients with metastatic renal cell carcinoma. J Clin Oncol 2006;24:2505–12.

15. Margolin K, Longmate J, Baratta T, et al. CCI-779 in metastatic melanoma: a phase II trial of the California Cancer Consortium. Cancer 2005;104: 1045–8.

16. Hu L, Zaloudek C, Mills GB, Gray J, Jaffe RB. *In vivo* and *in vitro* ovarian carcinoma growth inhibition by a phosphatidylinositol 3-kinase inhibitor (LY294002). Clin Cancer Res 2000;6:880–6.

17. Wymann MP, Zvelebil M, Laffargue M. Phosphoinositide 3-kinase signalling—which way to target? Trends Pharmacol Sci 2003;24:366–76.

18. Liu Y, Jiang N, Wu J, Dai W, Rosenblum JS. Polo-like kinases inhibited by wortmannin. Labeling site and downstream effects. J Biol Chem 2007;282: 2505–11.

19. Fan QW, Knight ZA, Goldenberg DD, et al. A dual PI3 kinase/mTOR inhibitor reveals emergent efficacy in glioma. Cancer Cell 2006;9:341–9.

20. Raynaud FI, Eccles S, Clarke PA, et al. Pharmacologic characterization of a potent inhibitor of class I phosphatidylinositide 3-kinases. Cancer Res 2007;67: 5840–50.

21. Chen JS, Zhou LJ, Entin-Meer M, et al. Characterization of structurally distinct, isoform-selective phosphoinositide 3′-kinase inhibitors in combination with radiation in the treatment of glioblastoma. Mol Cancer Ther 2008;7: 841–50.

22. Yaguchi S, Fukui Y, Koshimizu I, et al. Antitumor activity of ZSTK474, a new phosphatidylinositol 3-kinase inhibitor. J Natl Cancer Inst 2006;98: 545–56.

23. Kong D, Yamori T. ZSTK474 is an ATP-competitive inhibitor of class I phosphatidylinositol 3 kinase isoforms. Cancer Sci 2007;98:1638–42.

24. Casagrande F, Bacqueville D, Pillaire MJ, et al. G1 phase arrest by the phosphatidylinositol 3-kinase inhibitor LY 294002 is correlated to up-regulation of p27Kip1 and inhibition of G1 CDKs in choroidal melanoma cells. FEBS Lett 1998;422:385–90.

25. Blanco-Aparicio C, Pequeno B, Moneo V, et al. Inhibition of phosphatidylinositol-3-kinase synergizes with gemcitabine in low-passage tumor cell lines correlating with Bax translocation to the mitochondria. Anticancer Drugs 2005;16: 977–87.

26. Smalley KS, Haass NK, Brafford PA, Lioni M, Flaherty KT, Herlyn M. Multiple signaling pathways must be targeted to overcome drug resistance in cell lines derived from melanoma metastases. Mol Cancer Ther 2006;5: 1136–44.

27. Bedogni B, Welford SM, Kwan AC, Ranger-Moore J, Saboda K, Powell MB. Inhibition of phosphatidylinositol-3-kinase and mitogen-activated protein kinase kinase 1/2 prevents melanoma development and promotes melanoma regression in the transgenic TPRas mouse model. Mol Cancer Ther 2006;5: 3071–7.

28. Maira SM, Stauffer F, Brueggen J, et al. Identification and characterization of NVP-BEZ235, a new orally available dual phosphatidylinositol 3-kinase/mammalian target of rapamycin inhibitor with potent *in vivo* antitumor activity. Mol Cancer Ther 2008;.

29. Stauffer F, Maira SM, Furet P, Garcia-Echeverria C. Imidazo[4,5-c]quinoline as inhibitors of the PI3K/PKB-pathway. Bioorg Med Chem Lett 2007;.

30. Lin J, Adam RM, Santiestevan E, Freeman MR. The phosphatidylinositol 3′-kinase pathway is a dominant growth factor-activated cell survival pathway in LNCaP human prostate carcinoma cells. Cancer Res 1999;59:2891–7.

31. Wen Y, Hu MC, Makino K, et al. HER-2/neu promotes androgen-independent survival and growth of prostate cancer cells through the Akt pathway. Cancer Res 2000;60:6841–5.

32. Carson JP, Kulik G, Weber MJ. Antiapoptotic signaling in LNCaP prostate cancer cells: a survival signaling pathway independent of phosphatidylinositol 3′-kinase and Akt/protein kinase B. Cancer Res 1999;59:1449–53.

33. Andjelkovic M, Alessi DR, Meier R, et al. Role of translocation in the activation and function of protein kinase B. J Biol Chem 1997;272:31515–24.

34. Huang H, Tindall DJ. Dynamic FoxO transcription factors. J Cell Sci 2007; 120:2479–87.

35. van der Horst A, Burgering BM. Stressing the role of FoxO proteins in lifespan and disease. Nat Rev Mol Cell Biol 2007;8:440–50.

36. Ruckle T, Schwarz MK, Rommel C. PI3Kγ inhibition: towards an 'aspirin of the 21st century'? Nat Rev Drug Discov 2006;5:903–18.

37. Marone R, Cmiljanovic V, Giese B, Wymann MP. Targeting phosphoinositide 3-kinase—moving towards therapy. Biochim Biophys Acta 2007;.

38. Smalley KS, Lioni M, Dalla Palma M, et al. Increased cyclin D1 expression can mediate BRAF inhibitor resistance in BRAF V600E-mutated melanomas. Mol Cancer Ther 2008;7:2876–83.

39. Hussein MR. Tumour-infiltrating lymphocytes and melanoma tumorigenesis: an insight. Br J Dermatol 2005;153:18–21.

40. Sarbassov DD, Guertin DA, Ali SM, Sabatini DM. Phosphorylation and regulation of Akt/PKB by the rictor-mTOR complex. Science 2005;307:1098–101.

41. Feng J, Park J, Cron P, Hess D, Hemmings BA. Identification of a PKB/Akt hydrophobic motif Ser-473 kinase as DNA-dependent protein kinase. J Biol Chem 2004;279:41189–96.

42. Bozulic L, Surucu B, Hynx D, Hemmings BA. PKBα/Akt1 acts downstream of DNA-PK in the DNA double-strand break response and promotes survival. Mol Cell 2008;30:203–13.

43. Anand P, Gruppuso PA. Rapamycin inhibits liver growth during refeeding in rats via control of ribosomal protein translation but not cap-dependent translation initiation. J Nutr 2006;136:27–33.

44. Hanahan D, Weinberg RA. The hallmarks of cancer. Cell 2000;100:57–70.

45. Phung TL, Ziv K, Dabydeen D, et al. Pathological angiogenesis is induced by sustained Akt signaling and inhibited by rapamycin. Cancer Cell 2006;10: 159–70.

46. Del Bufalo D, Ciuffreda L, Trisciuoglio D, et al. Antiangiogenic potential of the mammalian target of rapamycin inhibitor temsirolimus. Cancer Res 2006;66: 5549–54.

47. Skinner HD, Zheng JZ, Fang J, Agani F, Jiang BH. Vascular endothelial growth factor transcriptional activation is mediated by hypoxia-inducible factor 1α, HDM2, and p70S6K1 in response to phosphatidylinositol 3-kinase/AKT signaling. J Biol Chem 2004;279:45643–51.

48. Wang X, Yue P, Chan CB, et al. Inhibition of mammalian target of rapamycin induces phosphatidylinositol 3-kinase-dependent and Mnk-mediated eukaryotic translation initiation factor 4E phosphorylation. Mol Cell Biol 2007;27:7405–13.

49. Li W, Petrimpol M, Molle KD, Hall MN, Battegay EJ, Humar R. Hypoxia-induced endothelial proliferation requires both mTORC1 and mTORC2. Circ Res 2007;100:79–87.

50. Rolink AG, Andersson J, Melchers F. Characterization of immature B cells by a novel monoclonal antibody, by turnover and by mitogen reactivity. Eur J Immunol 1998;28:3738–48.

51. Rudin M, McSheehy PM, Allegrini PR, et al. PTK787/ZK222584, a tyrosine kinase inhibitor of vascular endothelial growth factor receptor, reduces uptake of the contrast agent GdDOTA by murine orthotopic B16/BL6 melanoma tumours and inhibits their growth *in vivo*. NMR Biomed 2005;18:308–21.

52. Sini P, Samarzija I, Baffert F, et al. Inhibition of multiple vascular endothelial growth factor receptors (VEGFR) blocks lymph node metastases but inhibition of VEGFR-2 is sufficient to sensitize tumor cells to platinum-based chemotherapeutics. Cancer Res 2008;68:1581–92.

53. Garcia-Echeverria C, Pearson MA, Marti A, et al. *In vivo* antitumor activity of NVP-AEW541—a novel, potent, and selective inhibitor of the IGF-IR kinase. Cancer Cell 2004;5:231–9.

54. Knight ZA, Gonzalez B, Feldman ME, et al. A pharmacological map of the PI3-K family defines a role for p110α in insulin signaling. Cell 2006;125:733–47.

3.2. Identification of Novel Hits by Matrix-Template Strategy

It has been shown that marketed drugs are highly similar to the leads[h] from which they were derived [8]. Thus, the quality of lead classes available to medicinal chemists is very important for discovering best-in-class medicines. This makes lead generation a crucial step in the drug discovery process. Over the past decade, high-throughput screening (HTS[i]) has become the major paradigm for hit or lead discovery in pharmaceutical industry. However, in many cases, HTS either fails to deliver any promising hit or the identified hits cannot be turned into lead compounds with desirable *in vitro* potency and selectivity. Last but not least, there are still particular cases for which the set-up of the screen is expensive and time-consuming. In addition, *in silico* methods and fragment-based lead discovery can also be applied, either as an alternative to HTS, or as additional lead sourse when HTS hits are inadequeate to initiate a medicinal chemistry program. The most widely applied techniques used in the primary screening of fragment-like molecules include NMR [9], MS [10] and X-ray [11], which are limited related to target size, tendency to form crystals, or need for mutations or labelling. Once the hits are confirmed, the selection process begins for hit-to-lead follow up. For hits from HTS, selectivity, chemical tractability[j], binding mechanism, pharmacokinetic properties and patentability are usually viewed as more significant that the actual potency of the confirmed hits.

Here we present an alternative knowledge-based hit and lead strategy, which in case of PI3K/mTOR inhibitors demonstrated to be cost-friendly and highly efficient. With the aim to explore the chemical space of compounds, which are able to inhibit the activity of lipid kinases we did an in-depth analysis of >400 patents. Representatives from different chemical classes of lipid kinase inhibitors were selected and compounds from each class were synthesized. *In vitro* activity against PI3Kα as well as cellular activity of synthesized compounds were measured (Figure 4). For most chemotypes, a negative control compound, inactive against PI3Ks, was also synthesized. Based on this initial screen and known SAR[k] data from the literature (for summarized literature data see our published review [12]), a subset representing the most potent and selective agents was selected for further characterization step that we called *fragment validation step*. In this step we examined which structural fragments of the known PI3K inhibitors are significant for biological

[h] LEAD is "a prototypical chemical structure or series of structures that demonstrate activity and selectivity in a pharmacological or biochemically relevant screen. This forms the basis for a focused medicinal chemistry effort for lead optimization and development with the goal of identifying a clinical candidate. A distinct lead series has a unique core structure and the ability to be patented separately" (Bleicher et al., Nat Rev Drug Discov, 2003).
[i] HIGH-THROUGHPUT SCREENING is screening (of a compound collection) to identify hits in an *in vitro* assay usually performed robotically in 384-well microtitre plates.
[j] CHEMICAL TRACTABILITY is suitability of a compound for chemical modification.
[k] STRUCTURE-ACTIVITY RELATIONSHIP (SAR) is the consistent correlation of structural features or groups with the biological activity of compounds in a given biological assay (Bleicher et al., Nat Rev Drug Discov, 2003).

activity and which could serve for further chemical optimization. For this purpose, several derivatives of known PI3K inhibitors were synthesized, and the nature of their interactions with the target protein was analyzed by different cellular assays, X-ray and *in silico* experiments (Figure 5).

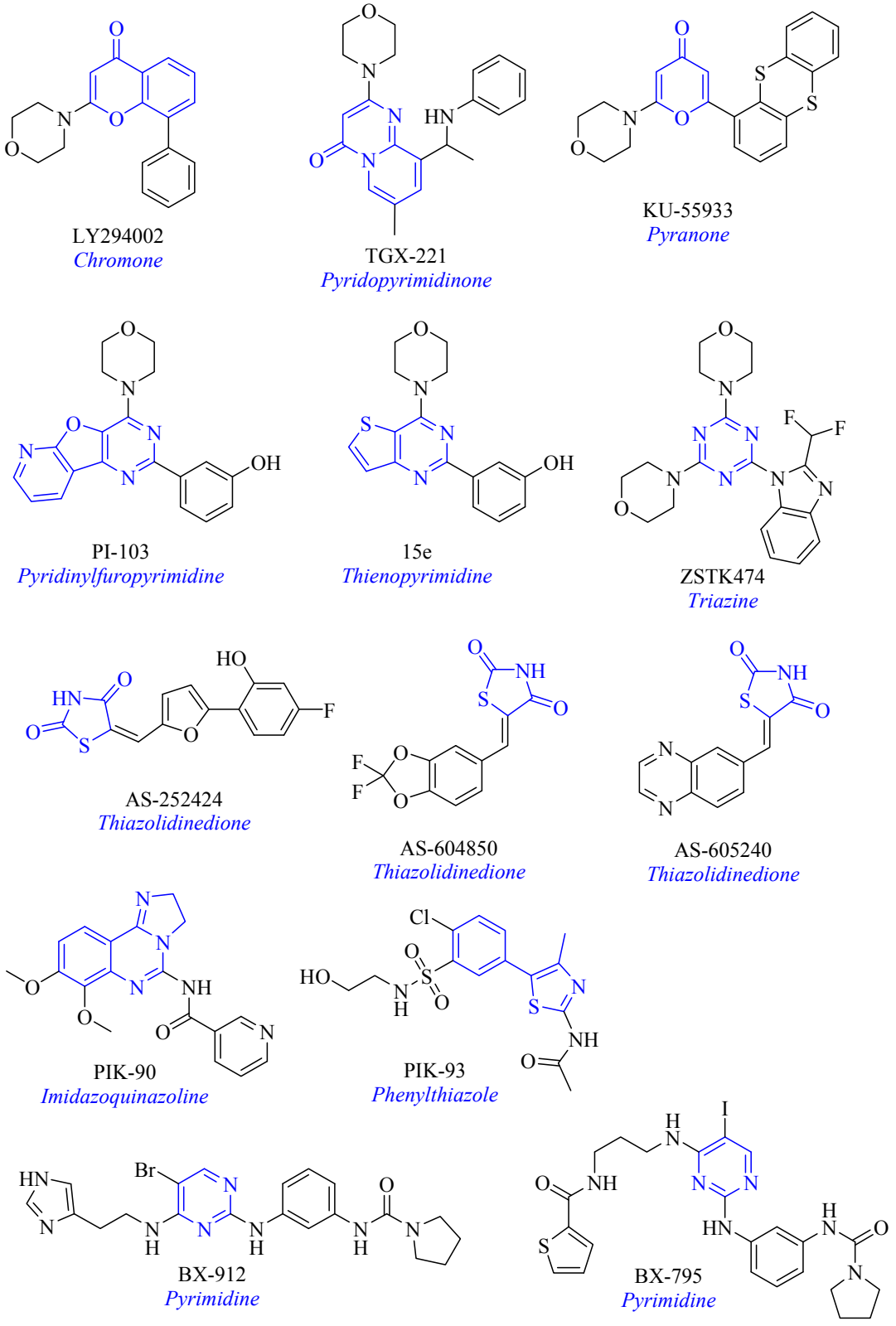

Figure 4. Structures of representative compounds from twelve classes of lipid kinase inhibitors that were selected from the public domain and tested *in vitro* against PI3Kα and *in cell*. The core chemotype is colored blue.

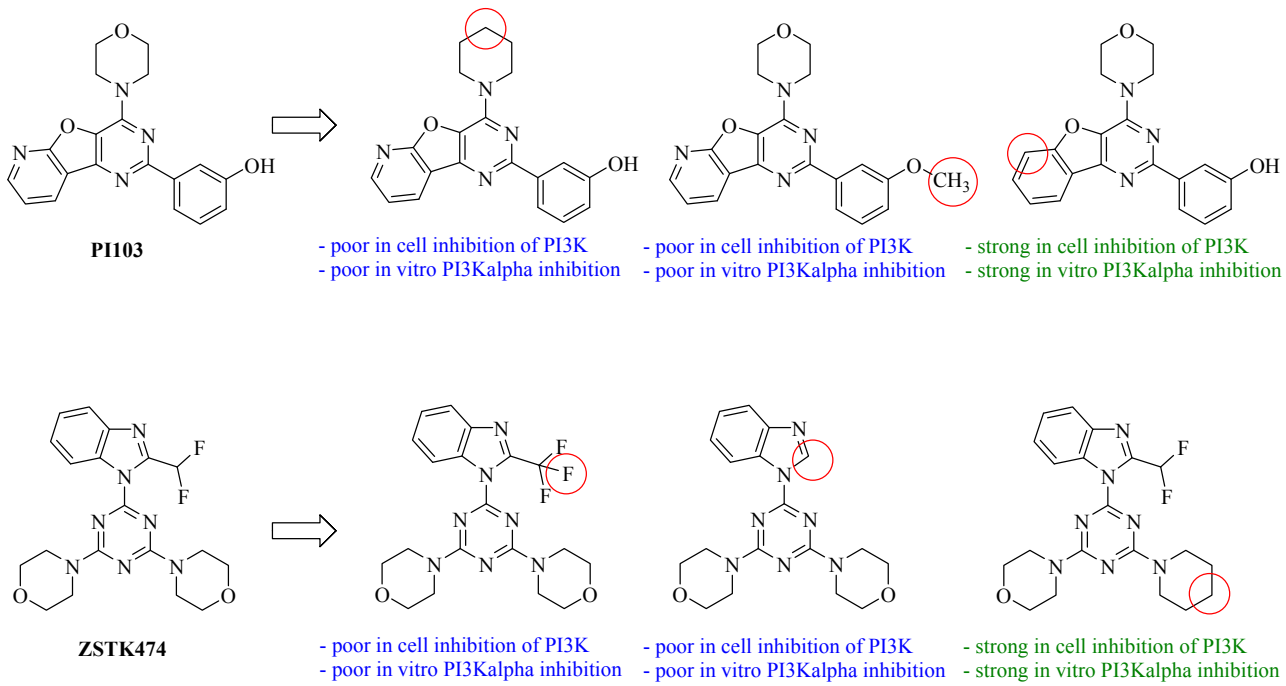

Figure 5. In the fragment validation step we examined, which structural fragments of the known PI3K inhibitors are significant for biological activity, and which could serve for further chemical optimization. For this purpose, we modified all possible positions around the molecular scaffold and synthesized several analogues of the known PI3K inhibitors, which activity and the binding mode was further analyzed by different cellular assays, X-ray and *in silico* experiments.

According to our results from different cellular and *in vitro* assays (e.g. competitive experiments with covalent natural inhibitor wortmannin, which binds covalently to a lysine in the ATP-binding pocket), X-ray crystal structures and published literature results, most PI3K inhibitors that have been developed for pharmaceutical applications work by competing with ATP binding. Similar to protein kinases, the ATP-binding site of PI3K is located in a cleft formatted by the N- and the C-terminal lobe of the catalytic domain [12], [13], [14]. The protein backbone and amino acid residues Met-804, Trp-812, Glu-880, Val-882 and Met-953 of PI3Kγ define a unique surface lining the ATP binding site, which provides more free space than typical protein kinases [14]. The crystal structures of the inhibitor•PI3Kγ complexes show that each of the inhibitors binds in the ATP-binding site, with one ring system partially overlapping and coplanar with the space occupied by the adenine moiety of ATP [12], [13]. All of the inhibitors have a hydrogen bond acceptor in a position equivalent to N1 of ATP. This is a feature that seems to be conserved in all kinase-inhibitor complexes [15]. This interaction in PI3Kγ involves the backbone of Val-882 and the morpholino oxygen of PI3K inhibitors such as LY294002 [13], PI-103 [1], and ZSTK474 (see the X-ray data obtained by Cmiljanovic et al.), and GDC-0941 [16] (for chemical structures of these compounds see Figure 6 and text below). Removal of the oxygen from a single morpholine resulted in a lost of

inhibitor activity (Figure 5). Additionally, known from the public domain and validated by our own research, morpholine-containing PI3K inhibitors are able to specifically target whether an individual PI3K isoform (compound TGX-221 targets selectively PI3Kβ isoform [17], Figure 6) or class I PI3Ks (p110α, p110β, p110γ and p110δ) without additional mTOR activity (compound ZSTK474 [18]) or mTOR[1] without affecting the PI3K activity (compound WYE-354 [19] and compound KU-0063794 [20], Figure 6).

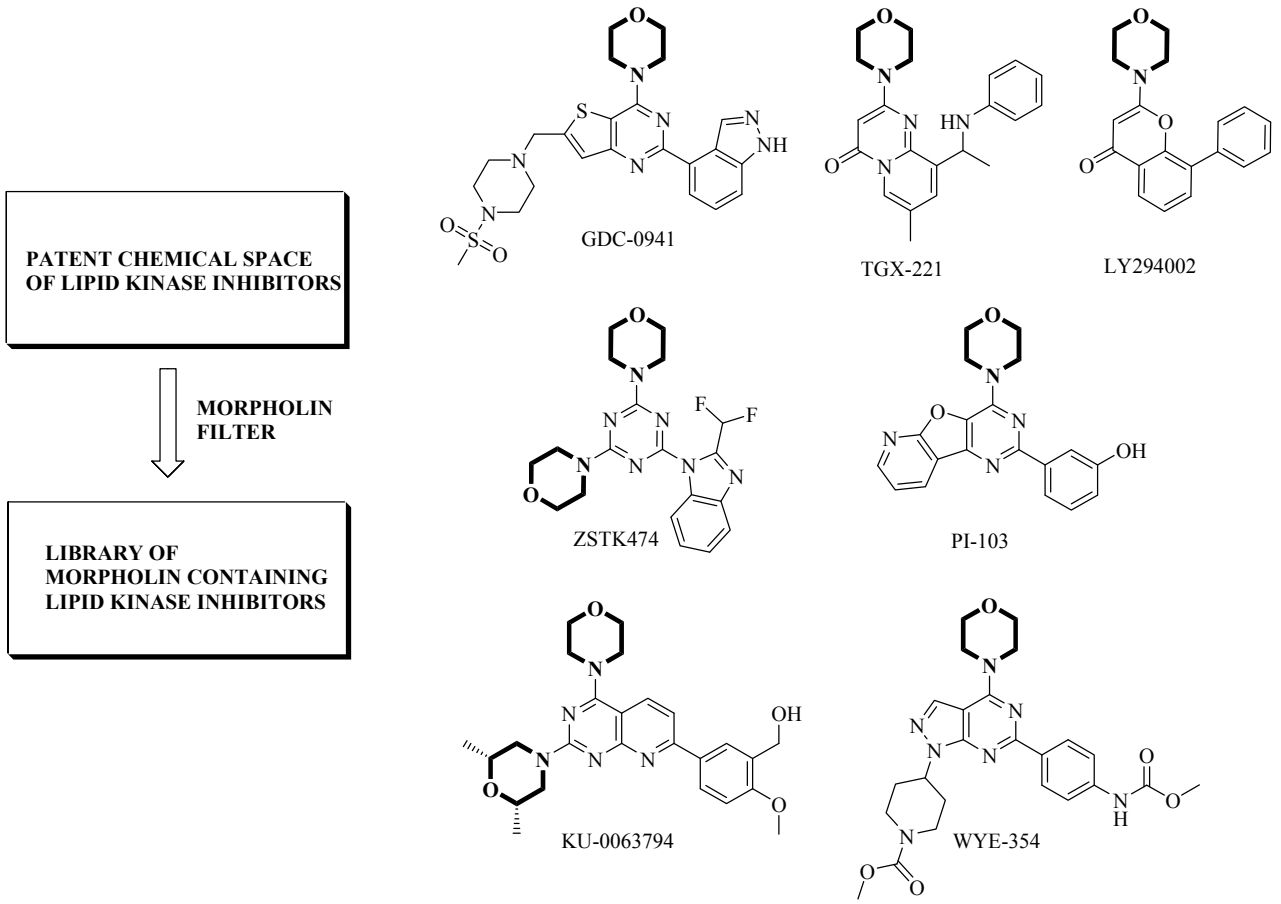

Figure 6. Representatives of morpholine-containing lipid kinase inhibitors known from the public domain. PI-103 targets with low-nanomolar activity the whole class I PI3Ks (isoforms p110α, p110β, p110γ and p110δ) as well as mTOR and DNA-PK (DNA dependent kinase) [1]. GDC-0941 targets with low-nanomolar activity class I PI3Ks and with sub-nanomolar activity mTOR [16]. TGX-221 is able to inhibit selectively the PI3Kβ isoform *in vitro* [17]. LY294002 is a broad lipid kinase inhibitor [12]. ZSTK474 is a selective class I PI3K inhibitor [18] without mTOR activity, and WYE-354 [19] and KU-0063794 [20] are selective mTOR inhibitors.

Because of available structural and promising biological data regarding target selectivity of morpholine-containing inhibitors as well as low cost availability of their building blocks, we used

[1] Targeting of mTOR includes complexes mTORC1 and mTORC2; mTORC1 is controlling the activation of S6K1 (ribosomal protein S6 kinase) and 4E-BP1 (so-called 4E-binding protein) and therefore ribosome biogenesis and translation. mTORC2 is making a positive feedback loop to phosphorylate PKB/Akt on Ser473. It is assumed that only mTORC1 is integrating nutrient and energy signals.

the morpholine pharmacophore[m] as a filter to select the relevant compounds from the patent chemical space for their further optimizations. Target selectivity, cellular activity measured by phosphoPKB-PKB[n] detection and *in vitro* activity against PI3Kα[o] activity were used as next filter criteria to eliminate specific scaffolds and their representatives from the chemical library (Figure 7).

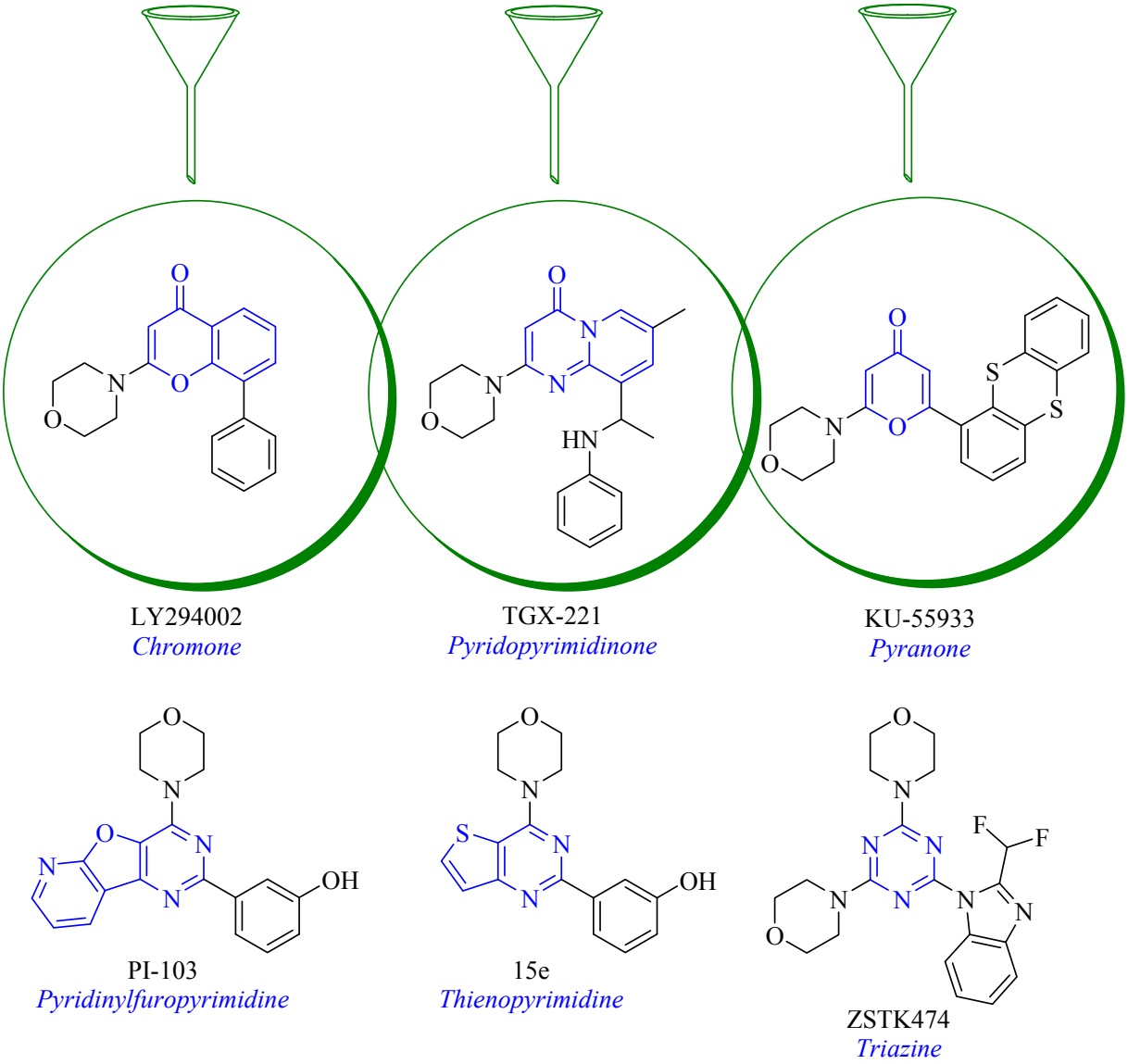

Figure 7. Filtering the morpholine-containing PI3K inhibitors according to their selectivity. Compound LY294002 is a broad range PI3K inhibitor with unwished toxicological effects [12], TGX-221 is selective inhibitor of PI3Kβ, which has no proven relevance in cancer therapy, and KU-55933 is a selective ATM (PI3K-related protein kinase) inhibitor. For PI-103, 15e and ZSTK474 a high anti-cancer potential was proofed [5].

[m] The IUPAC definition of a pharmacophore is "an ensemble of steric and electronic features that is necessary to ensure the optimal supramolecular interactions with a specific biological target and to trigger (or block) its biological response" (Wermuth, C.G., et al., Pure Appl. Chem., 1998).
[n] PKB also known as Akt is a downstream effector of PI3K in so-called PI3K/Akt signalling pathway.
[o] PI3Kα is the promising drug target in cancer.

Due to the importance of selective targeting of: i) mTOR, ii) PI3Kα, iii) class I PI3K or iv) class I PI3K/mTOR for cancer therapy, we wondered if we could design novel compounds with concerted selectivity by exploiting the structural properties of the known inhibitors with well-characterized selectivity profiles. More precisely, we aimed to explore how the specific changes in a chemical structure of small molecular weight lipid kinase inhibitors, could influence their selectivity within the same target family. For example, PI-103 (Figure 7) targets PI3K and mTOR at the same time, while ZSTK474 (Figure 7) is a pan-PI3K inhibitor without mTOR activity. We assumed that movement from ZSTK474 to PI-103 through the insufficient explored chemical space would lead us to novel molecules with refined target selectivity.

With the aim to systematically explore the previous described ideas and to close the gaps in knowledge of the specific function of different PI3K isoforms, we made a library of ~300 drug-like compounds, which were designed by applying specific combination of common medicinal chemistry methods such as scaffold hybridization[p] (also called scaffold morphing) and scaffold hopping on compounds selected in previous described steps. We firstly applied scaffold hybriding and scaffold hopping on ten different morpholin-containing compounds with the most active cellular properties and different selectivites. For example, the molecular fragments of compound PI-103, which is a PI3K/mTOR inhibitor, were crossed with the fragments of selective pan-PI3K compound ZSTK474 (Figure 8). The activity and selectivity of novel hybrid- and hopping-molecules was systematically investigated.

[p] For better understanding of the chemistry done for this project, the term “hybrid” should be explained. According to the Oxford English Dictionary the word “hybrid” is derived from Latin *hybrida*, meaning the “offspring of a tame sow and a wild boar”, “child of a freeman and slave”, etc. In general usage, “hybrid” is a thing made by combining two different elements, the offspring of two plants or animals of different species or varieties, such as a mule.

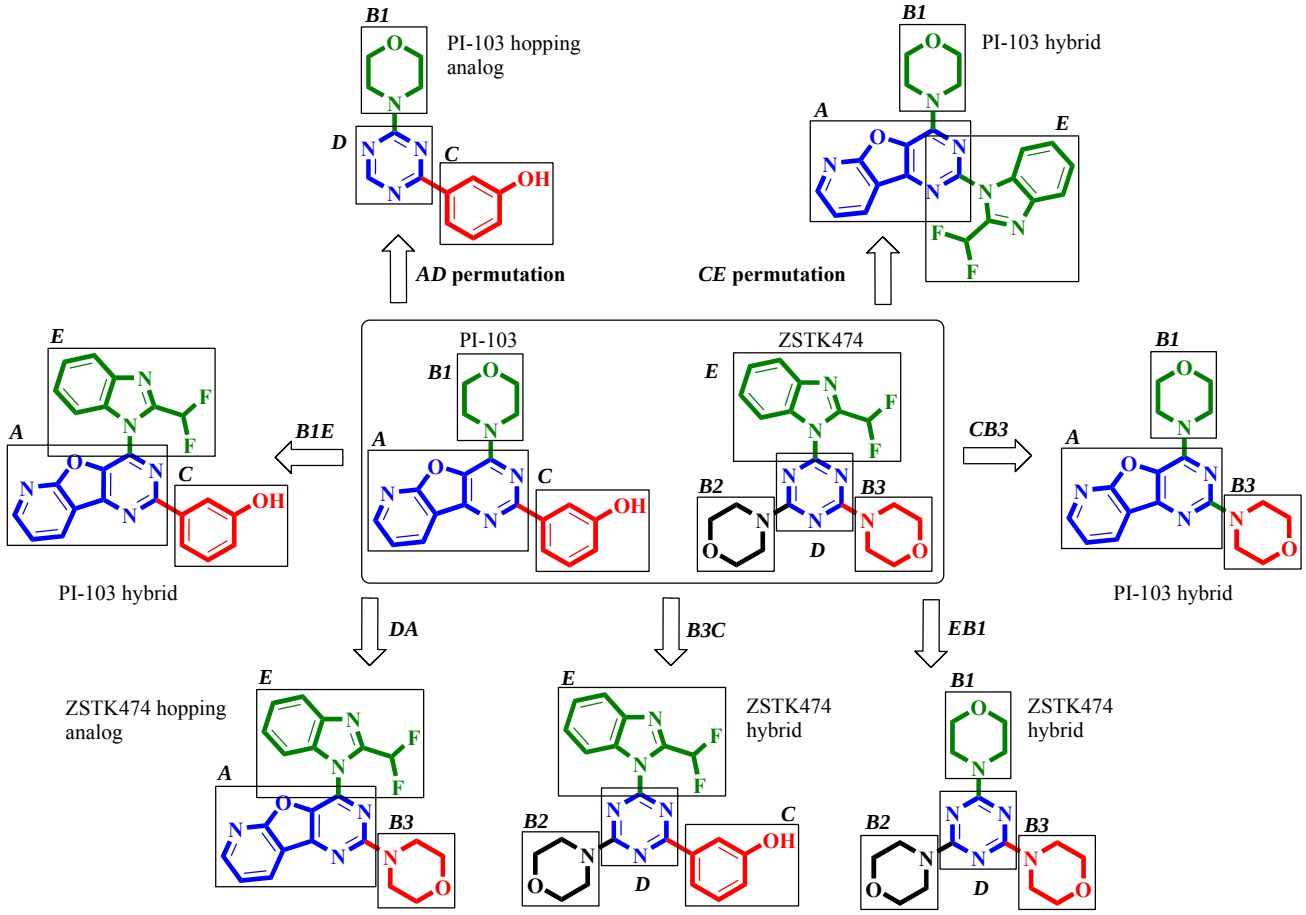

Figure 8. Presented is a strategy where the fragments of the known biologically active chemical compounds are crossed between each other, with the aim to obtain novel so-called hybrid-molecules. This offers the potential to modify existing leads in terms of selectivity, pharmacokinetic properties or side-effect profile. Novel hybrid molecules can be crossed with compounds obtained by crossing of two other PI3K inhibitors, with the aim to gain second generation hybrid molecules. In this example the chemical space of molecules PI-103 and ZSTK474 was rationally extended by applying scaffold hybriding and scaffold hopping strategies at the same time to provide novel molecules that are not covered by pharmaceutical industry and for which interesting biological properties where obtained. In comparison with the medicinal chemistry examples from the literature, where whether hybriding or hopping was obtained on a certain single scaffold, we obtained both strategies in a combinatorial way on several different scaffolds (see Matrix table, Figure 10).

In comparison with the known examples from the public domain, where only one scaffold relevant for a certain project was whether hybrided or hopped, we performed combinatorial optimization of our preselected molecules by parallel applying of scaffold hybriding and scaffold hopping strategies. Designed molecules were successfully synthesized and their activity was measured *in vitro* against PI3Kα and mTOR and *in cell*. Additionally, in close collaboration with computational scientists from the research group of Prof. Marketa Zvelebil (London Cancer

Research Institute) all molecules were docked[q] into the available crystal structures of PI3Kα and PI3Kγ isoforms and modelled structure of mTOR to explore the binding mode orientations of the docked ligands and their binding energies. Moreover, the first obtained *in silico* results were optimized with the results obtained from synthesis, X-ray and biological experiments, and were used as training sets for later experiments, where the docking of new molecules was successfully automated. In close collaboration with crystallographists from the research group of Prof. Roger Williams (Cambridge University, MRC Laboratory of Molecular Biology) an X-ray analysis of the most potent inhibitors was successfully accomplished. Such in-depth analysis led us to the fact that only morpholine moiety of the tested compounds is able to recognize the prominent valine entity making a key hydrogen bond; non-formation of the key hydrogen bond led to total inactivity of the relevant compounds. This criteria was used for the next filtering step, where all candidates without morpholine fragment were eliminated to avoid the synthesis; for example the PI-103 hybrid with the fragment sequence *AEC* (on the mid-left side of the Figure 8) did not fulfil the morpholine criteria and was eliminated; to confirm the quality of such morpholin-filter this compound and several analog compounds were synthesized and biologically characterized; they were inactive *in vitro* and *in cell* (for experimental results see the chapter 4 "Chemistry and Biology").

The previous results led us to a more focused library of 78 compounds that we called matrix-template library. Here we hopped from one into another morpholine-containing scaffold (see the first column from the left of the matrix table, Figure 10) and all these scaffolds were hybrided with appropriate fragments that we called "hybrid fragments" (see the first row at the top of the matrix table, Figure 10). Hybrid fragments were selected from the literature and patent domain. We supposed according to the structural data obtained for some hybrid fragments that all hybrid fragments from the matrix table are able to reach a deep hydrophobic pocket (also called "affinity pocket") within the ATP binding site (for more details see the chapter 3.3.5. "Insights into inhibitor activity and selectivity"). Within a column or a row of the matrix table the appropriate scaffolds and hybrid fragments were arranged according to *complexity rules* that we postulated.

[q] DOCKING AND SCORING is the process of computationally placing a virtual molecular structure into a binding site of a biological macromolecule (docking) and flexibly or rigidly relaxing the respective structures then ranking (scoring) the complementarity of fit (Bleicher et al., Nat Rev Dug Discov, 2003).

3.2.1. Complexity Rules for Design of Matrix-Template Libraries

By designing the drug-like matrix-template libraries we defined a set of complexity rules used to compare the appropriate scaffolds and hybrid fragments that are classified according to their complexity. The purpose of such system is to rationalize a designed drug-like matrix library in order to get a systematic overview which chemical fragments are responsible for the activity to the related targets and which of the most promising regions of the chemical space remain unexplored.

Two heteroatom containing aromatic groups within a scaffold hopping or a scaffold hybrid alignment of the matrix library are compared first by ring largeness of the heterocyclic aromatic system. The aromatic one-ring systems have lower complexity in comparison with two- or more-ring aromatic systems respectively fused aromatic systems; for example the aniline moiety as a one-ring system has lower complexity than the two-ring containing indole moiety (Figure 9A). Two aromatic one-ring systems (Figure 9B) or the aromatic two- or more-ring systems (Figure 9C) are compared by decreasing atomic number of the atoms directly attached to them or their substituents; the group having the atom of lower atomic number receives lower complexity (for example the toluene moiety has lower complexity as the aniline and further the aniline has lower complexity than phenol; additionally a pyridine has the lower complexity than pyrimidine, in turn a triazine has the higher complexity than pyrimidine (Figure 9B); for two-ring systems an indene moiety without a heteroatom has the lower complexity in comparison with an indole moiety containing a nitrogen atom, and further an indole moiety has lower complexity in comparison with the benzofuran group; the four heteroatom containing oxazolopyrimidine has in comparison with benzofuran and furopyrimidine the highest complexity (Figure 9C)). In addition, aromatic substitution with a primary amine provides a ligand, which has lower complexity than the ligand that was substituted with a secondary amine such as morpholine (see the matrix table, Figure 10). In case of regioisomers such as 6- and 2-substituted pyrimidine dimorpholine (matrix table, Figure 10), the lower complexity has such group whose aromatic carbon atom on which the hybrid fragment is attached has lower complexity according to the rule of decreasing atomic number of attached substituents (for example regioisomer 1 from figure 10 has lower complexity than regioisomer 2).

Comparison by:

(A) ring largeness

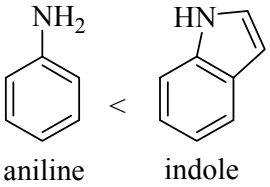

Purpose of the complexity rules:
systematic overview of chemical fragments
responsible for the inhibitor activity & selectivity

(B) decreasing atomic number of attached substituents

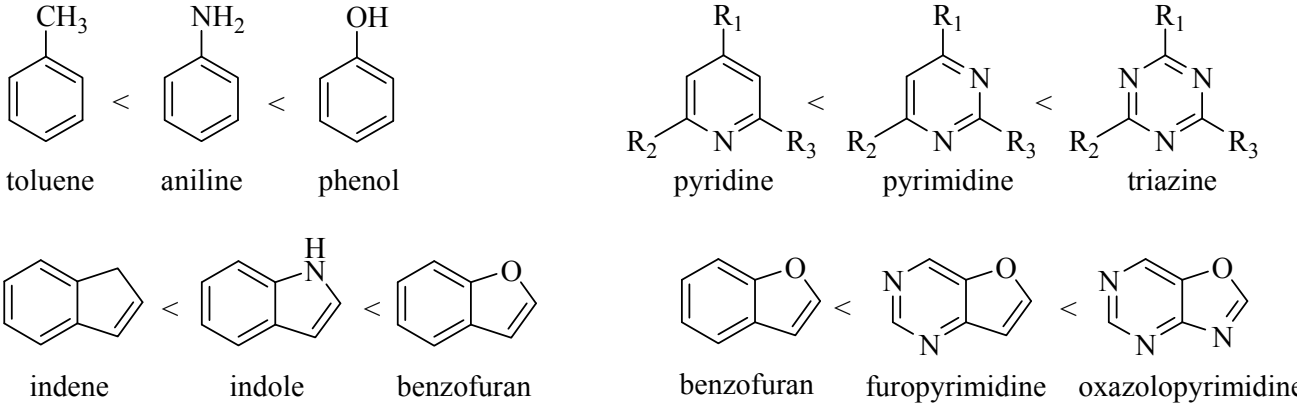

Figure 9. Complexity rules for the design of matrix-template libraries. Complexity increases from left to right. (A) Two heteroatom containing aromatic groups within a scaffold hopping or a scaffold hybrid alignment of the matrix library are compared first by ring largeness of the heterocyclic aromatic system. The aromatic one-ring systems have higher priority in comparison with two- or more-ring aromatic systems respectively fused aromatic systems; for example the aniline moiety as a one-ring system has higher priority than the two-ring containing indole moiety. (B-C) Two aromatic one-ring systems or the aromatic two- or more-ring systems are compared by decreasing atomic number of the atoms directly attached to them or their substituents; the group having the atom of lower atomic number receives higher priority; for example the toluene moiety has higher priority as the aniline and further the aniline has higher priority than phenol; additionally a pyridine has the higher priority than pyrimidine, in turn a triazine has the lower priority than pyrimidine; for two-ring systems an indene moiety without a heteroatom has the higher priority in comparison with an indole moiety containing a nitrogen atom and further an indole moiety has higher priority in comparison with the benzofuran group; the four heteroatom containing oxazolopyrimidine has the lowest priority and highest complexity in comparison with benzofuran and furopyrimidine.

Each scaffold fragment of the matrix table was correlated with each hybrid fragment leading to the appropriate compounds whose activity was measured *in vitro* and *in cell*. For every matrix

compound a pie chart (or a circle graph) is presented, which summarizes the biological activity of the compound; blue colour of the pie chart presents the cellular pPKB/PKB remaining activity, purple colour presents the cellular pS6 activity (phosphorylated S6 ribosomal protein, another marker of Akt/mTOR activation) and the brown colour presents *in vitro* activity for PI3Kα; for each pie it is imperative that the smaller the pie slice is the better is the appropriate activity (Figure 10). Additionally the backgrounds in the matrix table of the compounds with very good binding affinities are colored yellow, and those with good affinities are blue. Such matrix table gave us a great overview by visualising which scaffolds and hybrid fragments should be combined in order to refine the activity and the selectivity of relevant hit compounds.

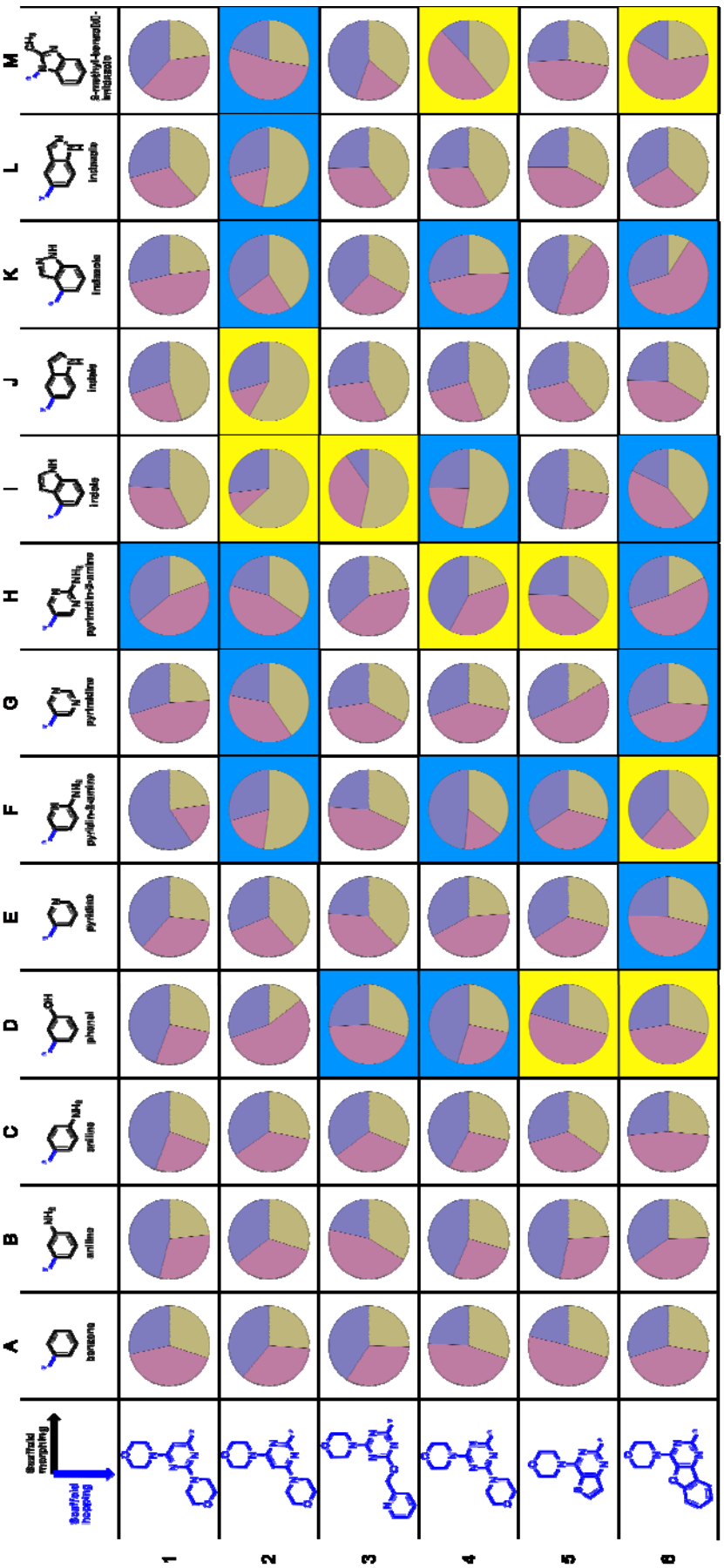

Figure 10. *Matrix-template library* of 78 compounds. Here we hopped from one into another morpholine-containing scaffold (see the first column from the left of the matrix table) and all these scaffolds were hybrided with appropriate fragments that we called "hybrid fragments" (see the first row at the top of the matrix table). Hybrid fragments were selected from the literature and patent domain. We supposed according to the structural data obtained for some hybrid fragments that all hybrid fragments from the matrix table are able to reach a deep hydrophobic pocket (also called "affinity pocket") within the ATP binding site. Within a column or a row of the matrix table the appropriate scaffolds and hybrid fragments were arranged according to *complexity rules* that we postulated (for the explanations of the rules consult the text). For every matrix compound a pie chart is presented; blue colour of the pie chart presents the cellular pPKB/PKB remaining inhibitor activity, purple colour presents the cellular pS6 activity and the brown colour presents *in vitro* inhibitor activity for PI3Kα; the smaller the pie slice is the better is the appropriate inhibitor activity. Compounds with yellow backgrounds have been shown to be very good active and those with blue backgrounds are good active.

3.3. Hit to Lead Optimization

After identification of hits[r] (compounds with yellow and blue backgrounds in matrix table, Figure 10) from the matrix library a hit-to-lead[s] follow up began by applying different medicinal chemistry strategies. By performing hit development using matrix-template strategy, we observed that the most compounds were cellular permeable and non-toxic in cellular systems. Last but not least, all compounds from the matrix-template library satisfy Lipinski's rule of five[t] [Lipinski, 1997 #145] in terms of drug-likeness[u].

By selecting the patented scaffolds for the matrix library, we considered ligand complexity and chemical tractability (suitability of a compound for chemical modification) as parameters for medicinal chemistry optimizations. Higher priority in the matrix library was given for molecules that are easier to synthesize and more amenable for structure-activity-relationship (SAR) development. The more positions on a scaffold that can be modified using robust chemistry, the more diverse are the analogs that can be accessible for the collection of SAR information. From 78 compounds of the matrix library 28 cell-permeable compounds were identified with good to very good *in vitro* and cellular activity. Figure 11 summarizes cellular and *in vitro* activity of the matrix-hit-compounds, which were further optimized by applying different medicinal chemistry strategies. Figure 12 summarizes the cellular pPKB/PKB and *in vitro* PI3Kα activity of all hit compounds and their analogues, which were obtained through the medicinal chemistry optimizations of our highly-motivated research team.

---

[r] HIT is „a primary active compound(s) with non-promiscuous binding behaviour, exceeding a certain threshold value in a given assay(s). The "active" is followed up with an identity and purity evaluation, an authentic sample is then obtained or re-synthesized and activity confirmed in a multi-point activity determination to establish the validity of the hit (validated hit)" (Bleicher, K.H., et al., *Hit and lead generation: beyond high-throughput screening.* Nat Rev Drug Discov, 2003. **2**(5): p. 369-378).

[s] LEAD is "a prototypical chemical structure or series of structures that demonstrate activity and selectivity in a pharmacological or biochemically relevant screen. This forms the basis for a focused medicinal chemistry effort for lead optimization and development with the goal of identifying a clinical candidate. A distinct lead series has a unique core structure and the ability to be patented separately".

[t] LIPINSKI'S RULE OF FIVE is a rule to evaluate druglikeness, or determine if a chemical compound with a certain biological activity has properties that would make it a orally active drug in humans. The rule was formulated by Christopher A. Lipinski in 1997, based on observation that most medication drugs are relatively small and lipophilic molecules. The rule says, that, in general, an orally active drug has to fulfil following criteria: (a) not more than 5 hydrogen bond donors (nitrogen or oxygen atoms with one or more hydrogen atoms); (b) not more than 10 hydrogen bond acceptors (nitrogen or oxygen atoms); (c) a molecular weight under 500 daltons; (d) an octanol-water partition coefficient log*P* is less than 5.

[u] DRUG-LIKENESS is a scoring metric (computational) for the similarity of a given structure to a representative reference set of marketed drugs (Bleicher, K.H., et al., *Hit and lead generation: beyond high-throughput screening.* Nat Rev Drug Discov, 2003. **2**(5): p. 369-378).

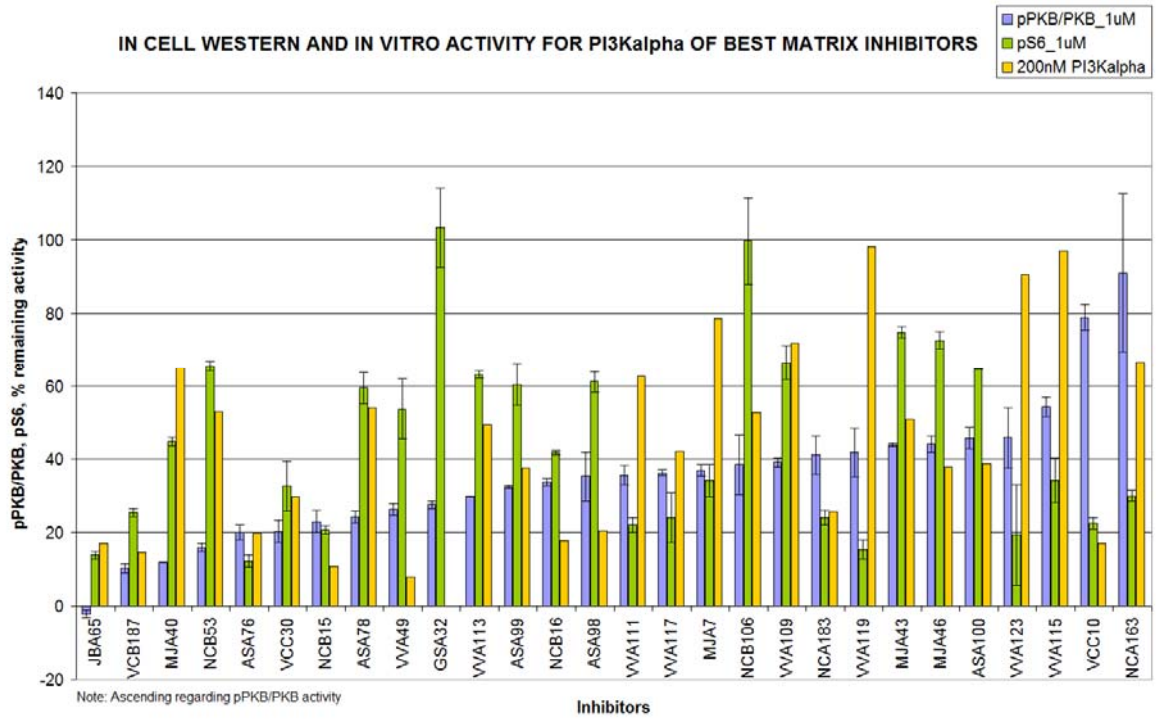

Figure 11. Biological activity of 28 cell-permeable compounds with good to very good biological activities that were identified from the preselected library of 78 compounds. All compounds were rapidly characterized by high-throughput screening assays such as in-cell Western method and *in vitro* method for profiling against PI3Kα. The identified hits were further optimized by applying different medicinal chemistry strategies.

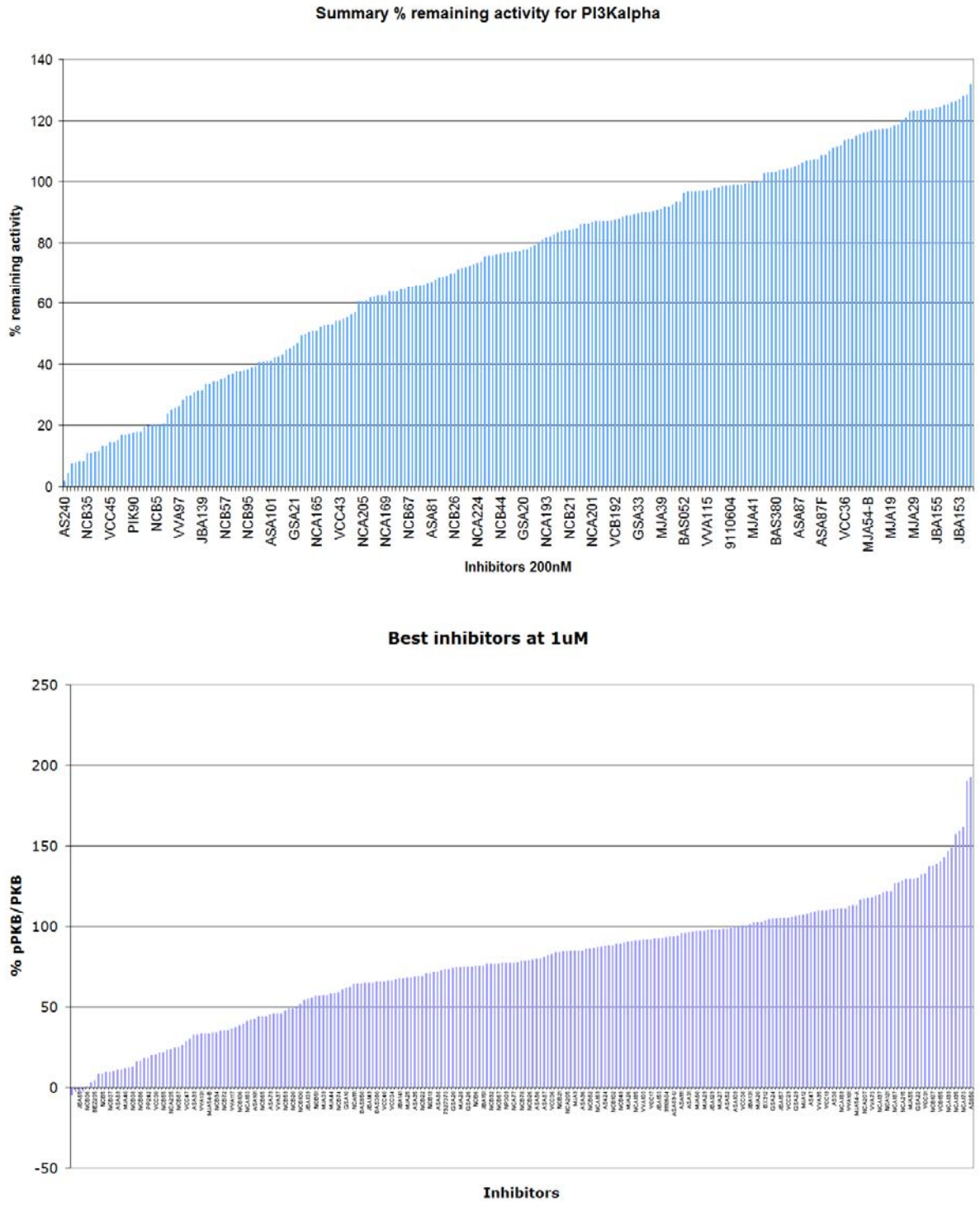

Figure 12. Summary of best inhibitors at 200 nM *in vitro* (above) and at 1 μM by in-cell Western method (below), where inhibitor efficacy was measured by pS6 Ser 235/236 detection. The higher the pPKB/PKB values are the less strong is the inhibition of signalling.

3.3.1. Medicinal Chemistry Application of Fluorine

Carbon-bound fluorine atoms are unique in organic chemistry. Fluorine is a small atom with a very high electronegativity [22]. With a van der Waals radius of 1.47 Å [23], covalently bound fluorine occupies a smaller volume than a methyl, amino, or hydroxyl group, but is larger than a hydrogen atom (van der Waals radius of 1.2 Å). While synthetic fluoro-organic chemistry has matured over recent decades, the specific use of fluorine in small-molecule drug-discovery research is more recent. Fluorinated compounds are nowadays synthesized in pharmaceutical research on a routine basis [24]. According to the World Drug Index (WDI), there are 128 fluorinated compounds with US trade names [25].

Current strategies for the introduction of fluorine atoms center on the following topics [25]:

3.3.1.1. Improving Metabolic Stability With Fluorine

Metabolic stability is one of the key factors in determining the bioavailability of a compound. Rapid oxidative metabolism by the liver enzymes, in particular the P450 cytochromes[v], is often found to limit bioavailability. A frequently employed strategy to circumvent this problem is to block the reactive site of the relative compound by the introduction of a fluorine atom. There are many examples illustrating that the replacement of an oxidizable C-H group by a C-F group increases metabolic stability of the molecule [25].

3.3.1.2. The Effect of Fluorine on Physicochemical Properties

3.3.1.2.1. The Effect of Fluorine on the pK_a

As the most electronegative atom, fluorine has a very strong effect on the acidity or basicity of nearby functional groups. Depending on the position of the fluorine substituent relative to the acidic or basic group in the molecule, a pK_a shift of several log units can be observed. For example, the pK_a's of acetic acid and its α-fluorinated analogues are 4.76 (CH_3COOH), 2.59 (CH_2FCOOH), 1.24 (CHF_2COOH), and 0.23 (CF_3COOH) [25]. Highly basic groups can have a limiting effect on the bioavailability. A fluorine atom introduced close to a basic group reduces its basicity; this results in

[v] CYTOCHROME P450 is a family of iron-haem-containing enzymes involved in oxidative metabolism of a broad variety of xenobiotics and drug compounds.

better membrane permeation of a compound and thus improved bioavailability. For example, the basicities of ethylamine and its β-fluorinated analogues, measured by the pK_a's of the protonated amines, decrease in an approximately linear fashion upon introduction of fluorine, the pK_a's being 10.7 ($CH_3CH_2NH_2$), 8.97 ($CH_2FCH_2NH_2$), 7.52 ($CHF_2CH_2NH_2$), and 5.7 ($CF_3CH_2NH_2$) [25]. Quite often, a change in the pK_a has a strong effect on both the pharmacokinetic properties of the molecule and its binding affinity. For example, a strongly basic group may be required for binding within a certain lead series, but at the same time this basic group may also be found to result in compounds with low bioavailability due to the limited ability of a strong basic group to pass through membranes.

3.3.1.2.2. The Effect of Fluorine on Molecular Lipophilicity

Lipophilicity is a key molecular parameter in medicinal chemistry. Typically, groups of substantial lipophilicity on the ligand are required to obtain a good binding affinity to the target protein [25]. However, a high lipophilicity typically results in a reduced solubility and a number of other undesirable properties for a compound. Therefore, the right balance between a required lipophilicity and a certain minimal overall polarity of the molecule is one of the recurring challenges for medicinal chemists.

The substitution of a hydrogen atom by fluorine increases lipophilicity slightly, by roughly 0.25 logD^w units [25]. Interestingly, there are quite a number of cases for which an H to F substitution decreases lipophilicity (Figure 12a) [25]. This is the case, when an oxygen atom is close to the fluorine by the relevant compound. One possible explanation, is that fluorine in close vicinity to an oxygen atom increases the overall polarity of the molecule, leading to a more pronounced gain in solvation energy in the polar medium relative to the nonpolar solvent [25]. However, it is also possible that the fluorine polarizes the neighboring oxygen atoms and this leads to stronger hydrogen bonds between the oxygen and neighboring water molecules.

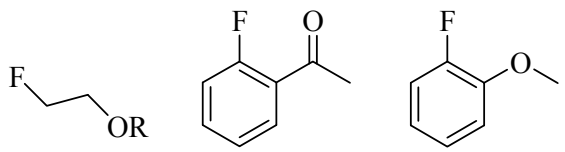

Figure12a. Examples where an H to F substitution decreases lipophilicity.

[w] Log*D* is the logarithmic coefficient of the distribution of the compound between octanol and water at a given pH (typically 7.4).

3.3.1.3. The Effect of a Fluorine Substitutent on Molecular Conformation

A fluorine substitutent can lead to a change in the preferred molecular conformation. Again, this effect can be explained by the size and electronegativity of fluorine. Based on a van der Waals radius of 1.47 Å for fluorine, the volume of a trifluoromethyl group is roughly twice that of a methyl group. As a result, the effect of fluorine substitution on molecular conformation is quite subtle and sometimes difficult to predict [25].

3.3.1.4. The Role of Fluorine in Protein-Ligand Interactions

Fluorine can have significant effects on the binding affinity in protein-ligand complexes. This effect can be direct by interaction of the fluorine with the protein, or it can be indirect by modulation of the polarity of other groups of the ligand that interact with the protein [25]. For example, most of the NK1 antagonists currently in clinical development contain a 3,5-di(trifluoromethyl)phenyl group to increase binding affinity [26]. Additionally, fluorine can have a role in polar interactions. Lessons from a set of fluorine-substituted thrombin inhibitors demonstrate that C-F···C=O interactions can play an important role in protein-ligand interactions and can lead to significantly increased binding affinities [25].

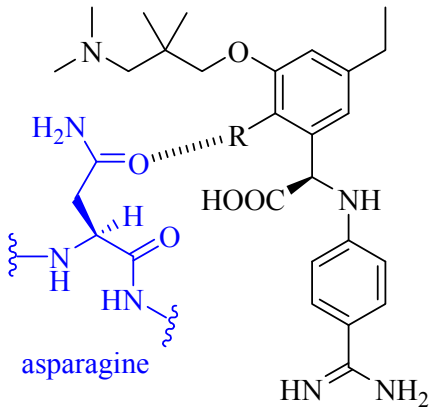

R	Ki - Thrombin [mM]
H	1.6
F	0.26

Figure 12b. Insertion of a fluorine to the presented thrombin inhibitor increases the inhibitor activity according to the C-F···C=O interaction of the thrombin inhibitor and the asparagine moiety of the target protein.

3.3.1.5. Applying Fluorine Strategy on PI3K Inhibitors

We could successfully apply fluorine strategy on our own research. Fluorine was systematically introduced at various positions of the inhibitor skeleton to explore the binding affinity and specific interactions of the halogen with active-site amino acid residues of the enzyme. In several examples insertion of fluorine dramatically enhanced the biological activity of the relevant hit-inhibitor. For example, compound **97** (NCA163) (Figure 13) from the matrix library was identified as a hit with good cellular and *in vitro* properties. Insertion of trifluoromethyl group on the 4-position of the pyridine ring of **97** (NCA163) led to the analog **98** (NCB5), which showed excellent activity in melanoma cancer cell lines (Figure 13). We determined the X-ray crystal structure of NCB5 in complex with PI3Kγ (Figure 13). 4-(trifluoromethyl)pyridin-2-amine group of **98** (NCB5) is going into deep hydrophobic pocket of the enzyme, where a fluorine atom of the trifluoromethyl group is within hydrogen-bonding distance of the N-H group of the catalytic Lys-883. Therefore, this interaction mode certainly constitutes a favourable dipolar interaction. Whether one wants to call this a hydrogen bond remains a matter of personal taste. Interestingly, insertion of CF_3-group led to nine times more potency *in vitro* against PI3Kα (Figue 13). Molecular modelling experiments with the PI3Kα crystal structure demonstrated that in comparison with PI3Kγ isoform the 4-(trifluoromethyl)pyridin-2-amine group of **98** (NCB5) was better fited within the ATP-binding pocket and therefore more hydrophobic contacts with the protein were obtained. IC_{50} measurements of **98** (NCB5) for class I PI3Ks and for mTOR demonstrate that this compound is selective pan-PI3K inhibitor with low-nanomolar activity (IC_{50}: PI3Kα (20 nM), PI3Kβ (15 nM), PI3Kδ (38 nM), mTOR (>1000 nM)). This example from our own research is an additional example, which demonstrates that fluorine can have significant effects on binding affinity in protein ligand complexes.

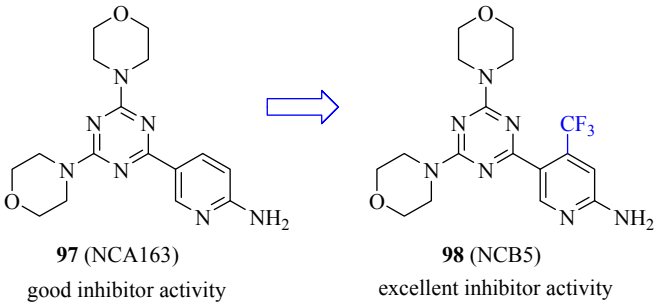

97 (NCA163)
good inhibitor activity

98 (NCB5)
excellent inhibitor activity

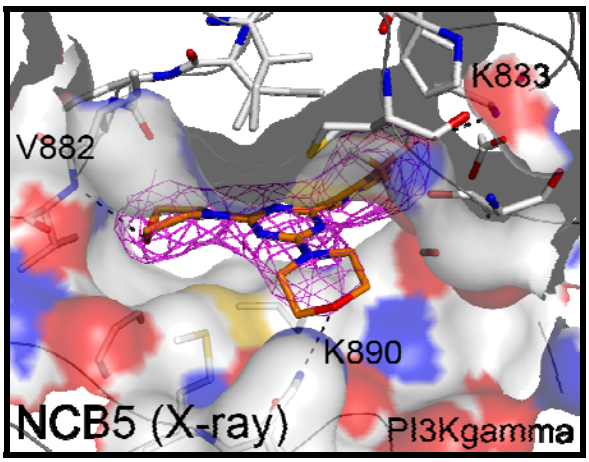

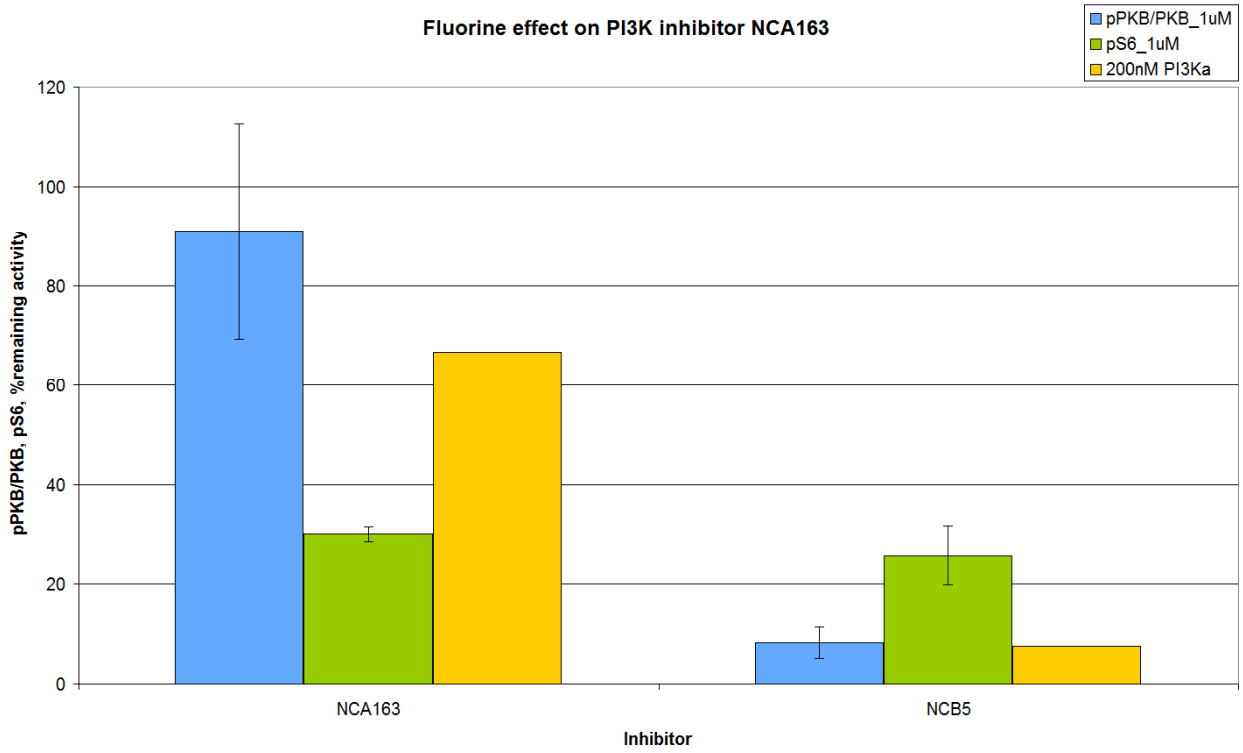

Figure 13. Fluorine effect on PI3K inhibitor **97** (NCA163). Presented is cellular activity (pPKB/PKB and pS6 bar charts) at 1 μM and *in vitro* activity against PI3Kα at 200 nM; the lower the bar chart the better is the activity of the relevant compound. Insertion of trifluoromethyl group led to considerable increased cellular activity and nine times more potency *in vitro* against PI3Kα. According to the X-ray crystal structure a fluorine atom of the trifluoromethyl group is within hydrogen-bonding distance of the N-H group of the catalytic Lys-883. Second morpholine moiety makes an additional H-bridge formation with Lys-890.

Another very interesting example from our own research is the fluorine effect on compound **114** (NCB53, matrix coordinate: M4) (Figure 13b). Compound **114** (NCB53) was identified as a hit from the matrix-template library. The literature known analog of this compound is the pan-PI3K selective inhibitor **115** (ZSTK474) from the Japanese pharmaceutical company Zenyaku Kogyo, which is the first orally available PI3K inhibitor. ZSTK474 is currently in clinical phase I.

We investigated the effect of replacing hydrogen atoms from the methyl group of compound **114** (NCB53) by a fluorine atom on the molecular conformation of the compound as well as protein-ligand interactions. Insertion of trifluoromethyl group to the benzimidazole moiety led to the compound **116** (NCA111), which was poorly active in cellular assays. Interestingly, insertion of difluoromethyl group to the benzimidazole provided the known compound ZSTK474, which has been shown to be the most potent benzimidazole-containing triazine derivative. With the aim to explore the effect of difluoromethyl group on the ligand activity, we determined the X-ray structure of ZSTK474 bound to PI3Kγ (Figure 13c). According to the X-ray structure fluorine of difluoromethyl group plays an important role as an acceptor for H-bridge formation. A similar H-bridge formation was observed for fluorine from the trifluoromethyl group of **98** (NCB5). Further efforts in analytical chemistry (NMR) explained that the reason for specific binding mode of ZSTK474 is an intramolecular H-bridge formation between hydrogen atom of the difluoromethyl group and nitrogen of the triazine scaffold (Figure 13c). The intramolecular H-bridge could not be obtained by NMR due to the symmetry of the ligand ZSTK474. To obtain the intramolecular H-bridge formation we broke the symmetry of the compound through the exchange of one morpholin ring with the dimethyl morpholin ring. By using Exchange NMR-Spectroscopy (EXSY) we were able to identify two possible conformers of the asymmetric ZSTK474 analog, compound NCB136, and to obtain their activation enthalpies $\Delta G^{\ddagger}[kJmol^{-1}]$ (Figure 13d). These results suggest that ZSTK474 is able, with help of the difluoromethyl group, to preorganize a specific symmetry before binding to the active-side of the protein. Intramolecular hydrogen bond formation of ZSTK474 can be explained with basicity of nitrogen atoms of triazine ring by analysing acid-base properties of well-characterized pyridine derivatives such as DMAP (Figure 13e). With such chemistry informations we were able to elucidate the selectivity mechanism of ZSTK474. One of two possible conformers of ZSTK474 within the protein binding pocket has been observed through the X-ray crystal structure where two H-bridge formations characterize the PI3K-ligand complex (Figure 13c). By docking the same ligand to the modeled mTOR structure we obtained the second possible conformer as the conformer with the highest binding energy to mTOR (Figure 13c). We proposed that due to the steric reasons and different ATP-binding pockets of class I PI3Ks and mTOR the conformer 1 is prefered by PI3Ks and conformer 2 by mTOR. Additionally by mTOR the H-bridge formation with the catalytic lysine residue is lost leading to the poor inhibitor activity to mTOR and therefore high class I PI3K selectivity (Figure 13c).

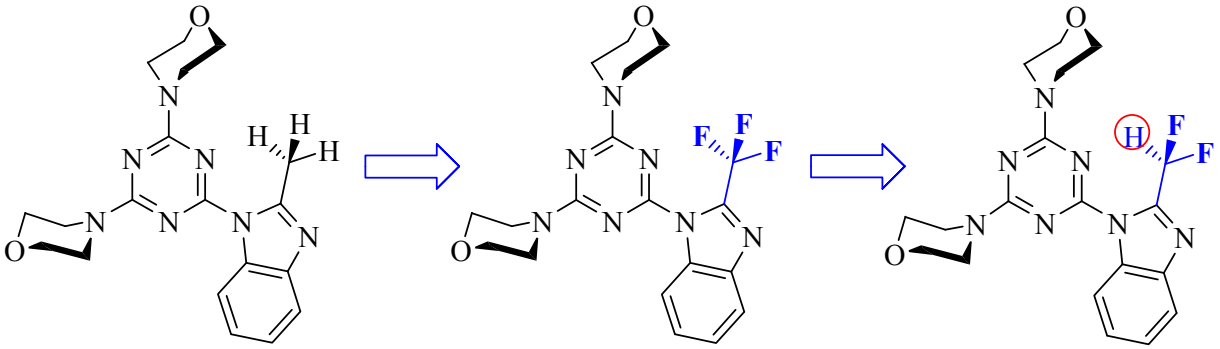

NCB53
very good pPKB inhibition
poor PI3Kalpha inhibition

NCA111
poor pPKB inhibition
good PI3Kalpha inhibition

ZSTK474
excellent pPKB inhibition
excellent PI3Kalpha inhibition

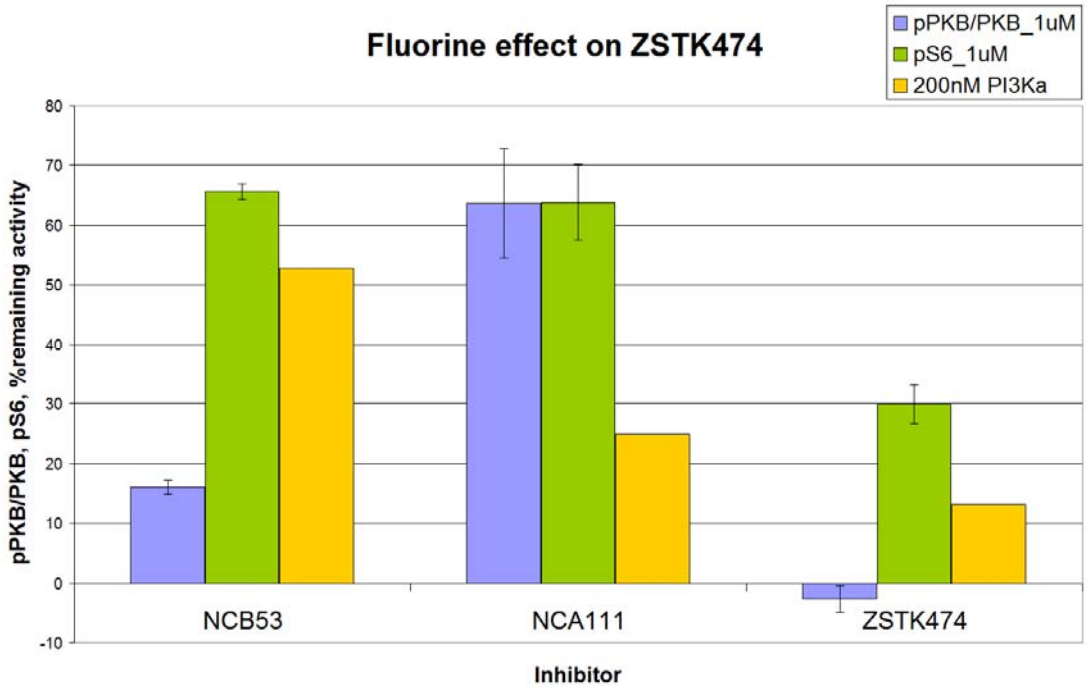

Figure 13b. Fluorine effect on ZSTK474. Presented is cellular inhibitor activity measured with pPKB, PKB and pS6 biomarkers in A2058 melanoma cells at 1 µM and *in vitro* inhibitor activity against PI3Kα at 200 nM; the lower the bar chart the better is the activity of the relevant compound. Trifluoromethyl group containing inhibitor **101** (NCA111) has lower activity as difluoromethyl group containing inhibitor (ZSTK474).

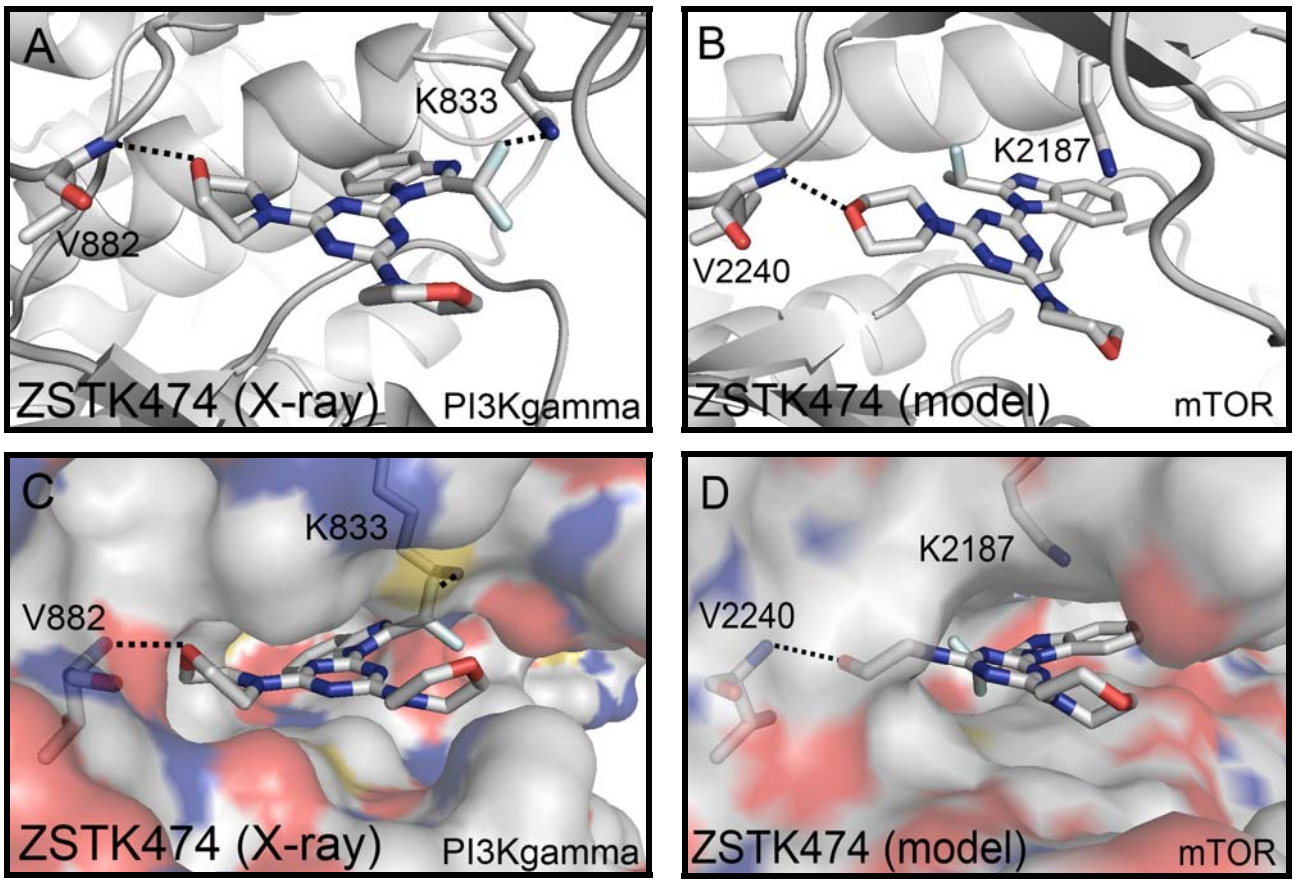

Figure 13c. (A) According to the X-ray crystal structure fluorine of the difluoromethyl group plays an important role as an acceptor for H-bridge formation. Specific interaction with Lys-833 within the ATP binding pocket leads to an appropriate binding mode of ZSTK474. Further efforts in analytical chemistry explained that the reason for such specific binding mode of ZSTK474 is an intramolecular H-bridge formation between hydrogen atom of the difluoromethyl group and the nitrogen atom of the triazine scaffold. (B) By docking the same ligand to the modeled mTOR structure the second possible conformer, as the conformer with the highest binding energy to mTOR and formed through the C-N bond rotation of the benzimidazole, has been observed. (C and D) We proposed that due to the steric reasons and different ATP-binding pockets of class I PI3Ks and mTOR the conformer 1 is prefered by PI3Ks and conformer 2 by mTOR. Additionally by mTOR the H-bridge formation with the catalytic lysine residue is lost leading to the poor inhibitor activity to mTOR and therefore high class I PI3K selectivity.

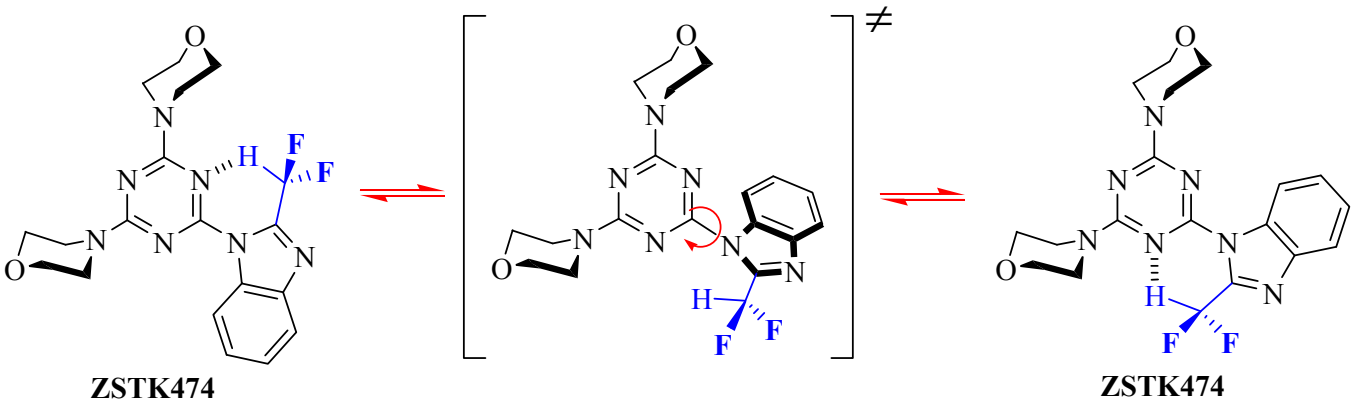

ZSTK474 **ZSTK474**

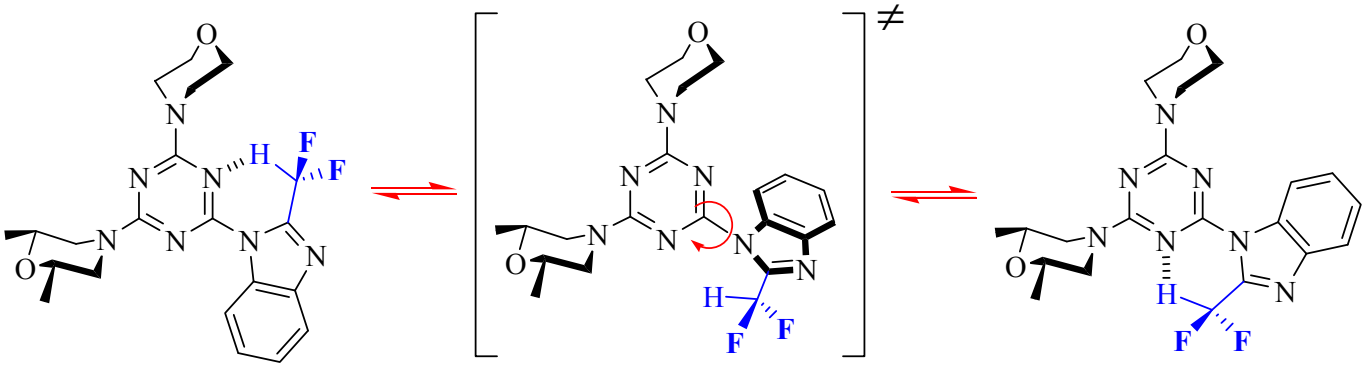

NCB136
NMR proven conformer 1

NCB136
NMR proven conformer 2

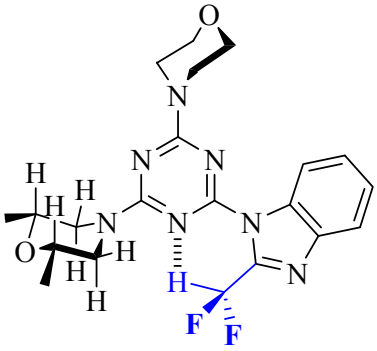

Asymmetric compound NCB136

LT/HT experiments on NCB-136:

assignment	*δ[ppm]*	*Δδ[Hz]*	$T_{coalesc.}[K]$	$\Delta G^{\ddagger}[kJmol^{-1}]$	$k(T_{coalesc.})[s^{-1}]$
H-3 Morph.	3.9	37.7	290	60.1	83.7
H-3e $Me_2M.$	4.5	58.3	336	68.9	129
H-3a $Me_2M.$	2.7	48.4	330	68.1	107

Figure 13d. With the help of Exchange NMR spectroscopy (EXSY-NMR) two possible conformers of the compound NCB136 have been identified. The obtained signals from EXSY spektren were used to calculate the activation enhalpie $\Delta G^{\ddagger}[kJmol^{-1}]$.

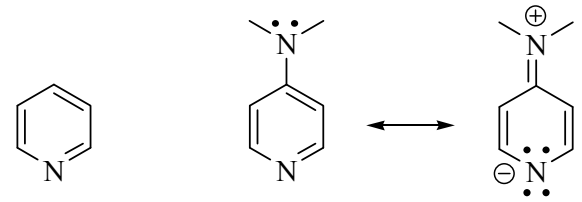

pyridine $pK_a = 5.2$ 4-dimethylaminopyridine (DMAP) $pK_a = 9.7$

Figure 13e. The nitrogen atom has high pK_a as pyridine through the influence of dimethylamino group, which has electron donor properties. DMAP can be compared with the morpholino group containing triazine derivative concluding that the nitrogen atoms on triazine scaffold are more basic and favour the intramolecular H-bridge formation with the difluoromethyl group.

3.3.2. Medicinal Chemistry Application of Sulfone Functional Group

The sulfone group is an important module in medicinal chemistry. It share its high electron withdrawing effects with groups like CF_3 or CN [27]. However, unlike the CF_3 group whose introduction into a given scaffold typically increases lipophilicity [25], or the nitrile group, which results in lipophilicity reduction only when introduced into saturated structural domains, a sulfone unit more or less lowers the lipophilicity of a compound independently of its structural location [27]. All three groups affect the basicity of nearby basic functional groups. The marked electron withdrawing and basicity-lowering effect of a sulfone group in a saturated system is best illustrated by the very weak basicity of thiomorpholine 1,1-dioxide (**1a**, Figure 14), the sulfone analogue of morpholine (**1b**, Figure 14). The reduction of the amine basicity, ΔpK_a, by approximately six log units relative to piperidine (**1c**) can be interpreted in terms of an amine basicity-lowering effect of almost three log units through each of the two σ-brances [27] in the six-membered ring, exerted by the SO_2 group in the β-position to the amine function.

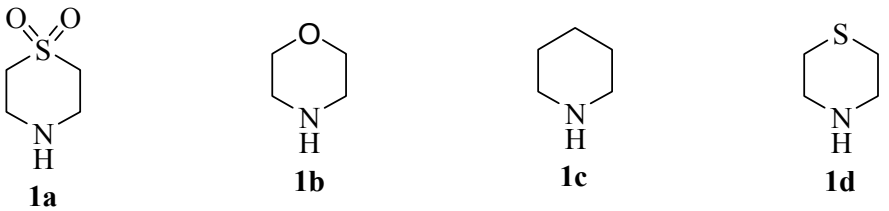

	1a	**1b**	**1c**	**1d**
pK_a	5.4	8.5	11.1	9.0
ΔpK_a	-5.8	-2.6	0	-2.1
½ ΔpK_a	-2.9	-1.3	0	-1.1

Figure 14. Experimental pK_a values of thiomorpholine 1,1-dioxide (**1a**), morpholine (**1b**), piperidine (**1c**), and thiomorpholine (**1d**) [27].

Sulfone strategy could be successfully applied for the optimization of ZSTK474, where a morpholine ring was replaced with thiomorpholine 1,1-dioxide (**1a**) providing compounds **140** and and **140b** (Figure 15), and sulfonyl piperazine derivatives (compounds **141** and **142,** Figure 15). Insertion of **1a** to ZSTK474 and to non-fluorinated ZSTK474 analog led to compounds **140** and **140b** (Figure 15) and reduction in biological activity. Interestingly, insertion of 1-(methylsulfonyl)piperazine led to **141**, which showed more potent activity *in vitro* and in cancer cell lines as ZSTK474. According to our molecular modelling experiments it was obvious that the oxygen atom of sulfonyl group has the potential to form an additional hydrogen bond with the target protein making this compound more potent. Advantageously, compound **141** has due to the polarity of the sulfonyl group better water solubility as ZSTK474.

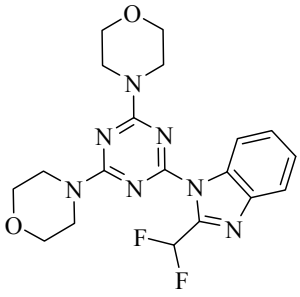

ZSTK474

Inhibitor activity:
in vitro excellent against PI3Kalpha
in cell excellent pPKB/PKB activity
in cell excellent pS6 activity
poor water solubility

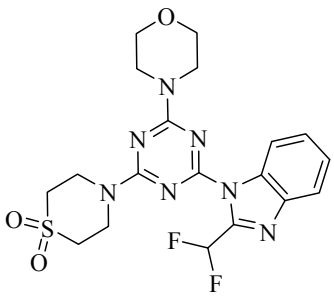

140 (NCB91)

Inhibitor activity:
in vitro good against PI3Kalpha
in cell poor pPKB/PKB activity
in cell poor pS6 activity

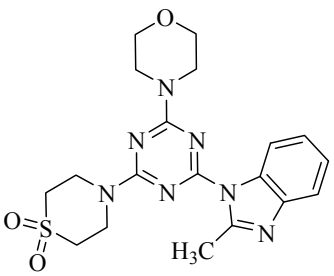

140b (NCB92)

Inhibitor activity:
in vitro poor against PI3Kalpha
in cell poor pPKB/PKB activity
in cell poor pS6 activity

Inhibitor activity:
poor>good>very good>excellent

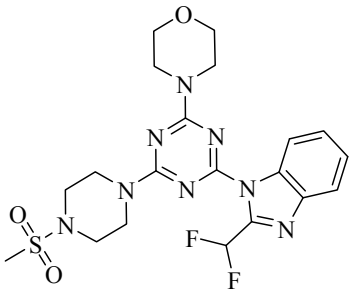

141 (NCB60)

Inhibitor activity:
in vitro excellent against PI3Kalpha
in cell excellent pPKB/PKB activity
in cell excellent pS6 activity
excellent water solubility

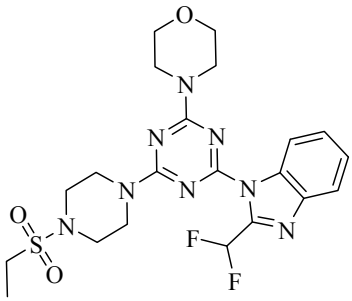

142 (NCB57)

Inhibitor activity:
in vitro good against PI3Kalpha
in cell very good pPKB/PKB activity
in cell poor pS6 activity

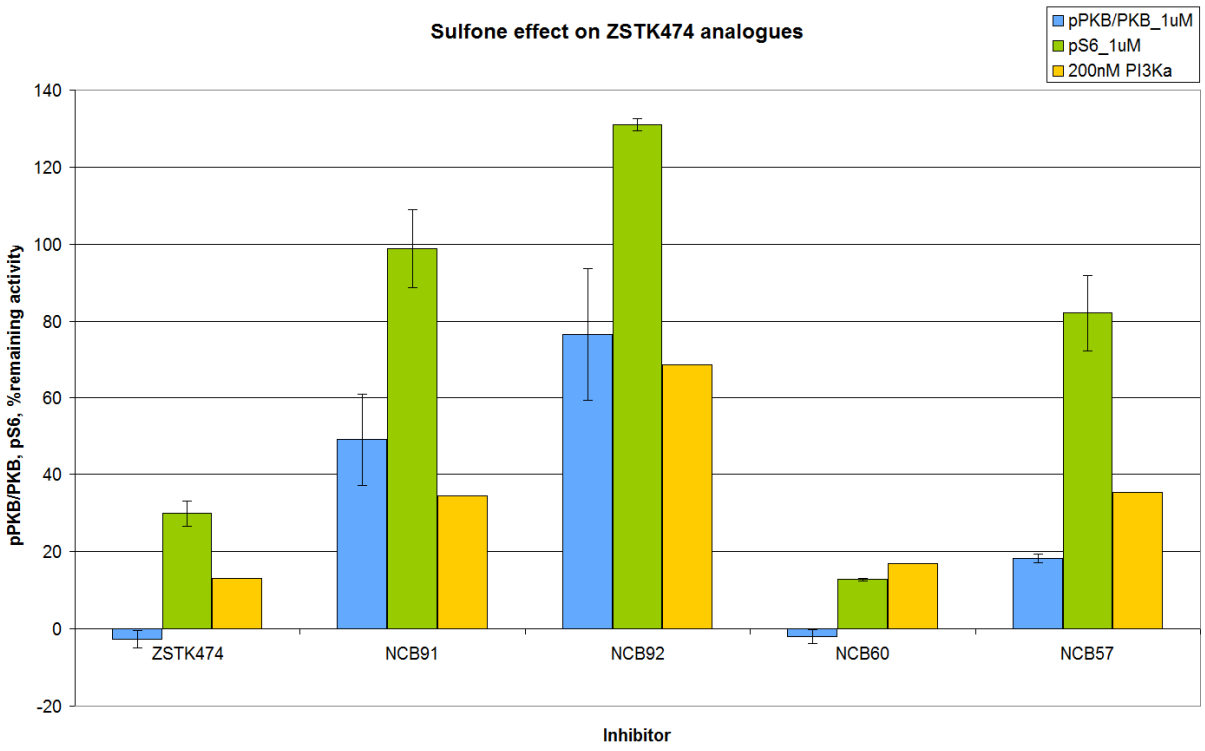

Figure 15. Optimization of ZSTK474 by applying sulfone strategie. The smaller the bar charts are the more potent are the relevant compounds.

3.3.3. Spirocyclic Oxetane Derivatives as Novel Promising PI3K Inhibitors

Despite very important function of morpholine in drug discovery making compounds more water soluble and less lipophilic, almost all of morpholino containing PI3K inhibitors have solubility problems under cellular conditions and therefore in several cases poor oral bioavailability (e.g. PI-103) (all literature known morpholino containing PI3K inhibitors were synthesized in the research group of Prof. B. Giese and their activity was tested in different cellular assays by colleagues from the research group of Prof. M. Wymann). With this background information we decided to expand the chemical space around morpholine. Novel molecules were designed where the morpholine moiety was exchanged with spirocyclic oxetane **263** (Figure 16), which is known from very recent studies of ETH Zürich and Roche Basel researchers (Prof. Erick M. Carreira, Prof. Klaus Müller and colleagues) to be able to successfully replace a morpholino unit [28]. By comparing spirocyclic oxetane **263** and morpholine (**262**) (Figure 16) one can reveal several interesting features. Spirooxetane **263** is more slender than morpholine (Figure 16), and the position of the oxygen atom of spirooxetane is in comparison with the oxygen atom of morpholine extended with 1.3 Å in the molecular symmetry plane. The lone pairs of electrons on the oxygen atom in spirooxetane have the spatial orientation, in morpholine (**260**) they are orthogonal (Figure 16). Furthermore, in spirooxetane the oxygen atom is colocated and in morpholine not according to different chair conformations of morpholine observed by X-ray structures of inhibitor•PI3Kγ complexes.

The spirocyclic analog of morpholine, 2-oxa-6-azaspiro[3.3]heptane (**263**), is with solubility of 24’000 μg/ml three times more soluble than morpholine (**262**) (Table 2). Such solubility feature is explained by lower Log*P* (intrinsic lipophilicity) and Log*D* (lipophilicity or logarithmic *n*-octanol/water distribution coefficient at pH = 7.4) than that of morpholine (Table 2). Additionally, the lipophilic parts of spirooxetane **263** (also called as “homospiromorpholine”) are concentrated around the central quaternary carbon while both its oxygen and nitrogen are exposed to the solvent. Moreover, according to human and in mouse liver microsomes, metabolic liability of spirooxetane is reduced [28]. All these observations together with its ease of preparation make spirooxetane **263** a very promising candidate of replacing morpholine as a solubilising group.

A

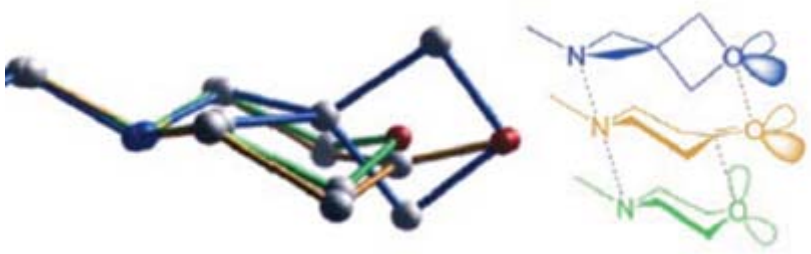

B

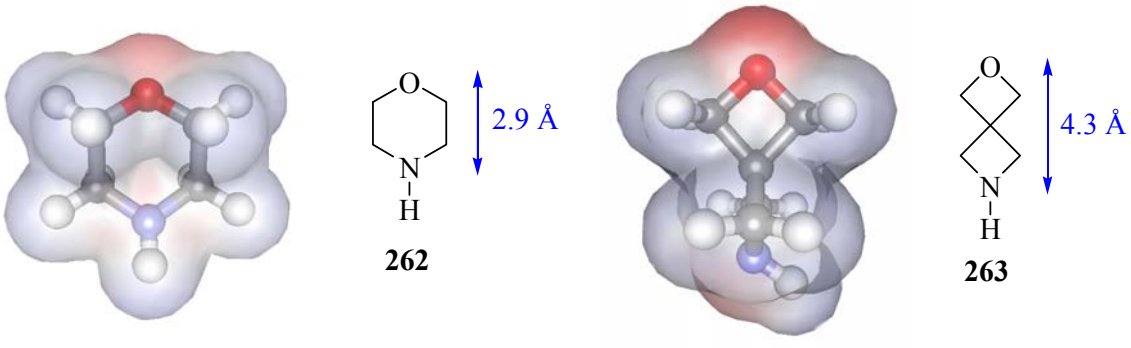

Figure 16. (A) Superposition of three structures: the X-ray crystal structures of the *N*-benzhydryl derivative of spirooxetane **263** and *N*-methylmorpholine (green), and a model of *N*-methyl-4-piperidone (ochre) (blue; the benzhydryl group is omitted, the crystallographic data can be obtained from The Cambridge Crystallographic Data Center via www.ccdc.cam.ac.uk/data_request/cif; the crystallographic data code for *N*-benzhydryl derivative of spirooxetane **263** is CCDC675323; adapted from Wuitschik et al. [28]). (B) Calculated van der Waals surfaces of spirooxetane and morpholine with the software Accelrys Discovery Studio 2.5. Position of the oxygen atom of spirooxetane is in comparison with the oxygen atom of morpholine extended with 1.3 Å in the molecular symmetry plane.

Table 2. Physicochemical and biochemical properties (adapted from [28]).[a]

Structure	log*D*[b]	log*P*[c]	Sol.[d]	CI_{int}[e]	pK_a[f]
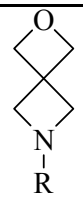	0.5	1.2	24000	3/7	8.0
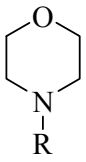	1.5	1.6	8000	9/8	7.0

[a]R = piperonyl. [b]Logarithmic *n*-octanol/water distribution coefficient at pH 7.4. [c]Intrinsic lipophilicity of the neutral base according to the equation $\log P = \log D + \log_{10}(1+10^{(pKa-pH)})$. [d]Intrinsic solubility of the neutral base. The values were obtained from the experimental thermodynamic solubility [$\mu g mL^{-1}$] in phosphate butter (50 mM) at pH 9.9 and 22.5±1 °C, and corrected for the pK_a value. [e]Intrinsic clearance rates [$min^{-1}mg^{-1}\mu L$] measured in human and mouse liver microsomes. [f]Amine basicity in water measured spectrophotometrically at 24 °C.

Designed spirooxetane derivatives (Table 3) were automatically docked in the crystal structure of PI3Kα (PDB code: 2RDO) and their binding mode orientations and binding energies were studied pre and after minimization and quick dynamics. The H-bridge formation of morpholino oxygen and the backbone amide of Val-851 was observed by all docked spirooxetane containing compounds from Table 3. The best energy scores were observed for compound **257** (GSA44), which was designed by substituting one morpholine ring with the spirooxetane **263** of inhibitor ZSTK474, which contains two morpholine units (Table 3 and Figure 17) both included in target binding according to our X-ray structure in complex with PI3Kγ. All of the docked spirooxetane containing compounds were successfully synthesized and tested *in vitro* for PI3Kα and in cellular cancer cell lines. The best experimental values were obtained for **257** (GSA44), which was in agreement with *in silico* results. Compound **254** (GSA61), which contains two spirooxetane units instead of two morpholines, was not active in cells and had poor activity *in vitro*. This compound was poorly soluble in all organic solvents and also in DMSO, which was used to dilute the substance for cellular assays and therefore we assumed that **254** (GSA61) could be also not cell permeable. To exclude the unfavourable solubility and the cell permeability factors of **254** (GSA61) we synthesized compounds **250** (GSA73) and **252** (GSA74) where one morpholine of the known inhibitor ZSTK474 (**115**) was exchanged with the spirooxetane moiety and the second morpholine was exchanged with certain piperazine derivatives known from previous experiments to be advantageous to increase the solubility and cell permeability of the whole ligand when attached directly to the triazine scaffold. Compounds **250** (GSA73) and **252** (GSA74) were also inactive in

cells and showed poor *in vitro* activity against PI3Kα concluding that only one morpholine ring of ZSTK474 (**115**) can be successfully replaced by spirooxetane **263**. According to the molecular modelling results, *in vitro* and *in cell* data observed by triazine derivative **257** (GSA44), the presence of one morpholine ring is essential for target recognition and key-hydrogen bonding with the hinge valine (Val-851 by PI3Kα, Val-854 by PI3Kβ, Val-882 by PI3Kγ and Val-828 by PI3Kδ) (Figure 18). Moreover, this observation was additionally confirmed by using the compound **264** (GSA65_2), where the morpholine ring of inhibitor PI-103, needed for the ligand activity by interacting with the hinge valine, was replaced with the spirooxetane moiety. Such morpholine-spirooxetane replacement induced a lost in biological activity of **264** (GSA65_2) (for cellular and *in vitro* data see below). Last but not least, our crystal structure of ZSTK474 in complex with PI3Kγ isoform and its direct comparison with the crystal structure of PI3Kγ in complex with *in silico* docked and minimized **255** (GSA44) provides a visual overview, that morpholine ring, which is going out of the binding pocket to solvent environment, is able to be successfully replaced with the spirooxetane **263** (Figure 19).

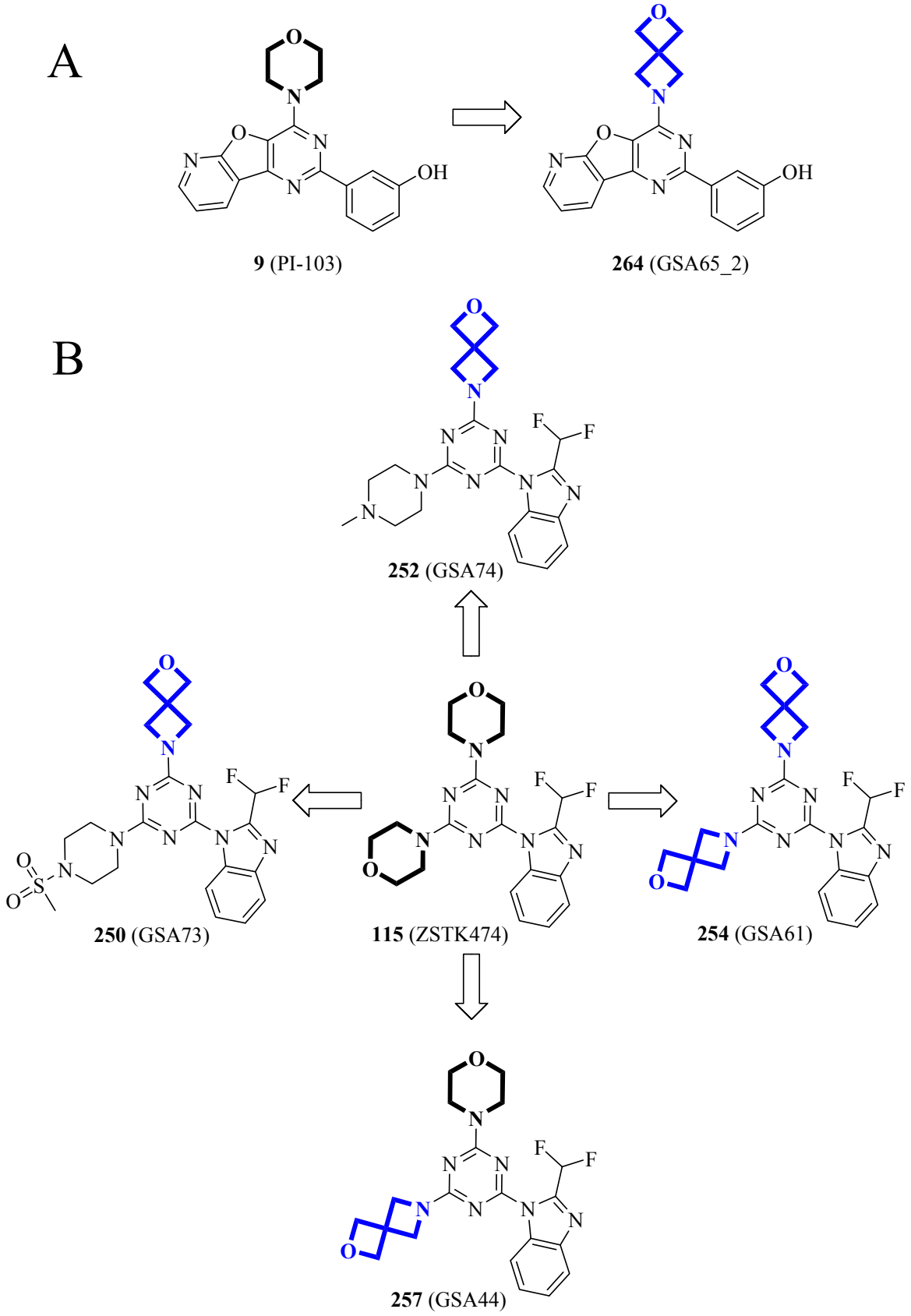

Figure 17. Design of spirocyclic oxetane containing phosphoinositide 3-kinase inhibitors. (A) The morpholine ring of pyridinylfuropyrimidine (PI-103), which is involved in the target binding, was replaced with spirooxetane (colored in blue). (B) The morpholino moieties of ZSTK474 were differently replaced with spirooxetanes leading to the active and inactive asymmetric compounds.

Table 3. Molecular modelling data obtained for spirooxetane containing compounds

Structure	ID	PI3Kα Score[a]	kcal bE before[b]	kcal/mol bE after[c]	Total	PI3Kγ Score[a]	mTOR Score[a]
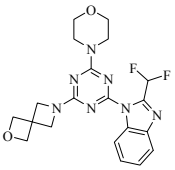	**257** (GSA44)	**59.34**	39.87	**114.844**	-23600	**69.03**	**71.53**
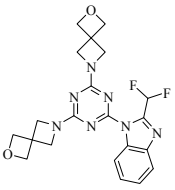	**254** (GSA61_s3)	55.26	-69.92	112.425	-23185	56.48	70.11
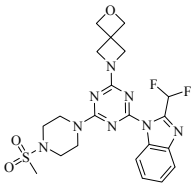	**250** (GSA73_s2)	57.58	82.8772	**127.719**	**-23047**	63.72	63.68
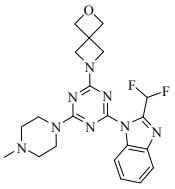	**252** (GSA74)	58.19	-137.991	70.123	-23154	67.75	66.74
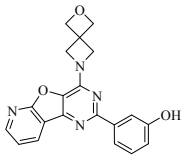	**264** (GSA65_2)	51.26	-657.304	108.056	-22824	58.46	67.27

[a]**Docking score** is the energy giving by the docking program, the more positive the better. There is no correlation between score and the binding energy. [b]**bE before** is the binding energy after docking prior any minimization and quick dynamics, the higher the better. [c]**bE after** is the binding energy after minimization and quick dynamics, the higher the better.

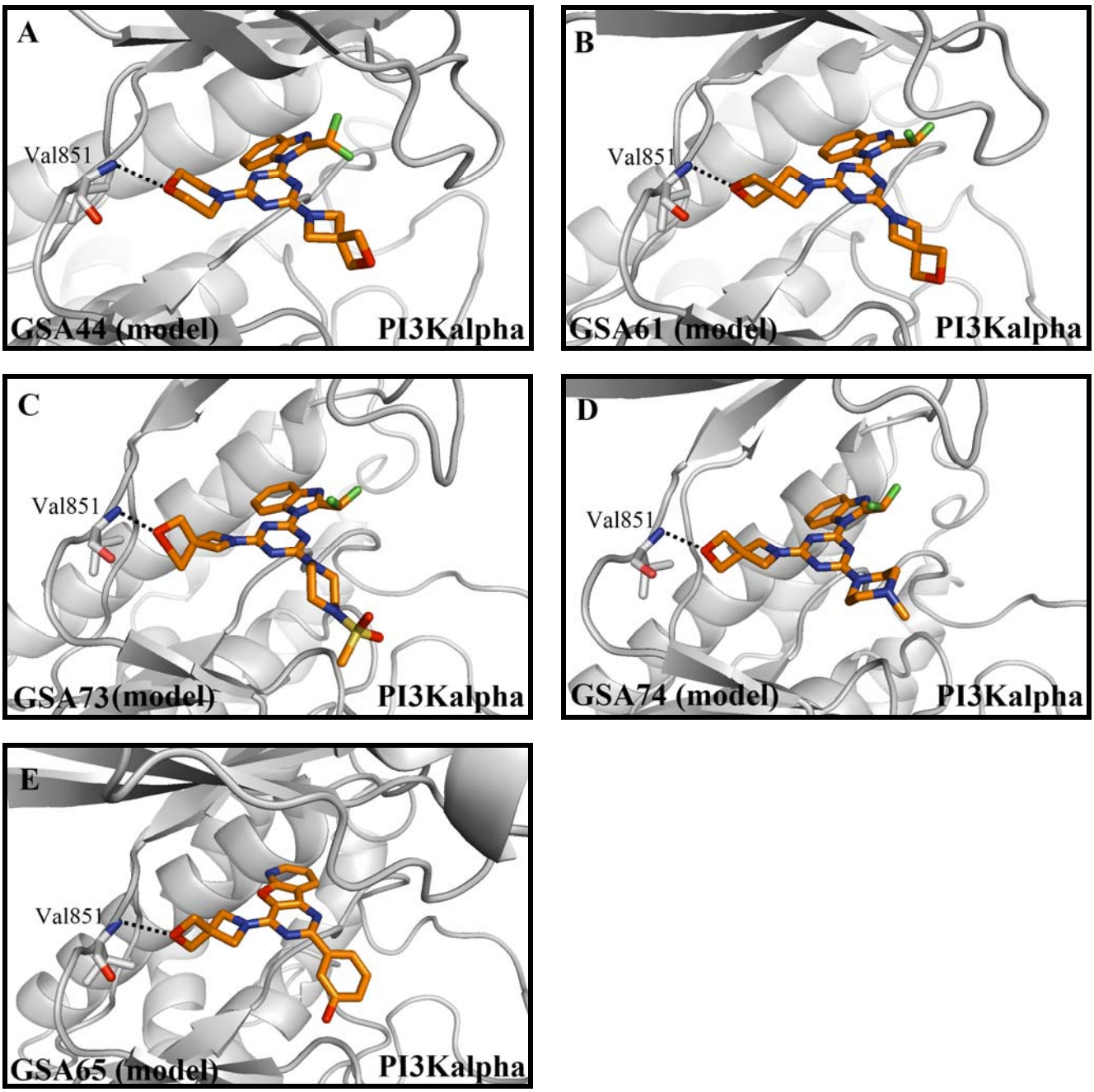

Figure 18. Targeting phosphoinositide 3-kinase (PI3K) with spirooxetane containing ATP-competitive inhibitors. (A-E) Ribbon diagrams of PI3Kα crystal structure (PDB code: 2RDO) in complex with *in silico* docked inhibitors and zoomed into the ATP-binding site. The binding energies and the binding mode orientations of the depicted inhibitors were compared pre and after the minimization and quick dynamics of the ligand·PI3Kα complexes. Val-851, which is responsible by PI3Kα for the interaction with the morpholino oxygen of morpholino ring containing PI3K inhibitors, and the ligands are represented in stick form, colored according to the element (C atoms in grey, N atoms in blue, O atoms in red). (A) Ligand **257** (GSA44) showed in comparison to all other docked ligands the best binding energies and it was obvious that the morpholino ring of **257** (GSA44) is required for high binding energy of the ligand by making an H-bridge formation with Val-851, where the spirocyclic oxetane moiety is located in the hydrophobic pocket II going outside of the binding pocket in a solvent environment direction. This observation was successfully confirmed with experimental *in vitro* and *in cell* results from the SAR studies (for data see below). (B-E) *In silico* the spirocyclic oxetane ring was able to successfully recognize Val-851 with satisfied ligand binding energies; *in vitro* and *in cell* the compounds were inactive leading to the observation that spirocyclic oxetane can not replace the morpholine responsible for binding with the hinge valine of PI3K.

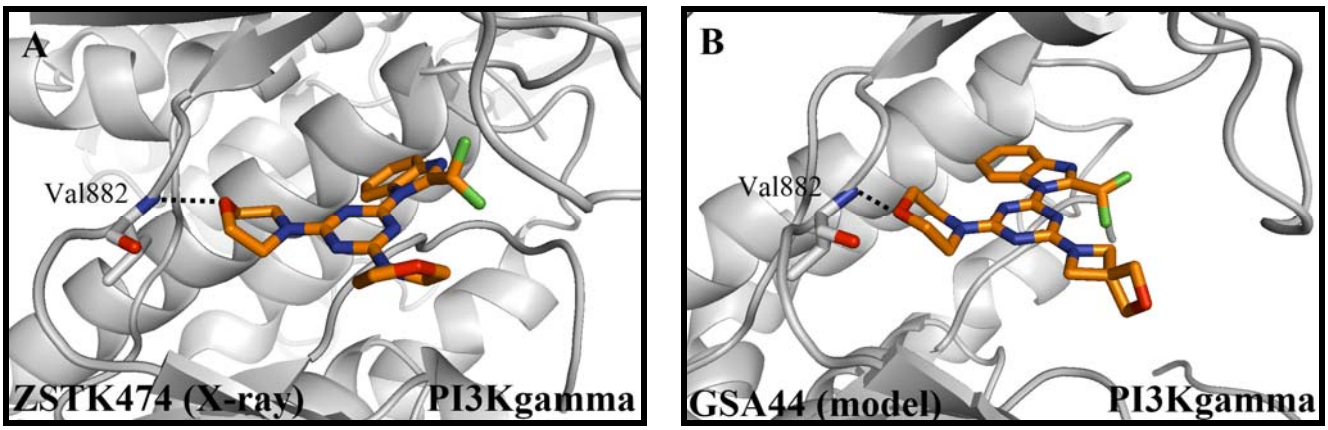

Figure 19. Targeting phosphoinositide 3-kinase (PI3K) with spirooxetane containing ATP-competitive inhibitors. (A-B) Ribbon diagram of PI3Kγ crystal structures zoomed into the ATP-binding site. Amino acids residues and the ligands are represented in stick form, colored according to the element (C atoms in grey, N atoms in blue, O atoms in red). Numbers denote highlighted, prominent side chains mediating PI3K/ligand interactions; the hydrogen bonds with Val-882 correspond to the contact lists. (A) Ribbon diagram of PI3Kγ crystal structure in complex with **115** (ZSTK474). One morpholine ring of the symmetric inhibitor makes the H-bridge formation with Val-882, an interaction conserved in all PI3K inhibitors; the second morpholine ring is located in so-called hydrophobic region II within the ATP-binding pocket, where it makes hydrophobic interactions with Lys-890 and is going out of the binding pocket to the solvent environment. (B) Ribbon diagram of PI3Kγ crystal structure with *in silico* docked asymmetric inhibitor **257** (GSA44). The binding energies of three most relevant binding mode orientations (interaction of Val-882 with whether the morpholine or benzimidazole or spirooxetane unit) were compared pre and after the minimization and quick dynamics of the ligand·PI3Kγ complex. The presented orientation of **257** (GSA44) showed the best binding energies and is comparable with the most stable binding orientation observed by PI3Kα isoform. The spirocyclic oxetane moiety is located in the hydrophobic region II going outside of the binding pocket in a solvent environment direction.

Table 4[a]. Cellular and *in vitro* data obtained for spirooxetane containing compounds

Structure	ID	*In vitro* PI3Kα 200nM	pPKB/PKB 1 µM	pPKB/PKB 10 µM	pS6 1 µM	pS6 10 µM
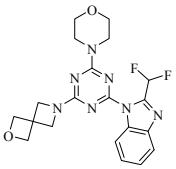	**257** (GSA44)	36	++++	++++	+(+)	++++
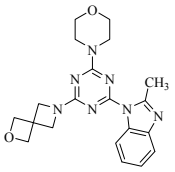	**256** (GSA42)	90	(+)	++++	-	-
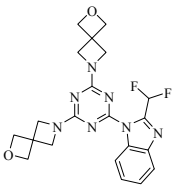	**254** (GSA61)	100	-	-	-	-
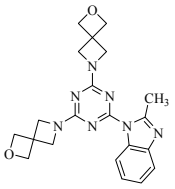	**253** (GSA53)	107	-	-	-	-
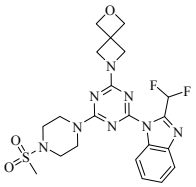	**250** (GSA73)	103	-	-	-	-
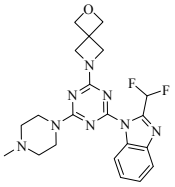	**252** (GSA74)	104	-	+	-	-
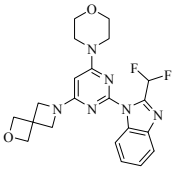	**261** (GSA81)	ND	ND	ND	ND	ND
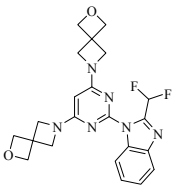	**259** (GSA80_2)	ND	ND	ND	ND	ND
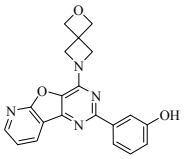	**264** (GSA65_2)	102	-	-	-	-

[a]Inhibitor efficacy and their cell permeability were measured by *in cell* Western inhibition assay on melanoma cell line A2058; "-" no activity, "+"/"++" poor activity; "+++" good activity; "++++" very good activity; *in vitro* PI3Kalpha inhibition was measured by *Kinase Glo* assay; given numbers represent %remaining activity, the smaller the value is the stronger is the inhibition. ND (not defined)

3.3.4. Summary of the Most Active Inhibitors

The follow figures summarize the most active inhibitors obtained after the hit-to-lead optimization of the compounds identified from the matrix library.

Figure 20 shows that ZSTK474 was one of the most potent benzimidazole-containing triazine derivatives followed by sulfonyl containing ZSTK474-derivative (compound NCB60), N-methyl piperazine ZSTK474 derivative (compound NCB36) and oxetane containing ZSTK474-derivative (GSA44). GSA44 has weaker inhibitor activity in comparison with ZSTK474, but it has better solubility. Further efforts are on-going to proof the oral bioavailability of GSA44.

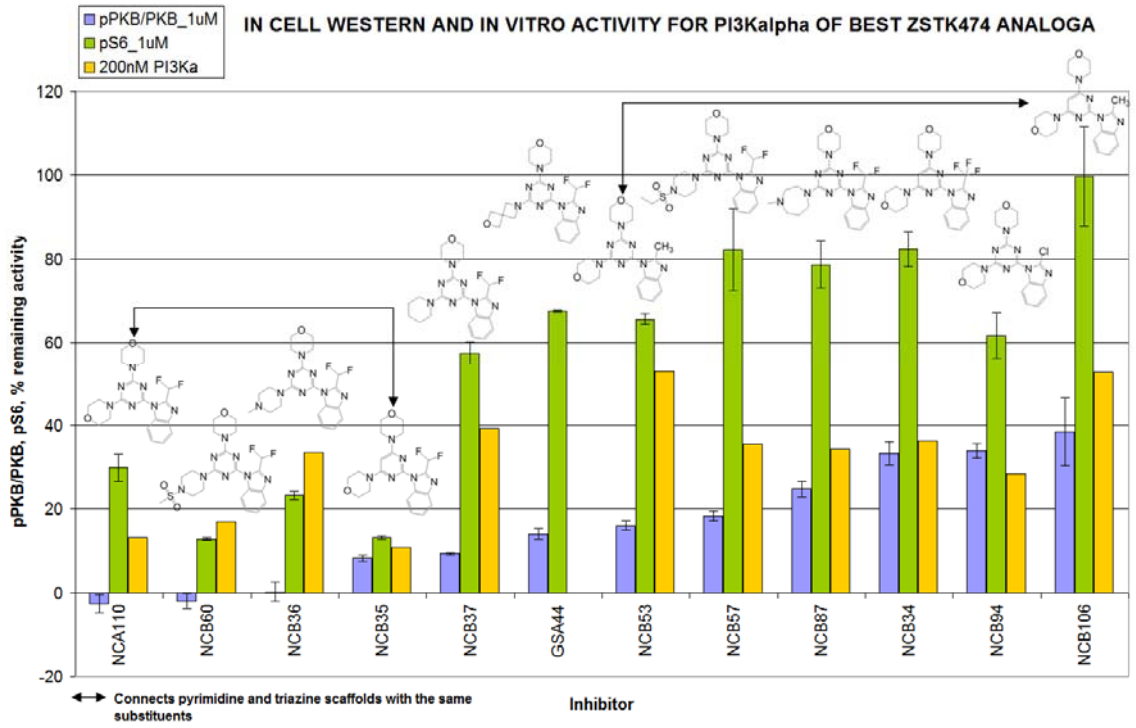

Figure 20. The most potent ZSTK474 analogues. Connected are pyrimidine and triazine scaffolds with the same substituents. The lower the bar charts the better are appropriate cellular and in vitro activities.

Figure 21 presents best triazine derivatives with an aminopyridine or aminopyrimidine moiety. By analyzing this figure one can obtain that in almost all cases a triazine derivative is more active *in cell* as the corresponding pyrimidine analog.

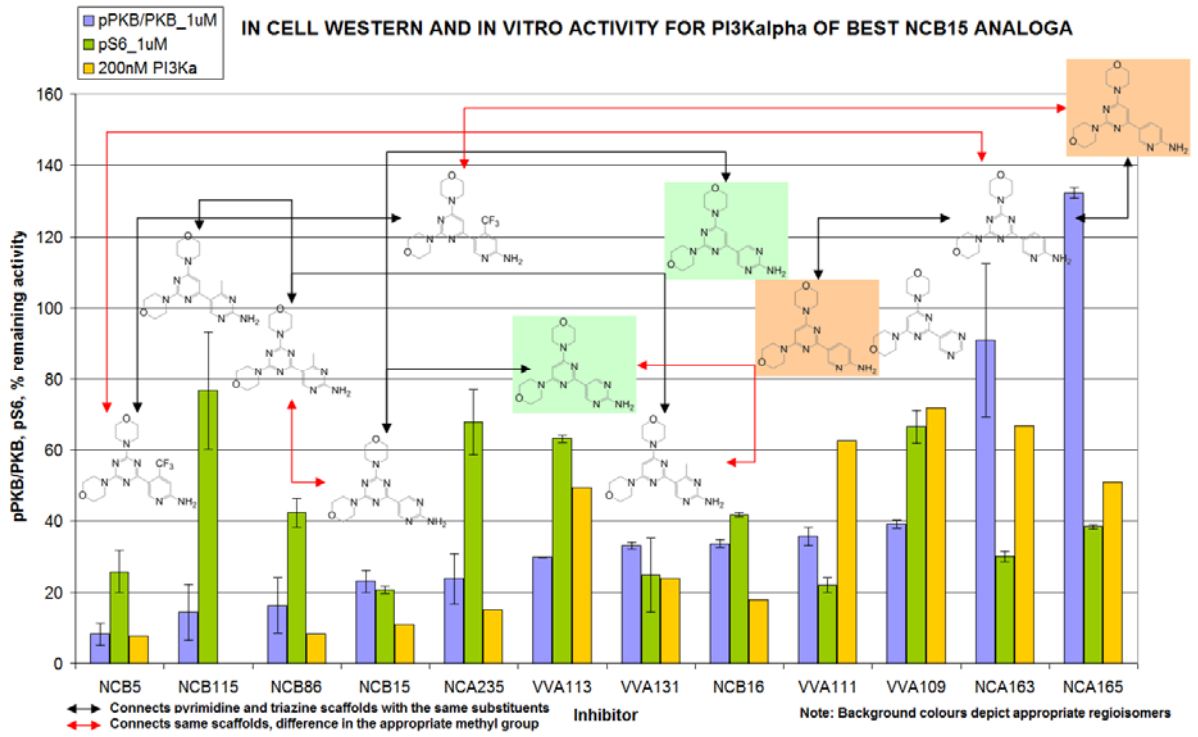

Figure 21. The most potent NCB15 analogues. Connected are pyrimidine and triazine scaffolds with the same substituents. Through the red line connection one can obtain the difference in the bioactivity by insertion of $-CH_3$ or $-CF_3$ groups. The lower the bar charts the better are appropriate cellular and in vitro activities.

Compound MJA40 (Figure 22) has been found to be a hit, which could not be optimized through the previous described strategies. Still, MJA40 is one of the most potent compounds identified from the matrix library. Very interesting is the selectivity of this compound; it shows high cellular activity and high isoform selectivity against PI3Kdelta. This compound did not inhibit PI3Kα, PI3Kβ and PI3Kγ. Further structural X-ray analysis in complex with PI3Kdelta is on-going, with the aim to explore the isoform selectivity of this compound.

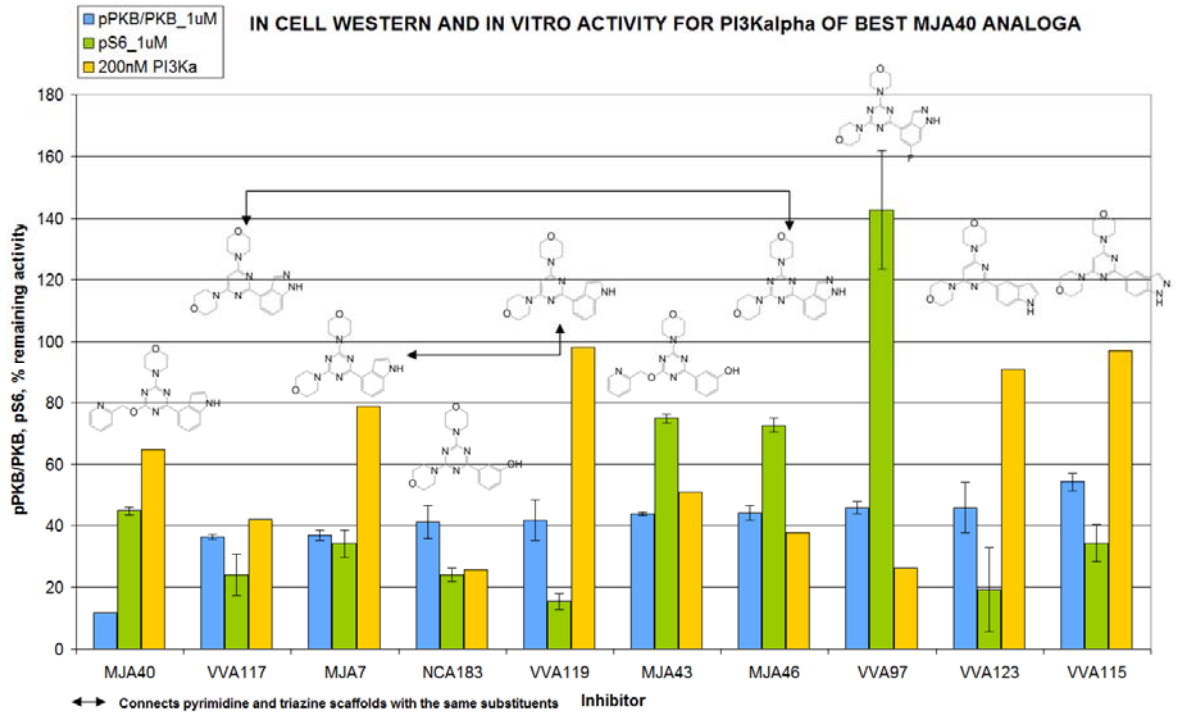

Figure 22. The most potent MJA40 analogues. Connected are pyrimidine and triazine scaffolds with the same substituents. Compounds VVA123 and VVA115 have been found to be mTOR active according to their cellular pS6 detection. The lower the bar charts the better are appropriate cellular and in vitro activities.

Several benzofuro- and thienopyrimidine derivatives were obtained to have attractive bioactivities (Figure 23 and Figure 24). The cellular and in vitro results suggest that the matrix strategy was successfully applied to gain novel pyridinylfuropyrimidine derivatives with non-dual character for further biological validation of PI3Ks. Further in vitro characterizations for mTOR are on-going and the novel results will complete the selectivity know-how.

Best matrix compounds with different selectivites have shown promising anti-proliferative effect (Figure 26).

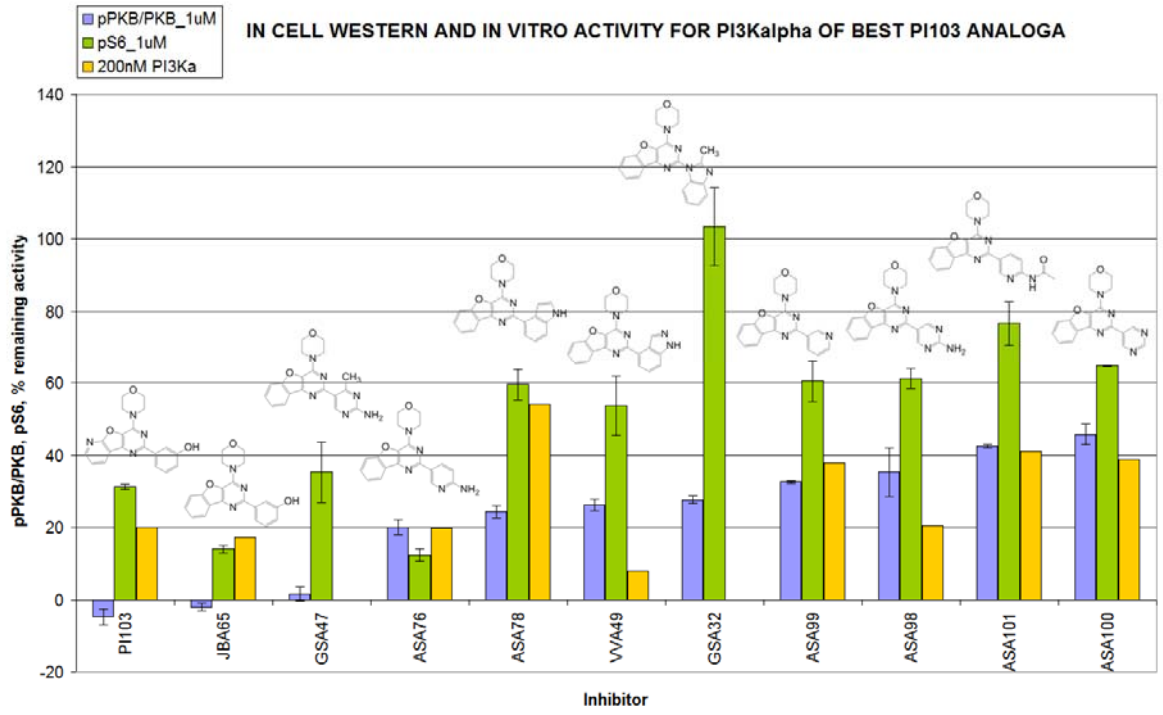

Figure 23. The most potent PI-103 analogues. The lower the bar charts the better are appropriate cellular and in vitro activities.

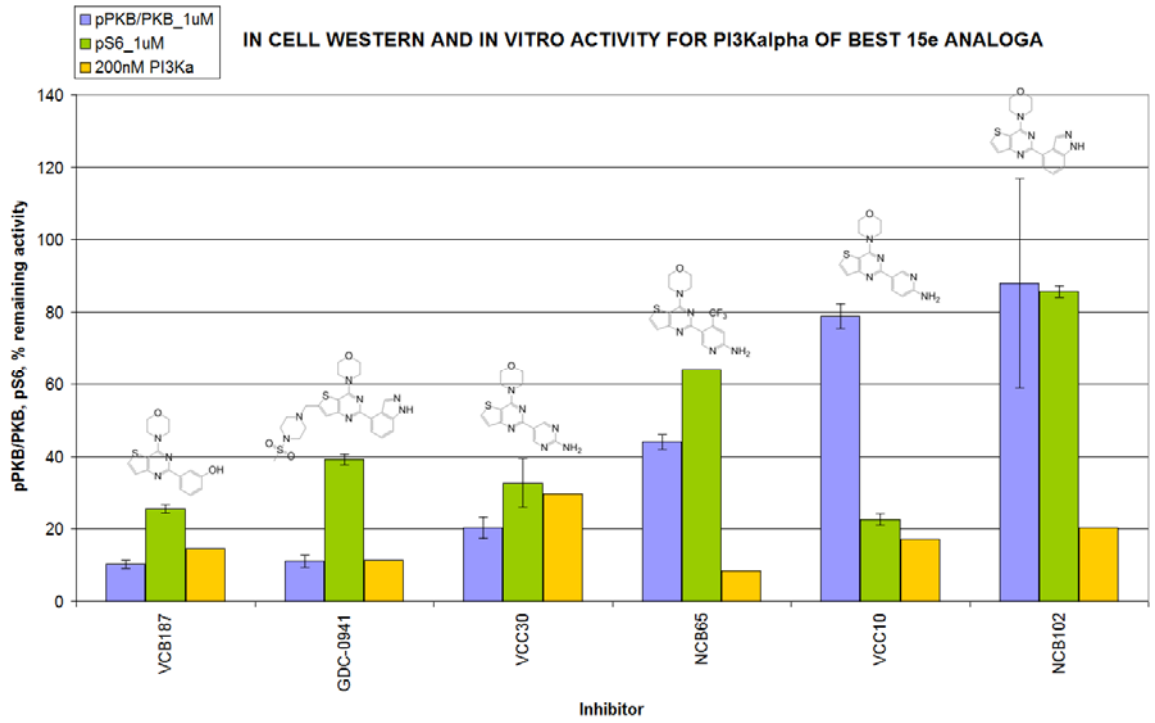

Figure 24. The most potent 15e (VCB187) analogues. The lower the bar charts the better are appropriate cellular and in vitro activities.

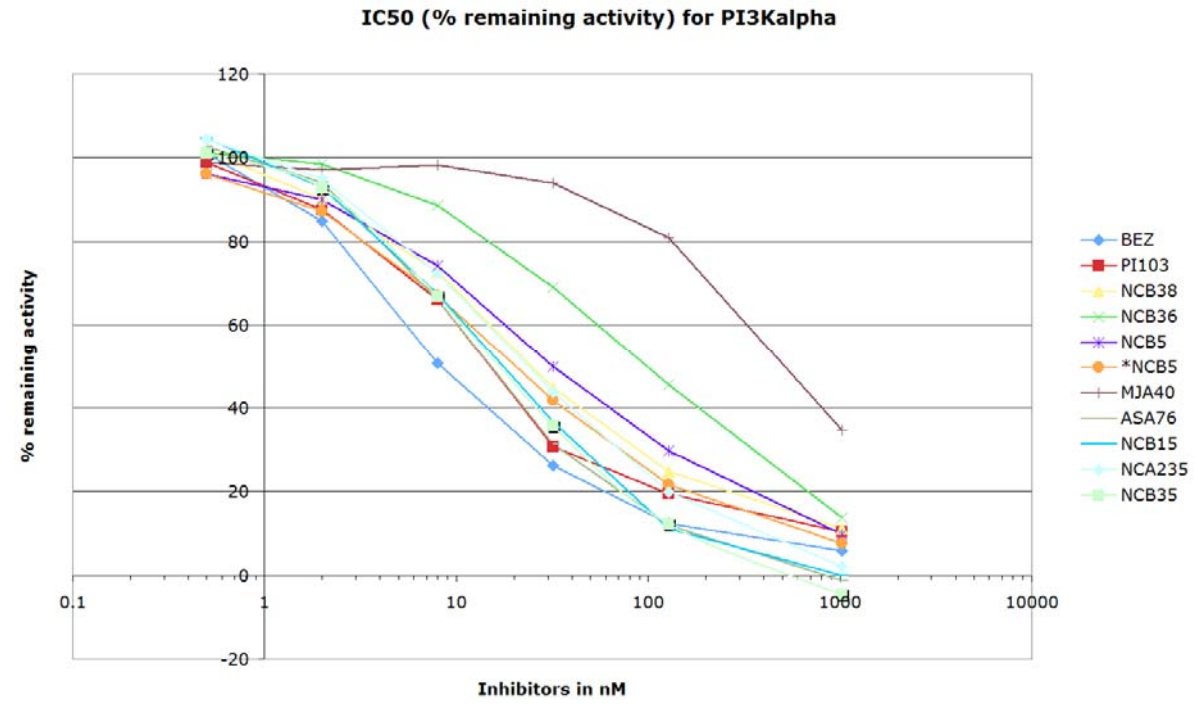

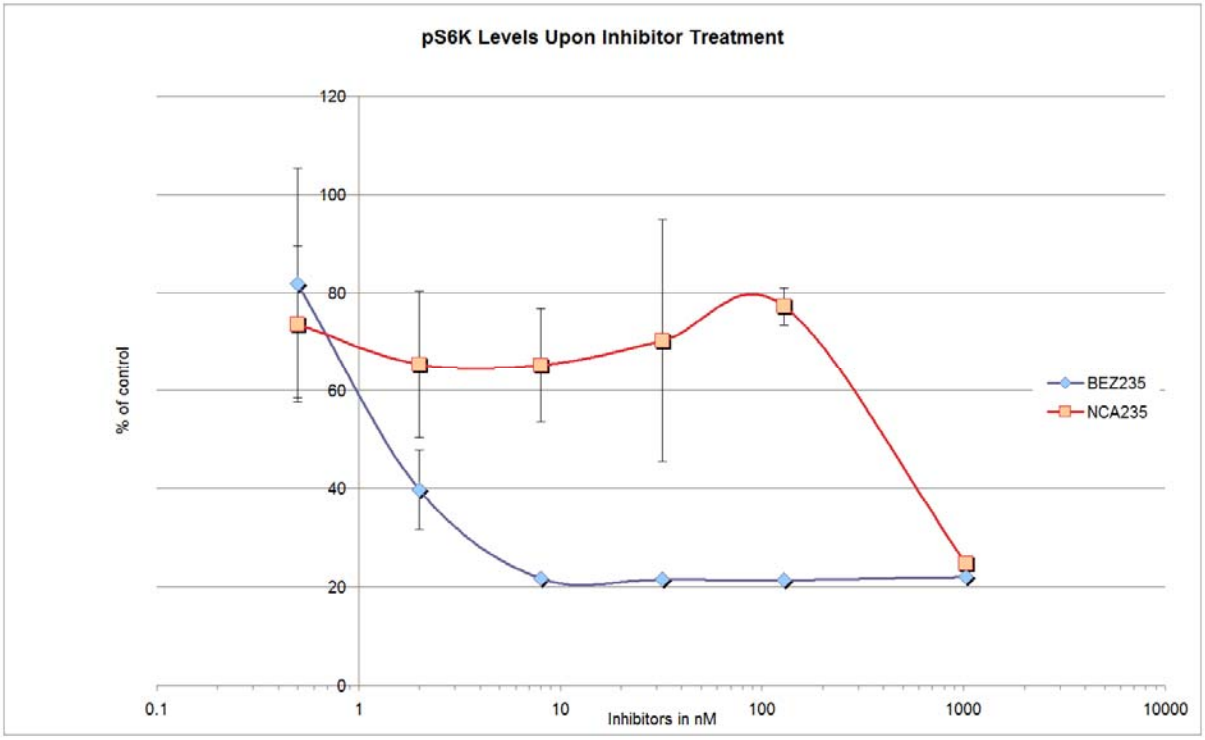

Figure 25. Concentration dependent inhibition of PKB phosphorylation. A2058 cells were exposed for 3 hours to increasing concentrations of NVP-BEZ235 and NCA235. Total cell lysates were subjected to immuno-blotting for total and phosphorylated PKB and phosphorylated $p70^{S6K}$. Emerging signals were quantified using fluorescent secondary antibodies, or enhanced chemiluminescence and ratios of phosphosphorylated over non-phosphorylated kinase for PKB and the quantified values for $p70^{S6K}$ are displayed. (n>2, mean ± SEM).

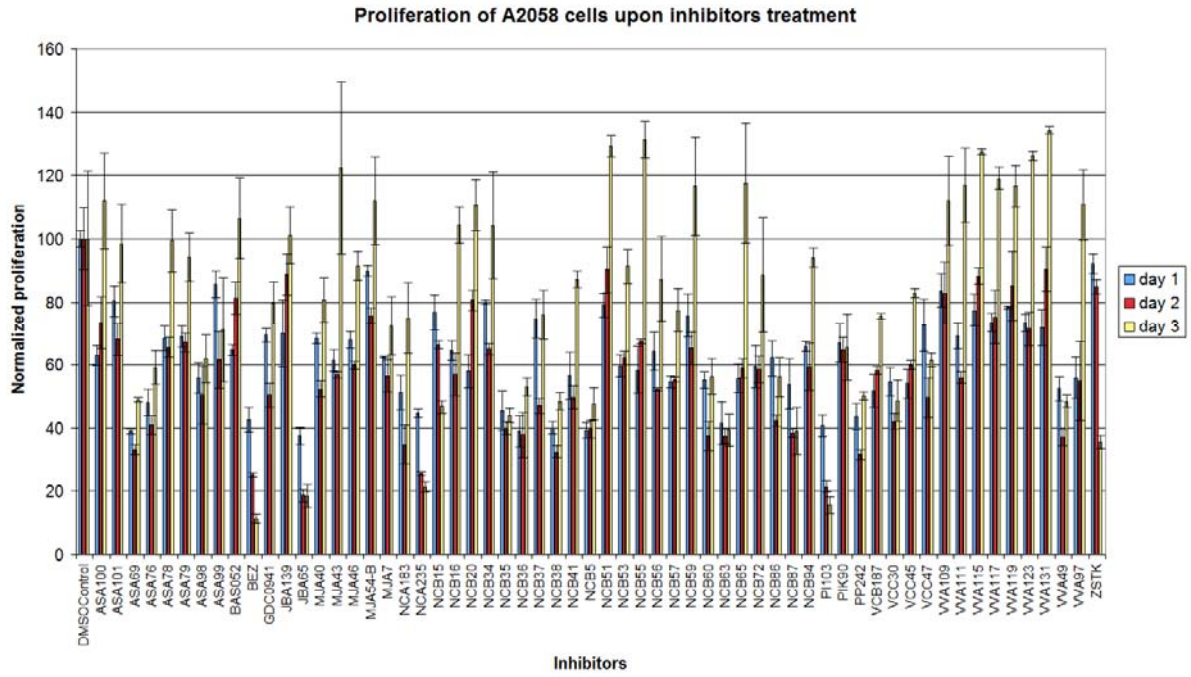

Figure 26. Anti-proliferative effect of PI3K inhibitors. Melanoma cells were exposed to the indicated inhibitors at 1 μM for one, two and three days, before cell numbers were determined with Alamar Blue. Cell numbers are depicted in relation to non-treated controls (ratio of treated over non-treated cultures). Data are means of triplicates ± SEM.

3.3.5. Structural Insights into Inhibitor Activity and Selectivity

3.3.5.1. The Active Site of Class I PI3Ks

All of the PI3Ks have a catalytic domain that shows homology with protein kinases. Like protein kinases, the catalytic domain of PI3Ks exhibits a bilobal organization with the ATP-binding pocket in a cleft between the N- and C-lobes, and PI3Ks share the same conserved catalytic residues in the phosphate-binding subsite of protein kinases [14]. Studies of protein kinases in complexes with small-molecule ATP-competitive inhibitors have suggested that conformational changes are often a part of the catalytic cycle of these enzymes. Most protein kinase inhbitors that have been developed target the active conformation of the enzymes so that the inhibitor-bound conformation is very similar to the ATP-bound conformation. These have been referred to as the type I inhibitors [29]. A pharmacophore model often used to describe binding by the type I protein kinase inhibitors divides the ATP-binding site into the hinge region, the hydrophobic pocket regions I and II, the adenine region, the ribose region and the phosphate region (Figure 27).

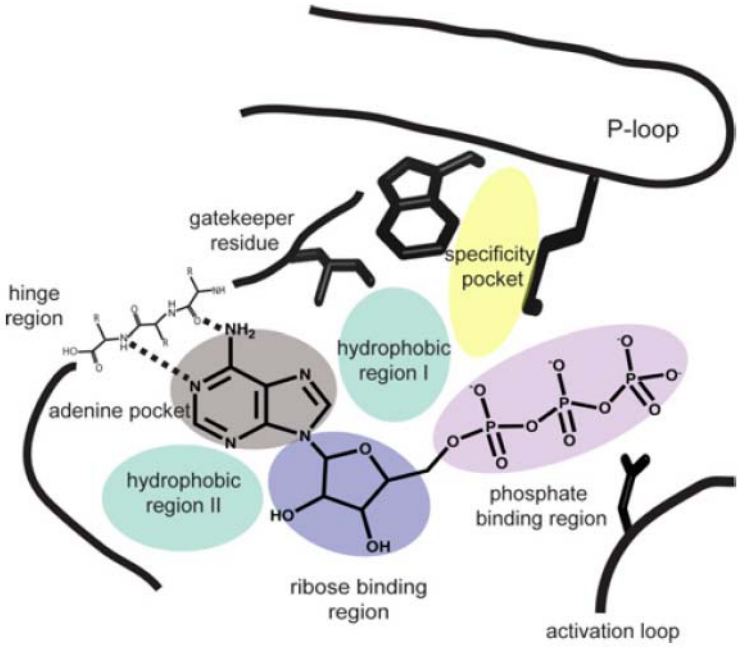

Figure 27. Schematic representation of a canonical PI3K/protein kinase ATP-binding pocket (adapted from [30]).

All PI3K-inhibitor complexes that have been reported are type I inhibitors, occupying the adenine region and making characteristic hydrogen bonds to the hinge of region of the PI3K [30]. A region that has been referred to as hydrophobic region I forms a deeper pocket behind the binding site for the ribose moiety of the ATP. In protein kinases, the “gatekeeper” residue, which forms part

of the wall of hydrophobic region I, partially restricts access to this region. Kinases with a large residue at the gatekeeper position cannot accommodate inhibitors with large substituents in hydrophobic region I, whereas kinases with a less bulky gatekeeper can. Among the most common resistance mutations of protein kinases is the mutation of a small gatekeeper residue into a larger more restrictive residue. The residue in PI3Ks analogues to the gatekeeper residue of the protein kinases is an isoleucine residue (Ile-871 in PI3Kγ, data obtained through the collaboration with Prof. Roger Williams, University of Cambridge), and this residue forms part of the wall of the very small PI3K hydrophobic region I. Many PI3K inhibitors occupy this region. This region has also been referred to as the "affinity pocket" in the PI3Kγ-inhibitor complexes [1].

3.3.5.2. Crystal Structures of PI3K/mTOR Inhibitors Developed by Matrix-Template Strategy

Here we report details of x-ray crystal structures, structural docking and modelling studies that we have conducted for small molecule inhibitors selected from the matrix library. All of these molecules are ATP-competitive antagonists (Figures 28, 29 and 30) that exhibit either:

a) broad class I activity, or
b) broad class I activity and mTOR, or
c) class I subtype selectivity and mTOR.

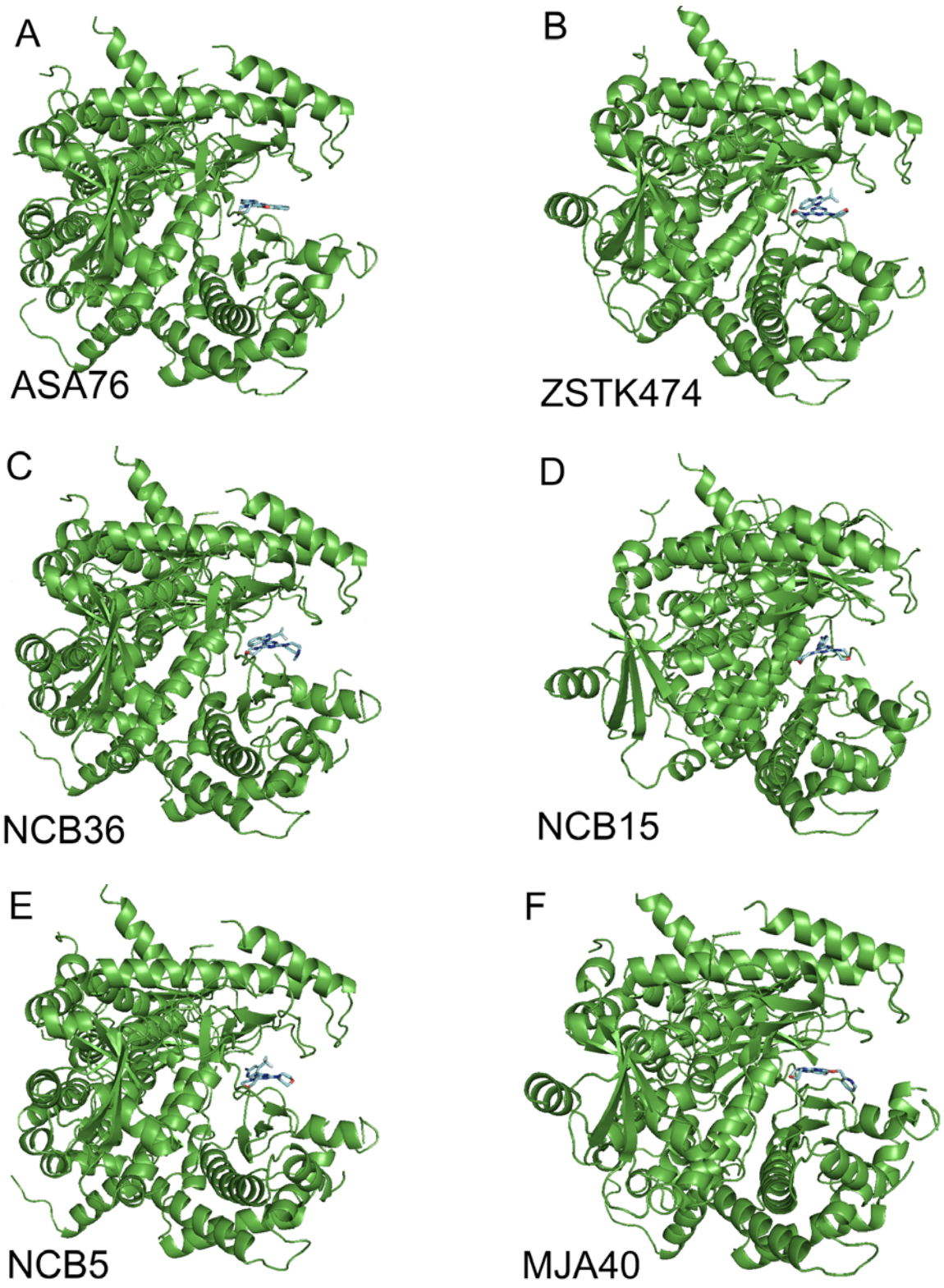

Figure 28. Targeting phosphoinositide 3-kinase (PI3K) with small molecule ATP-competitive inhibitors. (A-F) A ribbon diagram is presented in green, and the inhibitors, located at the ATP binding site, in the cleft between the N- and the C-terminal lobe of the catalytic subunit, are colored by elements.

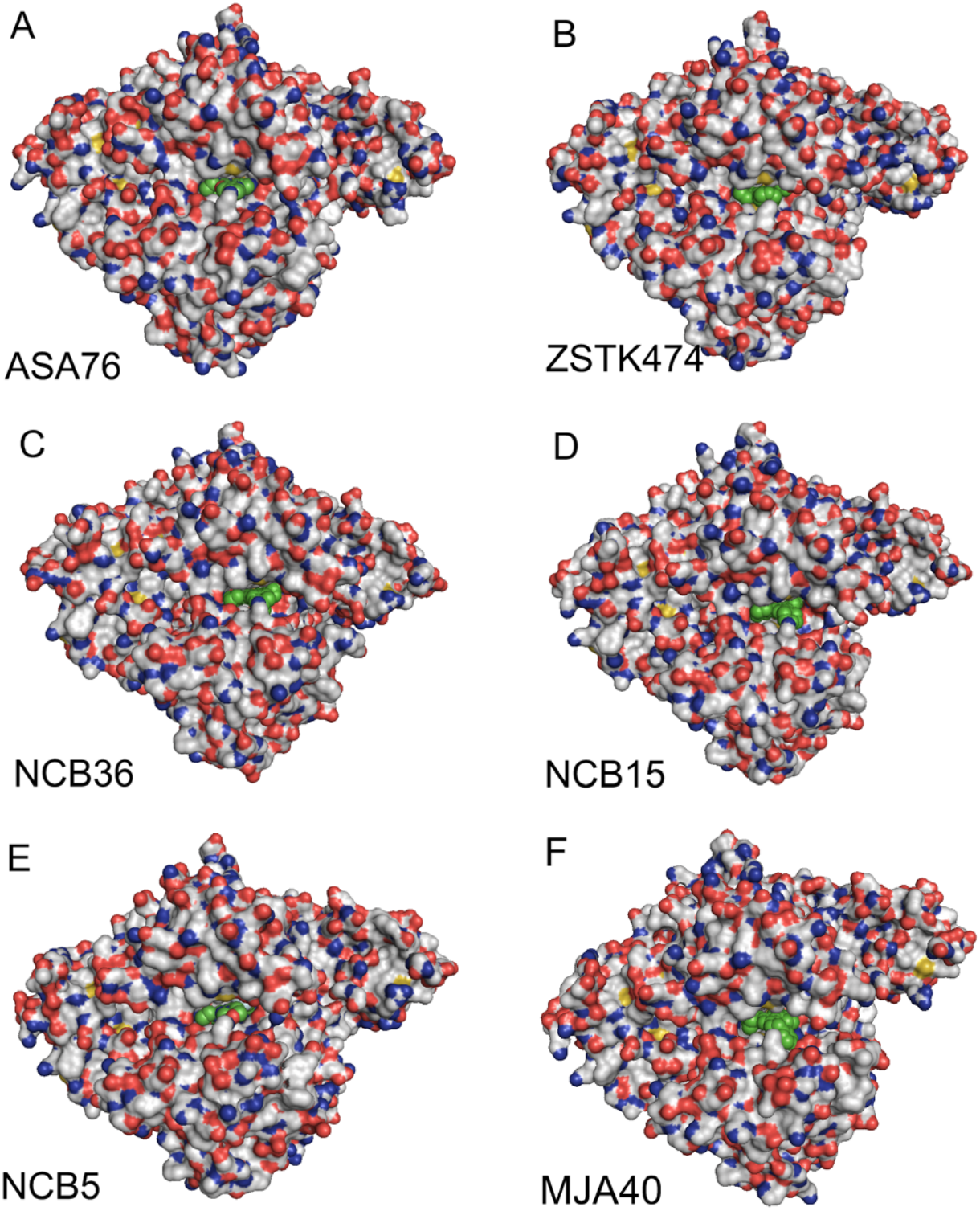

Figure 29. Targeting phosphoinositide 3-kinase (PI3K) with small molecule ATP-competitive inhibitors. (A-F) A surface diagram is presented, where the blue points characterize the N-atoms, red points O-atoms, yellow points S-atoms and grey points C-atoms of the enzyme; the relevant inhibitors, coloured in green, are presented as spheres with the aim to represent their filled space within the ATP-binding pocket.

We have determined the crystal structures of PI3Kγ in complex with inhibitors **34** (ASA76), **115** (ZSTK474), **139** (NCB36), **102** (NCB15), **98** (NCB5) and **208** (MJA40) (Figure 30). All of the compounds made the key hydrogen bond through the interaction of morpholine oxygen with the backbone amide of the hinge Val-882. The crystal structures confirmed that the matrix-hybrid-fragments are crucial for their high potency, because they are able to occupy the "affinity pocket" through the formation of several hydrogen bonds. The contact list with exact description of amino acids responsible for hydrogen bond formations and for hydrophobic interactions is given in Figure 31.

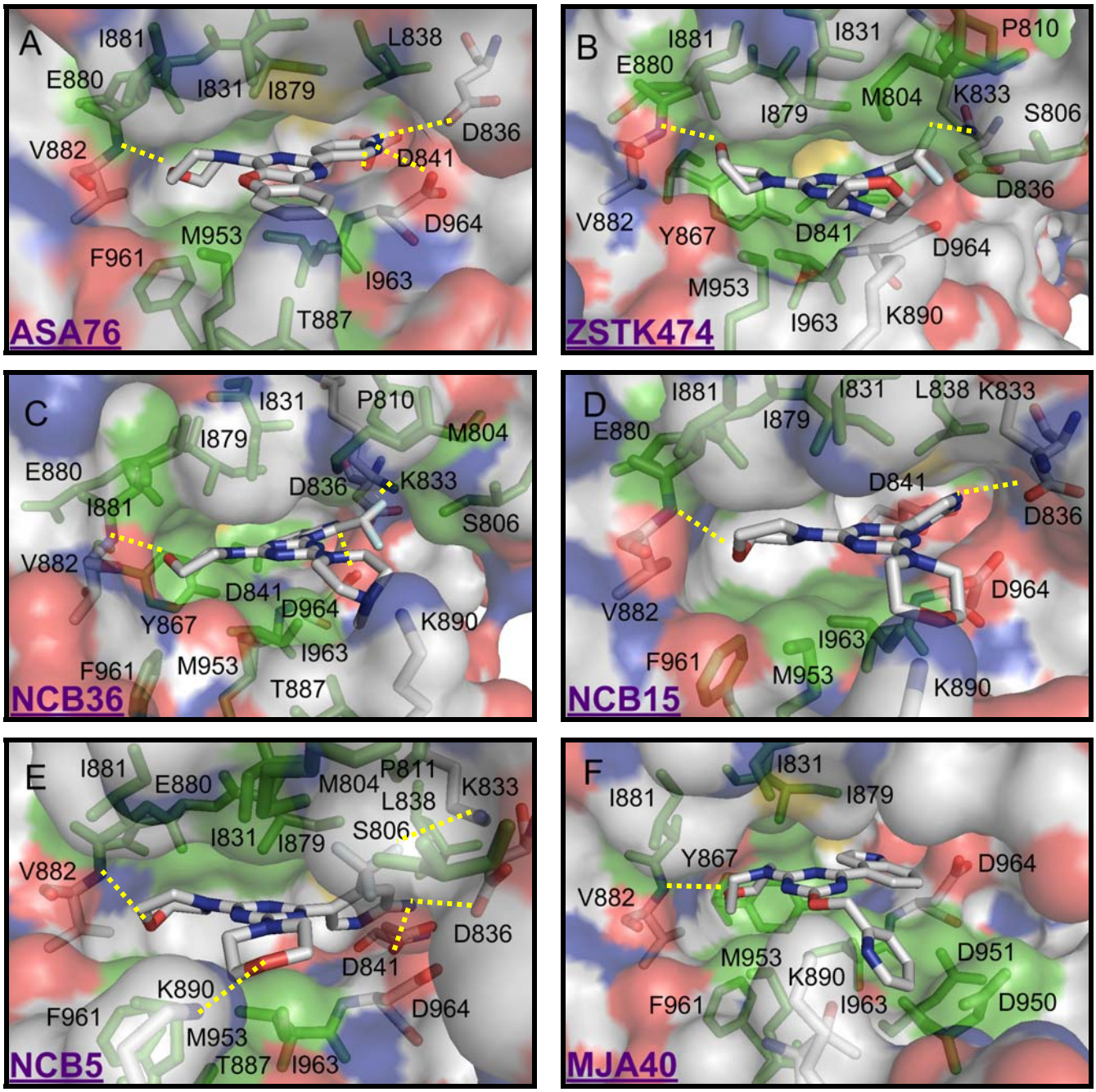

Figure 30. Targeting phosphoinositide 3-kinase (PI3K) with small molecule ATP-competitive inhibitors. (A-F) Surface diagram of ATP·PI3Kγ crystal structures zoomed into the ATP-binding site. Amino acids residues and the ligands are represented in stick form, colored according to the element (C atoms in grey, N atoms in blue, O atoms in red and S atoms in yellow). Numbers denote highlighted, prominent side chains mediating PI3K/ligand interactions; in green are colored amino acids for which hydrophobic contacts with the ligand could be obtained. For amino acids such as Asp836, Asp841, Glu880, Val882, Asp964, Lys833, and Lys890 both hydrophobic contacts and H-bridge formations could be obtained. Only hydrogen bonds that we are confident with are shown as yellow dashed lines. These correspond to the contact list from the Figure 31. For MJA40 there is only density for the morpholino group in contact with Val882 leading us to the conclusion that MJA40 is not able to reach the binding pocket of PI3Kγ; this observation was comparable with the experimental in vitro data and with the *in silico* data by docking MJA40 into PI3Kγ. For the cellular activity and isoform specificity of the depicted inhibitors consult text and data from the chapter "Chemistry and Biology".

	isoform				compounds				
mTOR	p110a	p110b	p110d	p110g	NCB5	ASA76	NCB15	NCB36	ZSTK474
Ile2163	Met772	Met779	Met752	Met804	✓			✓	✓
Ser2165	Ser774	Ser781	Ser754	Ser806	✓			✓	✓
Pro2169	Pro778	Pro785	Pro758	Pro810	✓			✓	✓
Leu2185	Ile800	Ile803	Ile777	Ile831	✓	✓	✓	✓	✓
Lys2187	Lys802	Lys805	Lys779	Lys833	✓ H-bond F29		✓	✓ H-bond F30	✓ H-bond F30
Glu2190	Asp805	Asp808	Asp782	Asp836	✓ H-bond N21	✓ H-bond N26	✓ H-bond N25	✓	✓
Leu2192	Leu807	Leu810	Leu784	Leu838	✓	✓	✓		
Asp2195	Asp810	Asp813	Asp787	Asp841	✓ H-bond N21	✓ H-bond N26	✓ H-bond N25	✓	✓
Tyr2225	Tyr836	Tyr839	Tyr813	Tyr867				✓	✓
Ile2237	Ile948	Ile851	Ile825	Ile879	✓	✓	✓	✓	✓
Gly2238	Glu849	Glu852	Glu826	Glu880	✓	✓	✓	✓	✓
Trp2239	Val850	Val853	Val827	Ile881	✓	✓	✓	✓	✓
Val2240	Val851	Val854	Val828	Val882	✓ H-bond O12	✓ H-bond O18	✓ H-bond O17	✓ H-bond O17	✓ H-bond O12
Thr2245	Thr856	Thr859	Thr833	Thr887	✓	✓		✓	
Ala2248	Gln859	Asp862	Asn836	Lys890	✓ H-bond O17				✓
Ser2342	Ser919	Asp923	Asp897	Asp950					
Asn2343	Asn920	Asn924	Asn898	Asn951					
Met2345	Met922	Met926	Met900	Met953	✓	✓	✓	✓	✓
Leu2354	Phe930	Phe934	Phe908	Phe961	✓	✓	✓	✓	
Ile2356	Ile932	Ile936	Ile910	Ile963	✓	✓	✓	✓	✓
Asp2357	Asp933	Asp937	Asp911	Asp964	✓	✓ H-bond N22	✓	✓ H-bond N21	✓

Figure 31. The contact list with exact description of amino acids responsible for hydrogen bond formations and for hydrophobic interactions is given.

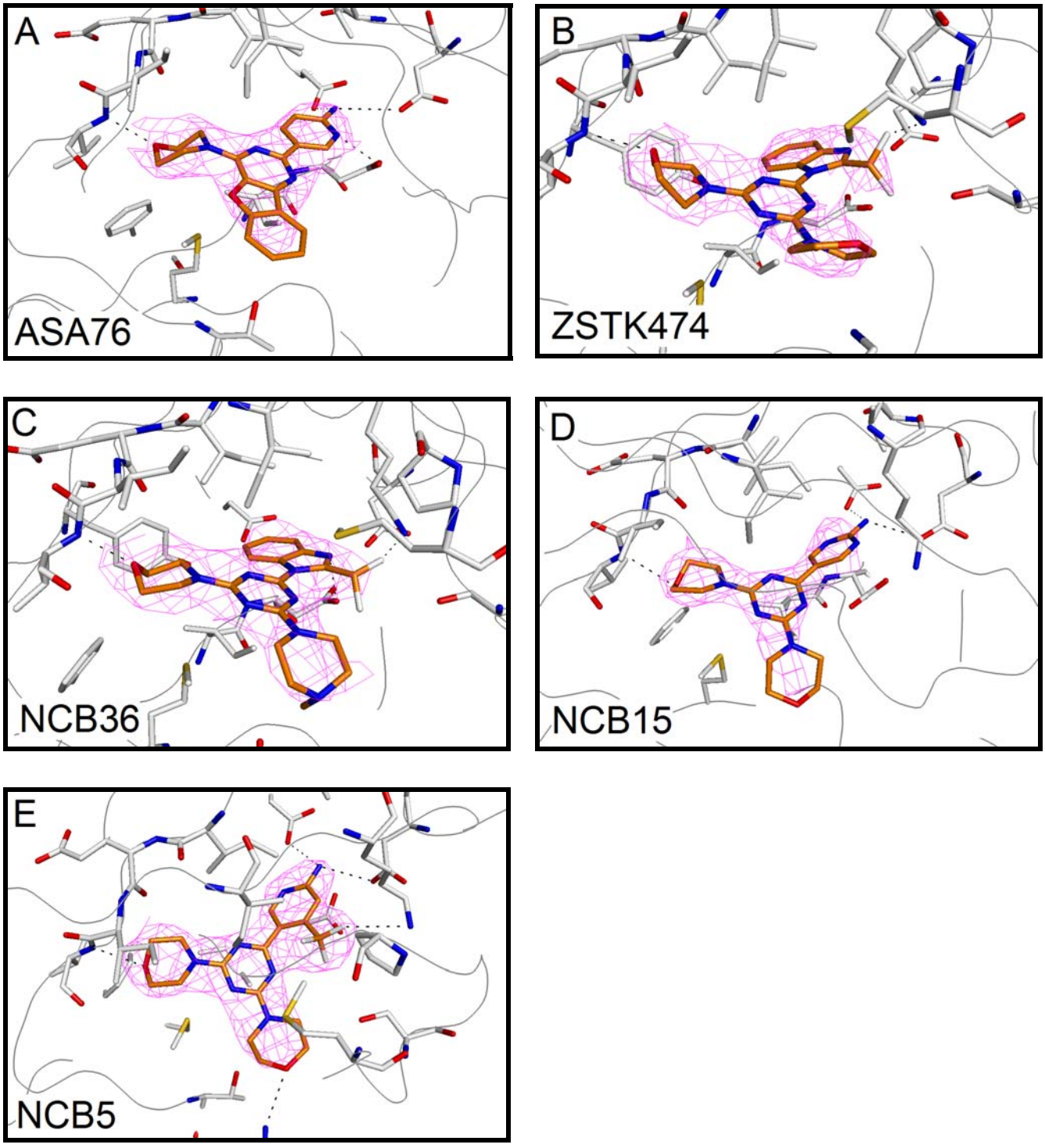

Figure 32. Targeting phosphoinositide 3-kinase (PI3K) with small molecule ATP-competitive inhibitors. (A-F) Extracted amino acids mediating PI3K/ligand interactions within the ATP-binding site; the electron density map of the compounds is presented in magenta mesh. Only hydrogen bonds that we are confident with are shown as black dashed lines.

The available crystal structures of PI3Kγ and PI3Kα from the Protein Data Bank were used for molecular modelling experiments. Three dimensional model of mTOR was created based upon the crystal structure of p110γ. The models were constructed as outlined by Pirola et al. [31]. For the docking studies, we used the genetic algorithm application GOLD [32]. Compounds were docked into the crystal structures and homology model by optimizing conformational and non-bonded contacts. The default scoring functions in GOLD are GoldScore and ChemScore; after an initial examination of LY294002 to compare the docked compound in p110γ to its X-ray structure, we elected to use GoldScore to dock the compounds, which produced nominally better results. Compound orientations using GOLD and GoldScore were generated and saved, and the highest-scoring orientation that also formed plausible hydrogen bond interactions was selected. The docked ligand and receptor structures were subsequently subjected to minimization and dynamics using the program *Yasara* and the *Yamber* forcefield. This was conducted mainly to relieve close contacts within the protein to the ligand, and to determine whether any of the docked compounds would be "ejected" from the pocket. Minimization and dynamics cycles were performed until the conformations of both the ligand and protein remained unchanged, and none of the docked compounds were "ejected".

To establish whether the docking results were enough authentic, we compared the data with the corresponding crystal structures of PI3Kγ complexed with the molecules from the matrix-template library. Analysis of the docked and crystal structures confirmed similar compound orientations, with the same hydrogen bonds being formed between the compounds and the ATP pocket in the protein (Figure 33).

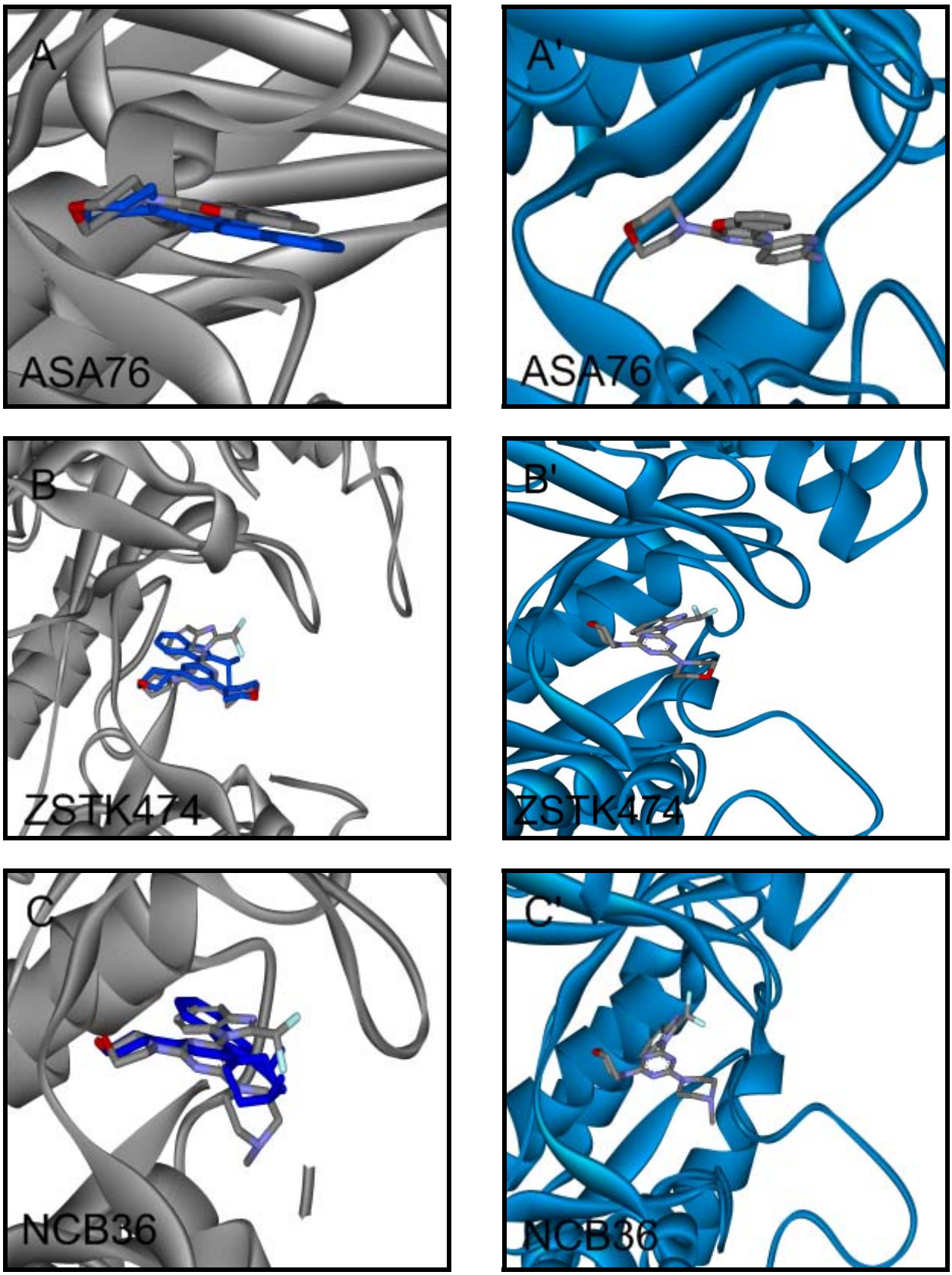
A
ASA76
A'
ASA76
B
ZSTK474
B'
ZSTK474
C
NCB36
C'
NCB36

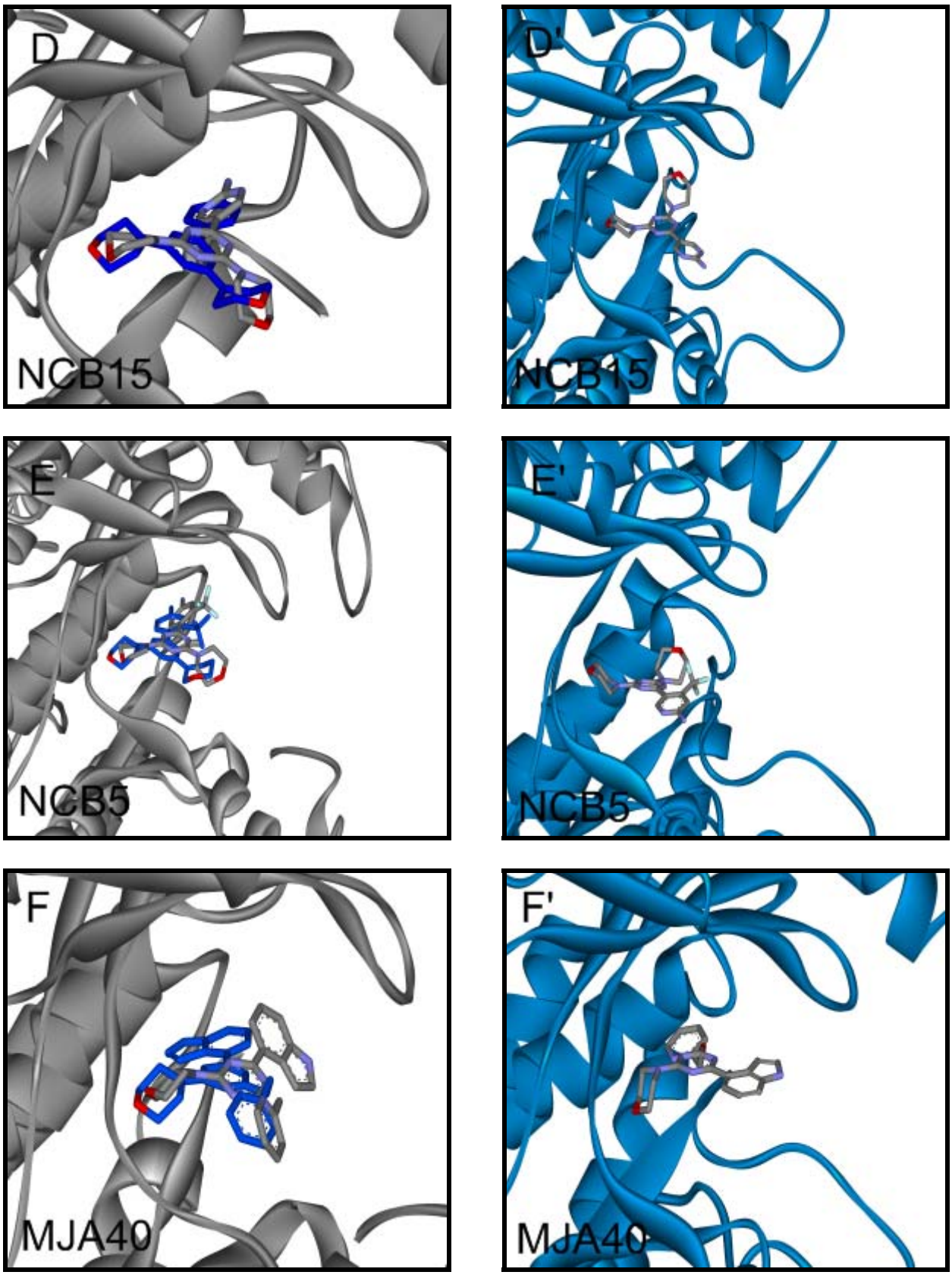

Figure 33. Targeting phosphoinositide 3-kinases (PI3Ks). (A-E) Comparison of the x-ray ligands (colored according to element) and docked ligands (colored in blue) in PI3Kγ (ribbon representation in gray). (A'-E') Docked ligands (colored according to element) in PI3Kα (ribbon representation in light blue). (A-A') Ligand ASA76 docked in PI3Kγ and PI3Kα in similar fashion. The binding mode of the docked structure of ASA76 is similar to the binding mode of the x-ray structure in PI3Kγ. (B-B') Ligand ZSTK474 docked in PI3Kγ and PI3Kα also in similar fashion. The binding

mode of the docked structure of ZSTK474 is similar to the binding mode of the x-ray structure in PI3Kγ. (C-C') The docked structure of the ligand NCB36 in PI3Kγ was planar and in PI3Kα was similar to the x-ray structure in PI3Kγ. (D-D') The PI3Kγ docking corresponds well with the x-ray structure, in PI3Kα the compound is flipped (in all 10 docked conformations), probably while the morpholine binding to the HingeVal is conserved to the other morpholine and the aminopyrimidine fragment is flipped to the hydrophobic pocket 2. This could be due to the different residues found in alpha versus gamma isoforms. (E-E') NCB5 docked in PI3Kγ in similar fashion compared to the x-ray structure. In all 10 docked orientations in PI3Kα, none of them have the second morpholine residue in the same orientation, even though the trifluoromethyl group comes close to that found in PI3Kγ. (F-F') MJA40 docks in the same orientation with the morpholine but the indole moiety flips round in all the docked structures; in PI3Kα the compound is rotated, where the indole moiety is facing the hydrophobic pocket II; this fragment is flipped towards the hydrophobic pocket 2. This could be due to the difference between an alpha and a gamma pocket.

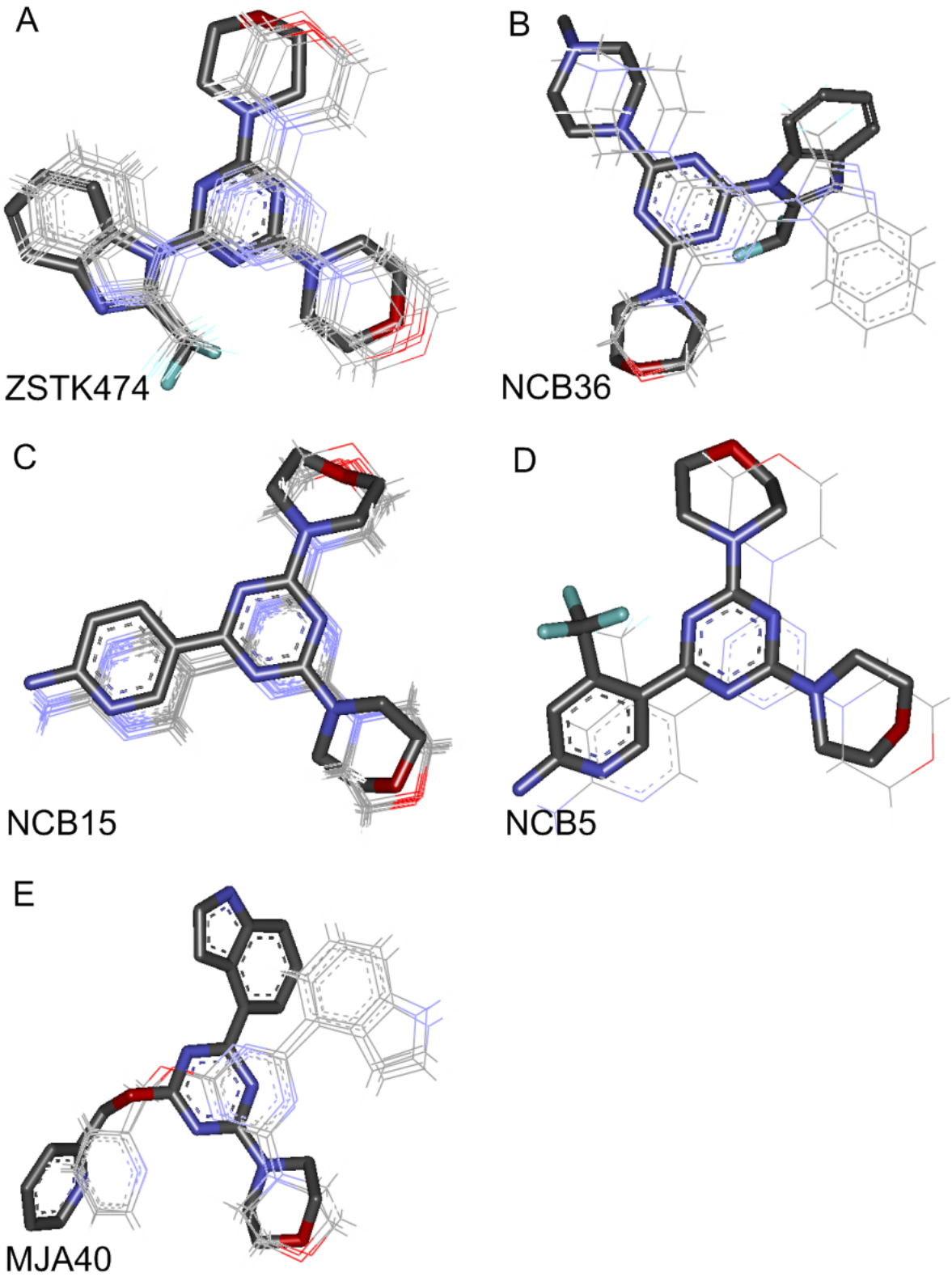

Figure 34. (A-E) Comparison of the x-ray ligands (stick forms and colored according to element) and docked ligands (line forms) in PI3Kγ. (A'-E') Comparison of the x-ray ligands (stick forms and colored according to element) and docked ligands (line forms) in PI3Kα.

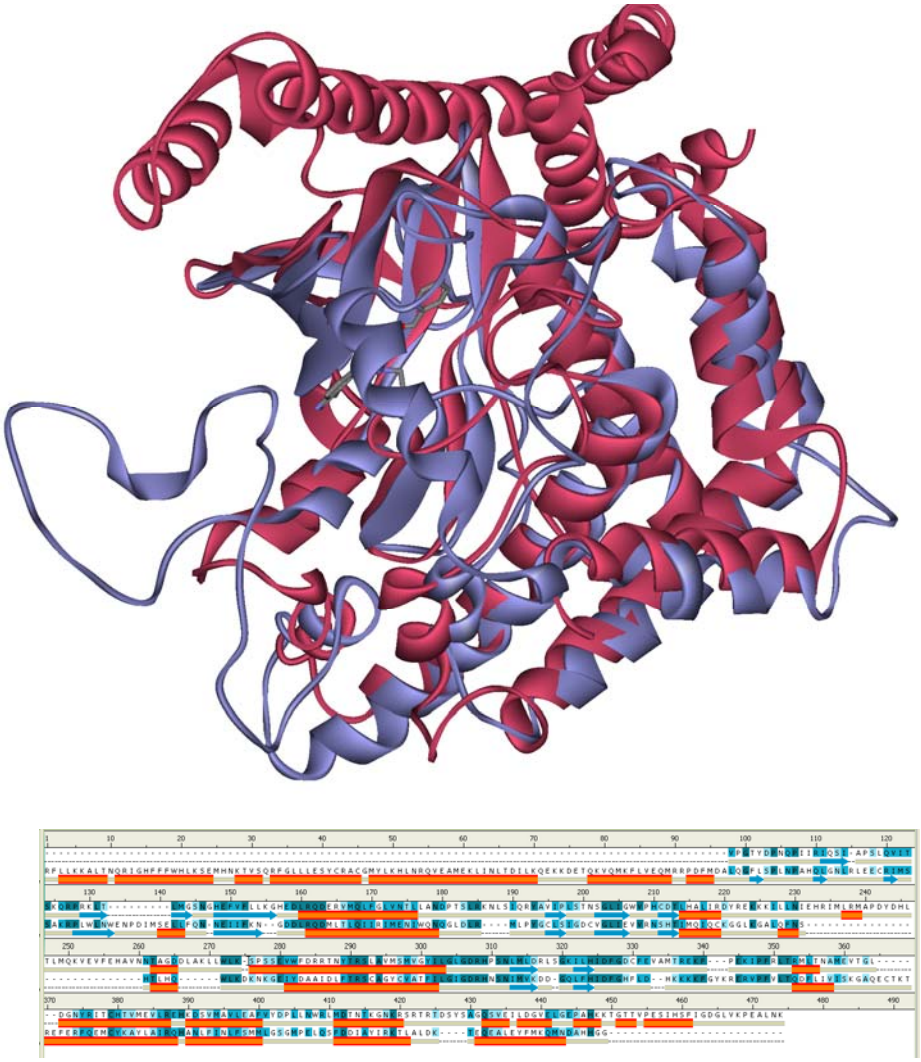

Figure 35. Designing the 3D structure of mTOR and its comparison with PI3Kα. A ribbon diagram of mTOR model (blueish), based on PI3Kγ, and superimposed on PI3Kα (pinkish) is presented. A relatively fast but detailed analysis shows a lot of differences between PI3Kα and mTOR, some of which are conducive to explain the difference of affinity between PI3Kα and mTOR for ligand MJA40 (thick lines). Also a picture of alignment between alpha and mTOR, where blue ovals show important differences, is presented. MJA40 was docked in mTOR (gold score of 75.9) and in PI3Kα (gold score 56.0) presenting much stronger affinity to mTOR, confirmed also by experimental IC50 estimation (IC_{50} (PI3Kα) = 500 nM).

4. Chemistry and Biology

4.1. Pyridinylfuropyrimidine Derivatives

The commercial available starting material 2-chloropyridine-3-carbonitrile **(1)** was treated with ethyl glycolate under basic conditions in the presence of 3-methylbutanol, where the aminofuropyridine **2** (AS3) was obtained. Amide formation of **2** with 3-methoxybenzoyl chloride yielded the furopyridine **3** (AS7). Further ester hydrolysis of **3** and directly amide formation with methanolic ammonia yielded the amide **4**, which was cyclized under basic conditions to the pyrimidinone **5** (AS18). Cleavage of the methyl group under acidic conditions, and further protection of the phenol group with acetic anhydride yielded the pyrimidinone **7** (AS21). Further treatment with phosphorus oxychloride ($POCl_3$) gave the chlorinated pyrimidine **8** (AS24), which was further substituted on the chlorine position with different secondary amines indicated in Table 5.

Scheme 2.

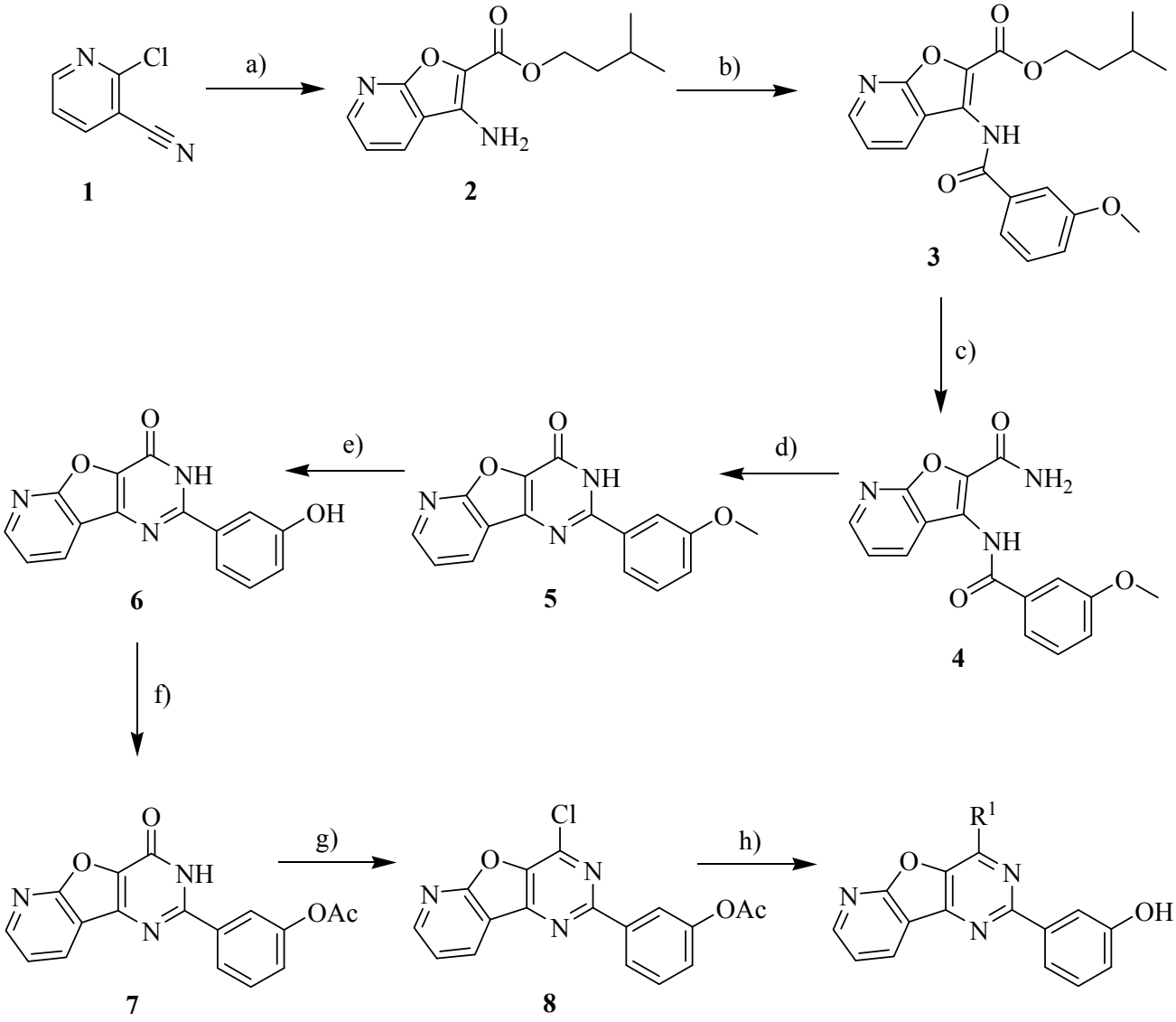

Reagents and conditions: (a) ethyl glycolate (1.1 eq.), Na_2CO_3 (2.0 eq.), 3-methylbutanol, reflux, 72 h, 31%; (b) 3-methoxybenzoyl chloride (1.1 eq.), Et_3N (1.1 eq.), CH_2Cl_2, room temp., 28 h, 86%; (c) $NH_{3(sat.)}$, MeOH, room temp., 4 h, 100%; (d) 5% $NaOH_{(aq.)}$ (10 eq.), EtOH, reflux, 1 h, 90%; (e) $AcOH_{(conc.)}$, $HBr_{(conc.)}$, reflux, 8 h, 100%; (f) Ac_2O (~100 eq.), Et_3N (1.6 eq.), reflux, 1 h, 42%; (g) $POCl_3$ (100 eq.), reflux, 3 h,100%; (h) amine ($2.2^{-3.5}$ eq.), n-butanol, 105 °C, 4^{-72} h, 6^{-85}%.

Table 5.

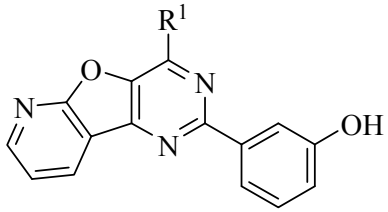

Compds	R^1	*In vitro* PI3Kalpha inhibition at 200nM	In cell inhibition	
			pPKB/PKB 1 µM pS6 1 µM	pPKB/PKB 10 µM pS6 10 µM
9 (PI103)	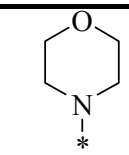	20	++++ +++	++++ +++
10 (AS44)	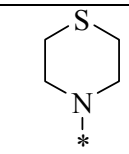	51	(+) +	++(+) ++
11 (VCC17)	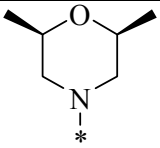	74	- -	++(+) +++
12 (VCC16)	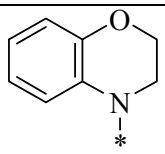	99	- -	+(+) ++
13 (VCC3)	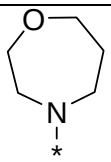	116	- -	- -
14 (AS38)	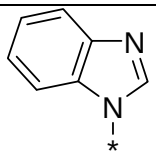	89	- -	- -
15 (AS47)	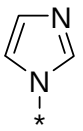	92	- -	- -
16	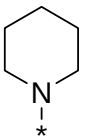	ND	- -	- -

[a]Inhibitor efficacy and their cell permeability were measured by *in cell* Western inhibition assay on melanoma cell line A2058; "-" no activity, "+"/"++" poor activity; "+++" good activity; "++++" very good activity; *in vitro* PI3Kalpha inhibition was measured by *Kinase Glo* assay; given numbers represent %remaining activity, the smaller the value is the stronger is the inhibition.

4.2. Benzofuropyrimidine Derivatives

One of the aims of this project was to investigate the biological activity of 3-(4-morpholinopyrido[3',2':4,5]furo[3,2-*d*]pyrimidin-2-yl)phenol (**9**, PI103) derivatives, where the phenol moiety on the 2-position of the pyrimidine ring is replaced with different isosteric heterocycles. Due to the poor water solubility of inhibitor **9** (PI103), we decided to produce and biologically characterize an analog of PI103, compound **23 (JBA65)**, by hopping from pyridinylfuropyrimidine scaffold to benzofuropyrimidine scaffold. Compound 3-(4-morpholinopyrido[3',2':4,5]furo[3,2-*d*]pyrimidin-2-yl)phenol **23 (JBA65)** was synthesized in a similar synthetic fashion as accomplished by **9** (PI103) (Scheme 3). After improved excellent biological activity of JBA65, which was comparable with the activity of PI103, and better water and DMSO solubility, a new synthetic route was developed, in order to produce 2-chloro-4-morpholinobenzofuro[3,2-d]pyrimidine **24** (ASA75), where on the 2-chloro position of the benzofuropyrimidine **24** different heterocyclic boronic acid pinacol esters were coupled by Suzuki-Miyaura reaction and different heterocyclic secondary amines by nucleophilic substitution (Scheme 4). Treatment of 3-aminobenzofuran-2-carboxamide **(17)** with ethyl chloroformate (Scheme 4) afforded the carbamate **21** (ASA82), which was converted into benzofuro[3,2-*d*]pyrimidine-2,4(1H,3H)-dione **(22)** (ASA70) by ring cyclization under basic conditions. Further chlorination of **22** with phosphorus oxychloride, followed by selective substitution with morpholine on the 4-chloro position of the pyrimidine ring, yielded the 2-chloro-4-morpholinobenzofuro[3,2-*d*]pyrimidine **(24)** (ASA75), which was further substituted on the 2-chloro position under Suzuki conditions.

Scheme 3.

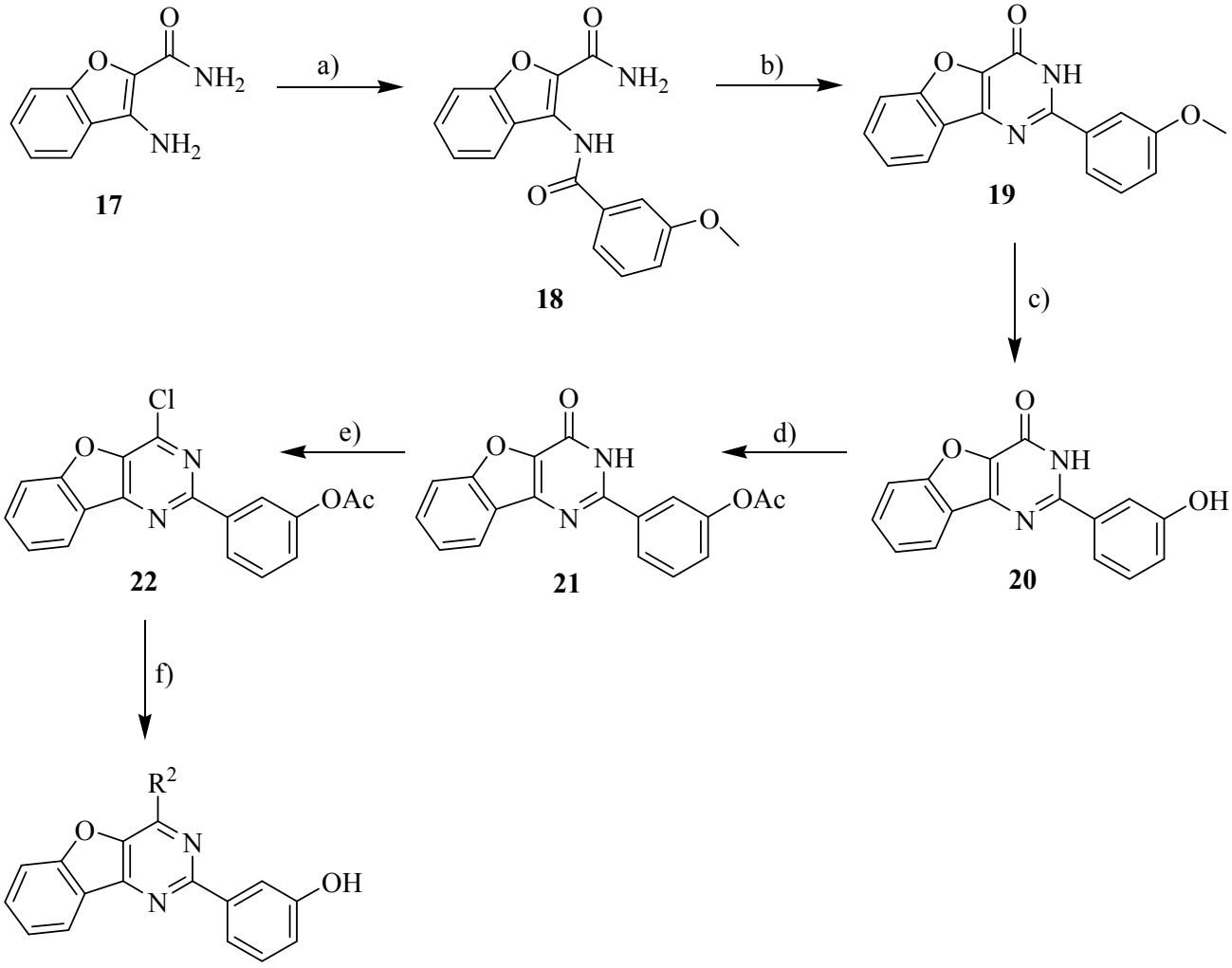

Reagents and conditions: (a) 3-methoxybenzoyl chloride (1.1 eq.), Et_3N (1.1 eq.), CH_2Cl_2, room temp., 18 h, 31%; (b) 5% $NaOH_{(aq.)}$ (10 eq.), EtOH, reflux, 1.5 h, 100%; (c) $AcOH_{(conc.)}$, $HBr_{(conc.)}$ (80 eq.), reflux, 8 h, 82%; (d) Ac_2O (100 eq.), Et_3N (1.6 eq.), reflux, 1.5 h, 100%; (e) $POCl_3$ (100 eq.), reflux, 4 h, 29%; (f) amine (2.2-3.5 eq.), n-butanol, 105 °C, 4-72 h, 10-100%.

Table 6.

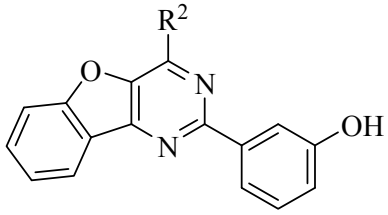

Compds	R^2	*In vitro* PI3Kalpha inhibition at 200nM	In cell inhibition	
			pPKB/PKB 1 µM	pPKB/PKB 10 µM
			pS6 1 µM	pS6 10 µM
23 (JBA65)	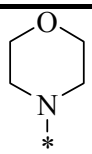	17	++++	++++
			++++	++++
24 (VCC19)	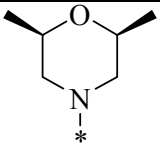	53	-	++
			-	+
25 (VCC18)	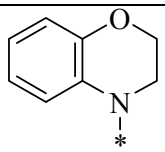	124	-	(+)
			-	+(+)

[a]Inhibitor efficacy and their cell permeability were measured by *in cell* Western inhibition assay on melanoma cell line A2058; "-" no activity, "+"/"++" poor activity; "+++" good activity; "++++" very good activity; *in vitro* PI3Kalpha inhibition was measured by *Kinase Glo* assay; given numbers represent %remaining activity, the smaller the value is the stronger is the inhibition.

Scheme 4.

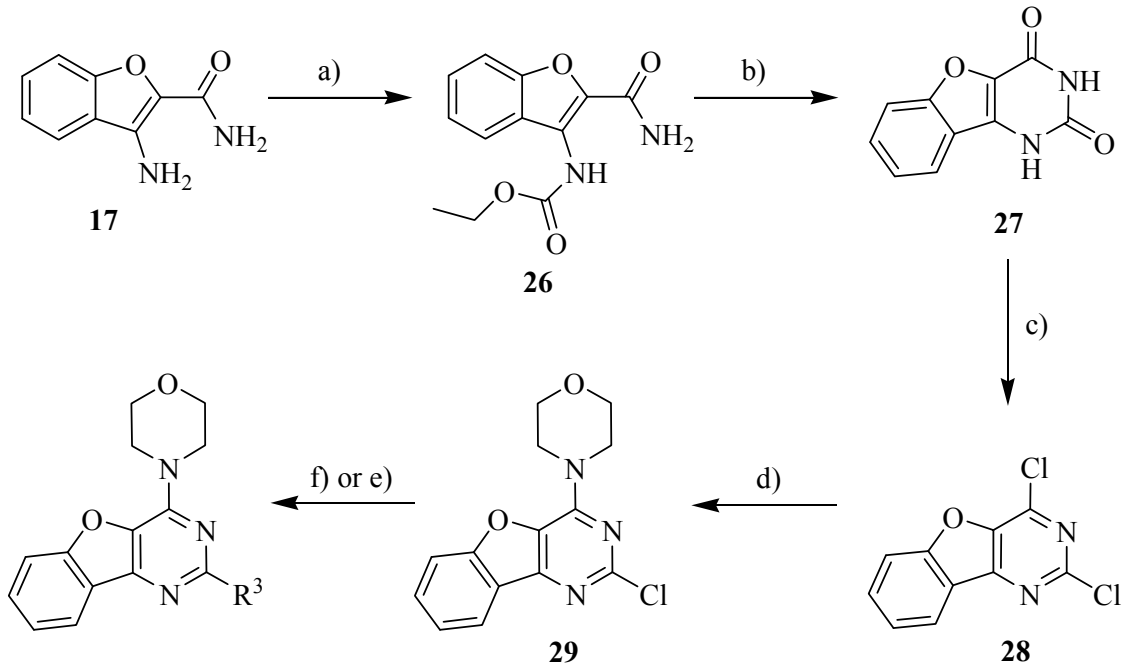

Reagents and conditions: (a) ethyl chloroformate (1.0 eq.), toluene, reflux, 6 h, 67%; (b) 5% NaOH(aq.) (10 eq.), EtOH, reflux, 1 h, 85%; (c) $POCl_3$ (5.0 eq.), DIPEA (5.0 eq.), 100 °C, 22 h, 52%; (d) morpholine (2.2 eq.), MeOH, reflux, 30 min., 95%; (e) boronic acid pinacol ester (4.0 eq.), 1,1'-bis(diphenylphosphino)ferrocene-palladium(II) dichloromethane complex (0.025 eq.), 2M Na_2CO_3(aq.):1,2-dimethoxyethane (1:3), reflux, 10-15 h; (f) amine (1.1 eq.), NaH (1.5 eq.), DMF, reflux, 4 h.

Table 7.

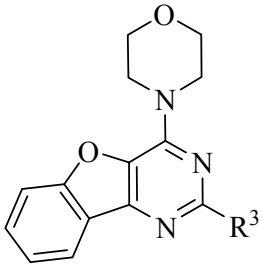

Compds	R^3	*In vitro* PI3Kalpha inhibition at 200nM	In cell inhibition pPKB/PKB 1 µM / pS6 1 µM	In cell inhibition pPKB/PKB 10 µM / pS6 10 µM
30 (GSA26)	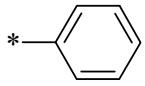	70	+ / -	++ / +
31 (GSA36)	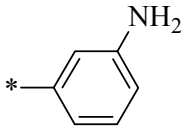	ND	+ / -	++++ / ++++
32 (GSA39) (HGA3)	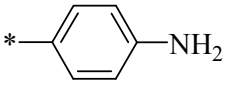	ND	++ / -	++++ / ++++
33 (ASA99)	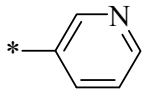	38	+++ / ++	++++ / ++++
34 (ASA76)	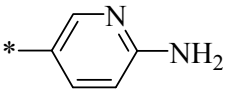	20	++++ / ++++	++++ / ++++
35 (ASA101)	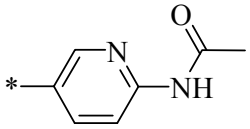	41	++(+) / +	++++ / ++++
36 (ASA100)	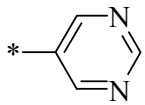	39	+++ / ++	++++ / ++++
37 (ASA98)	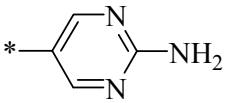	20	+++ / ++	++++ / ++++
38 (GSA47)	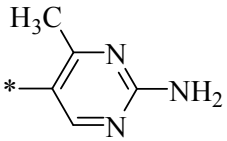	ND	++++ / ++(+)	++++ / ++++

Table 7 (continued).

Compds	R^3	*In vitro* PI3Kalpha inhibition at 200nM	In cell inhibition	
			pPKB/PKB 1 µM pS6 1 µM	pPKB/PKB 10 µM pS6 10 µM
39 (ASA78)	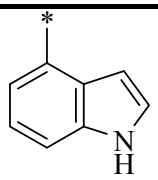	54	+++ ++	++++ ++++
40 (VVA75)	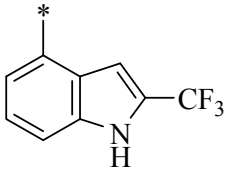	100	- -	+ -
41 (ASA79)	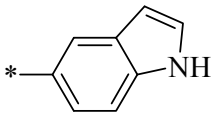	62	++ +	++++ ++++
42 (VVA49)	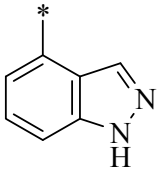	8	+++ ++	++++ ++++
43 (VVA73)	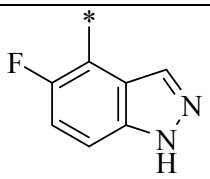	98	- -	- -
44 (VVA79)	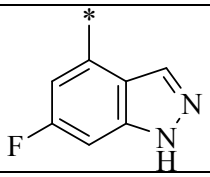	47	+ -	+++ -
45 (ASA80)	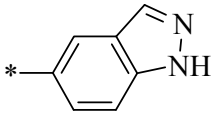	118	- -	+++ -
46 (ASA81)	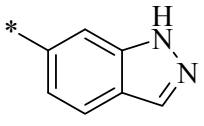	67	- -	+++ -
47 (GSA32)	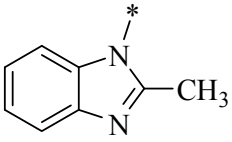	ND	+++(+) -	++++ ++++

Table 7 (continued).

Compds	R^3	*In vitro* PI3Kalpha inhibition at 200nM	In cell inhibition	
			pPKB/PKB 1 µM pS6 1 µM	pPKB/PKB 10 µM pS6 10 µM
48 (ASA92)	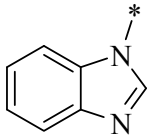	80	- -	+++ ++
49 (ASA95)	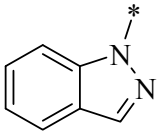	84	+ +	+++ ++++
50 (ASA94)	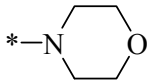	93	- ++	+++ ++++
51 (ASA113)	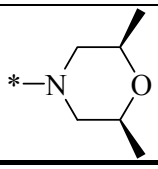	90	+ -	+++ +++

[a]Inhibitor efficacy and their cell permeability were measured by *in cell* Western inhibition assay on melanoma cell line A2058; "-" no activity, "+"/"++" poor activity; "+++" good activity; "++++" very good activity; *in vitro* PI3Kalpha inhibition was measured by *Kinase Glo* assay; given numbers represent %remaining activity, the smaller the value is the stronger is the inhibition.

4.3. Thienopyrimidine Derivatives

Scheme 5.

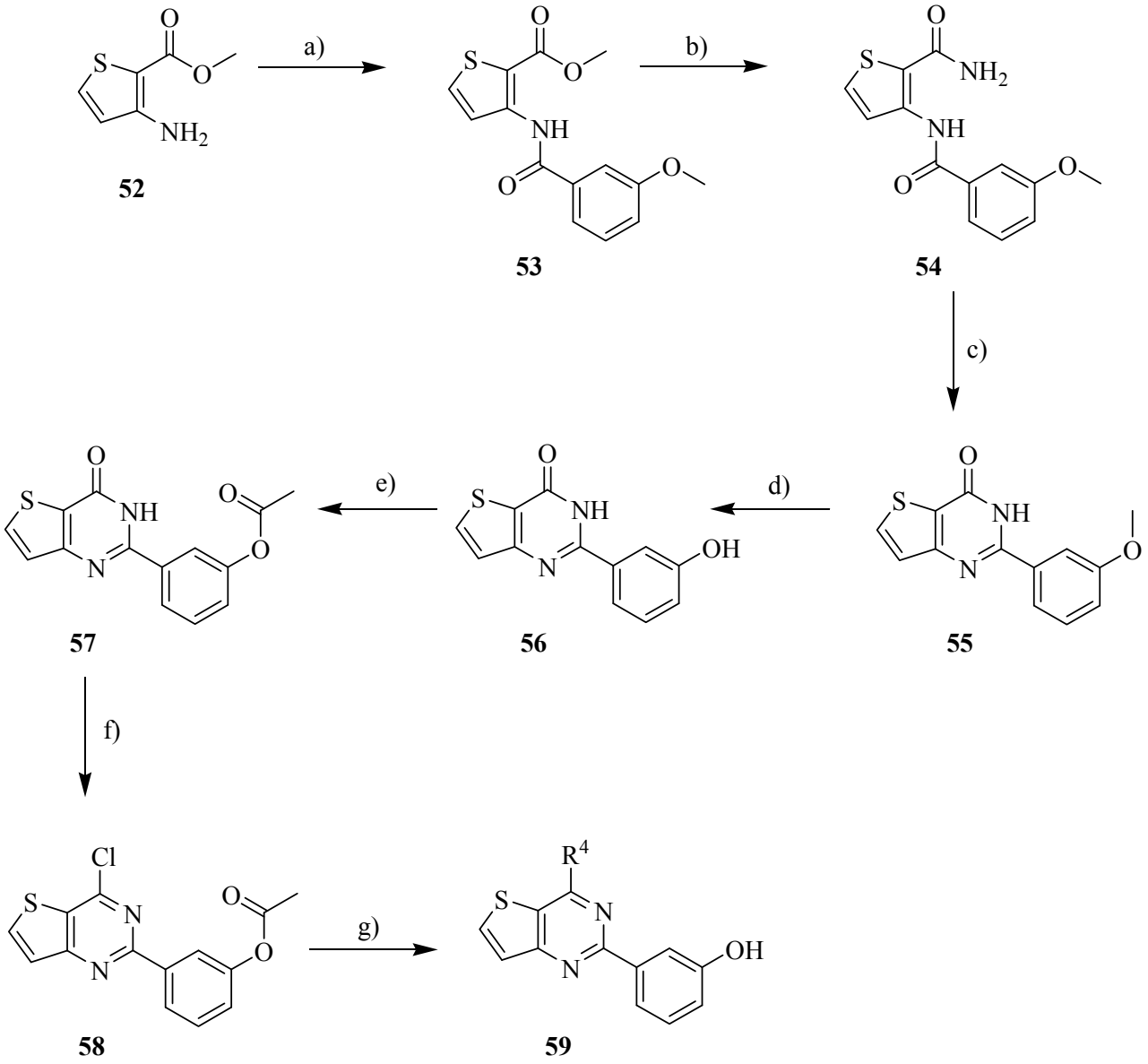

Reagents and conditions: (a) Et_3N (1.1 eq.), CH_2Cl_2, 0 °C to room temperature, 3 h, 100%; (b) methanolic ammonia (7N), 90 °C, 44 h, steel bomb at 50 psi (3.7 bar), 100%; (c) 5% $NaOH_{(aq.)}$ (10 eq.), EtOH, reflux, 1.5 h, 100%; (d) $AcOH_{(conc.)}$, $HBr_{(conc.)}$ (80 eq.), reflux, 8 h, 80%; (e) Ac_2O (100 eq.), Et_3N (1.6 eq.), reflux, 1.5 h, 100%; (f) $POCl_3$ (100 eq.), reflux, 4 h, 30%; (g) amine (2.2-3.5 eq.), n-butanol, 105 °C, 4-72 h, 50-80%.

Table 8.

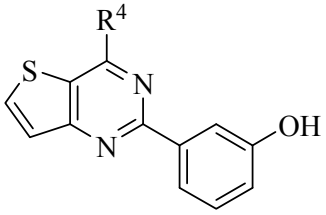

Compds	R^4	*In vitro* PI3Kalpha inhibition at 200nM	In cell inhibition	
			pPKB/PKB 1 µM	pPKB/PKB 10 µM
			pS6 1 µM	pS6 10 µM
60 (VCB187)	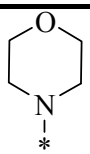	15	++++	++++
			+++	+++
61 (VCB192)	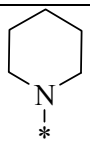	87	-	-
			-	-

[a]Inhibitor efficacy and their cell permeability were measured by *in cell* Western inhibition assay on melanoma cell line A2058; "-" no activity, "+"/"++" poor activity; "+++" good activity; "++++" very good activity; *in vitro* PI3Kalpha inhibition was measured by *Kinase Glo* assay; given numbers represent %remaining activity, the smaller the value is the stronger is the inhibition.

Scheme 6.

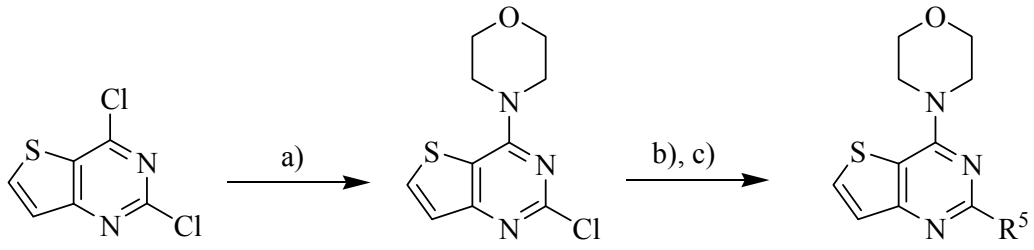

62 **63**

Reagents and conditions: (a) morpholine (2.2 eq.), methanol, room temperature, 1 h, 100%; (b) boronic acid pinacol ester (4.0 eq.), 1,1'-bis(diphenylphosphino)ferrocene-palladium(II) dichloromethane complex (0.025 eq.), 2M Na_2CO_3(aq.):1,2-dimethoxyethane (1:3), reflux, 10-15 h; (c) amine (1.1 eq.), NaH (1.5 eq.), DMF, reflux, 4 h.

Table 9.

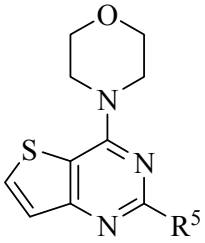

Compds	R^5	*In vitro* PI3Kalpha inhibition at 200nM	In cell inhibition[a] pPKB/PKB 1 µM / pS6 1 µM	In cell inhibition[a] pPKB/PKB 10 µM / pS6 10 µM
64 (NCB100)	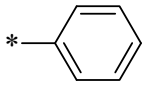	72	++	+++
			-	++(+)
65 (NCB101)	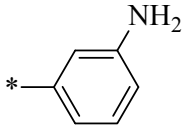	77	-	++++
			-	++++
66 (NCB98)	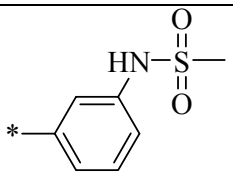	90	++	++
			-	++
67 (VCC33)	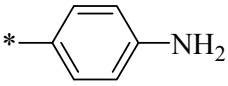	98	-	-
			-	-
68 (VCB155)	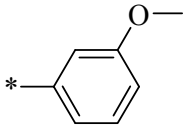	52	-	-
			-	++(+)
69 (VCB201)	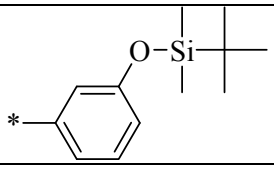	43	-	-
			-	+
70 (NCB67)	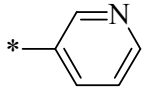	65	+	++++
			+	++++
71 (VCC41)	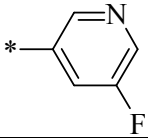	89	-	+++
			-	+
72 (VCC10)	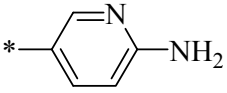	17	+	++++
			+++	+++

Table 9 (continued).

Compds	R^5	*In vitro* PI3Kalpha inhibition at 200nM	In cell inhibition[a] pPKB/PKB 1 µM / pS6 1 µM	In cell inhibition[a] pPKB/PKB 10 µM / pS6 10 µM
73 (NCB65)	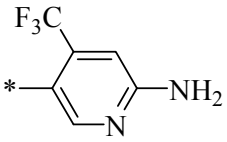	8	++	++++
			+(+)	++++
74 (NCB68)	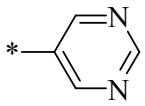	33	+(+)	+++
			-	++(+)
75 (VCC30)	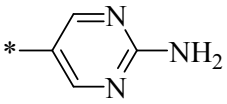	30	+++(+)	+++(+)
			+++	+++
76 (VCC31)	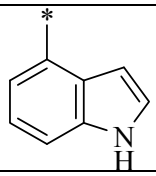	76	-	++++
			+	++++
77 (VCC40)	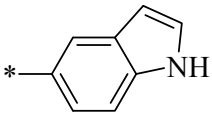	90	++	++++
			+	++++
78 (MJA19)	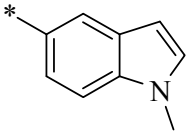	118	-	+
			+	+
79 (NCB102)	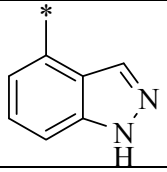	20	(+)	++++
			-	++++
80 (VCC34)	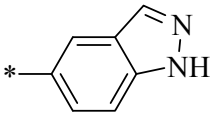	87	+	+++(+)
			-	+++(+)
81 (MJA18)	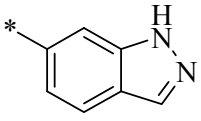	112	-	+
			+	+

Table 9 (continued).

Compds	R^5	*In vitro* PI3Kalpha inhibition at 200nM	In cell inhibition[a]	
			pPKB/PKB 1 µM pS6 1 µM	pPKB/PKB 10 µM pS6 10 µM
82 (VCC35)	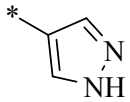	77	(+)	+++
			-	+++
83 (NCB74)	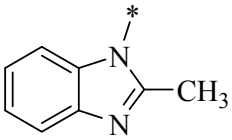	62	++	++++
			-	+(+)

[a]Inhibitor efficacy and their cell permeability were measured by *in cell* Western inhibition assay on melanoma cell line A2058; "-" no activity, "+"/"++" poor activity; "+++" good activity; "++++" very good activity; *in vitro* PI3Kalpha inhibition was measured by *Kinase Glo* assay; given numbers represent %remaining activity, the smaller the value is the stronger is the inhibition.

4.4. Di-Morpholine-Containing Triazine Derivatives

Scheme 7 shows a method for selectively displacing of two chlorines from 2,4,6-trichloro-1,3,5-triazine **(69)** with morpholine in dimethylformamide to prepare bis-morpholino triazine intermediate **70**, which was further coupled with heterocyclic boronic acid pinacol esters by Suzuki-Miyaura reaction and heterocyclic secondary amines by nucleophilic substitution.

Scheme 7.

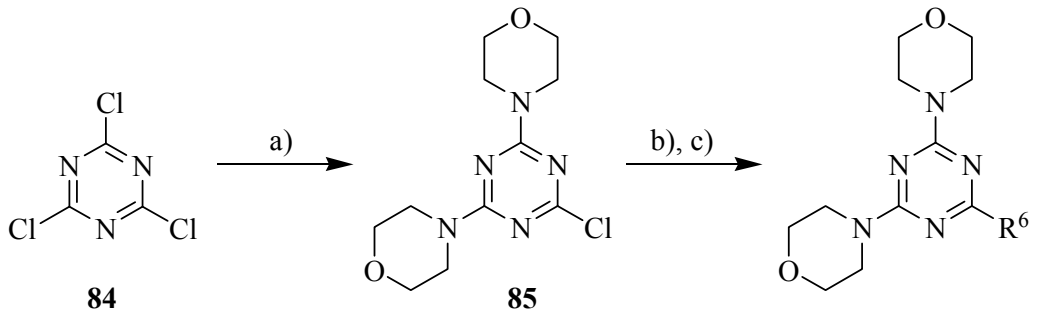

84 **85**

Reagents and conditions: (a) morpholine (4.5 eq.), DMF, 0 °C, 20 min., 56%; (b) boronic acid pinacol ester (4.0 eq.), 1,2-dimethoxyethane:2M Na_2CO_3 (3:1), dichloro 1,1'-bis(diphenylphosphino)ferrocene-palladium(II)dichloride dichloromethane complex (0.025 eq.), 90 °C, 15-20 h; c) amine (1.1 eq.), NaH (1.5 eq.), DMF, reflux, 4 h.

Table 10.

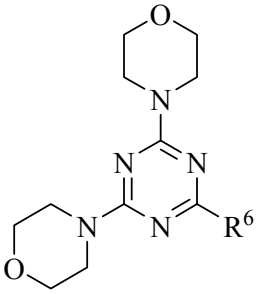

Compds	R^6	*In vitro* PI3Kalpha inhibition at 200nM	In cell inhibition[a] pPKB/PKB 1 µM pS6 1 µM	In cell inhibition[a] pPKB/PKB 10 µM pS6 10 µM
86 (GSA10)	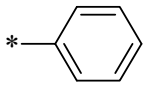	77	+(+)	++(+)
			-	+
87 (NCA197)	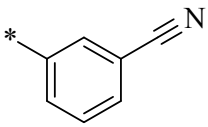	68	-	-
			-	-
88 (NCA201)	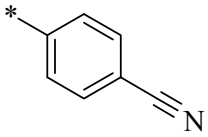	87	-	-
			-	-
89 (NCA193)	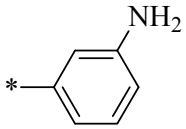	82	-	+
			+	+++(+)
90 (NCA189)	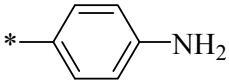	76	-	+++
			(+)	++++
91 (NCA183)	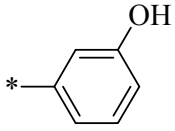	26	++	++++
			+++	++++
92 (NCA205)	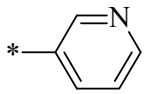	60	+	++++
			-	++(+)
93 (NCB9)	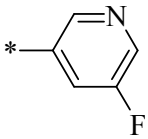	97	-	++
			-	+

Table 10 (continued).

Compds	R^6	*In vitro* PI3Kalpha inhibition at 200nM	In cell inhibition[a] pPKB/PKB 1 µM / pS6 1 µM	In cell inhibition[a] pPKB/PKB 10 µM / pS6 10 µM
94 (NCB90)	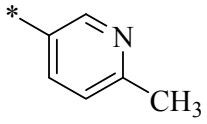	77	+	++++
			+	++++
95 (NCB89)	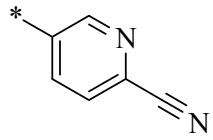	99	(+)	+
			-	-
96 (NCA215)	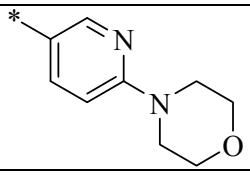	97	-	-
			-	-
97 (NCA163)	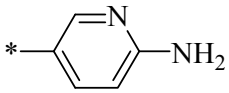	67	-	++++
			+++	++++
98 (NCB5/NCB63)	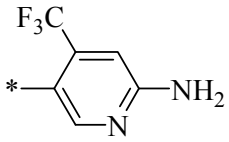	20	++++	++++
			+++(+)	+++(+)
99 (MJA47)	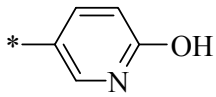	121	-	+
			+	+
100 (NCB78)	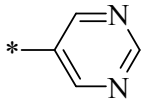	72	+	+(+)
			-	-
101 (NCB95)	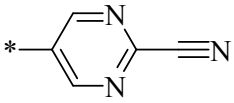	38	+(+)	++
			+	+
102 (NCB15)	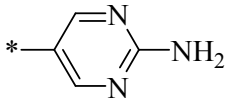	11	+++(+)	++++
			++++	++++

Table 10 (continued).

Compds	R^6	*In vitro* PI3Kalpha inhibition at 200nM	In cell inhibition[a] pPKB/PKB 1 µM pS6 1 µM	In cell inhibition[a] pPKB/PKB 10 µM pS6 10 µM
103 (NCB86)	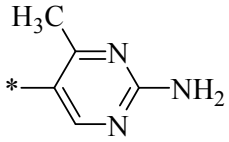	8	++++	++++
			++(+)	++++
104 (MZ-043)	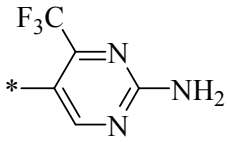	ND	ND	ND
			ND	ND
105 (MJA7)	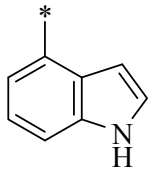	79	+++	++++
			++(+)	++++
106 (VVA81)	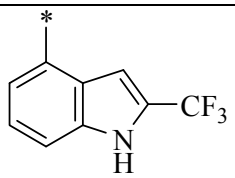	100	+	+++
			-	+
107 (MJA6)	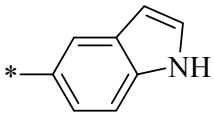	110	+	+++
			+	++++
108 (MJA46)	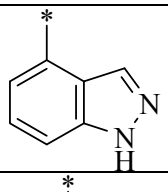	38	++(+)	++++
			+	++++
109 (VVA103)	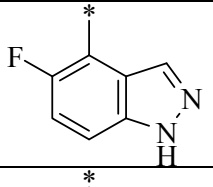	37	(+)	+++
			-	+++(+)
110 (VVA97)	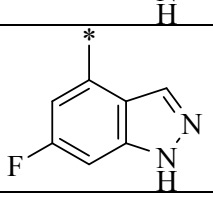	26	++(+)	++++
			-	+++(+)
111 (NCB22)	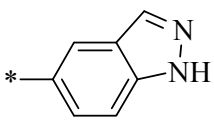	111	+	+++
			+	+(+)

Table 10 (continued).

Compds	R^6	*In vitro* PI3Kalpha inhibition at 200nM	In cell inhibition[a] pPKB/PKB 1 µM pS6 1 µM	In cell inhibition[a] pPKB/PKB 10 µM pS6 10 µM
112 (MJA14)	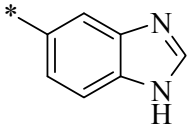	119	-	+(+)
			+(+)	++
113 (MJA44)	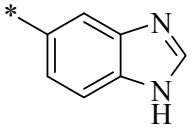	61	++	++++
			+	++++
114 (NCB53)	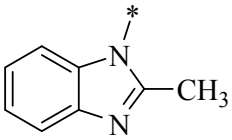	53	++++	++++
			+(+)	++++
115 (NCA110/NCB38/ ZSTK474)	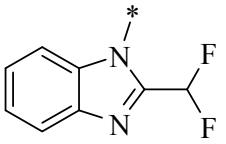	13	++++	++++
			+++(+)	+++(+)
116 (NCA111)	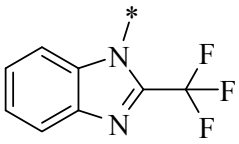	25	++	++++
			+	+++
117 (NCB82)	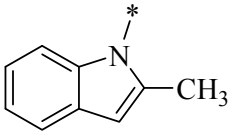	92	+	++
			-	(+)
118 (NCA77)	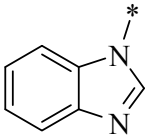	69	+	++++
			+	+++(+)
119 (NCA152)	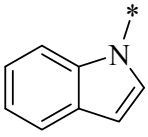	86	-	+
			-	+
120 (NCA181)	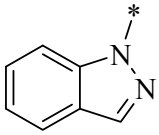	89	-	+
			-	++

Table 10 (continued).

Compds	R^6	*In vitro* PI3Kalpha inhibition at 200nM	In cell inhibition[a] pPKB/PKB 1 µM / pS6 1 µM	In cell inhibition[a] pPKB/PKB 10 µM / pS6 10 µM
121 (NCA173)	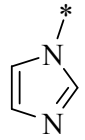	65	-	+
			-	++(+)
122 (BAS02828052)	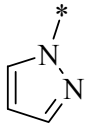	96	++	+++
			-	+(+)
123 (NCB94)	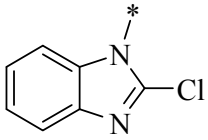	28	+++(+)	++++
			+(+)	+++
124 (BAS01056850)	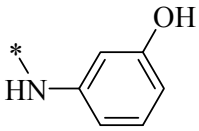	77	+(+)	++++
			-	+++
125 (MJA12)	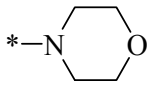	116	-	-
			-	-
126 (MJA32)	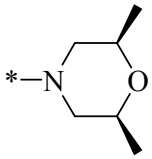	126	-	-
			-	-
127 (ASN09891537)	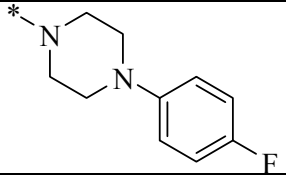	128	-	+(+)
			-	-
128 (BAS07354380)	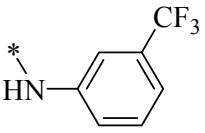	103	+(+)	-
			-	-
129 (7927373)	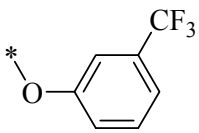	99	+(+)	-
			-	-

[a]Inhibitor efficacy and their cell permeability were measured by *in cell* Western inhibition assay on melanoma cell line A2058; "-" no activity, "+"/"++" poor activity; "+++" good activity; "++++" very good activity; *in vitro* PI3Kalpha inhibition was measured by *Kinase Glo* assay; given numbers represent %remaining activity, the smaller the value is the stronger is the inhibition.

4.5. ZSTK474 Derivatives

Scheme 8.

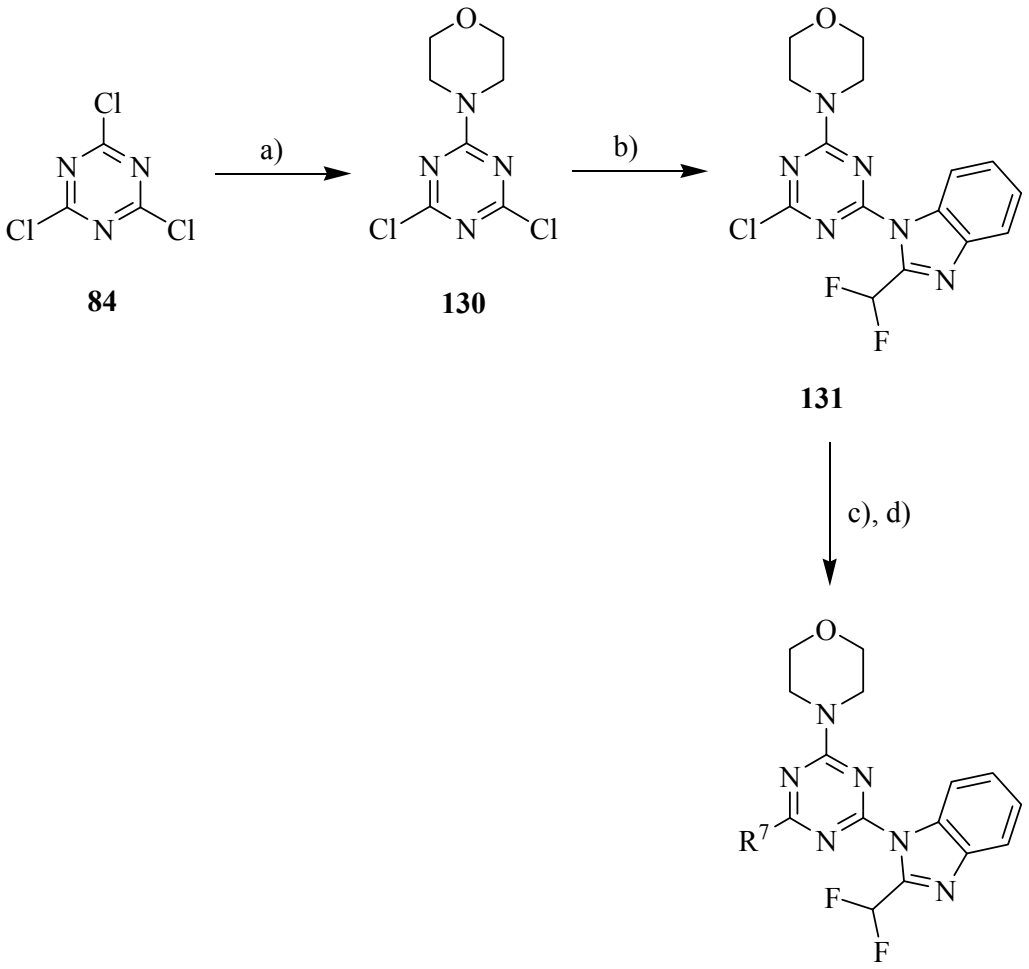

Reagents and conditions: (a) morpholine (1.0 eq.), CH_2Cl_2, -50 °C, 20 min., 28%; (b) K_2CO_3, (1.5 eq.), 2-difluoromethyl-1*H*-benzoimidazole (1.4 eq.), DMF, 30 min. at 0 °C, 4 h at room temp., 65%; (c) boronic acid pinacol ester (4.0 eq.), 1,2-dimethoxyethane:2M Na_2CO_3 (3:1), dichloro 1,1'-bis(diphenylphosphino)ferrocene-palladium(II)dichloride dichloromethane complex (0.025 eq.), 90 °C, 15-20 h; d) amine (1.1 eq.), NaH (1.5 eq.), DMF, reflux, 4 h.

Table 11.

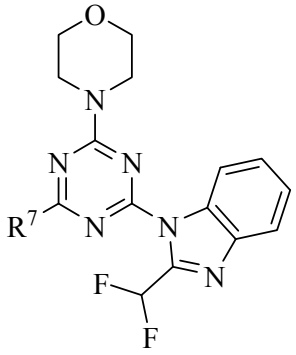

Compds	R^7	*In vitro* PI3Kalpha inhibition at 200nM	In cell inhibition[a] pPKB/PKB 1 µM / pS6 1 µM	In cell inhibition[a] pPKB/PKB 10 µM / pS6 10 µM
132	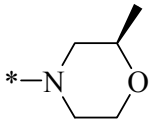	ND	ND ND	ND ND
133	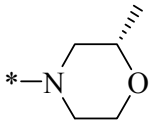	ND	ND ND	ND ND
134	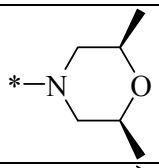	ND	ND ND	ND ND
135	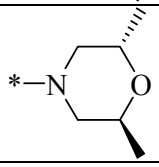	ND	ND ND	ND ND
136	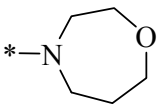	ND	ND ND	ND ND
137 (NCB87)	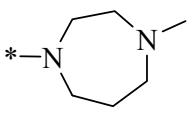	34	+++(+) +	++++ ++++
138 (NCB37)	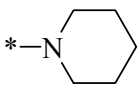	39	++++ +(+)	++++ ++++
139 (NCB36)	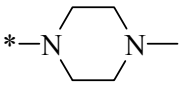	33	++++ ++++	++++ ++++

Table 11 (continued).

Compds	R^7	*In vitro* PI3Kalpha inhibition at 200nM	In cell inhibition[a]	
			pPKB/PKB 1 µM	pPKB/PKB 10 µM
			pS6 1 µM	pS6 10 µM
140 (NCB91)	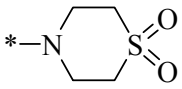	34	++	++++
			-	+++(+)
141 (NCB60)	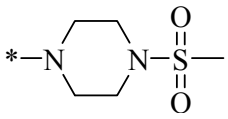	17	++++	++++
			++++	++++
142 (NCB57)	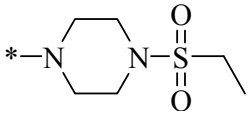	35	++++	++++
			(+)	+++
143 (NCB48)	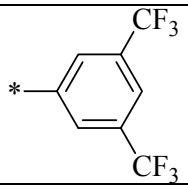	115	-	-
			-	-
144 (NCB51)	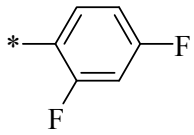	31	+(+)	++
			-	(+)
145 (NCB49)	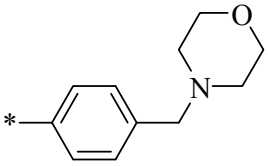	41	++	++++
			-	+++(+)

[a]Inhibitor efficacy and their cell permeability were measured by *in cell* Western inhibition assay on melanoma cell line A2058; "-" no activity, "+"/"++" poor activity; "+++" good activity; "++++" very good activity; *in vitro* PI3Kalpha inhibition was measured by *Kinase Glo* assay; given numbers represent %remaining activity, the smaller the value is the stronger is the inhibition.

4.6. Di-Morpholine-Containing Pyrimidine Derivatives

Scheme 9.

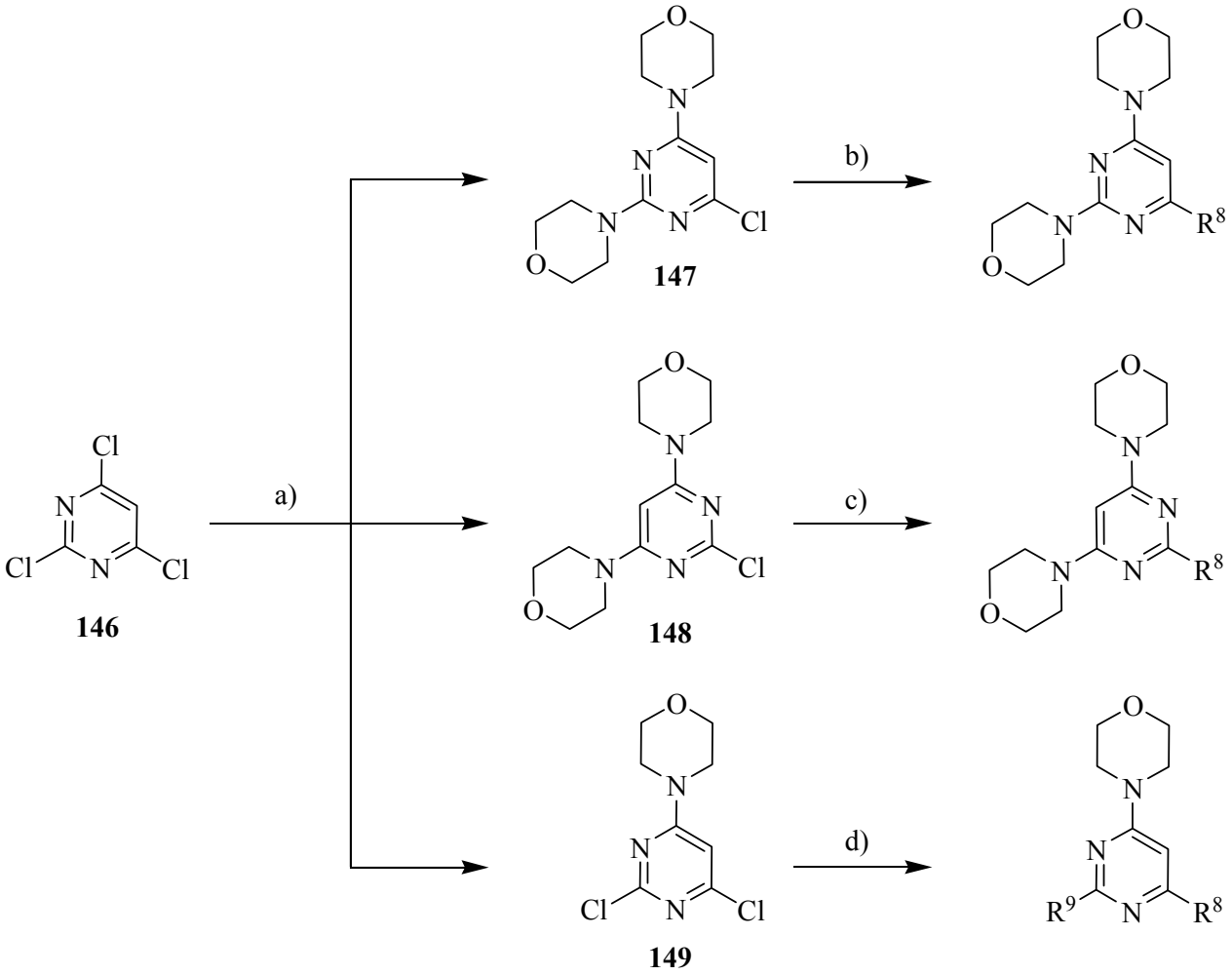

Reagents and conditions: (a) morpholine (2.5 eq.), N,N-diisopropylethylamine (3.0 eq.), ethanol, 0 °C to room temperature, 16 h, mixture of 132 and 133 (7:1); (b, c, d) boronic acid pinacol ester (4.0 eq.), 1,1'-bis(diphenylphosphino)ferrocene-palladium(II) dichloromethane complex (0.025 eq.), 2M Na_2CO_3(aq.):1 dimethoxyethane (1:3), reflux, 10-15 h; (c) amine (1.1 eq.), NaH (1.5 eq.), DMF, reflux, 4 h.

Table 12.

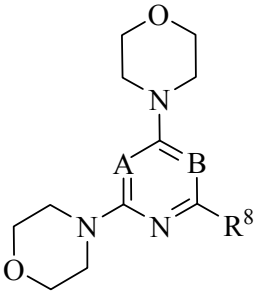

Compds	R^8	A	B	*In vitro* PI3Kalpha inhibition at 200nM	In cell inhibition[a] pPKB/PKB 1 µM / pS6 1 µM	In cell inhibition[a] pPKB/PKB 10 µM / pS6 10 µM
150 (GSA22)	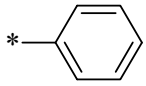	C	N	87	- / -	- / -
151 (GSA23)	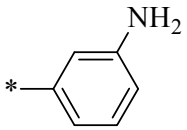	C	N	93	- / -	+ / -
152 (GSA24)	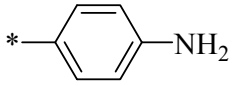	C	N	84	- / -	+ / -
153 (VVA105)	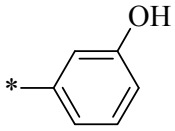	C	N	30	++ / -	++++ / +++(+)
154 (VVA107)	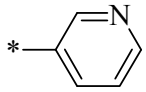	C	N	81	+(+) / +(+)	++(+) / +++
155 (VVA111)	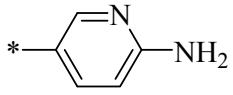	C	N	63	++(+) / +++	++++ / ++++
156 (VVA109)	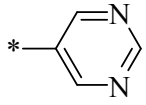	C	N	72	++(+) / +	+++ / +++
157 (VVA113)	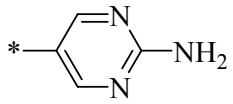	C	N	49	+++ / +(+)	+++(+) / ++++

Table 12 (continued).

Compds	R^8	A	B	*In vitro* PI3Kalpha inhibition at 200nM	In cell inhibition[a] pPKB/PKB 1 µM pS6 1 µM	In cell inhibition[a] pPKB/PKB 10 µM pS6 10 µM
158 (VVA131)	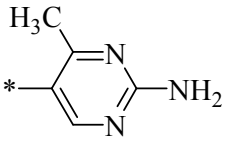	C	N	24	++(+) +++	++++ ++++
159 (ND)	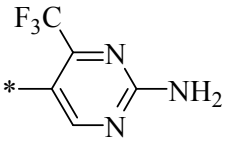	C	N	ND	ND ND	ND ND
160 (VVA119)	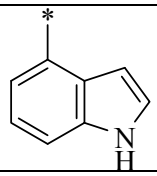	C	N	98	++(+) +++(+)	+++ ++++
161 (VVA123)	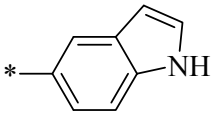	C	N	91	++ +++(+)	+++(+) ++++
162 (VVA117)	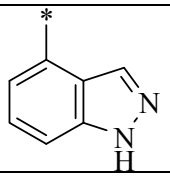	C	N	42	++(+) +++	+++(+) ++++
163 (VVA115)	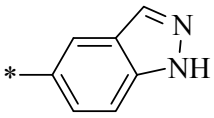	C	N	97	++ +++	++ +++
164 (NCB106)	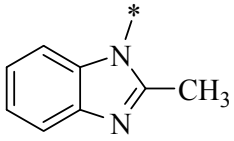	C	N	53	++(+) -	+++(+) +++
165 (NCB35)	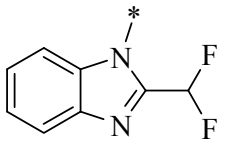	C	N	11	++++ ++++	++++ ++++
166 (NCB34)	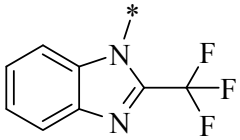	C	N	36	+++ +	++++ +++

Table 12 (continued).

Compds	R^8	A	B	*In vitro* PI3Kalpha inhibition at 200nM	In cell inhibition[a] pPKB/PKB 1 µM / pS6 1 µM	In cell inhibition[a] pPKB/PKB 10 µM / pS6 10 µM
167 (GSA20)	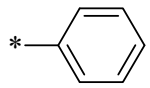	N	C	78	- / +	+(+) / ++
168 (NCA195)	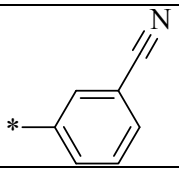	N	C	85	- / -	- / -
169 (NCA199)	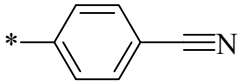	N	C	97	- / -	- / -
170 (NCA191)	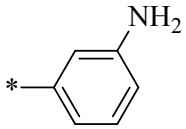	N	C	73	- / -	+ / ++
171 (NCA187)	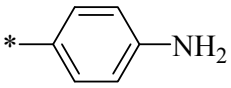	N	C	87	- / +	+ / +++(+)
172 (NCA185)	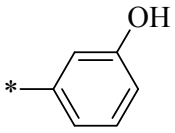	N	C	57	(+) / ++	++++ / +++(+)
173 (NCA203)	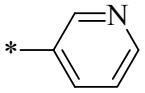	N	C	75	- / -	+ / -
174 (NCB11)	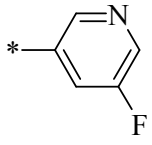	N	C	117	+ / -	+++ / +
175 (NCA207)	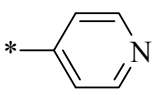	N	C	93	- / -	- / -

Table 12 (continued).

Compds	R^8	A	B	*In vitro* PI3Kalpha inhibition at 200nM	In cell inhibition[a] pPKB/PKB 1 µM pS6 1 µM	In cell inhibition[a] pPKB/PKB 10 µM pS6 10 µM
176 (ASA89)	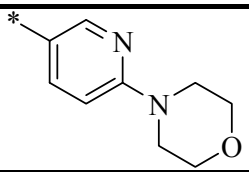	N	C	123	- -	+(+) -
177 (NCA165)	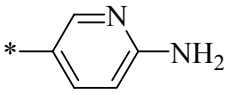	N	C	51	- ++	++++ ++(+)
178 (NCA235)	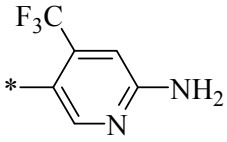	N	C	15	+++(+) +	++++ ++
179 (GSA28)	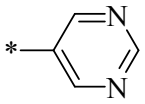	N	C	60	+ -	++ -
180 (NCB16)	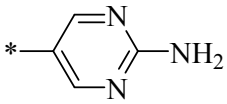	N	C	18	++(+) +++(+)	++++ ++++
181 (NCB115)	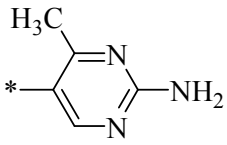	N	C	30	++++ +	++++ ++++
182 (ND)	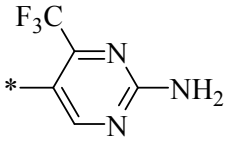	N	C	ND	ND ND	ND ND
183 (NCB20)	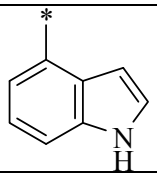	N	C	86	++ +	++++ ++++
184 (NCB19)	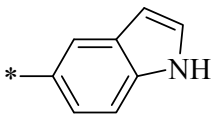	N	C	105	+ ++	++++ ++++

Table 12 (continued).

Compds	R^8	A	B	*In vitro* PI3Kalpha inhibition at 200nM	In cell inhibition[a] pPKB/PKB 1 µM pS6 1 µM	In cell inhibition[a] pPKB/PKB 10 µM pS6 10 µM
185 (GSA21)	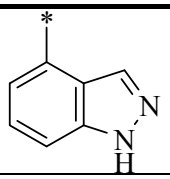	N	C	46	- ++	++++ ++++
186 (ASA87)	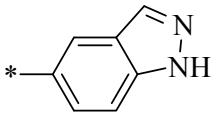	N	C	105	+ (+)	++ (+)
187 (ASA88)	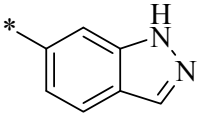	N	C	114	- -	+(+) -
188 (GSA29)	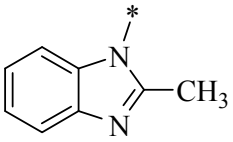	N	C	64	- -	++ ++++
189 (NCA169)	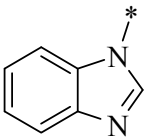	N	C	63	+ +	++++ +++
190 (ND)	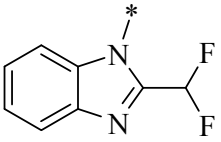	N	C	ND	ND ND	ND ND
191 (NCA171)	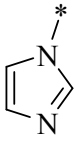	N	C	66	- +	+ ++
192 (ASA102)	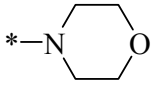	N	C	107	+(+) -	+(+) -
193 (ASA108)	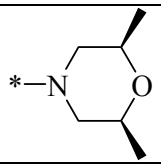	N	C	107	+(+) -	+(+) -
194 (ASA110)	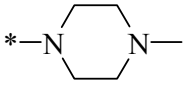	N	C	123	- -	- -

Table 12 (continued).

Compds	R^8	A	B	*In vitro* PI3Kalpha inhibition at 200nM	In cell inhibition[a]	
					pPKB/PKB 1 μM	pPKB/PKB 10 μM
					pS6 1 μM	pS6 10 μM
195 (ASA109)	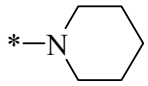	N	C	117	-	-
					-	-
196 (ASA111)	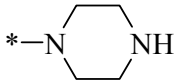	N	C	134	-	-
					-	-

[a]Inhibitor efficacy and their cell permeability were measured by *in cell* Western inhibition assay on melanoma cell line A2058; "-" no activity, "+"/"++" poor activity; "+++" good activity; "++++" very good activity; *in vitro* PI3Kalpha inhibition was measured by *Kinase Glo* assay; given numbers represent %remaining activity, the smaller the value is the stronger is the inhibition.

4.7. Linked Triazine and Pyrimidine Derivatives

Scheme 10.

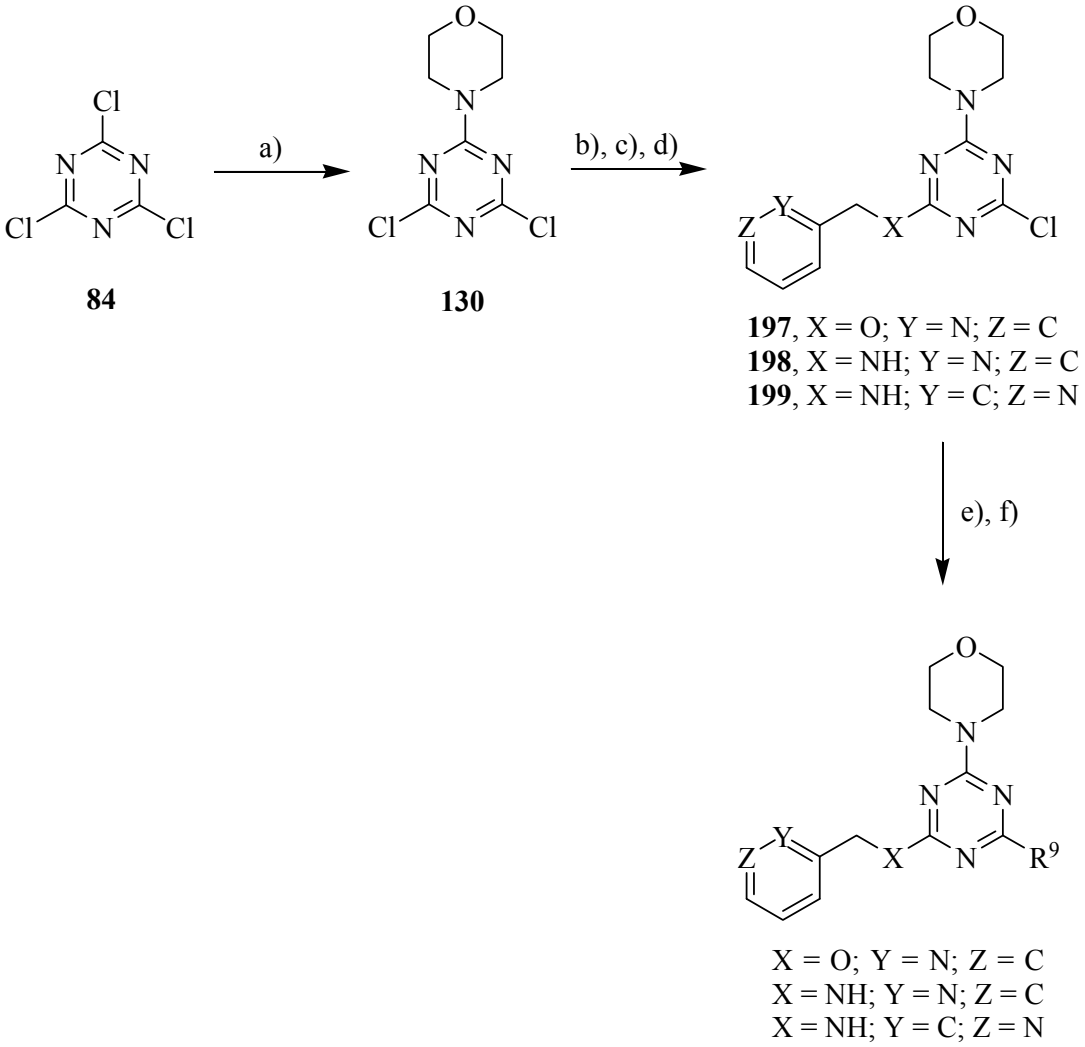

Reagents and conditions: (a) morpholine (1.0 eq.), CH_2Cl_2, -50 °C, 1 h, 41% **130** (MJA34); (b) 2-pyridylcarbinol (1.4 eq.), NaH (1.0 eq.), THF, room temperature, 2 h, 46% **197** (MJA33/35/36); (c) 2-picolylamine (1.1 eq.), CH_2Cl_2, room temperature, 21 h, 23% **198** (MJA11/17/22); (d) 3-picolylamine (1.5 eq.), CH_2Cl_2, - 5 °C, 16 h, 33% **199** (HGA12); (e) boronic acid pinacol ester (4.0 eq.), 1,2-dimethoxyethane:2M Na_2CO_3 (3:1), dichloro 1,1'-bis(diphenylphosphino)-ferrocene-palladium(II)-dichloride dichloromethane complex (0.025 eq.), 90 °C, 15-20 h; f) amine (1.1 eq.), NaH (1.5 eq.), DMF, reflux, 4 h.

Table 13.

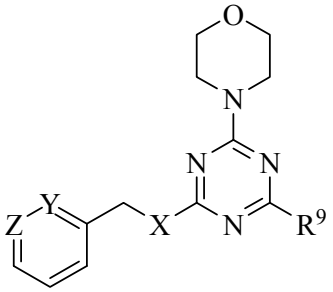

Compds	R^9	X	Y	Z	*In vitro* PI3Kalpha inhibition at 200nM	In cell inhibition[a] pPKB/PKB 1 µM / pS6 1 µM	In cell inhibition[a] pPKB/PKB 10 µM / pS6 10 µM
200 (NCB107)	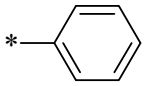	O	N	C	86	- / -	- / -
201 (NCB108)	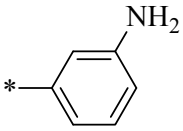	O	N	C	87	++ / -	++ / +(+)
202 (NCB109)	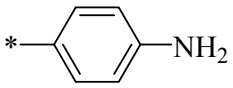	O	N	C	88	- / -	++(+) / -
203 (MJA43)	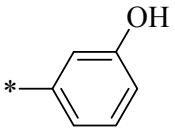	O	N	C	51	++(+) / +	++++ / ++++
204 (MJA39)	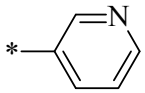	O	N	C	91	++ / -	++(+) / -
205 (MJA38)	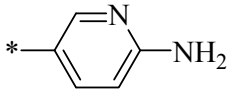	O	N	C	76	++ / -	++(+) / ++
206 (GSA33) (HGA1)	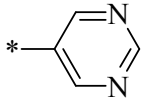	O	N	C	89	+ / -	+ / -
207 (MJA37)	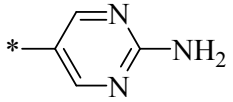	O	N	C	45	+ / +	+++ / ++++

Table 13 (continued).

Compds	R^9	X	Y	Z	*In vitro* PI3Kalpha inhibition at 200nM	In cell inhibition[a] pPKB/PKB 1 µM / pS6 1 µM	In cell inhibition[a] pPKB/PKB 10 µM / pS6 10 µM
208 (MJA40)	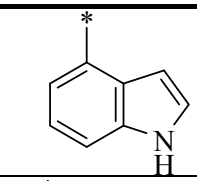	O	N	C	65	++++ / ++	++++ / ++++
209 (VVA77)	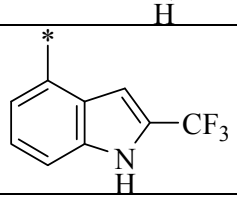	O	N	C	99	(+) / -	+++ / -
210 (MJA42)	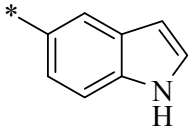	O	N	C	107	+ / +	+++ / ++++
211 (MJA60)	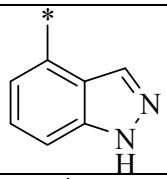	O	N	C	84	- / +	+++ / ++(+)
212 (VVA101)	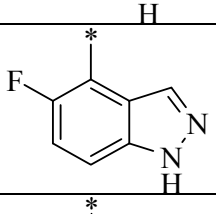	O	N	C	103	- / -	- / -
213 (VVA95)	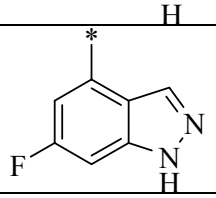	O	N	C	100	- / -	- / -
214 (MJA41)	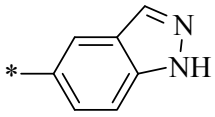	O	N	C	100	+(+) / -	++(+) / +
215 (GSA31) (HGA2)	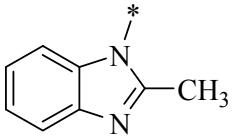	O	N	C	90	- / ++	+ / ++++
216 (MJA25)	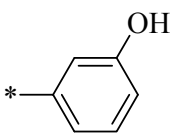	NH	N	C	66	+ / -	+++ / +++

Table 13 (continued).

Compds	R^9	X	Y	Z	*In vitro* PI3Kalpha inhibition at 200nM	In cell inhibition[a] pPKB/PKB 1 µM / pS6 1 µM	In cell inhibition[a] pPKB/PKB 10 µM / pS6 10 µM
217 (MJA29)	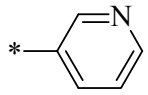	NH	N	C	123	- / -	- / -
218 (MJA30)	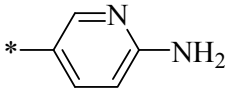	NH	N	C	71	+ / -	+ / +++
219 (MJA31)	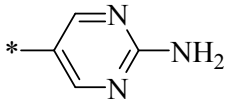	NH	N	C	40	+ / +(+)	+++ / ++++
220 (MJA28)	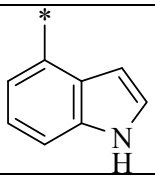	NH	N	C	104	+ / -	+++ / ++
221 (MJA26)	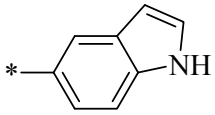	NH	N	C	123	- / -	+(+) / -
222 (MJA27)	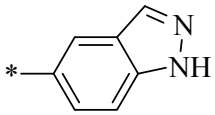	NH	N	C	125	- / -	- / -
223 (GSA59) (HGA13)	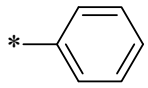	NH	C	N	98	- / -	(+) / -
224 (HGA14)	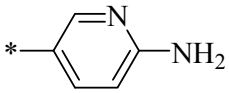	NH	C	N	67	- / -	- / +++(+)
225 (HGA15)	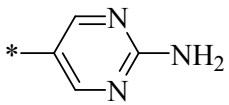	NH	C	N	19	+ / -	+++(+) / +++(+)

[a]Inhibitor efficacy and their cell permeability were measured by *in cell* Western inhibition assay on melanoma cell line A2058; "-" no activity, "+"/"++" poor activity; "+++" good activity; "++++" very good activity; *in vitro* PI3Kalpha inhibition was measured by *Kinase Glo* assay; given numbers represent %remaining activity, the smaller the value is the stronger is the inhibition.

Scheme 11.

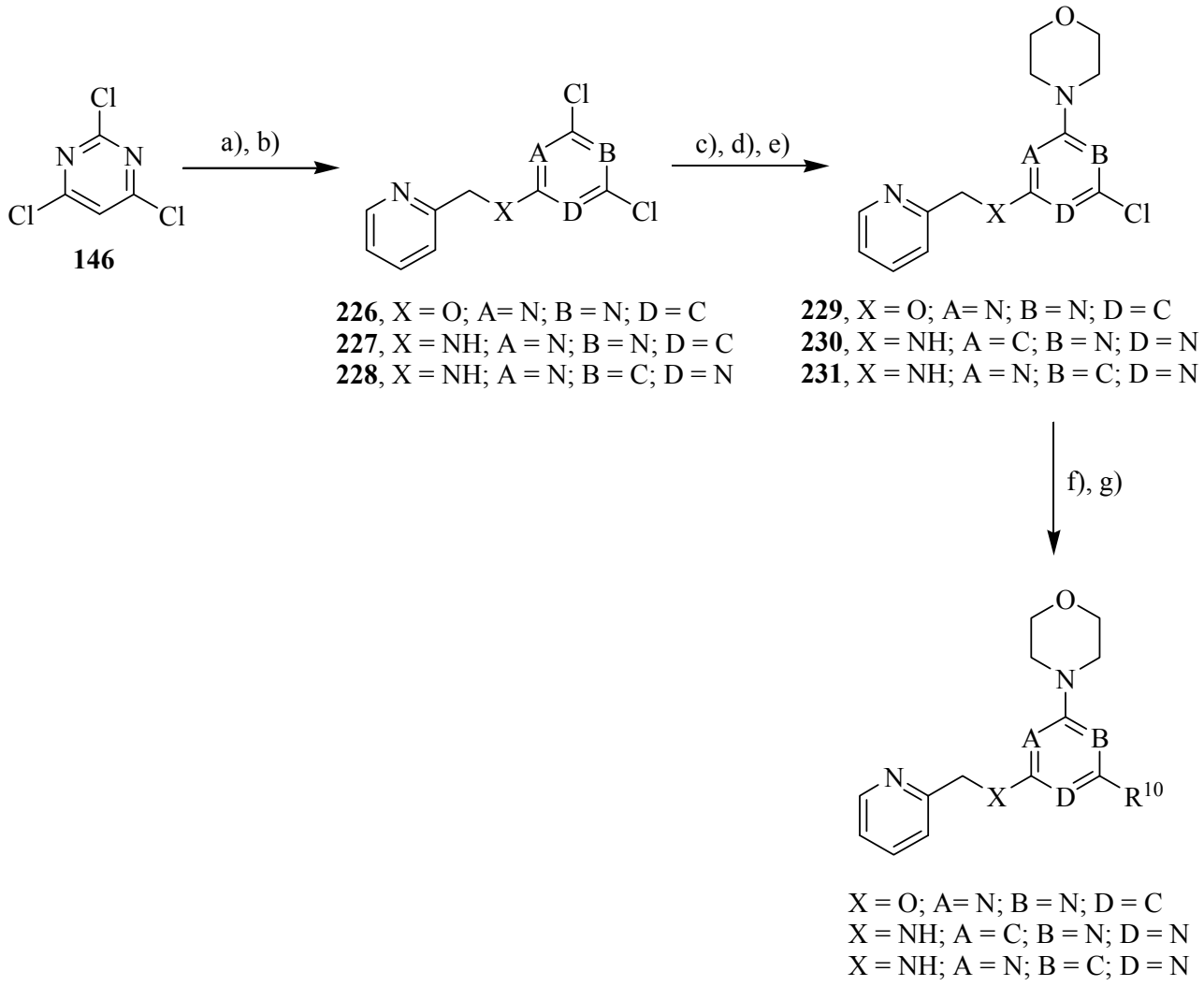

Reagents and conditions: (a) 2-pyridinemethanol (1.0 eq.), NaH (1.0 eq.), THF, room temperature, 3 h, 26% **226** (JBA133); (b) 2-aminomethylpyridine (1.1 eq.), DIPEA (1.1 eq.) dioxane, room temperature, 2 h, mixture of **227** (JBA113A) and **228** (JBA113B) (2:1); (c) **226** (JBA133) (1.0 eq.), morpholine (1.5 eq.), DIPEA (1.5 eq.), dioxane, room temperature, 2 h, 63% **229** (JBA147); (d) **227** (JBA113A) (1.0 eq.), morpholine (1.8 eq.), DIPEA (1.5 eq.), dioxane, reflux, 5 h, 84% **230** (JBA123); (e) **228** (JBA113B) (1.0 eq.), morpholine (1.5 eq.), DIPEA (1.5 eq.), dioxane, room temperature, 2 h, 71% **231** (JBA125); (f) boronic acid pinacol ester (4.0 eq.), 1,2-dimethoxyethane:2M Na_2CO_3 (3:1), dichloro 1,1'-bis(diphenylphosphino)-ferrocene-palladium(II)dichloride dichloromethane complex (0.025 eq.), 90 °C, 15-20 h; (g) amine (1.1 eq.), NaH (1.5 eq.), DMF, reflux, 4 h.

Table 14.

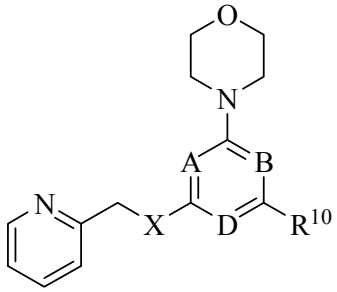

Compds	R^{10}	X	A	B	D	*In vitro* PI3Kalpha inhibition at 200nM	In cell inhibition[a] pPKB/PKB 1 µM / pS6 1 µM	In cell inhibition[a] pPKB/PKB 10 µM / pS6 10 µM
232 (JBA155)	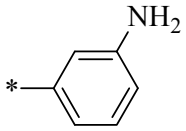	O	N	N	C	124	- / (+)	++ / (+)
233 (JBA153)	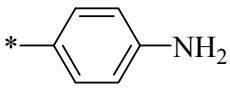	O	N	N	C	127	- / (+)	+(+) / (+)
234 (JBA139)	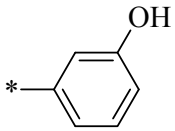	O	N	N	C	31	++ / -	++++ / +++
235 (JBA157)	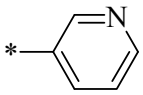	O	N	N	C	109	- / (+)	+(+) / (+)
236 (JBA151)	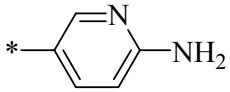	O	N	N	C	66	+ / -	+++ / +++
237 (JBA149)	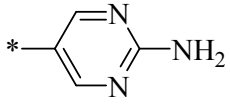	O	N	N	C	19	+ / +(+)	++++ / ++++
238 (NCB21)	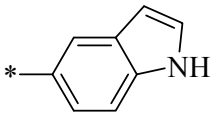	O	N	N	C	84	+ / +	++ / +
239 (JBA129)	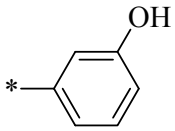	NH	C	N	N	103	- / -	++(+) / +++

Table 14 (continued).

Compds	R^{10}	X	A	B	D	*In vitro* PI3Kalpha inhibition at 200nM	In cell inhibition[a] pPKB/PKB 1 µM / pS6 1 µM	In cell inhibition[a] pPKB/PKB 10 µM / pS6 10 µM
240 (JBA141)	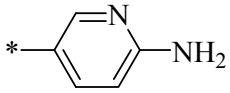	NH	C	N	N	62	+ / ++	++++ / ++++
241 (JBA131)	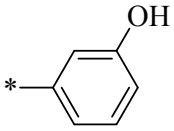	NH	N	C	N	88	- / +	++ / +
242 (JBA143)	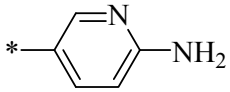	NH	N	C	N	123	- / -	- / -

[a]Inhibitor efficacy and their cell permeability were measured by *in cell* Western inhibition assay on melanoma cell line A2058; "-" no activity, "+"/"++" poor activity; "+++" good activity; "++++" very good activity; *in vitro* PI3Kalpha inhibition was measured by *Kinase Glo* assay; given numbers represent %remaining activity, the smaller the value is the stronger is the inhibition.

4.8. Spirocyclic Oxetane Derivatives

Due to the practical interest in view of its structural relationship to morpholine, we examined the biological properties of 2-oxa-6-azaspiro[3.3]heptane (spirooxetane, **261**) derivatives. Spirooxetane **261** was prepared by a recently published procedure of Wuitschick and colleagues [28]. Tribromopentaerythritol (**243**) provides ready access to 2-oxa-6-azaspiro[3.3]heptane (**261**), which can be stored conveniently as its stable oxalate salt **245**. Deprotonation of **245** with sodium hydride and the nucleophilic substitution with cyanuric chloride provided monosubstituted cyanuric chloride derivative **246**. Further displacement of chlorine with benzimidazole derivatives provided **247** and **248**. The last nucleophilic substitution of triazine derivatives **247** and **248** with different piperazine derivatives yielded the asymmetric end-products of Scheme 12. We observed that the nucleophilic substitution of cyanuric chloride with three different secondary amines could be obtained selectively under specific mild conditions. Collectivelly, this access route offers convenient pathway to diverse spirooxetane containing triazine libraries.

Scheme 12.

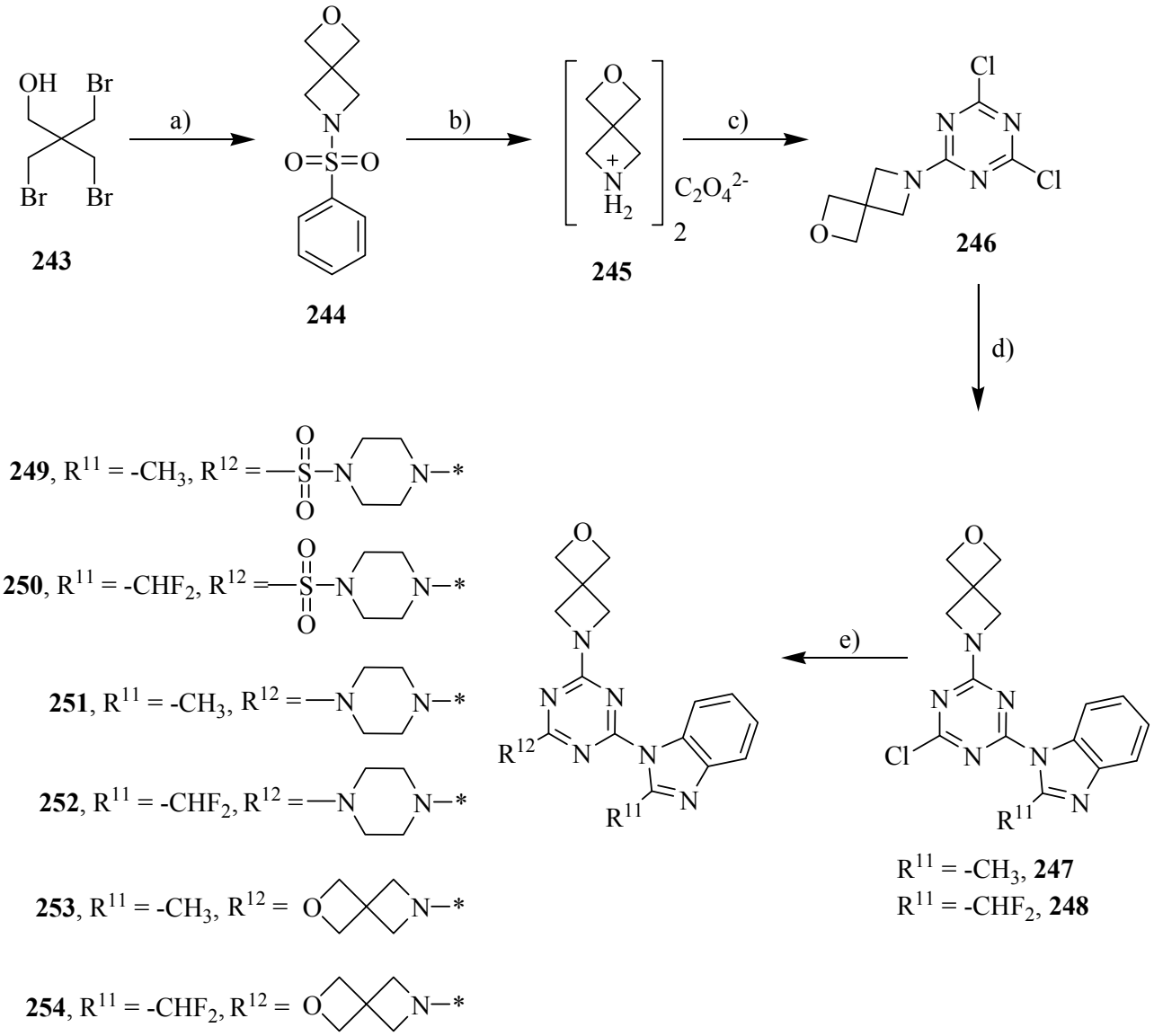

Reagents and conditions: (a) *p*-tosylamide (1.2 eq.), KOH (3.2 eq.), ethanol, reflux, 93 h, 63%; (b) Mg granulate (7.0 eq.), MeOH, ultrasound, 1 h, then $H_2C_2O_4$ (0.5 eq.), 75%; (c) NaH (2.0 eq.), room temperature, overnight, 86%; (d) K_2CO_3 (1.4 eq.), benzimidazole (1.4 eq.), DMF, 4 h, room temperature; (e) K_2CO_3 (3.2 eq.), piperazine (1.2 eq.), DMF, 2 h, room temperature.

The highly active lipid kinase inhibitor **257** (GSA44) was synthesized through a short three-step sequence (Scheme 13) in a same way as done by asymmetric ZSTK474 derivatives from the Scheme 8.

Scheme 13.

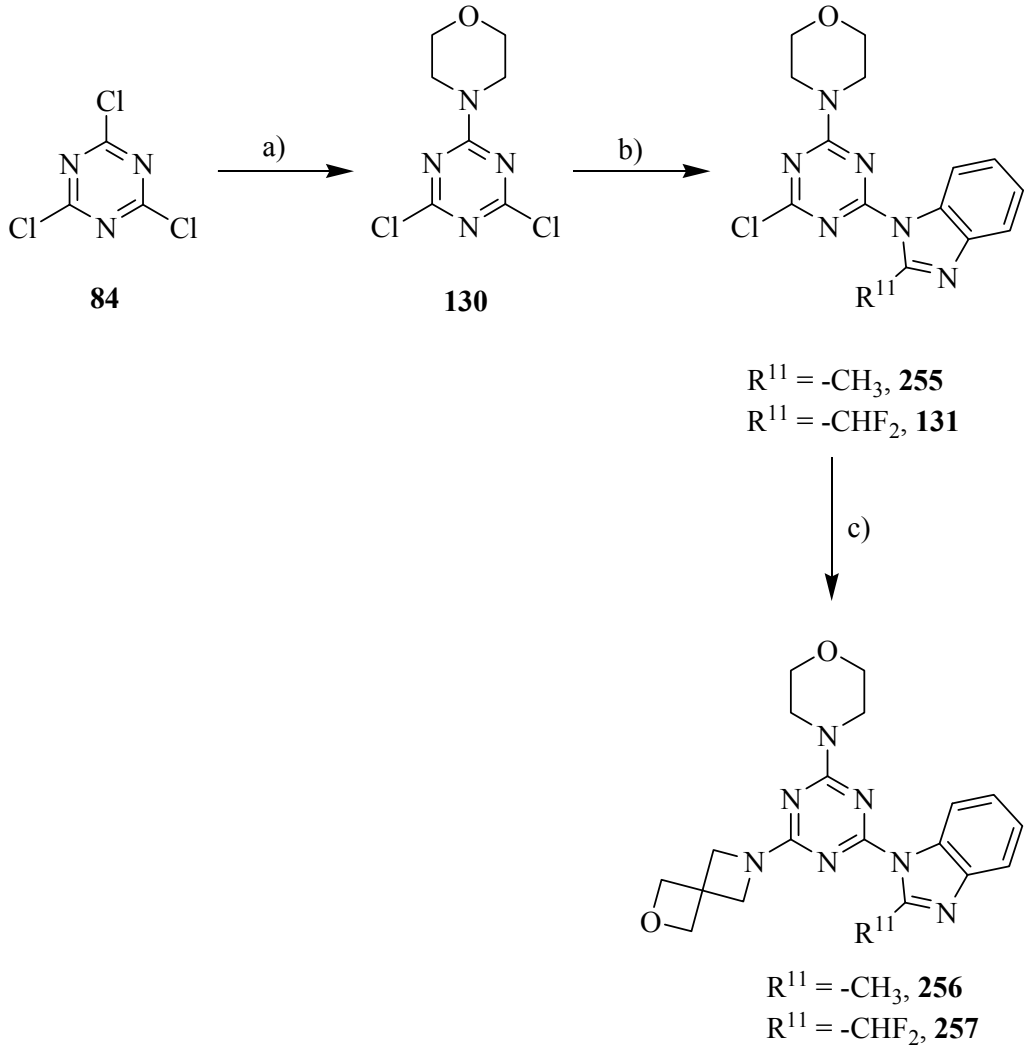

Reagents and conditions: (a) morpholine (1.0 eq.), CH_2Cl_2, -50 °C, 20 min., 28%; (b) K_2CO_3, (1.5 eq.), benzoimidazole (1.4 eq.), DMF, 30 min. at 0 °C, 4 h at room temperature; (c) K_2CO_3 (3.2 eq.), 2-oxa-azaspiro[3.3]heptane (0.6 eq.), DMF, room temperature, 3 h.

With the aim to proof the activity of the pyrimidine containing analog of **234** (GSA44), a similar synthesis as performed by triazine **234** (GSA44) is presented in Scheme x. The 2,4,6-trichloropyrimidine (**131**) was firstly substituted with 2-(difluoromethyl)-1*H*-benzo[*d*]imidazole at 2-chloro position of the pyrimidine ring. Further nucleophilic substitutions with the spirooxetane **261** and morpholine led to the desired analog of **234** (GSA44), compound **240** (GSA81). The systematic biological profiling of this compound is currently under investigation.

Scheme 14.

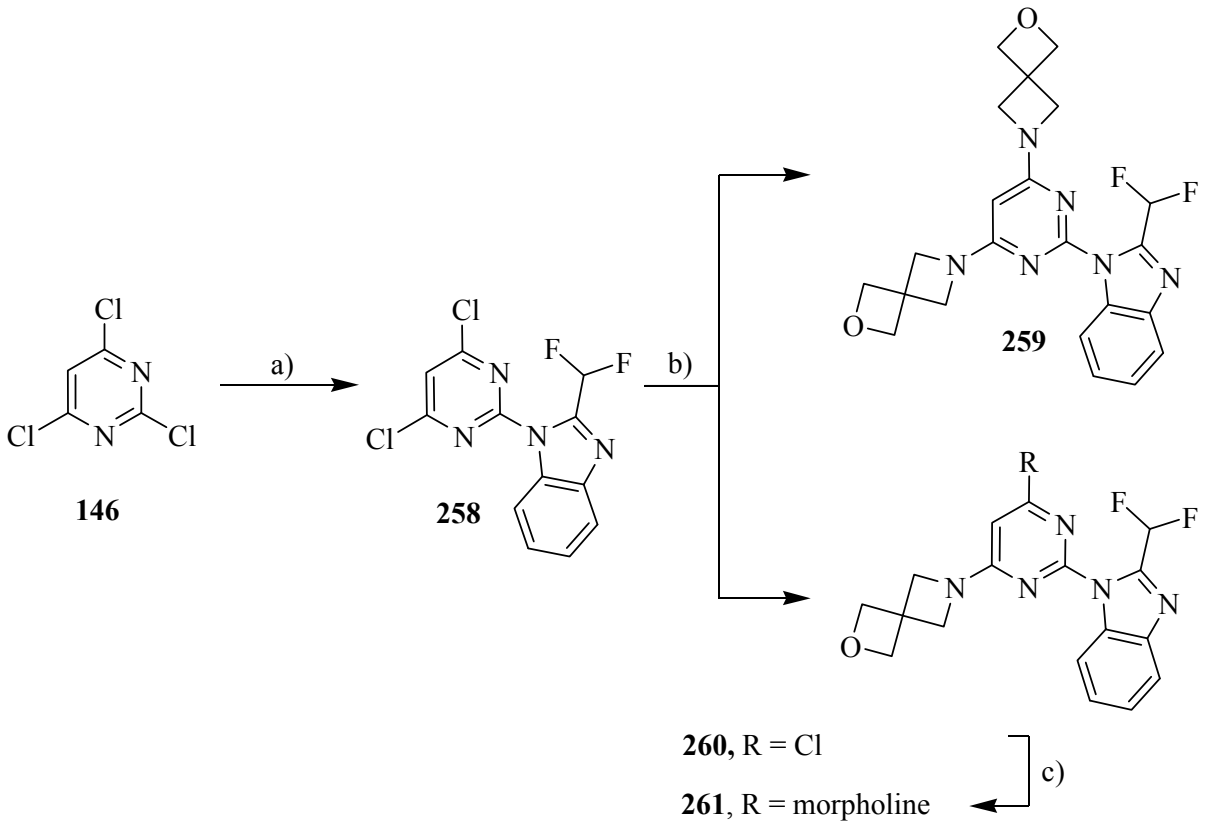

146 **258** **259**

260, R = Cl

261, R = morpholine

Reagents and conditions: (a) K_2CO_3 (1.74 eq), 2-(difluoromethyl)-1*H*-benzo[*d*]imidazole (0.9 eq.), DMF, 30 min. at - 5 °C and then 18 h at room temperature, 70%; (b) K_2CO_3 (2.8 eq.), 2-oxa-6-azaspiro[3.3]heptane (1.0 eq.), DMF, 30 min. at -5 °C and then 18 h at room temperature, 41% **261**, 19% **259**.

5. Summary and Outlook

The pharmaceutical development of PI3K inhibitors has made a great leap forward during the last 5 years. Promising molecules have entered clinical trials for cancer therapy, inflammation and coronary heart disease. First inhibitors with some isoform specificity have been lanced. While inhibitor selectivity is often impressive *in vitro*, *in vivo* selectivity, potency and efficacy will have to be united and improved for chronic treatment of non-fatal diseases, e.g. in inflammation and allergy. For some of the pan-PI3K developed for cancer therapy (e.g. BEZ235, PI-103, SF1126, XL765, XL147, ZSTK474), encouraging toxicity data has become available. Many experimental drugs are relatively well tolerated, even though the molecules cross-react with the whole PI3K family and PI3K-related kinases. As drug targeting of PI3K progresses, academia should close the gaps in knowledge of the specific function of the different PI3K isoforms. The race to occupy niches and markets in PI3K-directed therapies is on.

6. Experimental Part

6.1. Conditions of Measurements

Analytical thin layer chromatography (TLC) plates from Merck were used for reaction control (silica gel 60 on aluminium sheets) and chromatographic analysis (silica gel 60 on glass). Silica gel 60 (Fluka) was used for silica gel flash column chromatography. Preparative column chromatography employing silica gel was performed according to the method of Still.

Infrared spectra (IR) were recorded on a Perkin-Elmer 1420 spectrophotometer. Absorbance frequencies are reported in reciprocal centimeters (cm^{-1}).

Proton nuclear magnetic resonance (^{1}H NMR) spectra and carbon-13 nuclear magnetic resonance (^{13}C NMR) spectra were recorded on Bruker spectrometers (Avance400: 400 MHz for 1H and 101 MHz for 13C; Avance DRX500: 500 MHz for 1H and 125 MHz for 13C; Avance DRX600: 600 MHz for 1H and 150 MHz for 13C) at ambient temperature in the solvents indicated, and referenced to the residual solvent signal: $CDCl_3$ (7.26), DMSO-d_6 (2.50) or CD_3OD (3.31) for ^{1}H chemical shifts and $CDCl_3$ (77.0), DMSO-d_6 (39.0) or CD_3OD (49.0) for ^{13}C chemical shifts. Chemical shifts are reported in δ (ppm). Coupling constants are reported in Hertz (Hz). The following abbreviations are used: s (singlet), s, br (broad singlet), d (doublet), t (triplet), q (quartet) and m (multiplet). ^{13}C NMR spectra were routinely run with broadband decoupling.

Mass Spectrometry Electron Ionization (MS-EI) and **Fast Atom Bombardment (MS-FAB)** spectra were recorded on a VG70-250 (EI) and a MAT 312, using 3-nitrobenzyl alcohol as a matrix (FAB). **Mass Spectrometry Electron Spray Ionisation (MS-ESI)** spectra were recorded in methanol on a Finnigan MAT LCQ spectrometer. **High Resolution Mass Spectrometry (HR-MS)** was performed by the mass service at the University of Fribourg (CH). Mass signals are given in mass units per charge. The fragments and intensities are given in brackets.

Elemental Analyses (EA) were carried out on a Leco CHN-900 device. The values are given in mass percent.

6.2. Proliferation Assay

A2058 melanoma cells were plated in a black 96 well plate ($7 \cdot 10^3$ cells/cm^2). The next day the cells were exposed to different inhibitors at 1mM. Cell numbers were evaluated 1, 2 and 3 days after inhibitor treatment with Alamar Blue. Alamar Blue at a final concentration of 10% was added to the medium and the plate was left in the incubator for 4 hours. Then fluorescence was measured at an excitation wavelength of 560 nm and emission wavelength of 590 nm. The background value (well with no cells) was subtracted form all the values and the percentage of cell number compared to the control (DMSO treated cells) was calculated.

6.3. Western blot and IC_{50} determination

Melanoma cells were plated ($7 \cdot 10^3$ cells/cm^2), and NVP-BEZ235 and NCA235 (both at 1 mM) were added 24 hours later. After 3 hours of exposure to inhibitors, cells were lysed in NP-40-based lysis buffer (pH 8.0, 20 mM TrisHCl, 138 mM NaCl, 2.7 mM KCl, 5% glycerol, 1 mM $CaCl_2$, 1 mM $MgCl_2$, 1% NP-40, 20 mM leupeptin, 18 mM pepstatin, 1 mM Na-O-vanadate, 20 mM NaF and 100 mM PMSF). Proteins were separated on SDS-PAGE and transferred to Immobilon FL membranes (Millipore). Primary antibodies to pSer473-PKB/Akt and pThr389-$p70^{S6K}$ were from Cell signaling Technology (Danvers, MA); to pMAPK and MAPK from Sigma (St. Louis, Missouri), to PKB was a kind gift of E. Hirsch (Torino, Italy). Secondary antibodies (e.g. horseradish peroxidase-conjugated rabbit anti-mouse IgG (Sigma)) were visualized using enhanced chemiluminescence (Millipore), and fluorescent secondary antibodies (Alexa Fluor 680 or IRDye 800) were detected using the Odysee IR reader (LICOR).

6.4. Crystallization and Inhibitor Soaks

ΔABDp110γ crystals were obtained by the sitting-drop vapour diffusion method at 17˚C in the presence of 16% PEG 4000, 250mM $(NH_4)_2SO_4$ and 100mM Tris pH7.5. The crystals reached their maximum size (0.2 mm × 0.1mm × 0.1mm) in about 10 days.

The inhibitors NCB5, NCB15 and NCB36 were prepared in DMSO and diluted in cryoprotectant containing 25% PEG 4000, 15% glycerol, 250mM $(NH_4)_2SO_4$ and 100mM Tris pH7.5 to a final concentration of 1mM. The inhibitors ASA76 and MJA40 were prepared in DMSO and diluted in cryoprotectant consisting of 20% PEG 4000, 20% DMSO, 250mM $(NH_4)_2SO_4$ and 100mM Tris pH7.5 to a final concentration of 1mM. The inhibitor in cryoprotectant solution was added to the drop containing the crystals in a stepwise manner. The crystals were soaked in the final 1mM inhibitor solution for 3 hours (ASA76, MJA40), 4 hours (NCB15, NCB5, NCB36) or 16 hours (ZSTK474). Crystals were then transferred to fresh inhibitor in cryoprotectant solution for 30 seconds and flash frozen in liquid nitrogen.

6.4.1. Data collection and structure determination

Diffraction datasets were collected at the ESRF beamlines ID23-1 and ID29. Images were processed using Mosflm [33] or XDS [34] and scaled with SCALA [35].

The crystal structure of ΔABDp110γ/NCB5 complex was solved by molecular replacement using Phaser [36] with the previously published human ΔABDp110γ as the search model (PDB entry 1E8Y) and subsequent refined using Refmac [37]. Coot was used to manually build inhibitors in the unaccounted Fo-Fc difference electron density within the active site of the map [38]. Initial models of the inhibitors were generated using the PRODRG server (http://davapc1.bioch.dundee.ac.uk/prodrg) [39]. Refmac refinement was iterated with manual re-building using Coot until the structure converged.

Compound	NCB5	ASA76	MIA40	NCB15	NCB36	ZSTK474
PDB entry	****	****	****	****	****	****
Data Collection						
Wavelength (Å)	1.0072	0.9395	0.9395	1.0000	1.0000	0.9395
Spacegroup	C2	C2	C2	C2	C2	C2
Unit cell dimensions						
a, b, c (Å)	139.05, 67.22, 103.24	143.28, 67.29, 106.47	143.70, 67.47, 106.59	140.35, 66.96, 105.09	141.24, 67.11, 104.83	144.31, 67.73, 107.31
α, β, γ (°)	90.00, 96.94, 90.00	90.00, 95.74, 90.00	90.00, 95.73, 90.00	90.00, 96.40, 90.00	90.00, 96.21, 90.00	90.00, 95.05, 90.00
Resolution (Å)	60.44-2.66	40.83-2.70	35.62-2.43	61.20-2.90	61.43-3.20	71.88-2.69
% completeness (last shell)	98.3(97.2)	97.6(99.0)	99.4(100.0)	99.6(99.4)	99.4(99.3)	89.7(93.8)
R_{merge} (last shell)	0.065(0.468)	0.073(0.780)	0.096(1.51)	0.068(0.37)	0.077(0.368)	0.066(0.412)
<I/σI> (last shell)	11.9(2.5)	12.0(1.7)	11.6(1.4)	11.6(2.4)	12.7(3.8)	10.1(2.6)
Multiplicity (last shell)	3.5(3.5)	3.7(3.8)	7.2(7.5)	3.5(3.5)	3.5(3.6)	3.7(3.8)
Refinement						
Resolution (Å)	60.43-2.70	35.52-2.70	35.35-2.43	69.74-2.90	61.43-3.20	57.36-2.69
No. reflections	24861	26283	36862	20860	15623	24903
R_{work}/R_{free}	0.206/0.280	0.221/0.305	0.227/0.291	0.211/0.290	0.202/0.278	0.285/0.222
No. atoms						
Protein	6740	6791	6787	6729	6744	6735
Ligand	29	26	29	25	31	30
Water	35	39	53	13	24	16
Average B-factor (Wilson)	89.4(56.125)	89(72.66)	73.4(73.72)	79.3(74.7)	100.3(91.6)	92.5(83.8)
r.m.s. deviation from ideality						
Bond Lengths (Å)	0.015	0.015	0.017	0.014	0.015	0.019
Bond angles (°)	1.67	1.63	1.71	1.53	1.51	1.6
Dihedrals (°)	6.75	7.05	6.86	6.48	6.47	6.47
R.M.S.D.B for bonded main (side) chain atoms	0.70(1.93)	0.61(1.73)	0.78(2.21)	0.56(1.07)	0.49(1.24)	0.56(1.42)

6.5. Chemical Synthesis

6.5.1. Materials, Solvents and Reagents

All reactions were performed under an atmosphere of argon and stirred magnetically in oven-dried glassware. Anhydrous solvents were transferred via oven-dried syringe or cannula. Tetrahydrofuran (THF), dimethoxyethane (DME), diisopropylamine, triethylamine, diisopropylethylamine, dimethylsulfoxide, acetonitrile, hexane, toluene, diethyl ether, and dichloromethane were commercially available from Aldrich. Technical grade solvents used for extraction and column chromatography were distilled prior to use. Absolute solvents were purchased from Fluka or Aldrich in septum sealed bottles. Deuterated solvents were purchased from Cambridge Isotope Laboratories. Other materials and reagents were purchased from Fluka, Aldrich, Acros, Fluorochem, Boron Molecular, Frontier Scientific, Matrix Scientific or Activate-Scientific in the highest available grade and used without further purification.

References

1. Knight, Z.A., et al., *A Pharmacological Map of the PI3-K Family Defines a Role for p110alpha in Insulin Signaling.* 2006. **125**(4): p. 733-747.
2. Fan, Q.-W., et al., *A dual PI3 kinase/mTOR inhibitor reveals emergent efficacy in glioma.* 2006. **9**(5): p. 341-349.
3. Condliffe, A.M., et al., *Sequential activation of class IB and class IA PI3K is important for the primed respiratory burst of human but not murine neutrophils.* Blood, 2005. **106**(4): p. 1432-1440.
4. Mhaske, S.B. and N.P. Argade, *Regioselective Quinazolinone-Directed Ortho Lithiation of Quinazolinoylquinoline: Practical Synthesis of Naturally Occurring Human DNA Topoisomerase I Poison Luotonin A and Luotonins B and Eâ€* The Journal of Organic Chemistry, 2004. **69**(13): p. 4563-4566.
5. Marone, R., et al., *Targeting Melanoma with Dual Phosphoinositide 3-Kinase/Mammalian Target of Rapamycin Inhibitors.* Molecular Cancer Research, 2009. **7**(4): p. 601-613.
6. Maira, S.-M., et al., *Identification and characterization of NVP-BEZ235, a new orally available dual phosphatidylinositol 3-kinase/mammalian target of rapamycin inhibitor with potent in vivo antitumor activity.* Molecular Cancer Therapeutics, 2008. **7**(7): p. 1851-1863.
7. Raynaud, F.I., et al., *Pharmacologic Characterization of a Potent Inhibitor of Class I Phosphatidylinositide 3-Kinases.* Cancer Res, 2007. **67**(12): p. 5840-5850.
8. Proudfoot, J.R., *Drugs, leads, and drug-likeness: an analysis of some recently launched drugs.* Bioorganic & Medicinal Chemistry Letters, 2002. **12**(12): p. 1647-1650.
9. Villar, H., J. Yan, and M. Hansen, *Using NMR for ligand discovery and optimization.* Current Opinion in Chemical Biology, 2004. **8**(4): p. 387-391.
10. Swayze, E.E., et al., *SAR by MS: A Ligand Based Technique for Drug Lead Discovery Against Structured RNA Targets.* Journal of Medicinal Chemistry, 2002. **45**(18): p. 3816-3819.
11. Hartshorn, M.J., et al., *Fragment-Based Lead Discovery Using X-ray Crystallography.* Journal of Medicinal Chemistry, 2004. **48**(2): p. 403-413.
12. Marone, R., et al., *Targeting phosphoinositide 3-kinase—Moving towards therapy.* Biochimica et Biophysica Acta, 2007. **1784**(1): p. 159-185.
13. Walker, E.H., et al., *Structural Determinants of Phosphoinositide 3-Kinase Inhibition by Wortmannin, LY294002, Quercetin, Myricetin, and Staurosporine.* 2000. **6**(4): p. 909-919.
14. Walker, E.H., et al., *Structural insights into phosphoinositide 3-kinase catalysis and signalling.* Nature, 1999. **402**(6759): p. 313-320.
15. Lawrie, A.M., et al., *Protein kinase inhibition by staurosporine revealed in details of the molecular interaction with CDK2.* Nat Struct Mol Biol, 1997. **4**(10): p. 796-801.
16. Folkes, A.J., et al., *The Identification of 2-(1H-Indazol-4-yl)-6-(4-methanesulfonyl-piperazin-1-ylmethyl)-4-morpholin-4-yl-thieno[3,2-d]pyrimidine (GDC-0941) as a Potent, Selective, Orally Bioavailable Inhibitor of Class I PI3 Kinase for the Treatment of Cancer&#x2020.* Journal of Medicinal Chemistry, 2008. **51**(18): p. 5522-5532.
17. Jackson, S.P., et al., *PI 3-kinase p110 beta: a new target for antithrombotic therapy.* Nature Medicine, 2005. **11**(5): p. 507-514.
18. Yaguchi, S.-i., et al., *Antitumor Activity of ZSTK474, a New Phosphatidylinositol 3-Kinase Inhibitor.* J. Natl. Cancer Inst., 2006. **98**(8): p. 545-556.
19. Yu, K., et al., *Biochemical, Cellular, and In vivo Activity of Novel ATP-Competitive and Selective Inhibitors of the Mammalian Target of Rapamycin.* Cancer Res, 2009. **69**(15): p. 6232-6240.
20. García-Martínez, J.M., et al., *Ku-0063794 is a specific inhibitor of the mammalian target of rapamycin (mTOR).* Biochemical Journal, 2009. **421**(1): p. 29-42.

21. Bleicher, K.H., et al., *Hit and lead generation: beyond high-throughput screening.* Nat Rev Drug Discov, 2003. **2**(5): p. 369-378.
22. Pauling, L., *The Nature of the Chemical Bond.* Cornell University Presss, 1960.
23. Bondi, A., J. Phys. Chem., 1964. **68**: p. 441-451.
24. Smart, B.E., J. Fluorine Chem., 2001. **109**: p. 3-11.
25. Hans-Joachim, B., et al., *Fluorine in Medicinal Chemistry.* ChemBioChem, 2004. **5**(5): p. 637-643.
26. van Niel, M.B., et al., *Fluorination of 3-(3-(Piperidin-1-yl)propyl)indoles and 3-(3-(Piperazin-1-yl)propyl)indoles Gives Selective Human 5-HT1D Receptor Ligands with Improved Pharmacokinetic Profiles.* Journal of Medicinal Chemistry, 1999. **42**(12): p. 2087-2104.
27. Rainer , E.M., et al., *Remote Modulation of Amine Basicity by a Phenylsulfone and a Phenylthio Group.* ChemMedChem, 2007. **2**(3): p. 285-287.
28. Georg, W., et al., *Spirocyclic Oxetanes: Synthesis and Properties.* Angewandte Chemie International Edition, 2008. **47**(24): p. 4512-4515.
29. Liu, Y. and N.S. Gray, *Rational design of inhibitors that bind to inactive kinase conformations.* Nat Chem Biol, 2006. **2**(7): p. 358-364.
30. Williams, R., et al., *Form and flexibility in phosphoinositide 3-kinases.* Biochemical Society Transactions, 2009. **037**(4): p. 615-626.
31. Pirola, L., et al., *Activation Loop Sequences Confer Substrate Specificity to Phosphoinositide 3-Kinase alpha (PI3Kalpha). FUNCTIONS OF LIPID KINASE-DEFICIENT PI3Kalpha IN SIGNALING.* J. Biol. Chem., 2001. **276**(24): p. 21544-21554.
32. Jones, G., et al., *Development and validation of a genetic algorithm for flexible docking.* Journal of Molecular Biology, 1997. **267**(3): p. 727-748.
33. Leslie, A.G.W., *Joint CCP4 and ESF-EACMB (Daresbury Laboratory, Warrington, UK).* Newsletter on Protein Crystallography, 1992. **26**.
34. Kabsch, W., *Automatic processing of rotation diffraction data from crystals of initially unknown symmetry and cell constants.* Journal of Applied Crystallography, 1993. **26**: p. 795-800.
35. *CCP4, 1994, Acta Crystallogr. D, 50, 760-763.*
36. McCoy, A.J., *Solving structures of protein complexes by molecular replacement with Phaser.* Acta Crystallographica, Section D, Biological Crystallography, 2007. **63**: p. 32-41.
37. Murshudov, Acta Crystallogr. D, 1997. **53**: p. 240-255.
38. Emsley and Cowtan, Acta Crystallogr. D, 2004. **60**: p. 2126-32.
39. Schuttelkopf and v. Aalten, Acta Crystallogr D Biol Crystallogr, 2004. **60**(1355-63).
40. Phillips, M.A., et al., *Triazolopyrimidine-Based Dihydroorotate Dehydrogenase Inhibitors with Potent and Selective Activity against the Malaria Parasite Plasmodium falciparum.* Journal of Medicinal Chemistry, 2008. **51**(12): p. 3649-3653.

Curriculum Vitae, Vladimir Cmiljanovic

Vladimir Cmiljanovic, born August 12, 1979 in Kragujevac, *Languages*: fluent in Serbian, German and English.

Education, Professional Experience

2009 – present	PostDoc studies at Center for Biomedicine, University of Basel, Switzerland.
2006 - 2009	Assistant of Prof. Bernd Giese in Organic Chemistry.
2006 - 2009	Doctoral student, Institute for Organic Chemistry and Center for Biomedicine, University of Basel, Basel, Switzerland (Prof. B. Giese and Prof. M. P. Wymann): Targeting lipid signalling in disease; medicinal chemistry group leader and project initiator in targeting the lipid kinases with small chemical compounds; Ph.D. studies completed on 15th December 2009 with summa cum laude (the highest mark: 6.0).
2001 – 2006	University of Basel, Basel, Switzerland; Diploma in Natural Sciences, Master of Science in Chemistry, February 2006, the highest mark (6.0). Major subjects: organic chemistry, medicinal chemistry, biochemistry, molecular biology and microbiology.
2000 – 2001	Rector's Conference of the Swiss Universities, Fribourg, Switzerland; Diploma in General Qualification for Swiss University Entrance. Major subjects: chemistry, physics, mathematics, biology, German, English, world history and Swiss history.
1998 – 1999	University of Kragujevac, Kragujevac, Serbia.
1994 - 1998	Grammar school in Serbia; Diploma Type C, August 1998.

Professional Organizations

Swiss Chemical Society, Swiss Proteomics Society, American Association for Cancer Research, European Federation for Medicinal Chemistry (EFMC).

Publications

Targeting melanoma with dual phosphoinositide 3-kinase/mammalian target of rapamycin inhibitors.
Marone R, Erhart D, Mertz AC, Bohnacker T, Schnell C, Cmiljanovic V, Stauffer F, Garcia-Echeverria C, Giese B, Maira SM, Wymann MP. *Molecular Cancer Research* 2009 Apr;7(4):601-13.

Targeting phosphoinositide 3-kinase—Moving towards therapy (over 100 citations in 2 years).
Cmiljanovic V, Marone R, Giese B, Wymann MP. *Biochimica Biophysica Acta* 2008 Jan;1784(1):159-85.

Patents

Triazine, pyrimidine and pyridine analogs and their use as therapeutic agents and diagnostic probes.
Cmiljanovic V, Cmiljanovic N, Giese B, Wymann MP. International patent application, PCT/IB2009/007404.

Spirocyclic compounds and their use as therapeutic agents and diagnostic probes.
Cmiljanovic V, Cmiljanovic N, Giese B, Wymann MP, patent application ***.

Heterocyclic compounds and their use as therapeutic agents and diagnostic probes.
Cmiljanovic V, Cmiljanovic N, Giese B, Wymann MP. patent application ***.